Regulatory File Cy.

50-247

Feedwater Line Incident Report - Indian Point Unit No. 2

RECEIVED
JAN 14 1974
U.S. ATOMIC ENERGY COMMISSION
Regulatory Mail Section

DOCKETED
USAEC
JAN 14 1974
REGULATORY MAIL SECTION DOCKET CLERK

Consolidated Edison Company of New York, Inc.
Indian Point Unit No. 2
Facility Operating License DPR-26

January 14, 1974

8110210210 740114
PDR ADOCK 05000247
S PDR

TABLE OF CONTENTS

Section No.	Title	Page No.
1.0	Introduction	1-1
2.0	Sequence of Events	2-1
3.0	Damage to Equipment and Structures Resulting From the Incident	3-1
4.0	Investigations and Tests	4-1
5.0	Identification of Causitive Mechanisms	5-1
6.0	Modifications and Repairs	6-1
7.0	Evaluation of Safety Implications	7-1
8.0	Summary and Conclusions	8-1

Figures

A	Piping Penetration
B	Feedwater Piping Inside Containment for Steam Generator No. 22
C	Modified Piping to Steam Generator No. 22
D	Steam Temperature in Steam Generator No. 22 and at Break Location
E	Modified Feedwater Regulating System Showing Low Flow Bypass Regulator
F	Photomacrograph of Central Section of Fracture
G	Plastic Strain of Pipe at Crack

Figures

H	Tensile Properties of A-106, Gr. C, Pipe Material
I	Sketch of Glass and Plastic Model of Feedwater System
J	Experimentally Observed Slugging Mechanism
K	Simplified Sequence of Events

Appendices

I	Pertinent Data
II	Physical Damage Report
III	Metallurgical Report of Failed Sections of Feedwater Pipe
IV	Analysis of Containment Liner
V	Evaluation of Feedwater Line Check Valve
VI	Analytical Investigation of Feedwater Line Response to Postulated Water Hammer Effects

1.0 Introduction

Incident Description

On November 13. 1973, Indian Point Unit No. 2 experienced a turbine trip as a result of high water level in steam generator No. 23. At the time of the trip, the reactor was at about 7% of its rated power, and the plant was being prepared for synchronization of the generator to the system. As a result of the turbine trip, the normal feedwater flow was interrupted and auxiliary feedwater flow was supplying the steam generators. Level in Steam Generator No. 21, however, dropped, and the reactor tripped due to low-low steam generator level.

After reactor trip, level in Steam Generator No. 22 continued to decrease followed by a rise in containment temperature and humidity. Once it was determined that the steam generator level could not be restored, the plant was cooled down. During plant cooldown, investigation showed that the main feedwater pipe to Steam Generator No. 22 had cracked 180° circumferentially at the penetration inside containment. It was noted that the feedwater line to Steam Generator No. 22 experienced a shaking accompanied by a loud noise at about the time of reactor trip.

Investigation

As a result of the pipe break, a number of investigations and tests were conducted to determine the cause, results and implications of this incident. Consolidated Edison, with the

support of Westinghouse and their subcontractors, investigated various mechanisms in an effort to determine the most probable cause of the feedwater pipe break. These included an internal inspection of Steam Generator No. 22, an examination including a survey of the feedwater piping and penetration area, a metallurgical analysis of the failed section of pipe, a hydrostatic leakage test of feedwater Loop No. 22 check valve, and a review of the operating records.

A survey and examination of the electrical equipment inside containment was performed. The containment liner underwent an examination that included a pressure and leak test, and a leak test of the No. 22 feedwater line penetration. Additionally, a bending test of the liner material was performed to assure that this steel could withstand the cyclic stresses that it experienced in buckling and returning to its original shape.

Repairs

As a result of the incident, repairs to damaged equipment and certain modifications have been made. The most extensive of these modifications was lowering the horizontal run of the Loop No. 22 feedwater line at the steam Generator by approximately 1 ft. 4 in. The new modified section of feedwater piping was subjected to stress analysis to assure that original design criteria were met.

Additional restraints were also installed on the four feedwater lines inside containment to prevent pipe movement and "rebound" type stressing that appears to have contributed to the cracking of the pipe.

In order to improve the operability and control of the feedwater regulating system at low flow, the plug characteristics were modified. In addition, a bypass line will be installed at a subsequent outage on each of the four regulating valves, which will permit even more sensitive feedwater control at low flow. Additional vapor containment liner insulation has been added above the pipe break area completely around the inside of containment.

Safety Evaluation

A loss of feedwater incident, either as a result of a pipe break, pump failure or valve malfunction is analyzed in the Final Safety Analysis Report(FSAR), Section 14.1.9.

The analysis assumed the worst case situation where feedwater to all four steam generators is completely interrupted. Additionally, The plant is assumed to be operating at 3216.5MW_t (the maximum calculated turbine rating) with a primary system temperature of 570°F and a conservative core residual heat generation based upon long-term operation at the initial power level preceeding the trip.

In this analyzed case, as in the case of the November 13,1973 feedwater line break, the reactor trips on low-low level in one of the steam generators. This level signal, or the trip of any of the main feed pump turbines, then causes the two motor-driven auxiliary feedwater pumps(400 gpm each) to start. In the analysis, only one pump is assumed to start. This is shown, however, to be sufficient to supply enough flow to cool the primary system sufficiently and to preclude the primary

relief or safety valves from actuating.

The vapor containment is designed to withstand the blowdown from the reactor coolant system with the unit at full power. The analysis presented in the FSAR demonstrated that the reactor was adequately protected. The feedwater break which occurred on November 13, 1973 was much less severe with the reactor at only 7% of its rated power level, and T_{avg} equal to about 548°F. The size of the pipe failure, also was considerably smaller than a double-ended break. Thus, the system has been designed to withstand a substantially more severe pipe break without endangering the health and safety of the public.

The steam pressure in the vapor containment developed from blowdown from a single loop of the secondary side (as analyzed in Section 14.2.5 of the FSAR) is less severe than a primary side break. This analysis of the secondary side break at the exit of a steam generator computed the mass and energy release to be 2000000 lbs, and 182 x 10^6 Btu, respectively. Assuming an instantaneous release to the containment and no credit for containment safeguards, the containment pressure has been calculated to be 27 psig compared to the containment design value of 47 psig. The containment pressure generated by the feedwater pipe break was substantially less than this containment design pressure.

2.0 Sequence of Events

Time (approximate)	Event
Prior to Incident	Reactor critical, about 7% power T_{avg} = 548°F Turbine is at 1750 rpm No. 22 Steam Generator (s/g) level = 40%
7:38 a.m.	Turbine trip due to high level on No. 23 Steam Generator. In service No. 21 main boiler feed pump shutdown - 2 motor-driven auxiliary boiler feed pumps start and restore level in all but Steam Generator No. 22.
7:45 a.m.	Reactor trip due to low-low level in No. 21 Steam Generator. First shaking accompanied by a loud noise in No. 22 feedwater line observed.
7:50 a.m.	Primary system stabilized at T_{avg} = 533°F Pressure in steam generators = 890 psig. Level in No. 22 Steam Generator still dropping.
8:00- 8:30 a.m.	Evidence of moisture in containment.
8:30 a.m.	Second shaking accompanied by a loud noise was observed in No. 22 feedwater line.
9:10 a.m.	Level in waste holdup tank increases, indicating rising sump level.
9:15 a.m.	Containment temperature increases to a maximum of 110°F. Remaining two of five fan cooler units started. Containment humidity recorder indicates increased humidity to a wet bulb temperature of 90°F. Containment recirculation fan cooler units condensate collection system weirs indicate rising level. Isolation valves to and from No. 22 Steam Generator are shut.

Time (approximate)	Event
9:40 a.m.	Steam-driven auxiliary feed pump started. Additional shaking and noise was observed on the No. 22 feedwater line.
	Secured feed to No. 22 Steam Generator.
10:10 a.m.	Cooldown commenced to bring plant to a cold shutdown condition
10:15 a.m.	Containment entry made and possible break was identified.
10:45 a.m.	Safety injection initiated due to high differential steam generator pressure.
	Steam generator went dry.
11:05 a.m.	No. 22 Steam Generator was completely isolated by shutting the manual stop valves in the auxiliary feedwater water and chemical feed lines.
	Reactor Coolant Temperature - 450°F.

3.0 Damage to Equipment and Structures Resulting From the Incident

3.1 Feedwater Piping to No. 22 Steam Generator

The 18-inch feedwater line failed with a fracture adjacent to a fillet weld between the feedwater line and the endplate which is welded into the penetration sleeve. The fracture extended approximately 180° around the pipe.

Additionally, in the horizontal section of Line No. 22 feedwater piping at the steam generator, localized bulging was noted. The other loops were inspected and found to be all within acceptable tolerances.

An inspection of the No. 22 feedwater pipe alignment using surveying equipment indicated that movement had occurred with a small permanent deformation shown by an approximate 3/4 inch clearance at the elbow restraint near the penetration (prior clearance had been nominally zero). Some piping restraints and snubbers, both inside and outside containment showed evidence of displacement (see Appendix II).

3.2 Containment Liner

Areas of the containment liner above the feedwater pipe penetrations showed slight inward bulging away from the containment wall. Intermittent bulging of the liner occurred at the 73-foot elevation extending

clockwise on the northwest side of containment, starting in the area of the feedwater line penetrations over an arc of approximately 60 feet (see Appendix IV, Figure 2).

On the basis of surveying measurements, the stand-off distance of the bulge was estimated to be a maximum of 1.6 inches. The maximum deviation from the as-built condition was approximately 1.25 inches. The liner was apparently pulled away from a number of anchor studs that are imbedded in the concrete walls of the building and attached to the liner. A special ultrasonic inspection indicated that nine of the 28 studs in the bulged area were apparently broken. In addition, the ultrasonic inspection showed the spacing of studs at this elevation to be 28 inches instead of the specified 14 inches. Subsequent examination indicated the absence of two rows of studs around the containment circumference.

Throughout and subsequent to the incident, there was no evidence of any reduction in containment liner integrity. The weld channel penetration and pressurization system air consumption in this area of containment following the incident was normal.

4.0 Investigations and Tests

The investigations and tests described below have been undertaken and completed concerning all relevant areas associated with the incident, and to insure continued safe operation of the facility.

4.1 Examination of Feedwater Piping Including Penetration Areas

The visual inspection of the 18" diameter feedwater line inside containment indicated a fracture adjacent to the fillet weld between the feedwater line and the end plate which is welded into the penetration sleeve in the containment wall. The fracture extended approximately 180° around the pipe. The origin of the fracture was at the 3 to 4 o'clock position (from inside the containment when facing the containment wall). At this position, the fracture was at the toe of the fillet weld. The fracture appeared to have propagated up to the 12 o'clock position and down to the 6 o'clock position, and its path led away from the toe of the weld approximately 1/2". Immediately above the 3 o'clock position, a short branch of the crack traveled along the toe of the weld. The fractured portion of the pipe was offset from that portion remaining in the penetration so that at the 12 o'clock and 3 o'clock positions, it was raised 1/4 of an inch. The maximum measured width of the crack was 5/32 of an inch.

A survey of the feedwater piping to Steam Generator No. 22 inside containment included removal of insulation at Steam Generator No. 22 feedwater pipe nozzle area, points of restraint (hangers, snubbers, pipe whip restraints) and elbow welds. Visual and magnetic particle inspections performed at these critical areas disclosed no linear indications. In addition, two 8 radius sweeps of piping (about 13 feet of pipe per sweep) were stripped of insulation and visual and magnetic particle inspections indicated no abnormalities. Inspection of pipe alignment was performed using surveying equipment. This survey indicated that movement had occurred with a small permanent deformation shown by an approximate 3/4 inch clearance at the elbow restraint near the penetration (prior clearance had been nominally zero). Radiography was performed at the Steam Generator No. 22 feedwater nozzle to pipe weld and two elbow welds. No unacceptable indications were found by these inspections.

Visual examination of the Line No. 22 feedwater piping indicated some relative movement of insulation had occurred, but these indications were not necessarily related to this incident. Outside of containment, a survey of feedwater Line No. 22 indicated local cracking and spalling of insulation on piping.

Some relative movement of insulation can be expected with normal heatup and cooldown expansion of feedwater piping.

Examination of the balance of the piping revealed localized bulging in the area of the horizontal pipe run near the steam generator. Examination of the remainder of the feedwater piping for all four lines revealed no abnormalities. In addition, the penetration areas associated with all four feedwater lines were intact with no increased air consumption from the weld channel penetration and pressurization system, which serves to continually monitor such leakage paths from containment.

While performing these examinations of the feedwater piping, it was noted that structural steel shimming for pipe whip restraints BRD R-1 through R-4 had not been installed. Analysis by Westinghouse demonstrated that the lack of this shimming outside containment in no way caused or contributed to the incident. The feedwater piping to No. 22 Steam Generator has been hydrostatically tested following modifications and repairs, and determined to be within specifications and safe for continued operation.

4.2 Internal Inspection of Steam Generator No. 22

An internal inspection of the steam drum and the area above the tube sheet was made through existing inspection openings. In addition, the feedwater ring inside the steam generator was inspected internally by fiber optic means. The inspection of the feedwater ring indicated that the ring was free of blockage and no obstructions were found. The results of the other inspections also indicated no abnormalities. These inspections were performed with representatives from the manufacturer taking part in accordance with approved procedures. In addition, an inspection of the steam generator support structure was made with no evidence being found of distress, unusual movement or other anomalies.

4.3 Hydrostatic Leakage Test of Feedwater Loop 22 Check Valve

Hydrostatic leakage tests were performed on the check valves, located outside containment, in the feedwater line No. 22 to determine whether any incident-related damage had been caused and/or whether or not leakage was possible, which could have contributed to the incident. The results of the tests indicated that leakage past a valve seat was negligible for these valves.

4.4 Chemical Analysis of Surface Deposits From Steam Generator No. 22 Tube Sheet Area

Surface deposits were taken from Steam Generator No. 22 in the area of the tube sheet and sent to the Con Edison Chemical Laboratory for analysis. The purpose of this analysis was to determine if feedwater chemistry anomalies prior to or associated with the incident could potentially affect the startup and safe continued operation of the facility. The results of this analysis indicated that the feedwater chemistry had been and was being maintained within allowable specification limits. Therefore, no special precautions other than those normally maintained for feedwater chemistry are considered necessary for the startup following the incident and continued operation.

4.5 Metallurgical and Mechanical Examination of Failed Section of Pipe

A comprehensive metallurgical investigation was performed to classify the fracture so that the nature and magnitude of the loadings for initiation and propagation could be substantiated.

Metallurgical Investigation

A portion of the failed feedwater pipe was supplied to the Westinghouse Research Laboratories for fractographic analysis. This portion was from the pipe beyond the penetration toward the steam generator, and included the section which was suspected as the initiation site.

The initiation did not appear to start at a particular point but there was an area in which three arrest lines could be envisioned, Figure F. The first "thumbnail" type arrest line occurred at the toe of the circumferential weld connecting the pipe to the penetration assembly and was about 0.04 inches maximum depth by 0.44 inches long. The third area had a maximum depth of 0.22 inches and a length of 3.4 inches. These arrest lines were not caused by high-cycle fatigue, but were typical of overload strain concentrations. They could have been formed by several whipping motions of the pipe in one excitation event or by three separate events.

Course chevron markings are visible on each side and "point" to the initiation area, Figure F. The outer surface of the fracture is mostly shear and shows some rubbing which probably occurred during the decay of the whipping pipe and the slight torsion resulting from the final position of the piping run. The latter was evident when the pipe was cut since it displaced upward and rotated slightly counterclockwise (facing the penetration, inside the containment). Much of the fracture surfaces was cleavage with some shear present. The fracture surface did not run around the penetration weld but moved away from the weld on each side of the initiation area. The pipe under

plane strain showed a reduction in thickness and an accompanying axial extension which was confined to the volume near the fracture surface. These strains are described below, but the fracture analyses showed that the reduction in thickness caused a radial opening of the toe weld in some regions near the fracture surface. At the initiation area, the axial extension resulted in some cracking parallel to the fracture face. These two types of cracking are typical of exhaustion of ductility at the termination of a deformation process under tri-axial stress. They are "brittle type" failures similar to the "cup and cone" type failure of a tensile bar that has necked and generated tri-axial stress even though the prior stress was indicative of a ductile material. In general, material under tri-axial stress from the beginning of the deformation process has a lower theoretical ductility.

To demonstrate that this ductile material can be made to fail with a cleavage-type fracture surface, a tri-axial specimen was prepared by deep notching all sides of a rectangular section taken from the wall of this pipe near the fracture surface but away from the deformed area. This specimen failed at a net section stress of 116 ksi, (see mechanical investigation below). The fractographic analysis showed cracks

perpendicular to the surface as well (indicative of tri-axial stressing) and cleavage on these surfaces. The high net section stress under this severe notching is an indication of ductility since the peak stresses must relax because of plastic flow. A brittle-type material would have failed at a net section stress which is about the yield stress or lower.

The fractographic analysis was extensive and covered all sections of the fracture and features of adjacent welds. Over 75 macrographs, photomicrographs and SEM pictures are on file of the failed pipe covering a range of magnifications of various regions from 1 to 1000X.

In summary, there are no indications of any material defects which could have caused a low energy fracture initiation. The ductility observed is typical of a deformation process under the constraint of the geometry of the penetration.

Estimates of the Range of Loadings on Piping System

From the observations, metallurgical study, and measurements of the components which exhibited damage, an estimate can be made of the upper and lower values of the loadings which could crack the 18 inch feedwater piping.

Inspections: Thorough visual inspections were made of the feedwater piping system and the adjacent components by several parties. Detailed records were made of damage to pipe restraints, bumpers, and integral components. A review of the operational data indicated that the piping system received three loadings before the actual failure. Two of these loadings caused minor damage to some valves and pipe hangers.

Measurements and Observations

(1) Radial Strain. The 18-inch pipe cracked at the inner side of the containment wall. The crack extended from the 12:30 o'clock position to the 6:00 o'clock position, looking toward the containment wall from the inside. The plastic deformation was confined to a narrow band near the circumferential weld which anchors the pipe to the containment wall. The constraint of the pipe is such that a high degree of plane strain is maintained so that the axial strain is nearly equal to the radial strain but opposite in sign. A plot of the magnitude of the radial strain around the pipe is illustrated in Figure G(b). Two distinct peaks can be seen. It is probable that the peak at the 7:00 o'clock position was caused either

by whipping of the pipe during the final failure or by an earlier loading in a different vibration mode. The peak plastic strain is about 7%, and, therefore, this piping material exhibited reasonable ductility for this plane strain loading.

The plastic strain is confined to the highest stressed area near the high constraint of the circumferential weld at the penetration. The axial strain distribution, Figure G(a), shows that the deformation is confined to a band along the pipe about twice the pipe thickness away from the fracture. The crack in this position is along the toe of the weld. The crack propagated only a short distance along the weld but moved away from the weld as it propagated further around the pipe. This results from the plastic distortion of the pipe under and around the high constraint at the circumferential weld. Although the final failure was by cleavage because of the constraint, considerable plastic deformation occurred before propagating rupture. The pipe dimensions were within tolerance and the pipe thickness was a maximum of 0.775 inches at the area of failure initiation.

(2) Bumper Depression. The lateral bumper, at the first inner elbow away from the penetration, is assembled with about 1/16 to 1/8 inch clearance. A depressed area at the edge closest to the containment wall was about 2-1/4" wide by 6" long with a maximum plastic compression of about 0.030 inches. This bumper prevents motion in a direction which would close the pipe break. After the break, this bumper clearance had increased to about 0.7 inches. This is consistent with the direction of the plastic strain of the pipe. The larger clearance could also allow the plastic straining of the pipe on the opposite side at the 7:00 o'clock position noted in Figure G(b).

The only constraints of the pipe in a direction away from the bumper are the pipe whip constraints, hangers, and the run of pipe to the steam generator. The records, mentioned above under observations, show that lateral and axial motions of the pipe occurred along its run.

(3) Pipe Motion at Steam Generator. The pipe whip restraint at the steam generator consists of a cable around the generator attached to a yoke clamped to the horizontal run of the feedwater

pipe. The markings of the yoke on the pipe and the deformation of the clamping bolts of the yoke indicate that lateral whipping of pipe had occurred.

(4) Pipe Displacement at Cutting. The feedwater pipe was cut at the first elbow just inside the containment to make repairs. The face end of the piping run displaced upward and rotated slightly counterclockwise, facing the inner containment wall. These small motions are probably a result of the shifting the piping restraints since any plastic strain would be greatly magnified by the long piping runs.

Fracture Analyses

The analyses of the areas of the fracture are described in detail above, but it should be noted that the area of initiations does show three zones of fracture. These zones could have been formed in the three loadings mentioned above, or in three bending cycles during the final fracture. The maximum depth of the three zones is about 0.22 inches (28% of wall thickness) and the maximum area of the zones is about 1% of the wall area.

There are no indications of any material defects which could have caused a low energy fracture initiation,

Material Properties

The mechanical properties of the pipe material, A-106 Gr. C, are given by the nominal curves of Figure H for plane stress tensile loading as a function of temperature. The pipe at the region of the failure is constrained circumferentially so that the circumferential or hoop strain is nearly zero. The pipe under tension or bending is thus under plane strain conditions. The axial strain is equal to the radial strain but opposite in sign. The result of this constraint is a reduction in strain to failure, and an increase in fracture stress. The latter was demonstrated by testing a rectangular section of A-106 pipe with side notches. The test point of 82 ksi is plotted in Figure H and identified as "Bi-axial Specimen", because of the bi-axial stress generated by the constraint.

Because of the radial constraint at the penetration and the geometry of the circumferential weld, the stresses are tri-axial at the toe of the weld. The high degree of tri-axiality results in a further reduction in ductility and a higher fracture stress at the more probable temperature of the pipe. To demonstrate the latter, and to determine the fracture mode, a rectangular section of the feedwater pipe just beyond the fracture was notched on four sides using a 1/16-inch saw with a 0.005 inches tooth

radius. This "tri-axial specimen" was tested at 196°F. It began to yield at about 96 ksi and failed at 116 ksi. This test proved that this pipe material is notch insensitive, and that a high tensile load is required to initiate and propagate the failure. The fracture surface was examined, and the same type of cleavage was found as that observed for the in-plant pipe failure.

Estimate of Loading to Cause Observed Pipe Failure

Two cases of loading will be postulated for the pipe failure to cover the upper and lower ranges of load and energy.

CASE 1. Energy pulse to generate a moment sufficiently large to plastically deform pipe to fracture and cause damage to pipe supports and bumpers.

As the moment increases beyond yield at the point of maximum stress, the neutral axis for bending will move away from the diameter perpendicular to the diameter through the maximum stress point. Thus, a plastic hinge is developed so that the total deflections are proportional to the distance from the relocated neutral axis. This allows the plastic strain to spread over a large portion of the pipe, as shown in Figure G(b).

This case gives the upper or maximum moment and energy for fracture.

Moment$_{(max)}$	$\int_A r\sigma dA$	$= 10^6$ lb-ft
Energy for pipe fracture	$\int_C P\Sigma dt$	= 6000 ft-lbs
Energy for bumper damage	$\int_A \sigma\Sigma dA$	= 1500 ft-lbs
Energy for restraints hangers and friction (est.)		= 2500 ft-lbs
Total energy for single event		= 10,000 ft-lbs

CASE 2. Four individual loadings.

The moment maximum is practically the same as in Case 1 (10^6 lb-ft.) since the highest strained area must be taken to fracture. Subsequent moments are reduced to 99%, 98% and 92%, as the net section decreases. As demonstrated by the multi-axial stress tests, there is no reduction of material strength due to the propagating fracture surface.

The total energy is increased because of the additional friction losses due to multiple pipe vibrations. The energy for the fourth loading after fracture initiation is about 3300 lb. ft. This is a lower bound of the energy range.

Postulated Energy Source

The source of the loading is postulated to be a pulse of a water slug produced by the steam and cool water interface in the horizontal run at the entrance to the steam generator. The energy can be transferred to the piping system as the pressure pulse is propagated along the pipe. Much of the energy could be

transferred through the check valve, but some reflections would occur. The pipe at the inner wall penetration will whip as the pipe is deflected away from the bumper as the pipe run is laterally displaced. The final position of the pipe run is in a direction to have placed a moment on the pipe at the penetration.

4.6 Review of Operating Records

A detailed review of operating records, computer printout and strip recorder charts of events prior to, during, and following the incident was conducted. The data from these records pertinent to the incident are presented in Appendix I. Based on a review of these data, and interviews with operators, it was determined that the break in the feedwater line to Steam Generator No. 22 occurred subsequent to the reactor trip. In addition, the data indicate that the feedwater rings inside Steam Generators 21 and 22 were uncovered shortly after the reactor trip. While the level in Steam Generator No. 21 recovered, the level in Steam Generator No. 22 did not, and continued to decrease.

This data review also demonstrated proper functioning of equipment inside containment for detection of reactor coolant system leaks. The equipment available for detection of non-radioactive leaks; humidity detectors, the moisture collection system associated with the cooling coils for the main air

recirculation units, and sump level instrumentation provided useful information to the operators to enable them to follow the course of the incident.

4.7 Survey and Examination of Electrical Equipment

An inspection after the incident was made to determine the condition of electrical equipment within containment. At Elevation 68 feet, a few minor traces of water were noticed, but the area otherwise appeared dry. At Elevation 46 feet, the presence of approximately 6 to 8 inches of water over the entire floor area was observed. An inspection of the cables and electrical equipment in the area of the electrical penetrations indicated that the lowest cable tray running on the floor along the missile shield wall was partially submerged in water (the cable in this tray, however, is designed and tested for such conditions). The cabling in the upper trays appeared dry. The level of the cable tray immediately above the lowest tray was observed to contain moisture on the bottom of the cables, but appeared dry on top. The electrical penetration area appeared intact. The lowest tray in this area was above the water level. The cabling did exhibit evidence of having been sprayed with water. There were a number of splices in this area in cabling, but no obvious water damage to the splices. An inspection of other

areas within containment indicated that all valve operators, transmitters and two drain tank pump motors were located well above the water level, and the equipment, including fittings, appeared dry.

- The electrical equipment inside containment appears to have suffered no adverse effects from the feedwater line leak. No electrical equipment is located in the immediate vicinity of the feedwater piping penetrations. It should be noted that all safeguards related equipment inside containment is designed to operate under substantially more severe containment moisture and heat conditions than those resulting from the leak in the No. 22 feedwater line.

4.8 Analysis of Examination of Containment Liner

(1) Survey of Liner Profile

The first program conducted after the discovery of the bulge in the liner was a profile survey performed by Con Edison surveyors.

The area of the liner survey extended from the midpoint between Columns 8 and 9 over to Column 11 in plan, and from Elevation 68'-8" to Elevation 81'-8".

In the surveyed area, vertical chalk lines were strung on 1'-0" centers and horizontal lines were marked on 0'-6" centers, except that

in the 2' wide horizontal band in which the bulge was concentrated (approximately Elevation 73'-75'), the spacing of the horizontal lines was reduced to 0'-3". By hanging plumb lines from overhead piping opposite each vertical chalk line, a base line was established from which the liner profile could be established.

The liner survey data is included in Appendix IV.

(2) Ultrasonic Testing of Liner Studs

Con Edison employed the services of the Conam Testing Labs to operate an ultrasonic scanner in an attempt to locate the anchor studs behind the liner plate in the bulged area.

By observing a change in signal, the Conam technicians were at first able to locate the liner studs. By further refining their technique, the technicians gained the ability to determine whether the located stud was intact and securely welded to the liner, or whether the stud or stud weld had broken.

The results of this ultrasonic examination indicated nine studs out of 28 in the bulged area apparently were broken (2 of these readings were questionable and are included for purposes of analysis).

(3) Magnetic Particle Inspection of Liner

A 2' wide band centered along the ridge (or high point) of the bulge was inspected by the magnetic particle technique for the entire length of the bulge.

The coating on the liner in the area examined was removed by power grinding.

No evidence of cracking was found. After the 47 psi containment proof test, the same area of the liner will again be inspected by magnetic particle technique.

(4) Bend Tests

Bend tests were performed to demonstrate the ductility of the liner plate and the ability of the plate to perform under a cycle loading condition.

Welded and unwelded plates were subjected to cycle tensile loads (20 cycles) and examined non-destructively for cracking. Test results obtained showed no evidence of cracking due to cyclic load.

(5) Liner Behavior During Pressure Test

In order to determine the movement of one section of the deformed liner plate, the following steps were taken:

a) a ruler mounted on a bracket was fixed perpendicularly to the liner at the high point of a long deformation.

b) a second bracket was fixed to the liner directly above the ruler-mounting bracket in a non-deformed area of the liner.

c) a plumb line which crossed the ruler-mounting bracket was hung from the upper bracket.

d) television cameras with remote monitors were focused on the point, where the plumb line crossed the ruler.

Any shift of the rules would indicate movement of the deformed plate. As the containment pressure was increased from 0 to 15 psig, the ruler shifted 5/8 of an inch from the zero reference point. The liner movement increased linearly with the increase in pressure.

After the 5/8 of an inch movement was recorded at 15 psig, no further movement was observed for the balance of the pressure increase to 47 psig. This leads to the conclusions that the liner made contact with the concrete after the 5/8 inch shift, and that the extent of

the deformation on this area was not as great as originally suspected. The 5/8 inch movement of this liner during the 0-15 psig pressure rise agrees closely with the results predicted by analysis.

4.9 Pressure and Leak Tests of Containment Liner

Prior to startup of the facility, and following modifications and repairs, special tests were conducted to determine the integrity of the containment liner and of the penetration for No. 22 feedwater line.

The pressure and leak test of the containment liner was performed as follows:

1. A 100% magnetic particle examination of the bulged section of containment liner was performed. This examination indicated no abnormalities or cracks.

2. The weld channel penetration and pressurization system was energized in the area of the bulged section of the containment liner. No abnormal air consumption was observed. The weld channel penetration pressurization system in this area was then de-energized.

3. Special provisions were made to assure that all potential leakage paths other than the liner were eliminated prior to performing a special pressure leak test of the liner. These provisions included placing the isolation valve seal water

system in service, removing weld channel penetration pressurization system air from all penetrations and the liner, and checks to assure that other valve paths were closed.

4. Containment pressure was increased gradually to 47 psig and stabilized at that pressure after which a leak rate test was performed.

5. While at 47 psig following the leak rate test, the weld channel penetration and pressurization system in the area of the containment liner was energized to 46 psig, and the air consumption measured.

6. The difference between the measurement at Steps 4 and 5 is the leak rate through the containment liner. The results of this leak rate test demonstrated that the leakage associated with the containment liner was well within the acceptance criteria of .04% per day of the containment volume.

7. After depressurization of the containment, the weld channel penetration pressurization system will be energized in the area of the bulged containment liner, and this measurement compared to that taken in Stpe No. 2. The results of this comparison demonstrate any increased leakage caused by the pressurization tests to the weld

channel system in this area. In addition, following depressurization, a 100% magnetic particle examination will be performed on the bulged area of the containment liner.

Following the replacement of the pipe and endplates in Line No. 22 feedwater penetration, a Type B (10CFR50, Appendix J) leakage test was performed. The results of this test indicated that the leakage was small and acceptable for continued service and safe operation of the facility.

4.10 Investigation of Water in Reactor Vessel Cavity

Following the feedwater pipe break approximately six hours after the failure of the feedwater line to No. 22 steam generator, an inspection team proceeded to the cavity underneath the reactor vessel to determine the amount of water collected in this area as a result of the failure. Reference points were noted, and subsequent measurements indicated that the water level in the cavity was approximately 56" above the cavity floor. This level is well below the level of the bottom of the reactor vessel, and there was no evidence of the water having contacted the vessel.

All of the in-core movable detector conduit horizontal runs were submerged. These conduits

14 Jan 84
IP#2 F.W. line
Incident (Nov 13, 1978)

are fabricated of stainless steel and did not suffer any damage as a result of this submergence. They were wiped down and smear checked to assure the absence of any potentially damaging surface contaminants.

4.11 Startup Test Program

Strain gages, thermocouples and pressure transducers are being placed on feedwater lines, both inside and outside containment at various critical points to monitor their behavior during startup and plant trips. This instrumentation is part of a special startup test program to the conclusion reached in Section 7.0 which concerned the determination and elimination of probable cause.

4.12 Westinghouse Experiment for Feedwater Line Break

Westinghouse Research experimentally investigated the possibility of generating a pulse of water in the feedwater line as a result of steam intrusion through the ring header in the steam generator. A portion of the ring header was simulated by a straight section of clear plexiglass having a series of flow holes along the underside. A second straight run of clear plexiglass representing the feedwater piping made a tee-junction at the mid-section of the plexiglass ring header; a

vacuum line and water trap were connected to a port on the upper side of the simulated feedwater piping.

Open channel flow of water was initiated in the feedwater line, allowed to partially fill the plexiglass ring header and drain through the flow holes. When steady flow was achieved, the vacuum line was activated and air exhausted from the free pipe volume over the water surface, some air was sucked in through those flow holes not covered by water. A rippling wave-like surface was established on the flowing water. As all the flow holes became covered with water, air bubbles could be observed entering the ring header and rising through the water. The surface activity became more agitated and soon developed a chugging effect. Pulses of water completely filled the feedwater pipe volume for a limited axial region, swept down the pipe length to the vacuum port, and were exhausted to the water trap in the vacuum line. The test demonstrated that if open channel flow had been established in the feedwater piping, and if a low pressure region could have been established over the water surface - say, by condensing steam, then a chugging flow of water pulses could be established experimentally.

A sketch of the glass and plastic model is shown in Figure I.

The general pattern of the unstable condition is illustrated in Figure J. Figure J(a) indicates how, for very low feedwater flow rates, a stable condition exists where there is enough space above the flowing liquid to allow pulling the air back through the feedwater conduit with no amplified disturbances. As the feedwater rate increases the counterflow of air cannot smoothly pass the constriction in the junction block, but rather, must pass through as large bubbles, i.e., the pipe becomes locally flooded as indicated in Figure J(b). A slug of water forms across the pipe separating the air trapped in the upper portion of the feedline from the counterflowing bubble and, as the air is evacuated from the upper section, this slug is accelerated toward the back of the pipe and collapses (Figures J(c) and J(d)) with considerable shock to the system.

After collapse of the trapped air bubble, the remaining slug of water initiates a surface wave, which moves back in the direction of the feedwater flow to initiate the plug formation indicated in Figure J(b). There are variations on the above

behavior of course, e.g., at higher feedwater flow rates condition J(b) could be obtained before the collapse of the first bubble so that the return surface wave is unnecessary to initiate the second slug, but it appears that for the conditions of gas counterflow through a change in cross-section, there is some liquid flow rate which will produce the slugging pehnomenon.

5.0 Identification of Causitive Mechanism

Following the performance of various investigations, a number of possible mechanisms for producing the feedwater line break that occurred on November 13, 1973 were postulated. The three mechanisms that were identified which could have produced energy and piping loads of high magnitude were:

(1) Fast closure of a feedwater regulating valve or feedwater check valve could produce a water hammer type shock (refer to Appendix VI). This mechanism was ruled out as a possible cause because:

(a) The plant was at a condition where feedwater flow was very low

(b) The observed shock occurred some time after the main feed flow had stopped and the auxiliary feedwater system was supplying feedwater

(c) The main feedwater regulating valve No. 22 was not found in a closed position after the incident

(2) Malfunction of a check valve could permit backflow of hot water and steam from a steam generator to enter areas of the feedwater lines back toward the penetration and regulating valves. Sudden quenching of steam voids by introduction of cool auxiliary feed flow could cause water slug shocks. This mechanism was ruled out as a credible cause of the incident because:

(a) The check valves associated with this mechanism in the main feedwater and auxiliary feedwater systems were pressure tested. The pressure test showed that the valves would not permit back

flow under static conditions.

(b) The main feedwater check valve (BFD-6) was evaluated to assure that the valve would function as intended under flow and static conditions. The evaluation showed that the valve would perform the desired function.

(3) Water slug loading caused by water-steam reaction in the horizontal feedwater line adjacent to Steam Generator No. 22 which followed the uncovering of the steam generator feed ring and partial drainage of the connected feed piping. The nature of this mechanism has characteristics that represent the conditions present at the time of the incident. These conditions were:

(a) The observed shaking of the pipe and noise occurred at about the time the No. 22 steam generator level decreased to a point below the feedwater ring center line.

(b) Low temperature water from the auxiliary feedwater system was being supplied to the steam generator.

In addition, the flow model test demonstrated the principle of water slugging and an evaluation of model observations showed that significant loads could be produced. The evaluation of the shock loads associated with regulating valve rapid closure showed that significant loads could be produced by this mechanism at elevated power levels(refer to Appendix VI). The magnitude of this load could cause excessive stresses. Therefore, the regulating valves were modified in such a manner

as to eliminate this shock loading.

6.0 Modifications and Repairs

As a result of the incident, repairs to damaged equipment have been made and the equipment retested to demonstrate its acceptability. In addition, as a result of examination and analysis, certain modifications were made to eliminate the most likely causitive mechanisms. The modifications also improve operability of the feedwater system to further preclude conditions that may have contributed to the incident.

6.1 Feedwater Piping Inside Containment

Steam Generator No. 22 feedwater piping is unique in that it represents the only line with a relatively long (10 ft. 8 in.) horizontal run of piping leading to the steam generator feedwater nozzle. Lines 21, 23 and 24 all have horizontal runs one half or less the length of Line No. 22. A modification has been made to the Line 22 horizontal run of piping (see (Figure C). This modification consists of lowering the elevation of the horizontal run immediately outside of the feedwater inlet nozzle approximately 1 ft. 4 in. to preclude the possibility of water in this horizontal run draining into the steam generator whenever the water level drops below the feedwater ring. This modified section of piping has been analyzed, tested and found to be acceptable in accordance with the design criteria for Indian Point Unit No. 2.

A similar modification to Lines 21, 23 and 24 feedwater piping which have short horizontal runs is not necessary, since these lines do not show evidence of damage or excessive movement.

6.2 Feedwater Piping Supports

The failure of feedwater Line No. 22 near the containment penetration occurred when the pipe impacted on the bumper restraint and rebounded. Additional restraint is being added near the first elbow in the pipe runs inside containment, on all four feedwater lines to prevent excessive feedwater line motion in the event forces are generated that could cause a similar rebound situation. These restraints have been designed so that they will not interfere with normal line movement. In addition, structural steel spacers for pipe restraints BFD R-1 through BFD R-4 outside containment, previously not installed, have been installed.

6.3 Feedwater Regulating Valves and Bypass System

As a result of investigations into various mechanisms that could have caused the incident, it was determined that a rapid closure of a main feedwater regulating valve could cause waterhammer forces. Hydraulic dampers are being added to the main feedwater regulators to preclude rapid closure of the valves

in the event the internal valve plug "hangs up" when the trip solenoid operates. These hydraulic dampers will not, however, adversely affect the closing time of the regulating valves during normal operation.

The review of operating data and history indicates that feedwater flow and steam generator level are difficult to control in the transient conditions associated with plant startup. The plug trim on the main feedwater regulating valves was modified in accordance with manufacturer's recommendation to provide improved low flow characteristics. A six-inch startup bypass line will be installed in the near future to all four main feedwater regulating valves (see Figure E).

6.4 Containment Liner

The containment liner is presently insulated up to and immediately above the elevation around the feedwater line penetrations to limit liner compressive stress due to heating during a loss-of-coolant accident. An additional 18 feet of insulation is being added above the pipe break area completely around the inside of containment. This additional insulation will preclude local heating and the resultant bulging similar to that which occurred with this incident. In the vicinity of feedwater and steam lines, the insulation was extended an additional eight feet.

6.5 Replacement of Broken Feedwater Pipe

The failed section of feedwater piping was removed and replaced with a new section extending from the first elbow outside containment through the penetration, to near the first elbow inside containment. The containment penetration end plates and expansion joints were replaced. The undamaged containment penetration sleeve and cooling coils were retained.

7.0 Evaluation of Safety Implications

A similar, but much more severe, accident was postulated in the Final Facility Description and Safety Analysis Report (FSAR), where a complete loss of feedwater to all SG's was assumed to occur. The reactor is assumed to be operating at 102% of the 3216.5 mw_t (the maximum calculated turbine rating) just prior to the interruption in boiler feed flow. Further assumptions are that the reactor is tripped by the smallest possible "low-low" level in a steam generator; only one auxiliary motor-driven boiler feed pump is available; and the residual core heat generation is conservative (maximized) and based on long-term reactor operation at the power level preceeding the trip. The power-operated steam relief valves and condenser dump valves are also not assumed to be available in the analysis, and a conservatively low heat transfer coefficient in the steam generator is used.

The conditions that are postulated in the FSAR far exceed in severity those that actually occurred before and during the November 13, 1973 incident. On that date, feedwater flow to only one steam generator was lost and the reactor was at only 7% power. Thus, the reactor was producing substantially less power than the maximum assumed in the analysis, and residual heat was much less than the postulated value. Further, both motor-driven auxiliary boiler feed pumps operated, and the levels in two of the other

three steam generators did not drop below the "low-low" alarm point. Blowdown of the No. 22 steam generator caused no significant pressure rise in the vapor containment building as this structure is designed to handle the full blowdown of the reactor coolant system with the unit initially at full power.

Following the break, equipment functioned as expected, and at no time was there any danger of violation of containment integrity, or loss of cooldown capabilities for the reactor. The health and safety of the public was, thus, not endangered by this incident.

8.0 Summary and Conclusions

Based on the observations, analysis and tests performed following the November 13, 1973 incident, three mechanisms were identified which could have developed suficient energy to cause the piping failure or could have contributed to the failure. These mechanisms were:

a) Waterhammer caused by the sudden closure of the feedwater regulating valve.

b) Water slug loading caused by check valve malfunction which results in feed line back flow from the steam generator and subsequent quench of steam voids.

c) Water slug loading caused by water-steam reaction in the horizontal feedwater line adjacent to Steam Generator No. 22 which followed the uncovering of the steam generator feed ring and partial drainage of the connected feed piping.

The sudden closure of a feedwater regulating valve was ruled out as the cause of failure because adequate energy was not available at the low flow rates involved to produce failure. However, the regulating valves were modified to eliminate the possibility of subjecting the piping system to loads which would result in excessive stresses.

Back flow in a feedwater line was ruled out as the cause of failure because the main feedwater check valve was found to be leak tight and it was determined that it would function as intended. Therefore, no mechanism for back flow was available.

The water-steam reaction in the horizontal feedwater line adjacent to the steam generator was determined to be a mechanism which could develop a significant load and was representative of a set of conditions that existed at the time of the incident. Therefore, the feedwater line adjacent to the steam generator was modified in such a way as to minimize the potential steam void volume that can develop the water/steam contact area. This modification would preclude this loading condition.

The bulging of the containment liner in the vicinity of the steam generator No. 22 feedwater line at the penetration was caused by the impingement of steam and water on the liner. Based on the analysis and tests performed, it was determined that the integrity of the liner was not violated by the incident. However, insulation was added to preclude bulging if future steam leaks impinge on the liner.

Feedwater system modifications are being made to provide for improved low feedwater flow control. These modifications will assist the operator in maintaining the steam generator levels in the proper range during start-up and shut-down evolutions. The main feedwater regulating valves have been modified to incorporate improved plug trim. At a subsequent outage a low flow bypass feedwater regulating system will be installed.

In addition, to verify the above conclusion and to test the effectiveness of the modifications, the feedwater piping will be instrumented to monitor the temperature, pressure and piping displacement performance.

Since the incident which occurred on November 13, 1973 was significantly less severe than the similar incident analyzed in the FSAR, and for which the plant's safety systems are designed, and all safety systems performed as designed, there was no resulting hazard to public health and safety.

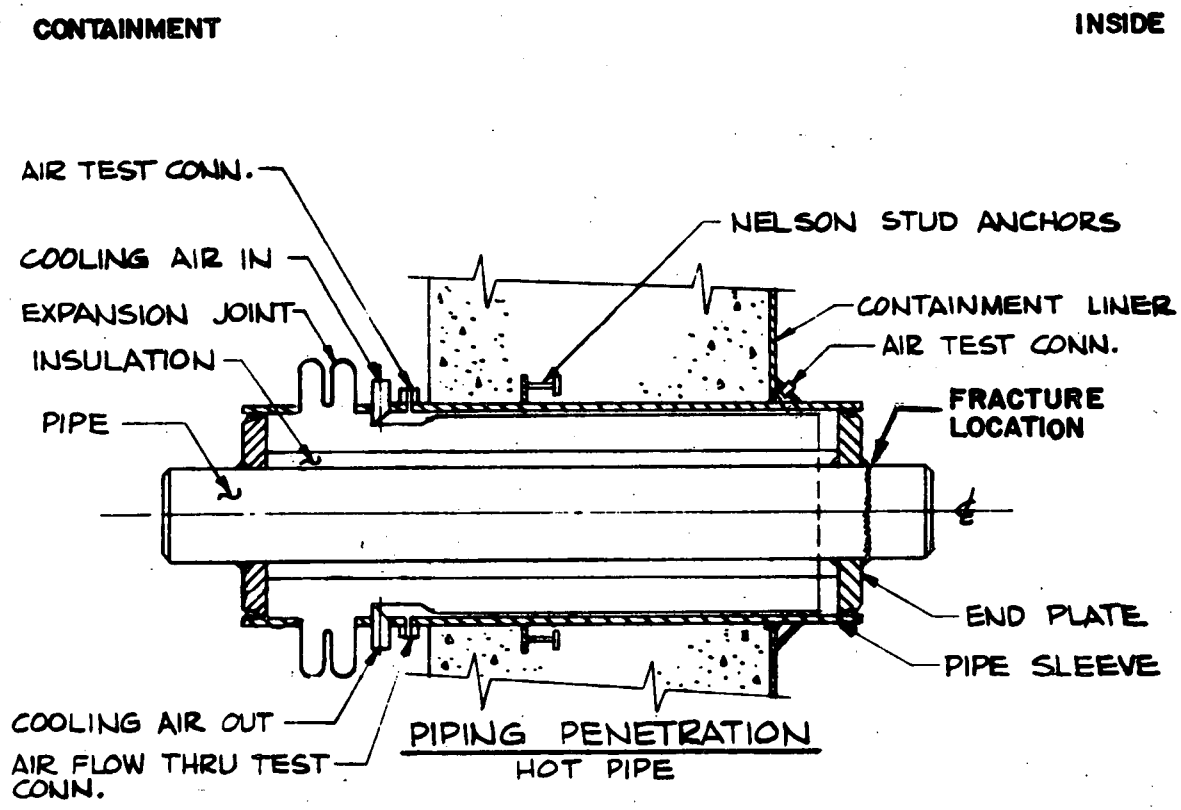
OUTSIDE CONTAINMENT
INSIDE CONTAINMENT
AIR TEST CONN.
COOLING AIR IN
EXPANSION JOINT
INSULATION
PIPE
NELSON STUD ANCHORS
CONTAINMENT LINER
AIR TEST CONN.
FRACTURE LOCATION
END PLATE
PIPE SLEEVE
COOLING AIR OUT
AIR FLOW THRU TEST CONN.
PIPING PENETRATION
HOT PIPE

Figure A

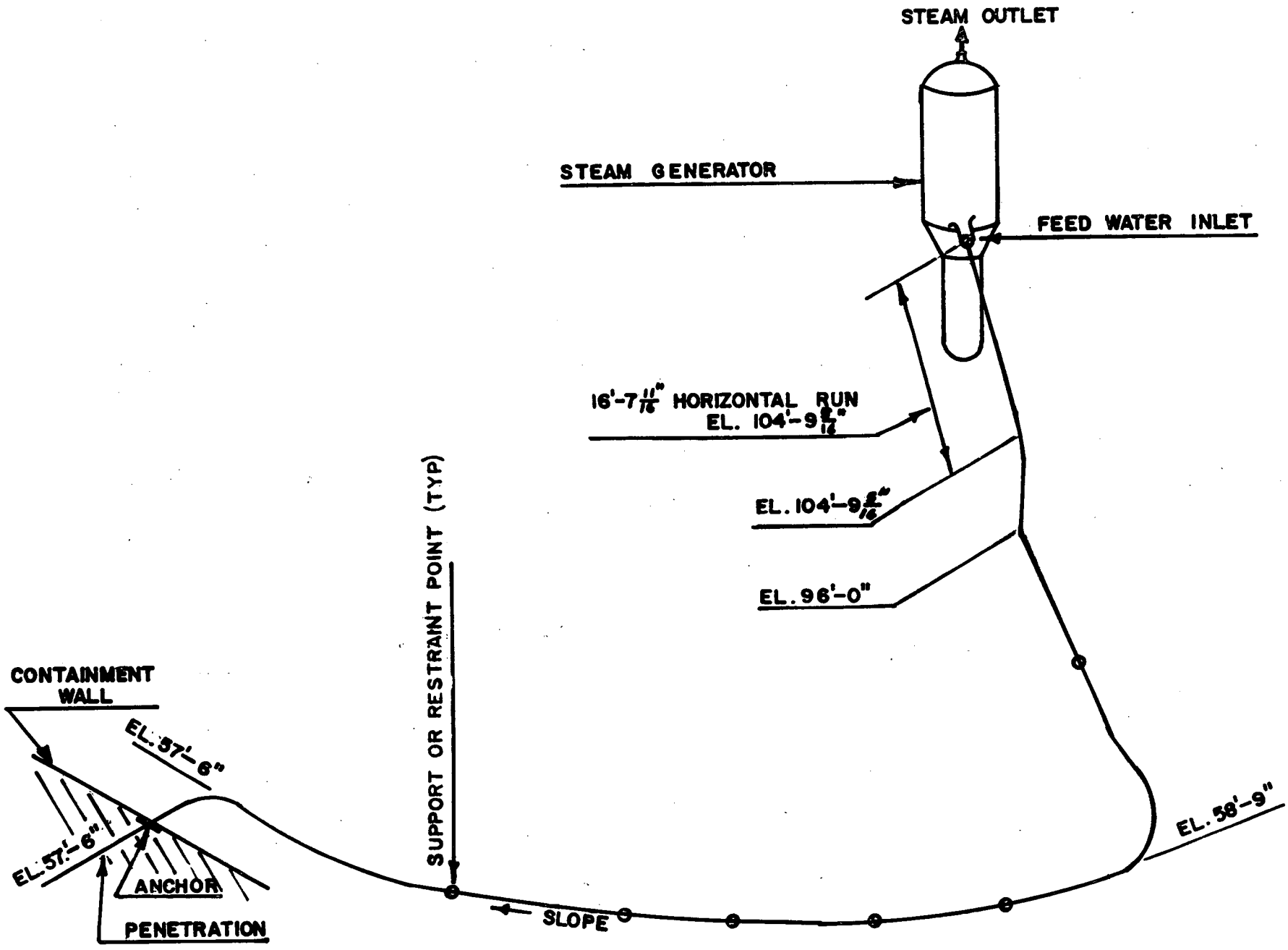

FEED WATER PIPING INSIDE CONTAINMENT
FOR STEAM GENERATOR NO. 22

Figure B

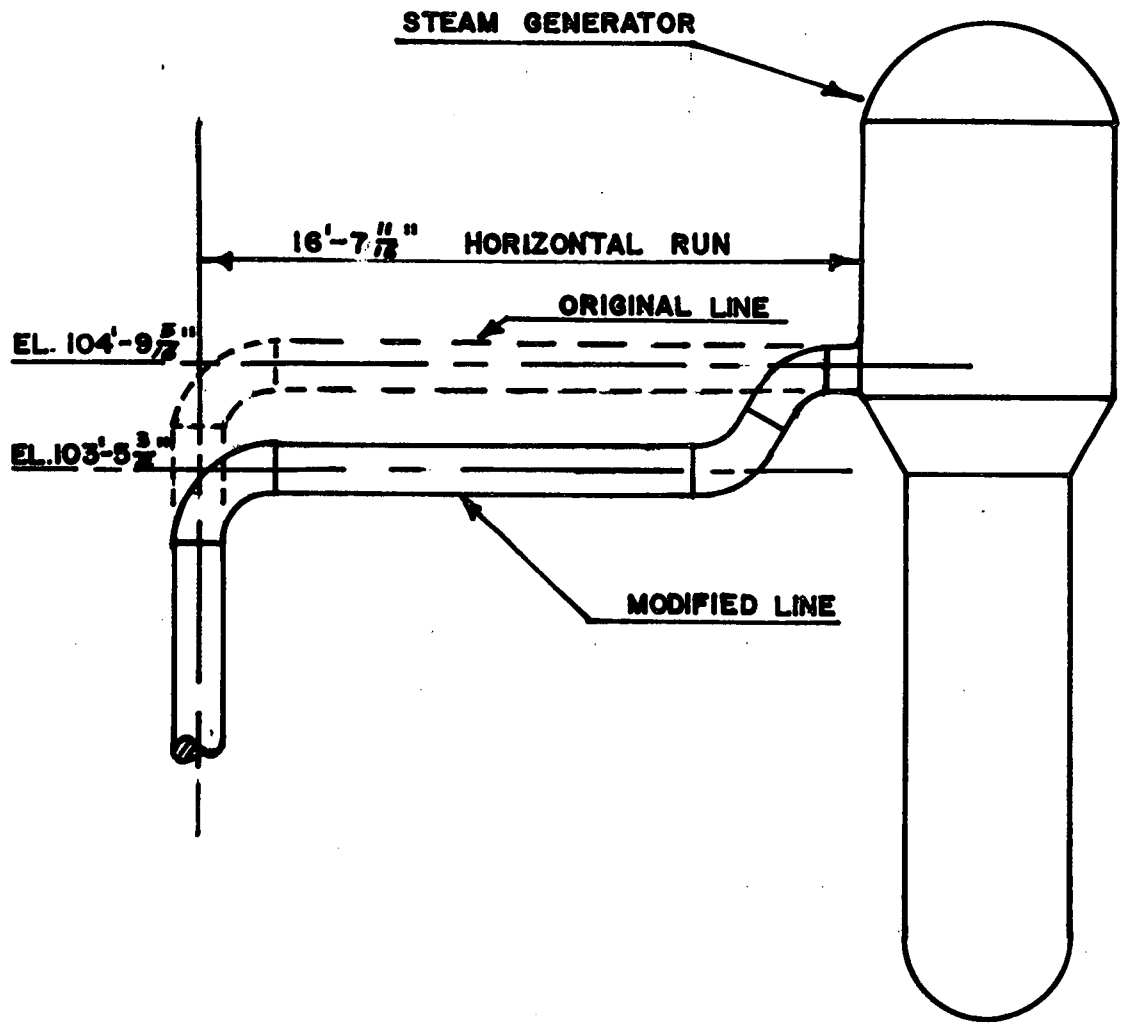

MODIFIED FEED WATER PIPING TO
STEAM GENERATOR NO. 22

Figure C

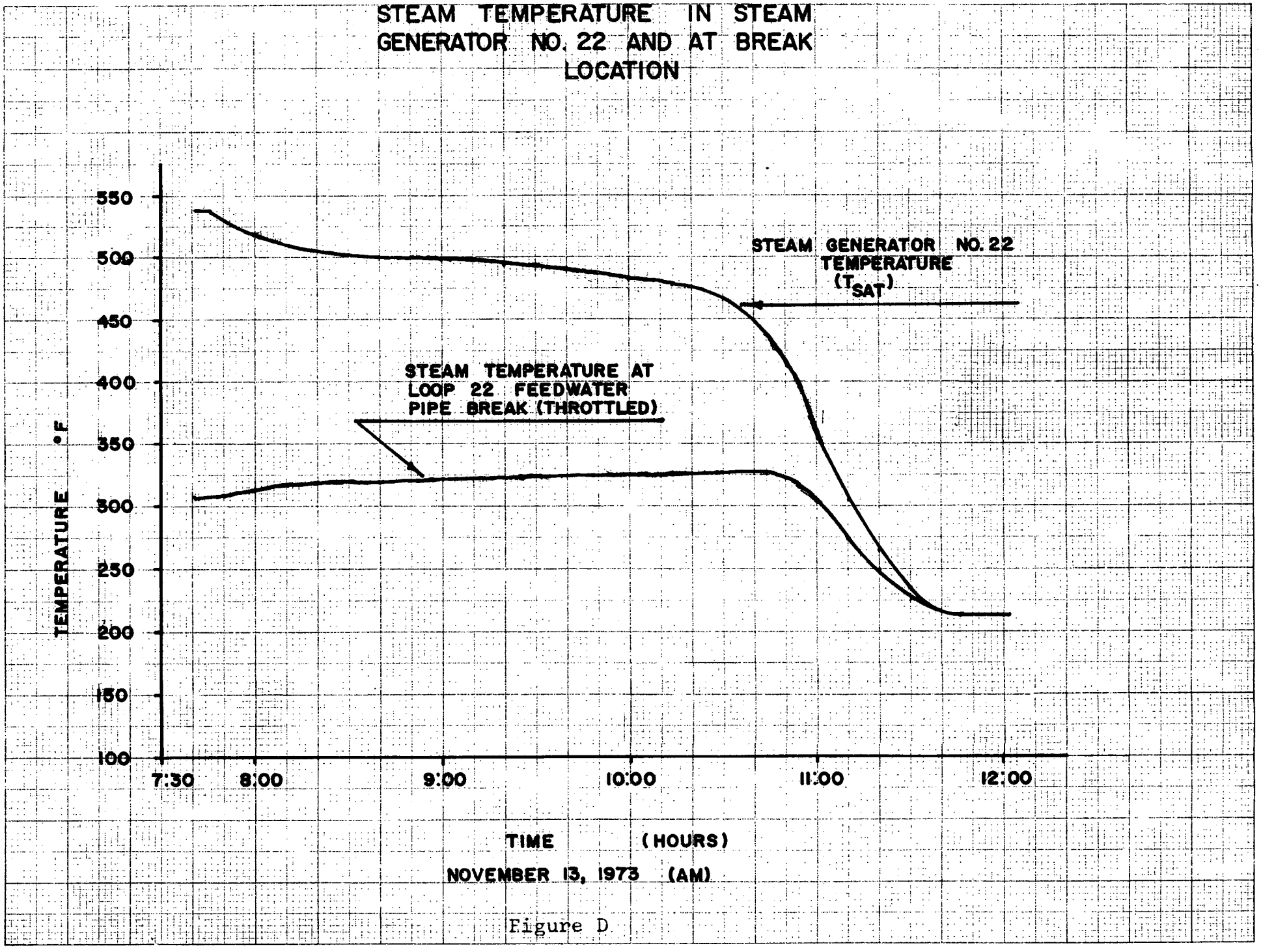
STEAM TEMPERATURE IN STEAM GENERATOR NO. 22 AND AT BREAK LOCATION
STEAM GENERATOR NO. 22 TEMPERATURE (T_{SAT})
STEAM TEMPERATURE AT LOOP 22 FEEDWATER PIPE BREAK (THROTTLED)
TEMPERATURE °F
550
500
450
400
350
300
250
200
150
100
7:30
8:00
9:00
10:00
11:00
12:00
TIME (HOURS)
NOVEMBER 13, 1973 (AM)

Figure D

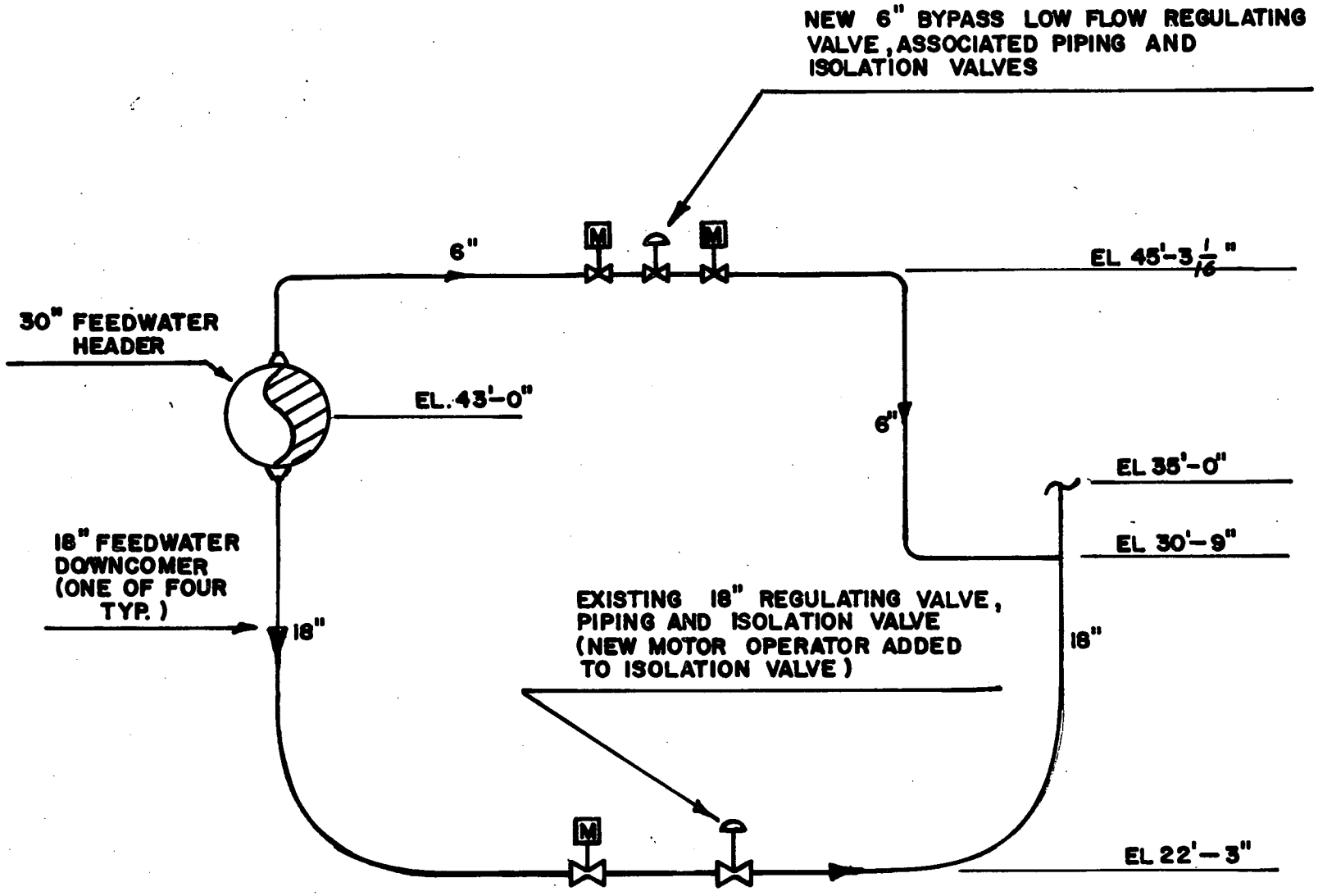

MODIFIED FEEDWATER REGULATING SYSTEM
SHOWING LOW FLOW BYPASS REGULATOR
(ONE OF FOUR TYP)

Figure E

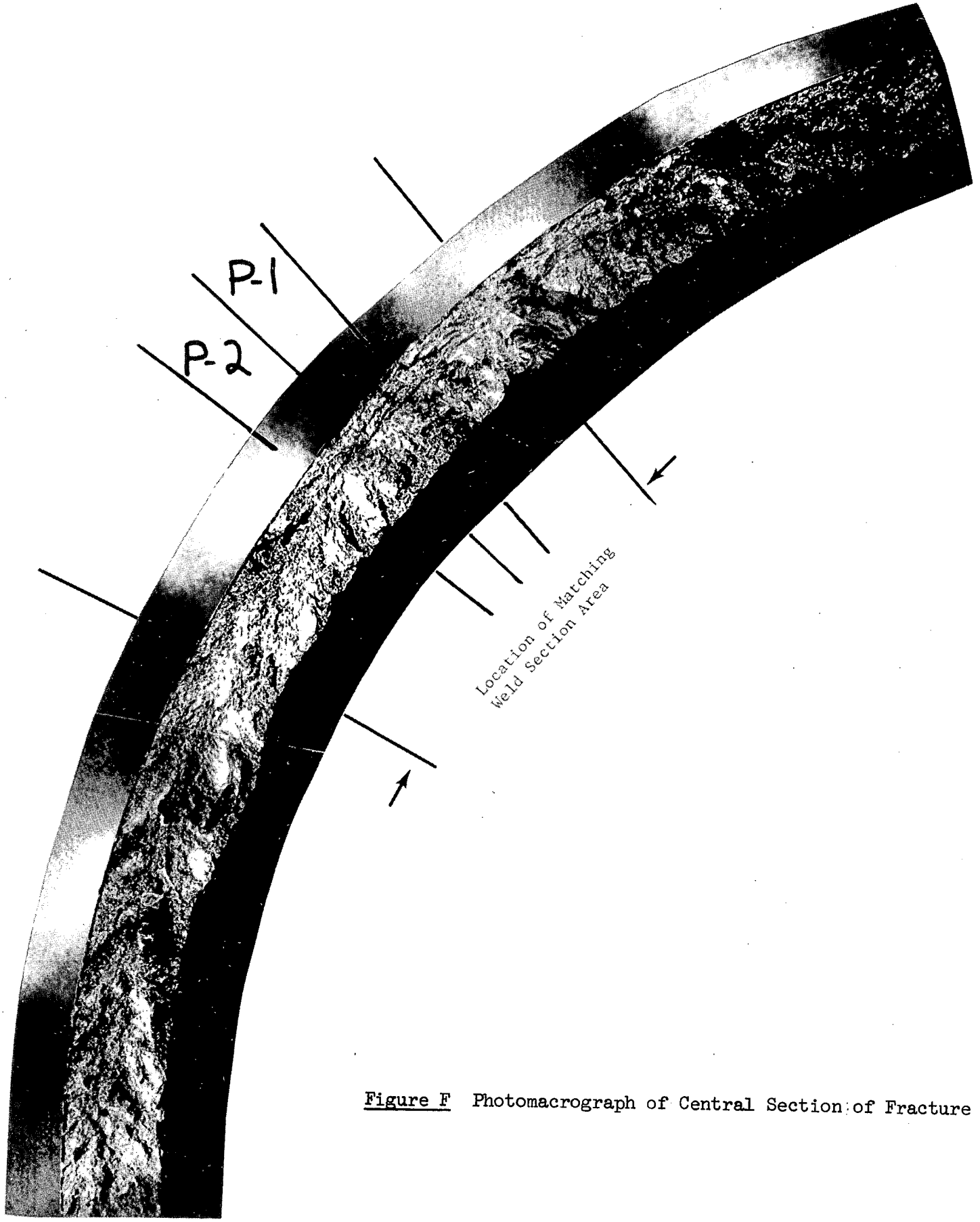

Figure F Photomacrograph of Central Section of Fracture

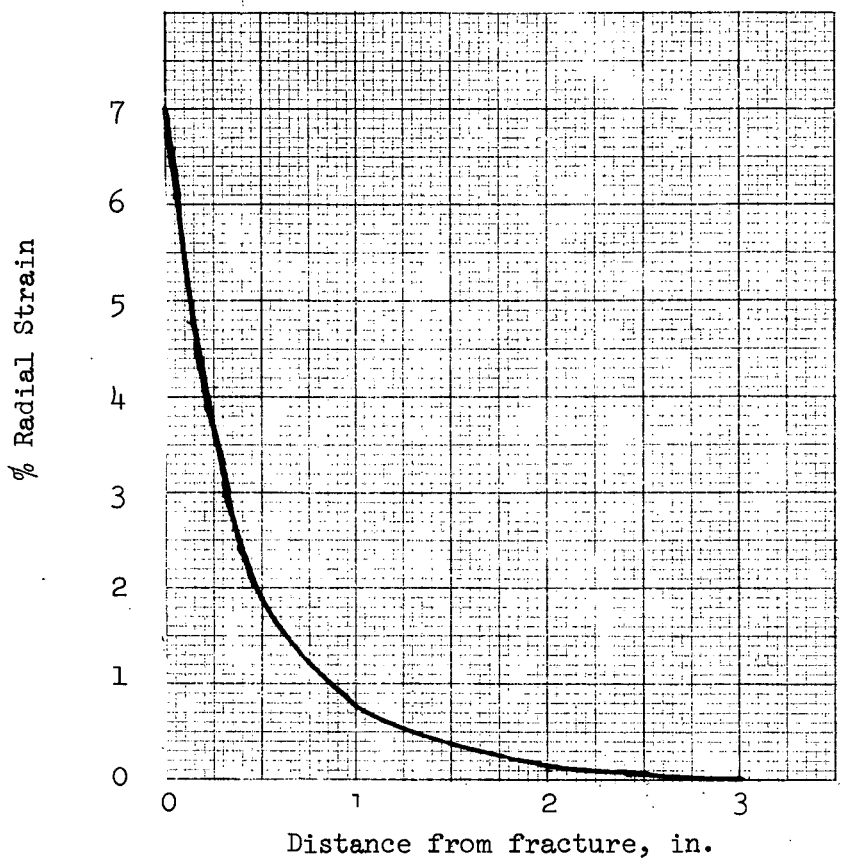

(a) Axial strain distribution at 2:00 clock position

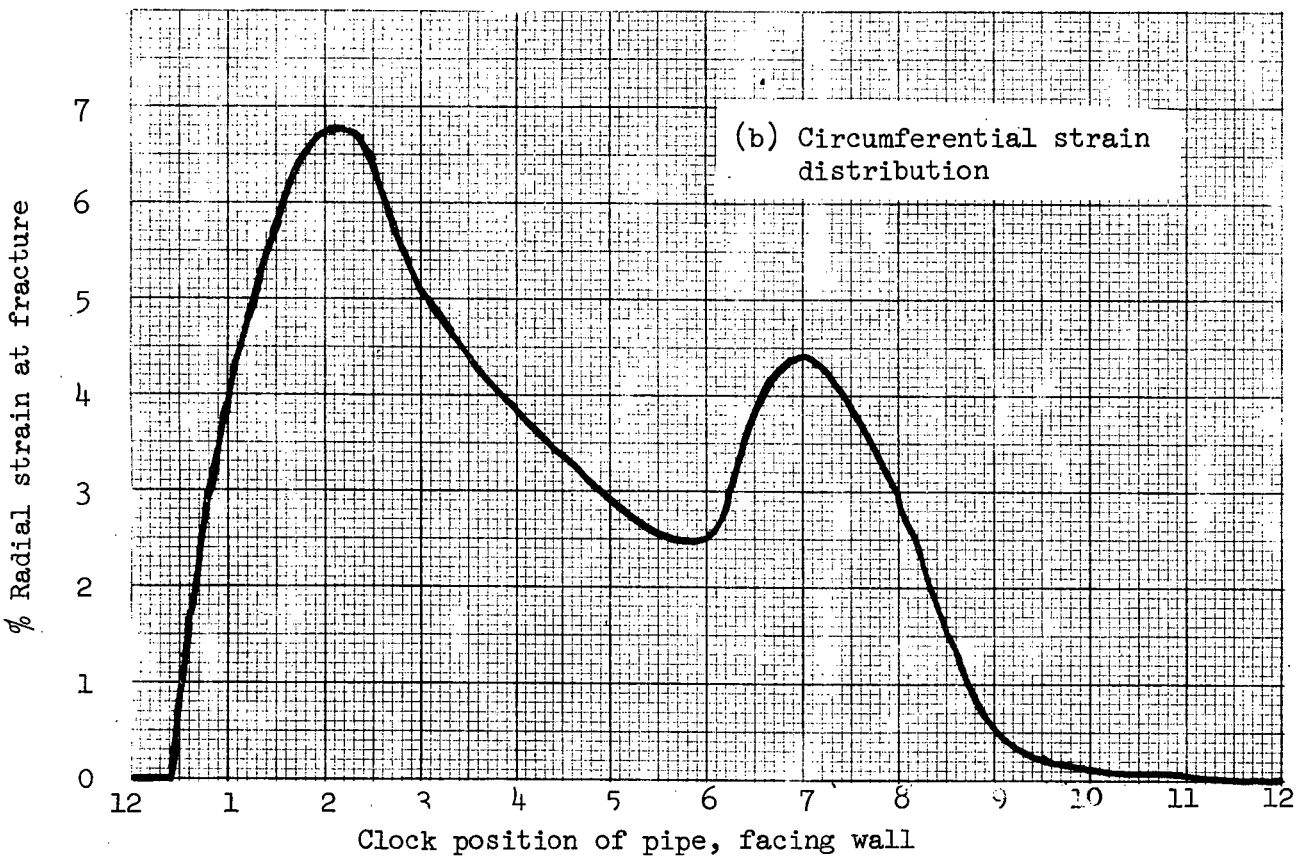

(b) Circumferential strain distribution

Figure G Plastic strain of pipe at crack

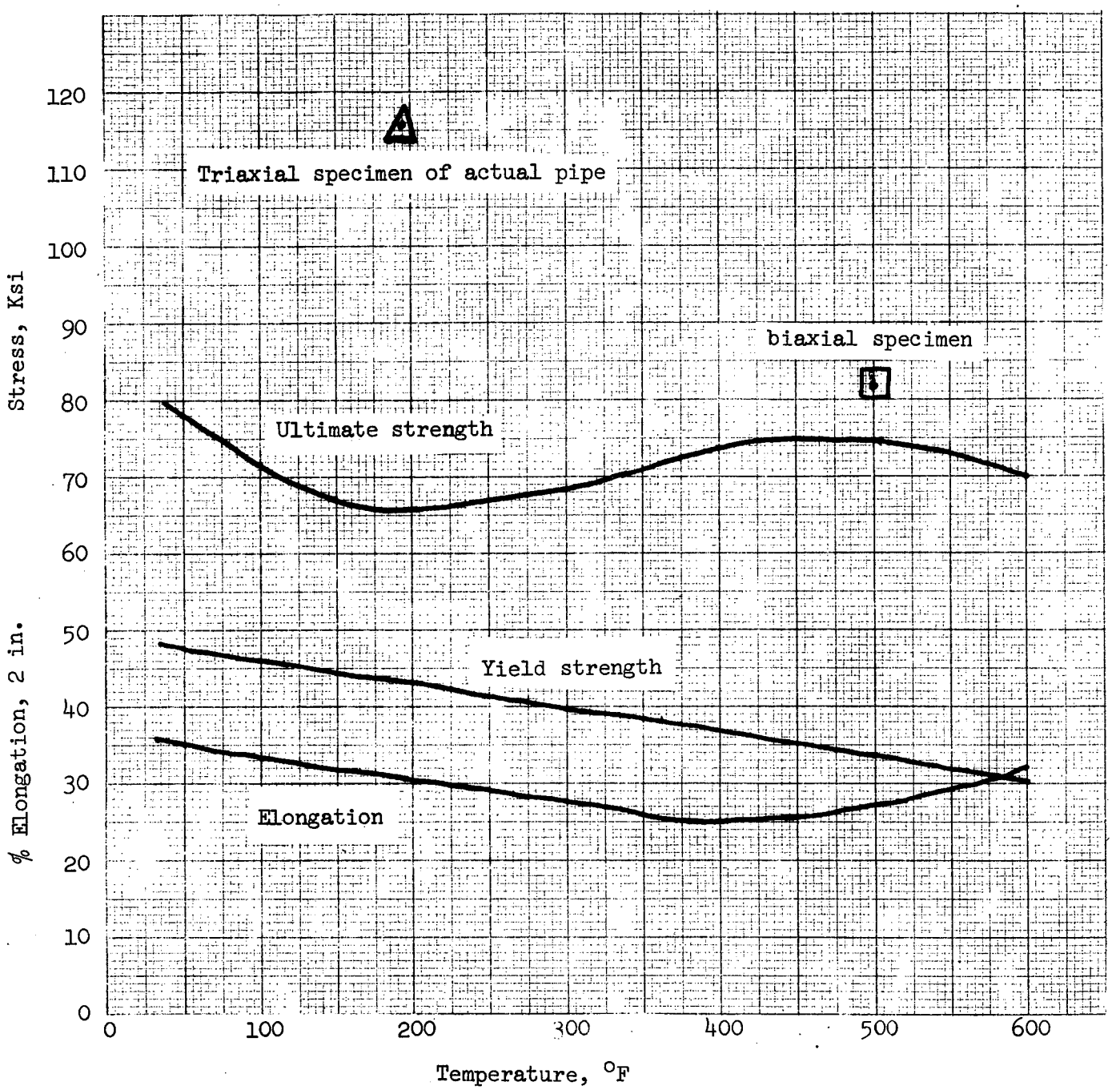

Figure H Tensile properties of A-106, Gr. C, pipe material

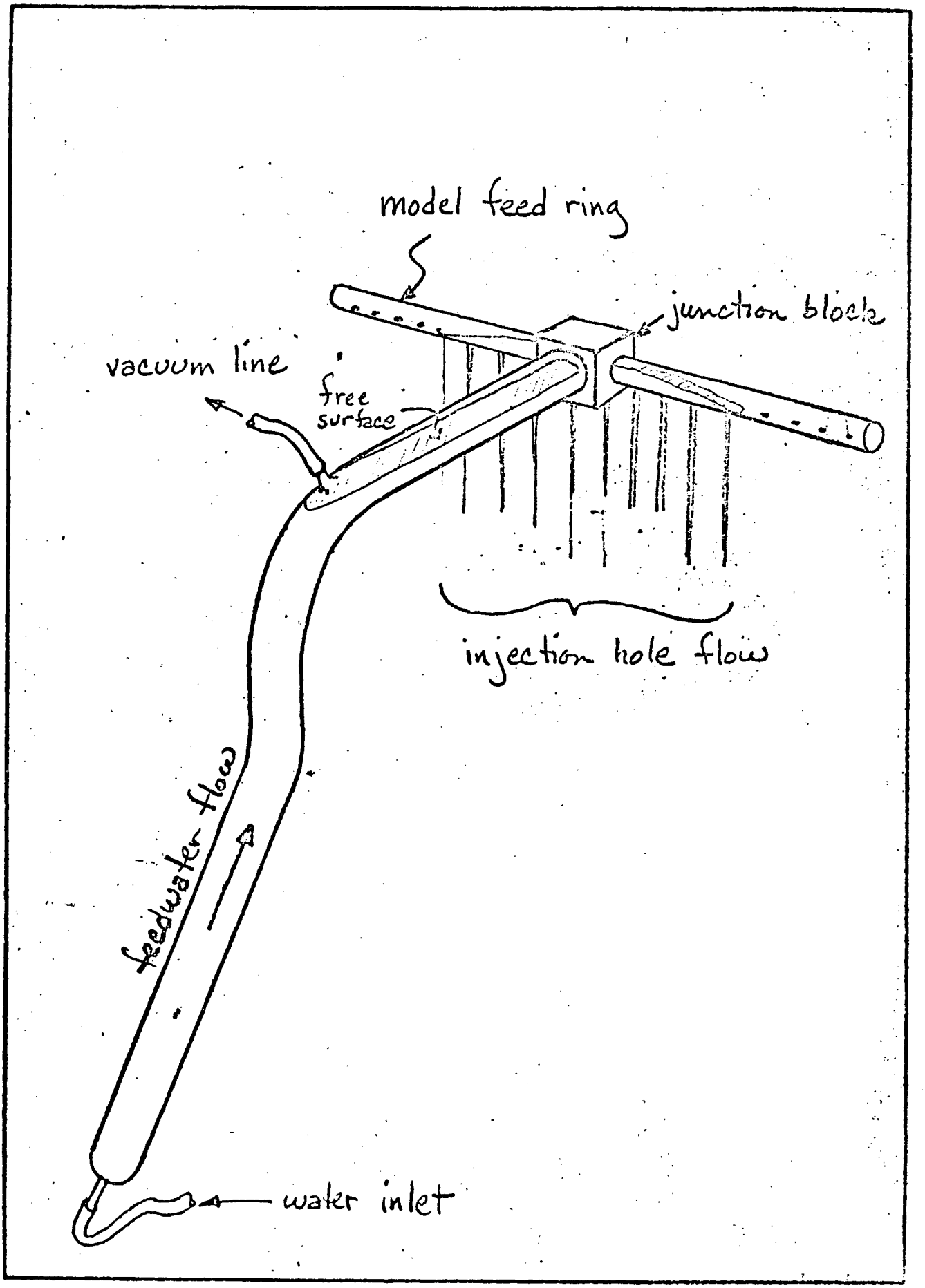

Figure I Sketch of Glass & Plastic Model of Feedwater System

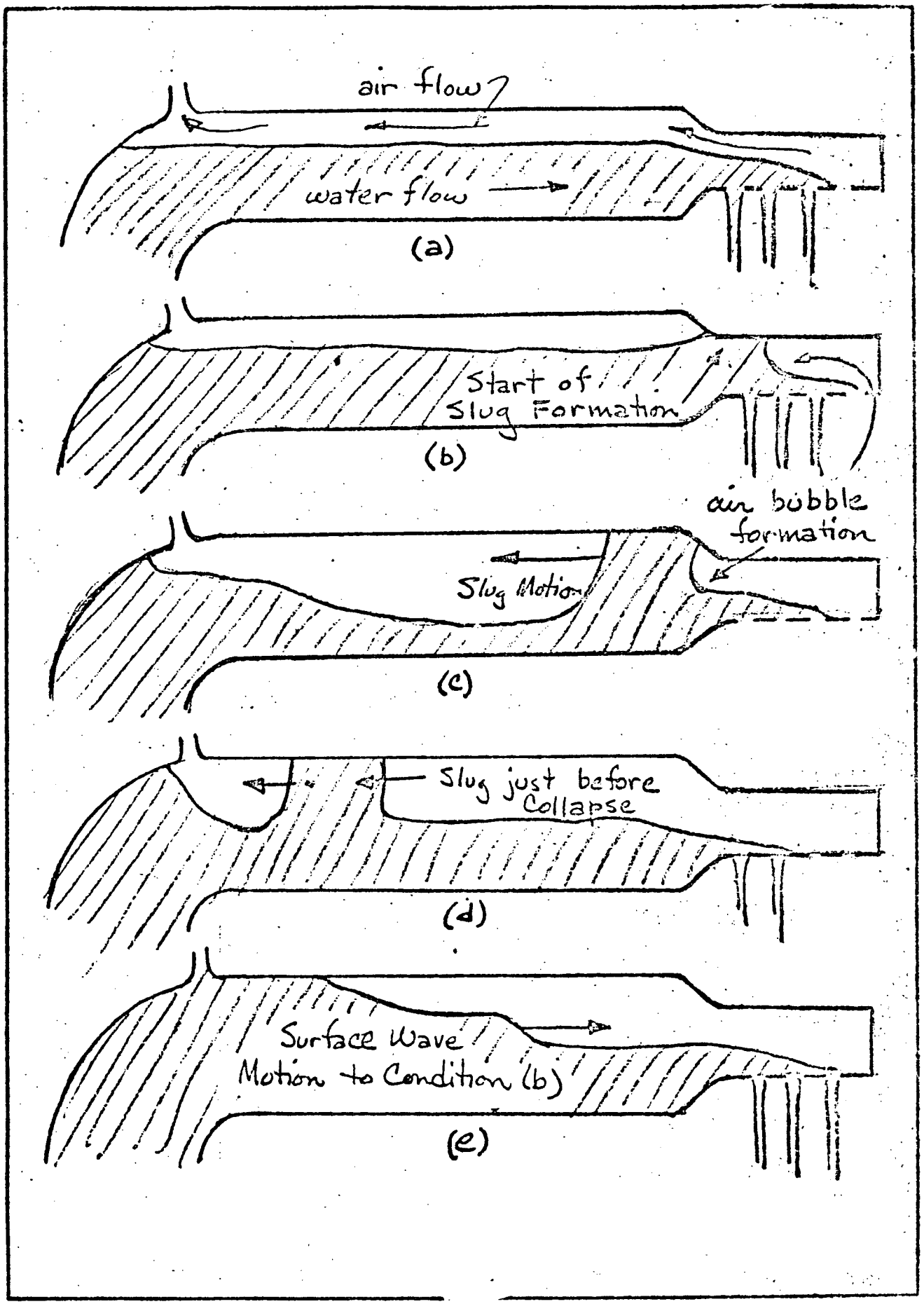

Figure J Experimentally Observed Slugging Mechanism

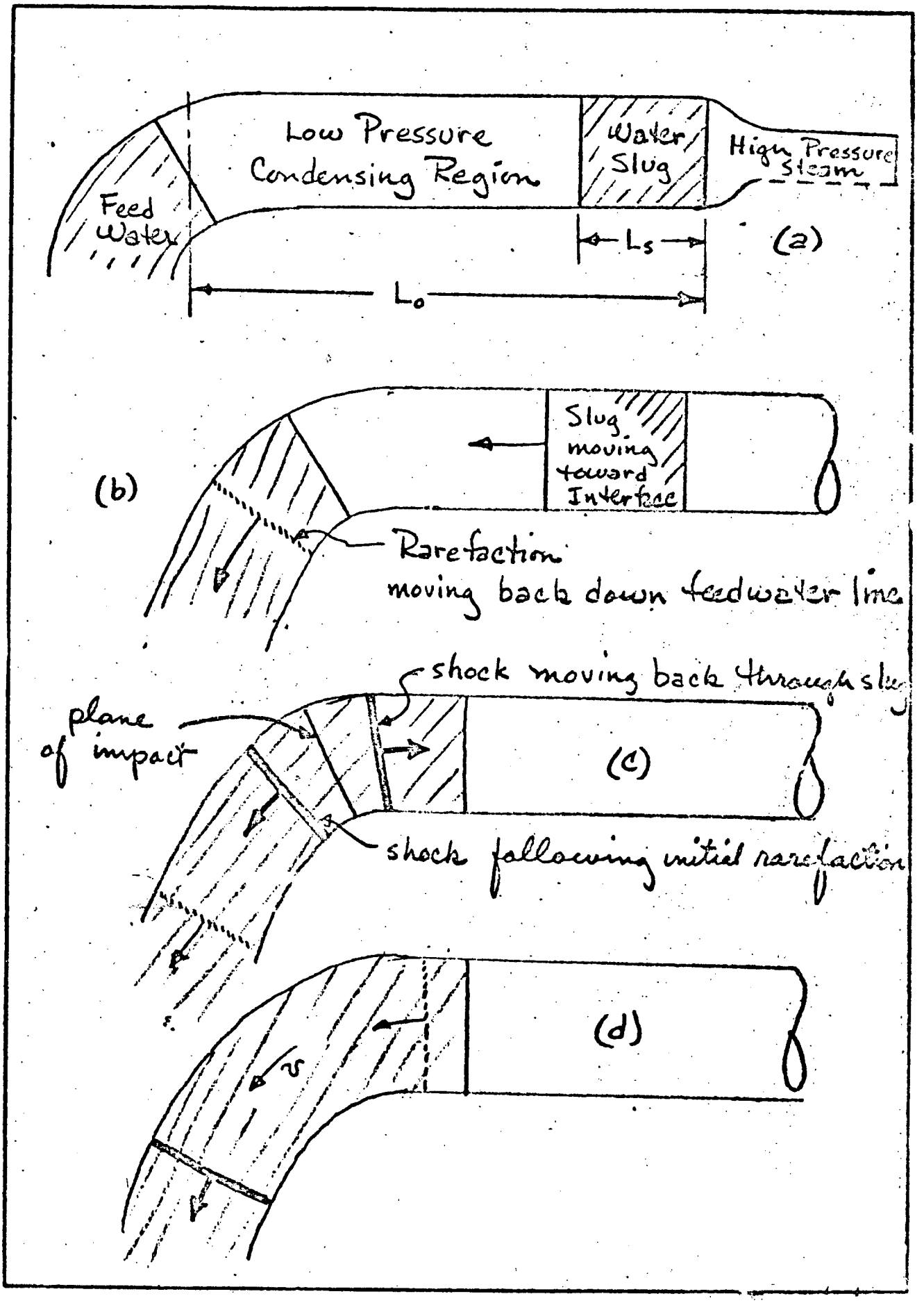

Figure No. K Simplified Sequence of Events

Appendix I

Pertinent Data

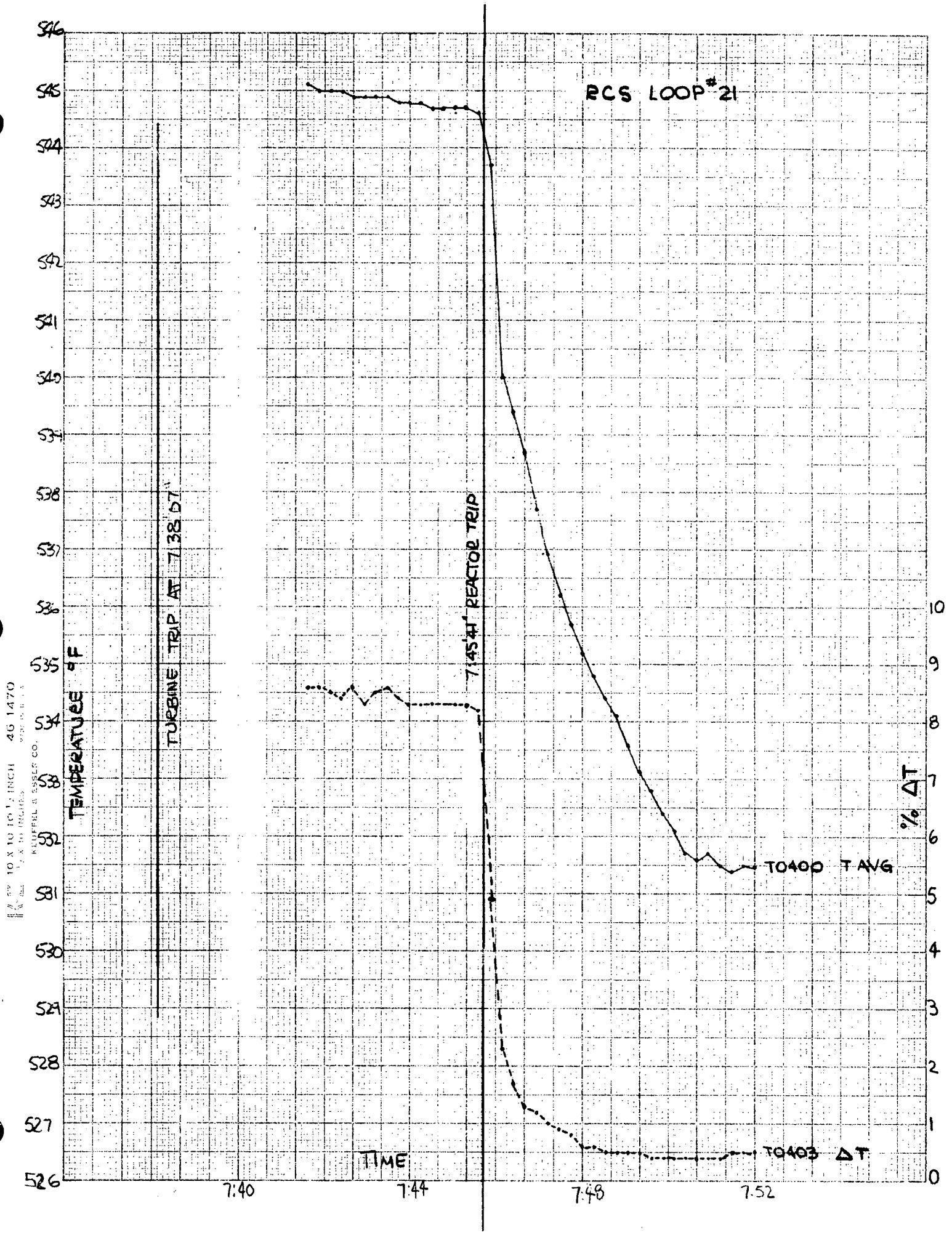
RCS LOOP #21
TEMPERATURE °F
546
545
544
543
542
541
540
539
538
537
536
535
534
533
532
531
530
529
528
527
526
TURBINE TRIP AT 7:38:07"
7:45:41" REACTOR TRIP
TO400 T AVG
TO403 ΔT
% ΔT
10
9
8
7
6
5
4
3
2
1
0
TIME
7:40
7:44
7:48
7:52

F. L. MOSELEY COMPANY
PASADENA, CALIF.
NO. H-100150 FOR USE ON AUTOGRAF
MODEL 2 & 4
PRINTED IN U.S.A.

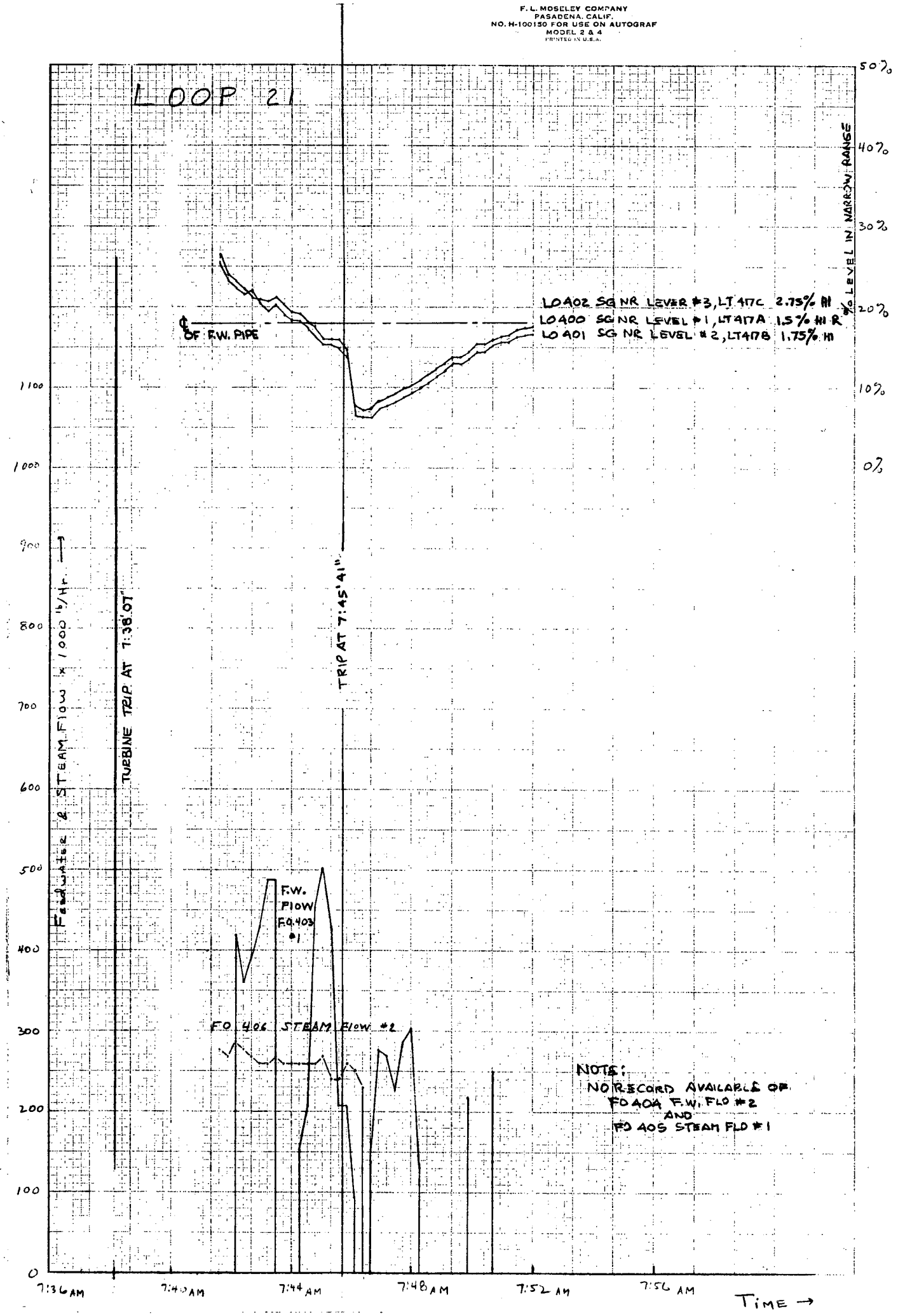

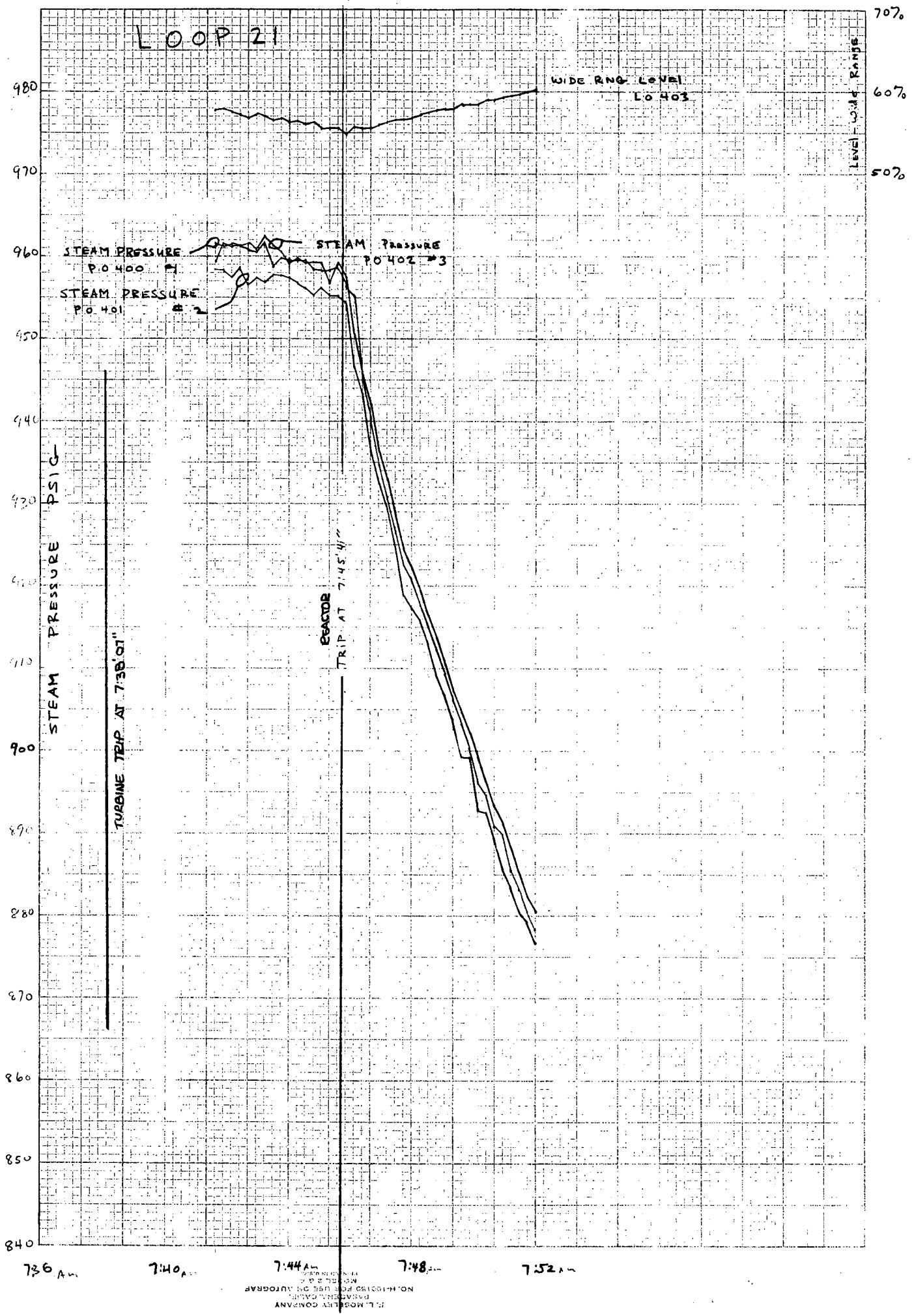
LOOP 21
WIDE RNG LEVEL
LO 403
STEAM PRESSURE
PO 400 #1
STEAM PRESSURE
PO 402 #3
STEAM PRESSURE
PO 401 #2
TURBINE TRIP AT 7:38'01"
REACTOR TRIP AT 7:45'41"
STEAM PRESSURE PSIG
LEVEL 0-4 RANGE
980
970
960
950
940
930
920
910
900
890
880
870
860
850
840
70%
60%
50%
7:36 AM
7:40 AM
7:44 AM
7:48 AM
7:52 AM

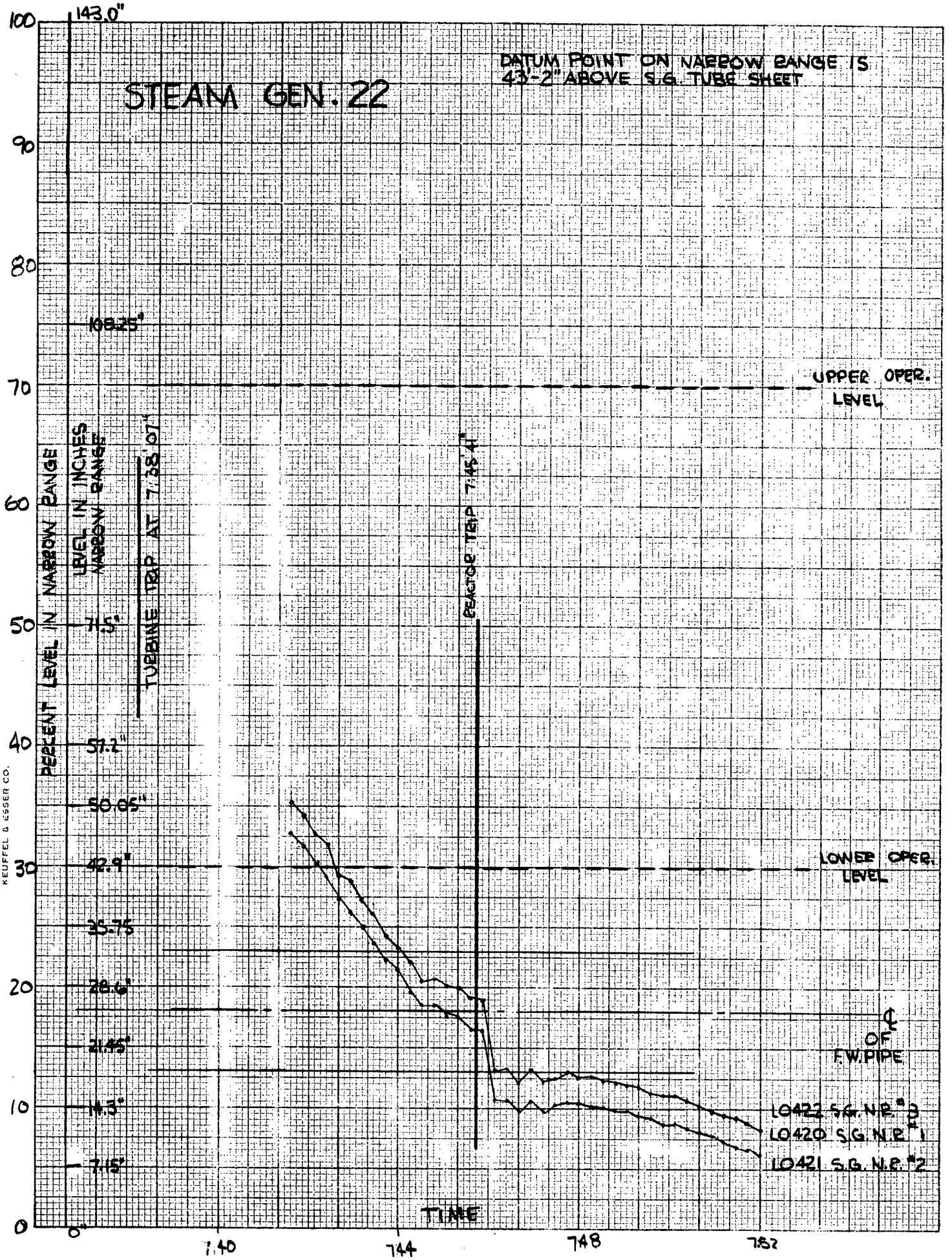

K&E 10 X 10 TO ½ INCH 46 1470
7½ X 10 INCHES MADE IN U.S.A.
KEUFFEL & ESSER CO.

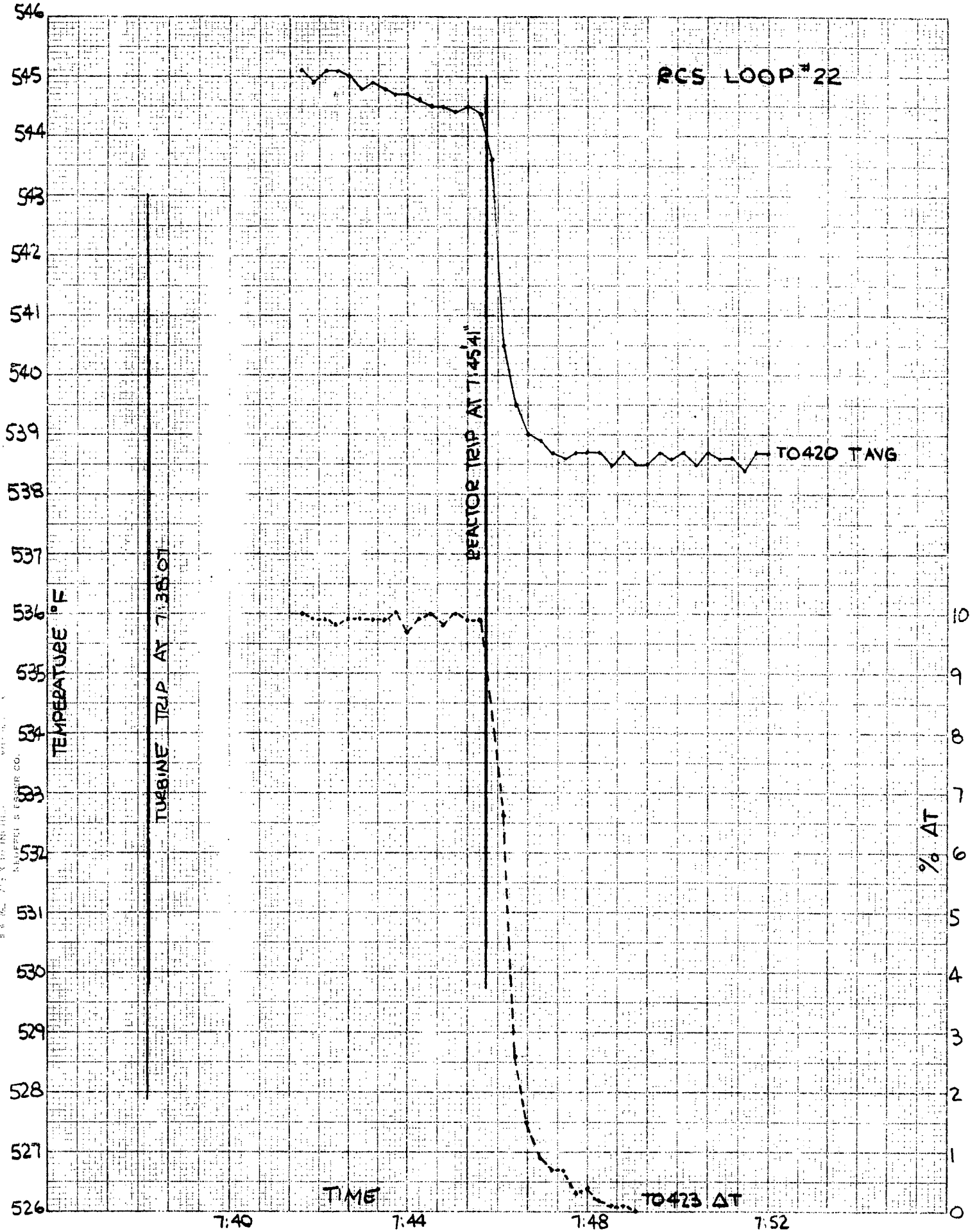
RCS LOOP #22
TEMPERATURE °F
546
545
544
543
542
541
540
539
538
537
536
535
534
533
532
531
530
529
528
527
526
% ΔT
10
9
8
7
6
5
4
3
2
1
0
TURBINE TRIP AT 7:38:01
REACTOR TRIP AT 7:45:41
TO420 TAVG
TO423 ΔT
TIME
7:40
7:44
7:48
7:52

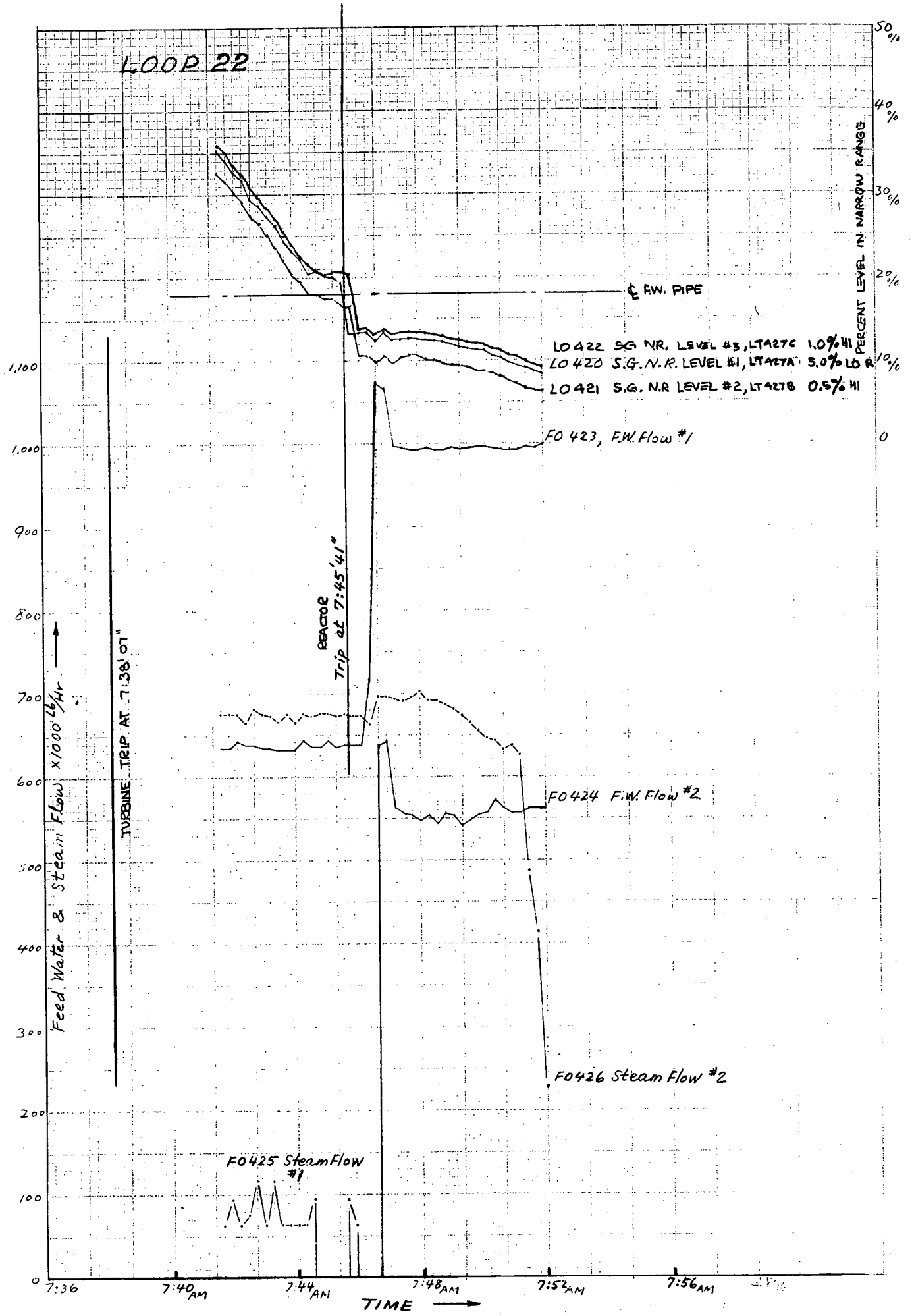
LOOP 22
℄ F.W. PIPE
LO422 SG N.R. LEVEL #3, LT427C 1.0% HI
LO420 S.G. N.R. LEVEL #1, LT427A 5.0% LO R
LO421 S.G. N.R LEVEL #2, LT427B 0.5% HI
FO 423, F.W. Flow #1
FO424 F.W. Flow #2
FO426 Steam Flow #2
FO425 Steam Flow #1
TURBINE TRIP AT 7:38'07"
REACTOR Trip at 7:45'41"
Feed Water & Steam Flow x1000 Lb/Hr
PERCENT LEVEL IN NARROW RANGE
50%
40%
30%
20%
10%
0
1,100
1,000
900
800
700
600
500
400
300
200
100
0
7:36
7:40AM
7:44AM
7:48AM
7:52AM
7:56AM
TIME

F. L. MOSELEY COMPANY
PASADENA, CALIF.
NO. H-100150 FOR USE ON AUTOGRAF
MODEL 2 & 4
PRINTED IN U.S.A.

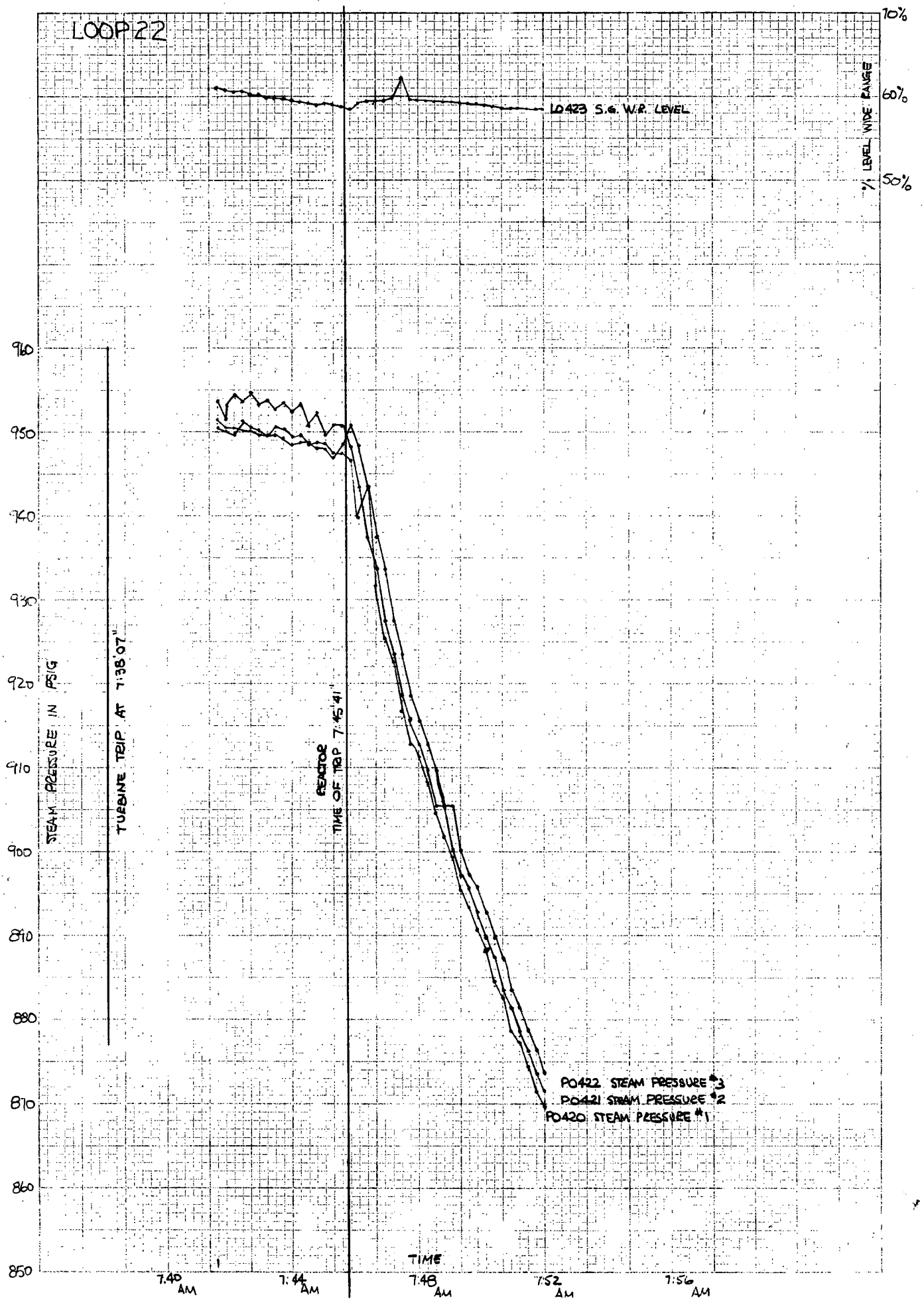

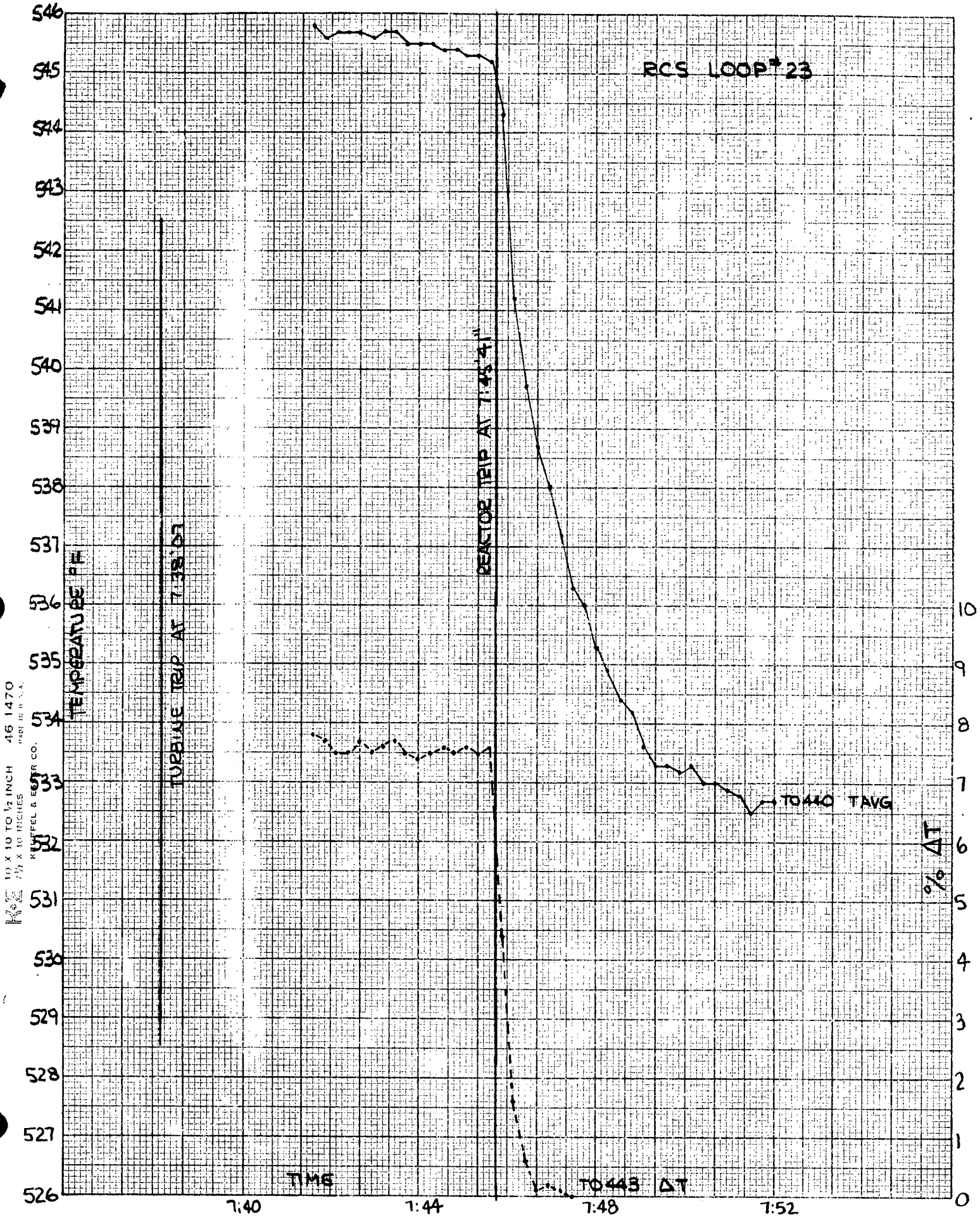
RCS LOOP #23
TEMPERATURE °F
TURBINE TRIP AT 7:38'05"
REACTOR TRIP AT 7:45'41"
TO440 TAVG
TO443 ΔT
% ΔT
TIME
7:40
7:44
7:48
7:52
546
545
544
543
542
541
540
539
538
537
536
535
534
533
532
531
530
529
528
527
526
10
9
8
7
6
5
4
3
2
1
0
10 X 10 TO ½ INCH
2½ X 10 INCHES
KEUFFEL & ESSER CO.
46 1470

F. L. MOSELEY COMPANY
PASADENA, CALIF.
NO. H-100150 FOR USE ON AUTOGRAF
MODEL 2 & 4
PRINTED IN U.S.A.

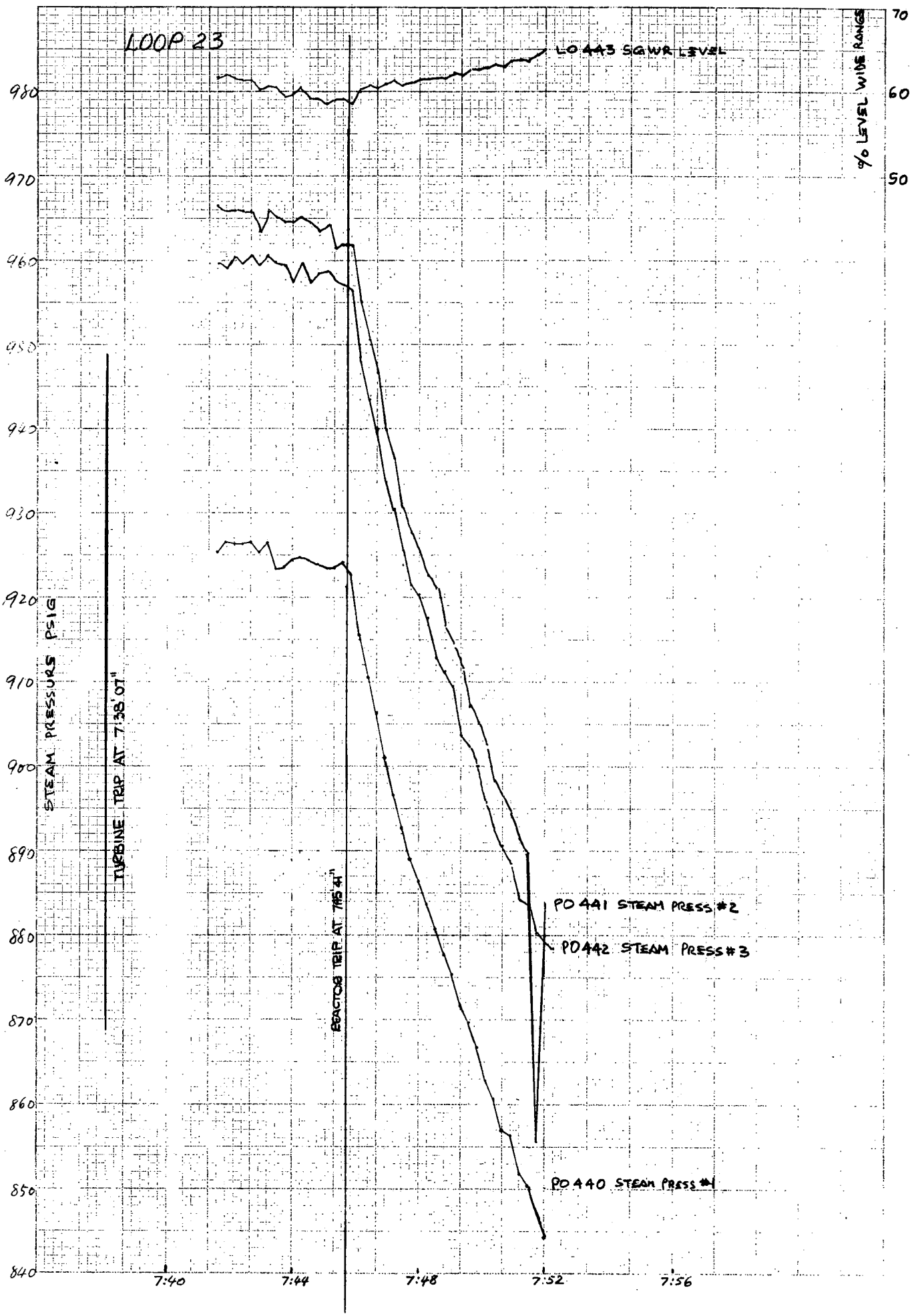

F. L. MOSELEY COMPANY
PASADENA, CALIF.
NO. H-100150 FOR USE ON AUTOGRAF
MODEL 2 & 4
PRINTED IN U.S.A.

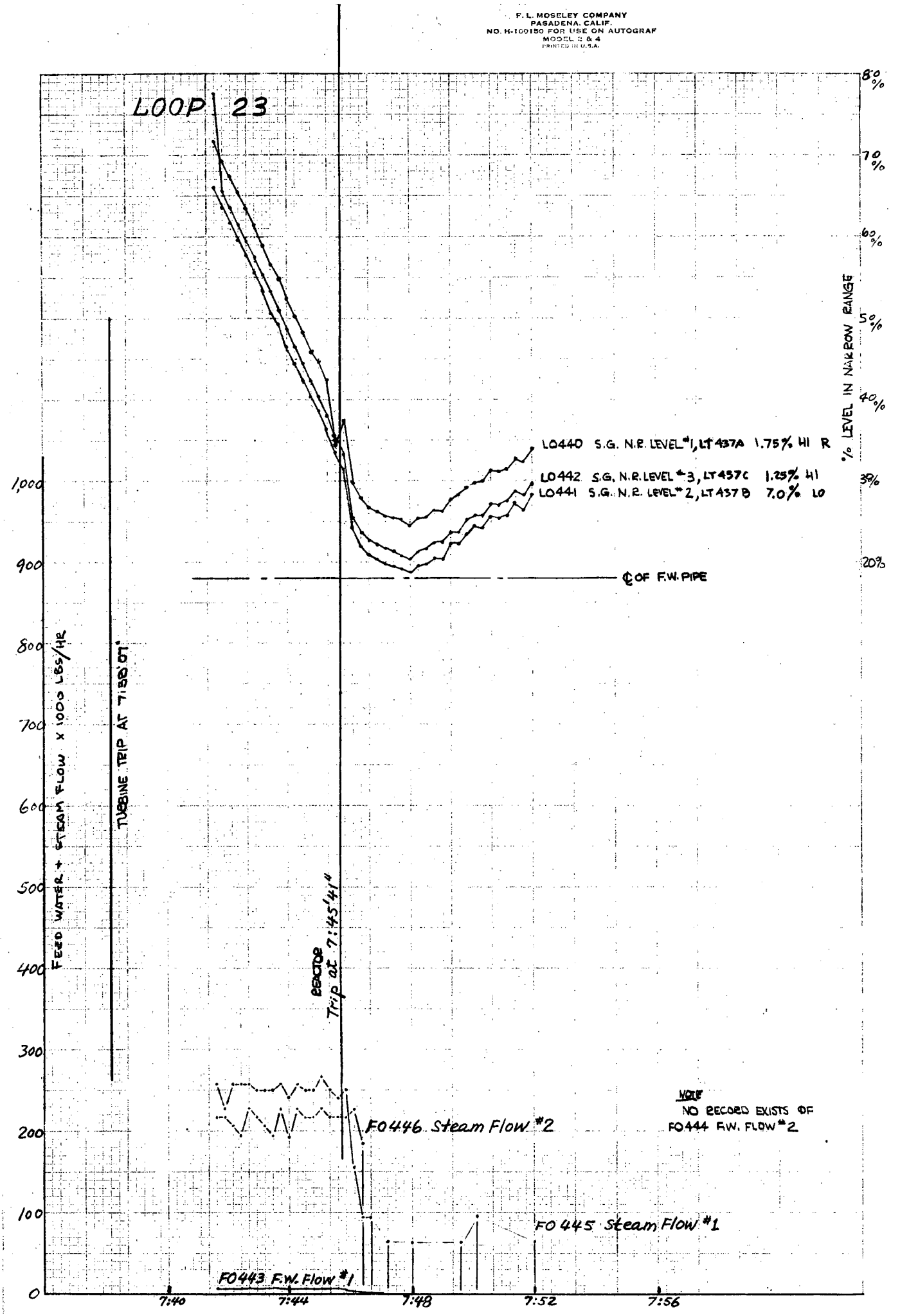

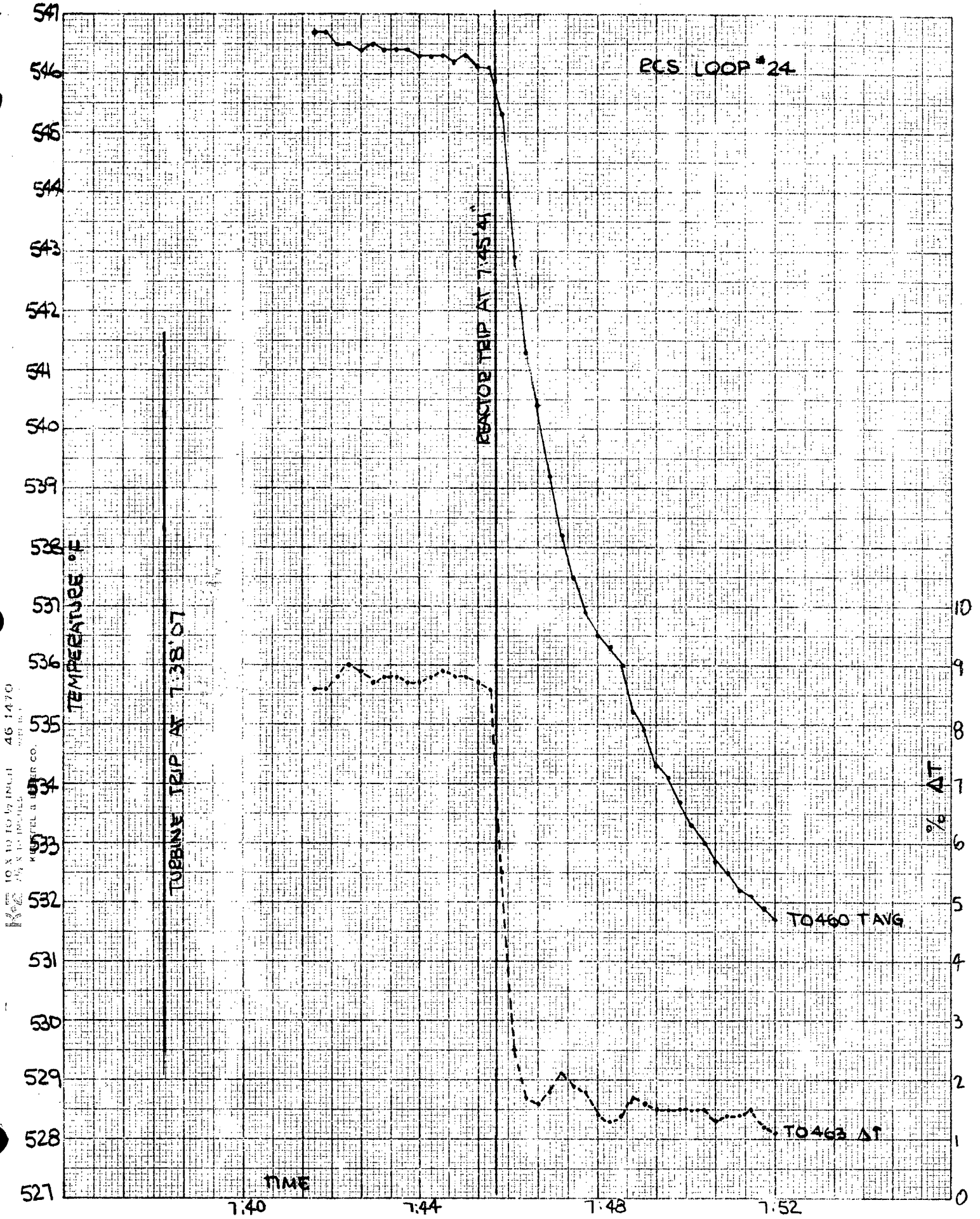
RCS LOOP #24
TEMPERATURE °F
TURBINE TRIP AT 7:38'07
REACTOR TRIP AT 7:45'41
TO460 TAVG
TO463 ΔT
% ΔT
TIME
7:40
7:44
7:48
7:52
541
546
545
544
543
542
541
540
539
538
537
536
535
534
533
532
531
530
529
528
527
10
9
8
7
6
5
4
3
2
1
0

F. L. MOSELEY COMPANY
PASADENA, CALIF.
NO. H-100150 FOR USE ON AUTOGRAF
MODEL 2 & 4
PRINTED IN U.S.A.

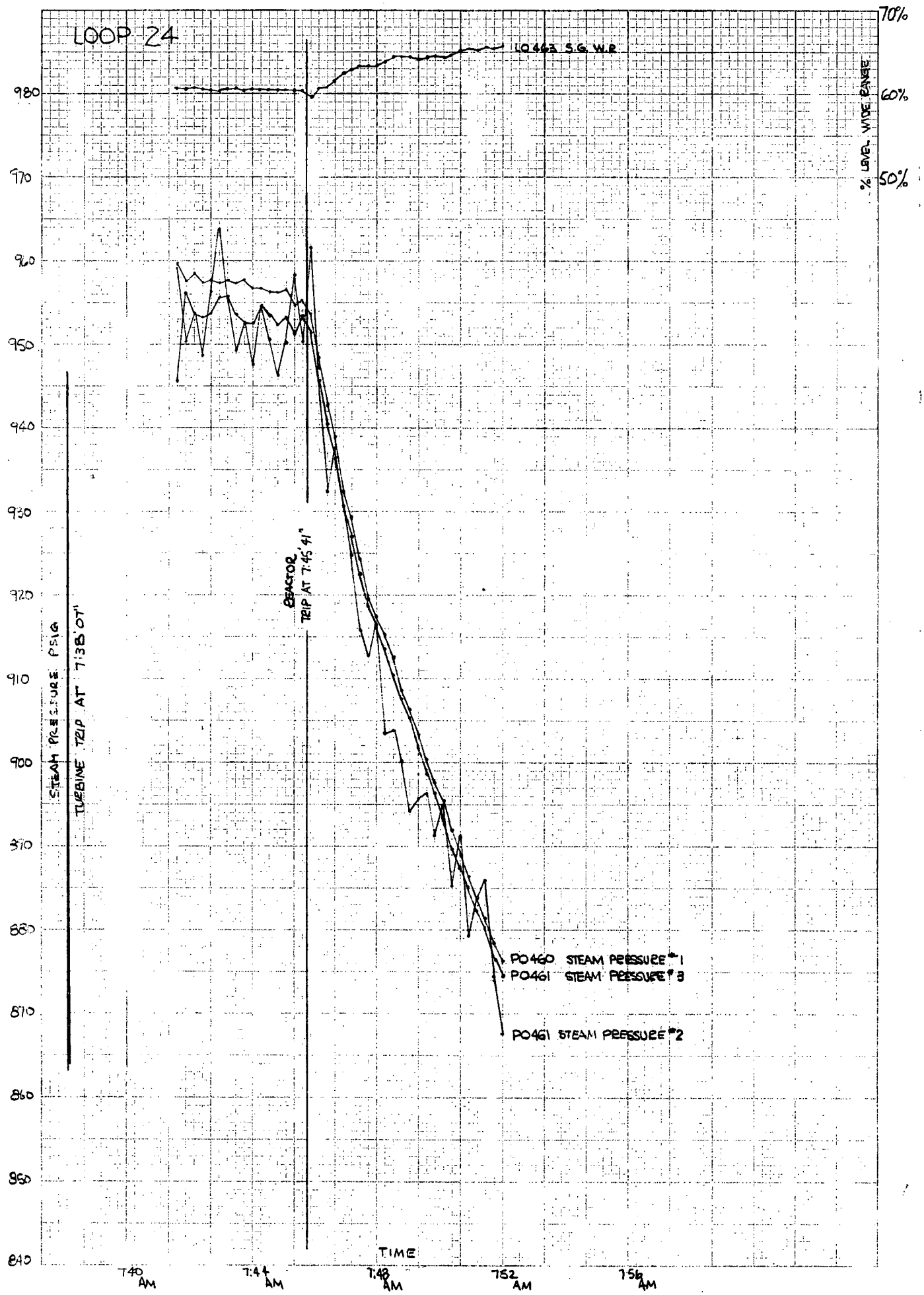

F. L. MOSELEY COMPANY
PASADENA, CALIF.
NO. H-100150 FOR USE ON AUTOGRAF
MODEL 2 & 4
PRINTED IN U.S.A.

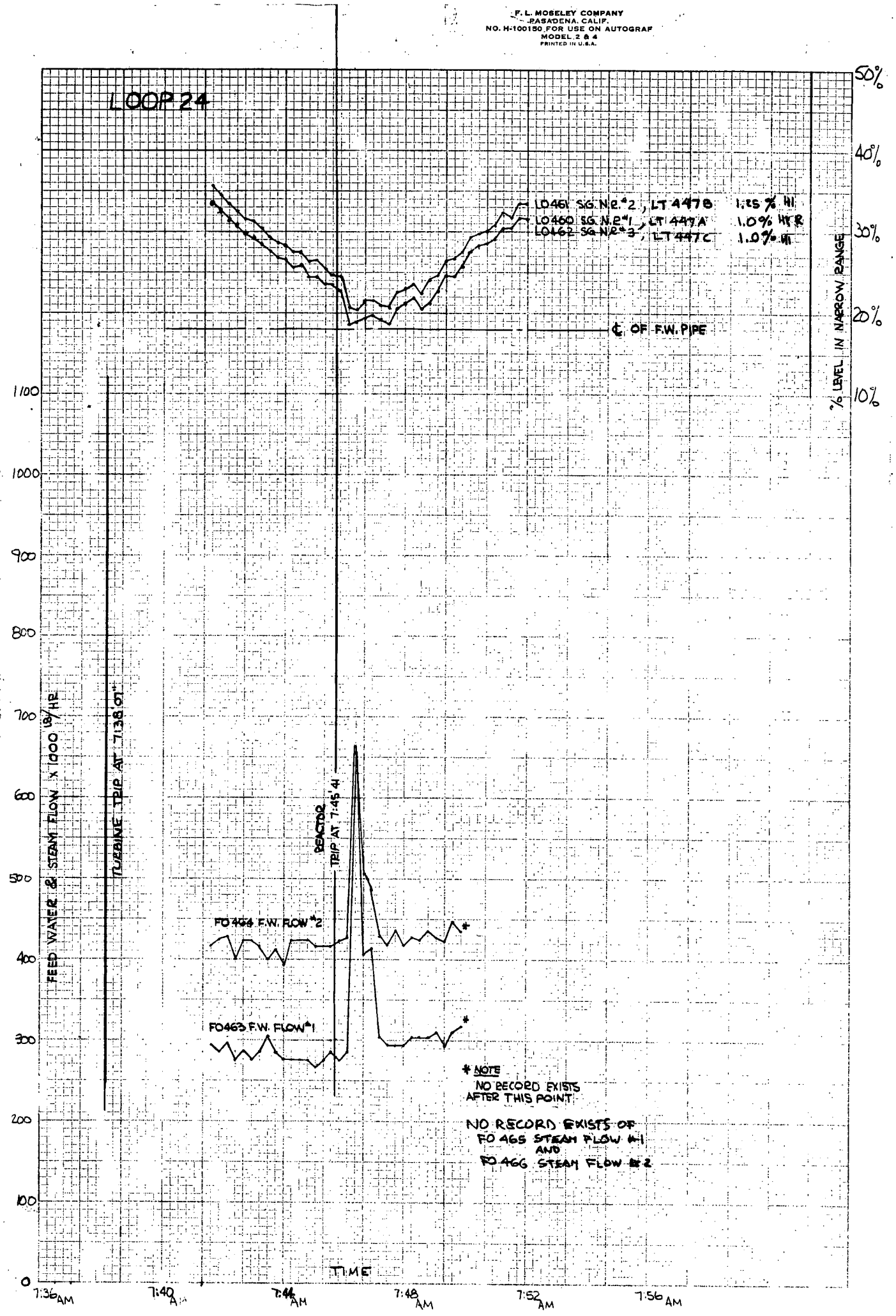

Appendix II

Summary of Visual Inspections on Feedwater Line No. 22 Following the Pipe Break on November 13, 1973

Support BFD 33 - Base-mounted spring unit:

Deadweight load appeared satisfactory, using pin hole as approximate indicator, however, unit was 5/8" east and 5/8" south of proper location.

Support BFD 23 - Base-mounted spring unit:

Deadweight load appeared satisfactory, however, unit was approximately 1" east & 1-1/8" south of proper location.

Sliding Rigid Support - Upstream of shut-off and regulator valves:

No indication of recent north/south movement, but it could have had a 1" east/west movement.

Sliding Rigid Support - Downstream of regulator valve:

no indication of recent north/south movement but jacket and insulation indicated a 1/2" east/west deformation.

Restraint BFD-3A:

The clamp was rotated on the pipe with a nominal gap of 5/8" from the underside of the bumper to the restraining member. The end gaps were 1/4" x 1".

Total north/south and east/west movement was 3-1/2" and 1-1/4", respectively.

Support BFD-38 - Rod-mounted spring unit:

Deadweight load appeared satisfactory. The insulation was compressed at the clamp, leaving a north and south gap of 5/8" and 1", respectively.

Support - BFD-41 - Base-mounted spring unit:

Deadweight loading appeared satisfactory. Paint scrapings on load indicator showed maximum movements of 1-7/16" down and 5/8" up from present position. Insulation disturbance at pipe support was 1" and 5/8" on north and south sides, respectively.

Restraint - SR-B-Q - Hydraulic snubber unit - 20000# capacity:

Clamp on pipe was rotationally displaced. Makeup spacer pipe was bent approximately 5°±. All anchor bolts were tight.

Restraint - SR-B-4 - Hydraulic snubber unit - 20000# capacity:

There was 1-1/2" open gap between the clamp and the insulation on the underscale of the clamp. Several anchor bolts were loose in the concrete and others were still tight in the concrete, but the nuts were loose.

Restraint SR-B-3 - Hydraulic snubber unit - 20000# capacity:

Common clamp with SB-B-4. On the column-type support, all anchor bolts were loose in overhead concrete and tight in floor concrete.

Restraint BFDR-13 - Pipe whip:

Everything appeared satisfactory.

Support - BFD-45 - Trapeze rod-mounted spring units:

Deadweight load appeared satisfactory. Dial indicator showed maximum movement of 1/4" up and 5/8" down. Insulation was depressed on pipe by bumping against bottom inside of spring can.

Restraint - BFDR-8 - Pipe Whip:

The insulation was disturbed, could be partially by compression and partially by own deadweight and displacement.

Restraint - BFDR-2 - Pipe Whip:

Restraining spacers not installed. The auxiliary boiler feed line ties into the boiler feed line near BFD-45. Movement of the feed line affected the auxiliary feed line and caused disturbance on the supports as shown. There are signs of movement in the auxiliary feed line supports for a considerable distance upstream towards the pumps.

BFD-83 - Rod-mounted spring unit:

Deadweight load appeared satisfactory. Everything looked undisturbed.

BFD-84 - Support and Seismic Restraint:

Seismic restraining angles were damaged, and broken off completely on one angle. The other had a fractured weld causing the angle to open up enough to be inoperable.

SR-464 - Seismic restraint:

Seismic restraint dropped from Elevation 49' to Elevation approximately 43 ft. and was lying inside a 10" Ø pipe sleeve. The bolts were loose on the clamp but the west half of the clamp was tight against the sleeve, being pressed hard by the pipe in a southwest direction.

Restraint - Pipe Whip:

Located 2 feet from penetration anchor: Contact had taken place between the outside surface of the reinforcing ring on the pipe, and the bore of the 1" plate restraint over a 7" length at approximately 4 o'clock, when looking from penetration side.

HBF-9 - Restraint - Pipe Whip:

The north/south pipe whip had indentations or depressions, indicating a substantial sudden application of load.

This loading caused a fracture on the horizontal structural beam.

HBF-10a - Restraint - Pipe Whip:

No evidence of contact.

HBF-17 - Support, Seismic & Pipe Whip:

The 8W58 vertical member was bent to a depth of 3/16". The reinforcing ring on the pipe was flattened slightly on the outside of one side to a height of 2-5/8" with a maximum horizontal width of 1/2". The bottom of the ring was seated on the support steel.

PR4 - Restraint - Pipe Whip:

There were two longitudinal shear-type tears in the 2-7/8" diameter pins caused by the bore of the lug, approximately 7/8" long x 1-1/2" wide x 1/32" maximum depth. The south side end collar had apparently been forced off the end of the pin.

HBF-18 - Support, Seismic & Pipe Whip:

The 8W58 vertical member was bent 1/4" towards the crane wall on one half of the pipe side flange at the center line of the pipe. The bottom of the ring was seated on the support steel.

PR5 - Restraint - Pipe Whip:

There was very little damage and no indication of how much longitudinal movement had taken place.

HBF-19 - Support, Seismic & Pipe Whip:

The reinforcing ring on the pipe was bearing against the upper and vapor containment liner sides of the restraining steel, but had a 5/16" and 1/2" clear gap on the bottom and crane wall sides, respectively. The reinforcing ring appeared slightly flattened on the bearing sides.

Insulation disturbance approximately 12 ft. downstream of HBF-19

Local damage to the stainless steel jacketed insulation caused by the combination of longitudinal and vertical movement of the pipe and the gravity displacement of the insulation was noted.

HBF-2 - Support - Rod-mounted spring unit:

Deadweight loading appeared satisfactory. The insulation above and below the lug was compressed and broken out respectively to a considerable depth. The stainless steel jacket seam, which was vertically in line with the lug, was compressed and deformed on the top side and burst open on the underside of the lug.

Slightly above HBF-2:

The depression in the insulation jacket indicated a movement of several inches by the pipe at this point.

PR-19 - Restraint - Pipe Whip:

There were a few small indentations and shiny surfaces indicating a total displacement of 3/16" at the worst point. The two half clamps are held together by four 2" diameter bolts.

Appendix III

Metallurgical Report of Failed Section of Feedwater Pipe

From : RESEARCH LABORATORIES
WIN : 236-7337
Date : December 19, 1973
Subject: Fractographic Analysis of a Steam Condensate, Return Pipe Failure From Consolidated Edisons' Indian Point #2 Installation

PENN CENTER, PWR

E. U. Powell

A sample of a failed steam condensate return pipe was supplied us with a request for a fractographic analysis. The following is a discussion of this analysis.

Figure 1 shows photographs of the pipe failure and identifies the area of suspected fracture initiation. Figure 2 is a 1X composite photograph of part of the fracture surface and includes the suspected initiation site.

Visual examination of the fracture surface showed a general battered condition, but nevertheless indicated the failure initiated in the suspected area, which is at approximately the 3 o'clock position of the original pipe location. However, the failure initiation did not appear to be a point type, but rather an area type. What appeared to be arrest lines were observed parallel to the outside pipe surface to a depth of about 1/4 inch. These lines are visible on Figure 2 and Figure 3. Also visible in Figure 2 are coarse chevron markings pointing to this area. Figure 3 is a photomacrograph of an area of the fracture surface designated as P-1 on Figure 2 and shows the location of the fractographs in Figures 4 through 9 inclusive, with relation to the lines.

Figure 4 shows a region, Area 1 (from Figure 3), adjacent to the outside surface of the pipe, this surface is mostly shear with some rubbing evident. Area 1A, in Figure 4, is mostly cleavage with some shear present. Figures 5, 6 and 7 are quite similar in appearance and show shear with signs of rubbing. Figure 8 is from an area approximately 1/2 inch from the outside pipe surface and is mostly cleavage with small areas of shear.

Subsequently, a section of the pipe fracture from the weld side of the failure was provided for examination. Figure 9 shows a photograph of this section and a sketch showing the location of the various samples subsequently removed for examination and the approximate original location of the section. The location of this section with respect to the pipe side of the failure is shown on Figure 2.

Visual examination of the fracture face of the section from the weld side revealed nothing that was not observed on the pipe side of the failure. Figures 10 and 10A are composite SEM fractographs of this surface. However, further examination of the sample revealed what appeared to be a crack at the toe of the weld and visible for several inches. Two areas of this defect are shown in Figure 11.

Section 1, Figure 9, was removed and macroetched to examine the weld area, Figure 12 is a photomacrograph showing the weld and the penetration into the pipe (left) and the plate (right).

Several sections of the weld side of the failure were examined metallographically to determine if the defect shown in Figure 11 was a weld toe crack or a cold weld. Microscopic examination confirmed the defect as a weld toe crack, Figure 13 shows two typical examples at different magnifications. During the microscopic examination some internal cracking was noted in the pipe material, several of these cracks are visible in Figure 13. When these internal cracks were observed there was some concern that they might have been pre-existing; however on examination of sections adjacent to, and in, the area of fracture initiation they approached the fracture face and disappeared indicating that their occurrence was probably coincident with the fracture. Section 7, Figure 14 tends to confirm this since it was located within the fracture initiation area.

Figure 15 shows photomicrographs of typical fracture edge areas. A and B of Figure 15 show cleavage with some cracks under the fracture face. C and D show the typical microstructural distortion of shear. D is particularly interesting because on the right side of the photomicrograph a cleavage crack and shear are clearly visible; however, it can be seen that the distortion from the shear does not extend to the left side of the crack, demonstrating that the crack occurred first (perhaps microseconds). Therefore, the failure mode is cleavage with the planes connected by shear.

In order to determine if anything might be learned from an examination of fracture faces of the internal cracks a section was ground until the ligaments between the cracks could be fractured without damaging the crack faces. This was done by cooling below the ductile-brittle transition temperature with liquid nitrogen.

Figure 16 shows photomacrographs of the cracked area chosen for examination and the sample after fracturing. Figure 17 shows a photomacrograph of Section W-4-A and SEM fractographs of cleavage in virgin metal which occurred when the cracks were opened. The area identified by arrow 1 is the surface of the toe crack, the discoloration is a heavy oxide. This oxide is clearly visible in the SEM fractographs in Figure 18, W-4-A1. Area W-4-A2 in Figure 18 shows a cleavage type fracture.

Figure 19 is a photomacrograph of the fracture face of Section W-4-B, from Figure 15, showing the locations of the SEM fractographs in Figures 20, 21, and 22. The light areas are cleavage obtained on opening the cracks. The dark areas are oxidized crack surfaces. Figures 20, 21 and 22 are examples of different areas of the fracture W-4-B and in some of these cleavage is visible despite the oxide. W-4-B5 of Figure 22 is an example of a freshly cleaved surface.

The pipe material was reported to be a plain carbon steel with a tensile strength of 77-79 ksi, yield strength of 44-45 ksi and an elongation of 27%. With these mechanical properties it would be expected that with an overload condition this steel would fail in a ductile manner. Since it did not it was postulated that the high load, estimated to have been 500 ksi to 1,000 ksi, in conjunction with the constraint on the pipe was the cause. In order to confirm this a sample of the pipe material was stressed to failure, at 200°F, in a simulated, triaxially loaded tensile test. Figure 23 shows a photomacrograph of the fracture surface of the test sample as well as SEM fractographs of this surface. Figure 24 is also SEM fractographs of the fracture surface. Figure 25 shows photomicrographs of the microstructure of the fracture surface. In all three Figures cleavage is visible confirming that this material can be made to fail in a brittle (cleavage) manner under selected conditions of loading and constraint.

The heavy oxide on the surface of the weld toe crack indicates that it probably occurred first and at an earlier period of time or, at least, was subjected to an elevated temperature subsequent to cracking.

The lines on the fracture surface are quite probably crack arrest lines indicating that the fracture propagated from the weld toe crack to final failure in one or more cycles of loading.

C. J. Dorsch/mjl

C. J. Dorsch
Materials Science

M. W. Hagadorn

M. W. Hagadorn
Metals Processing & Fabrication

mjl

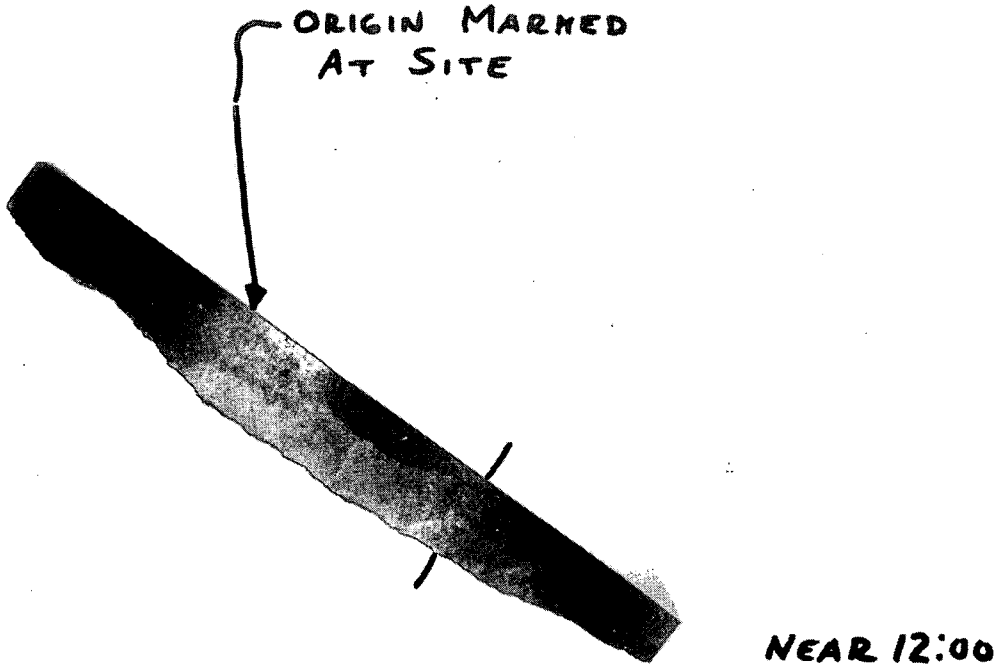

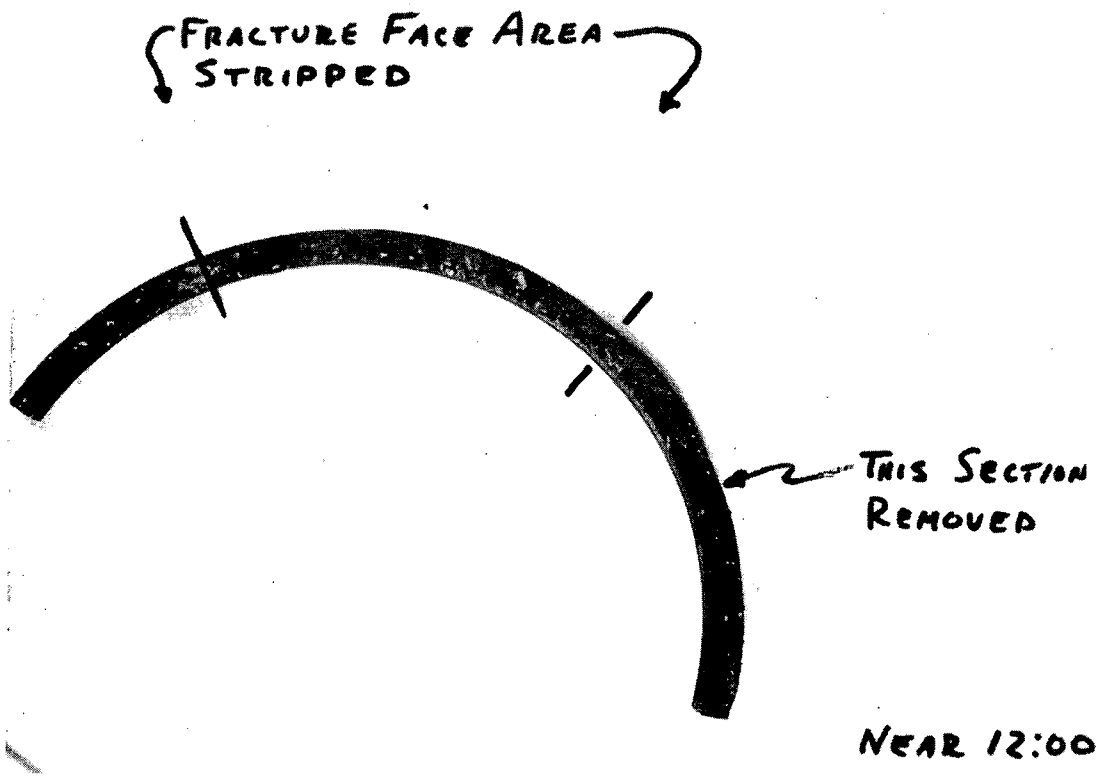

Figure 1 -- Photographs of Pipe Section of Failure 1/4 X

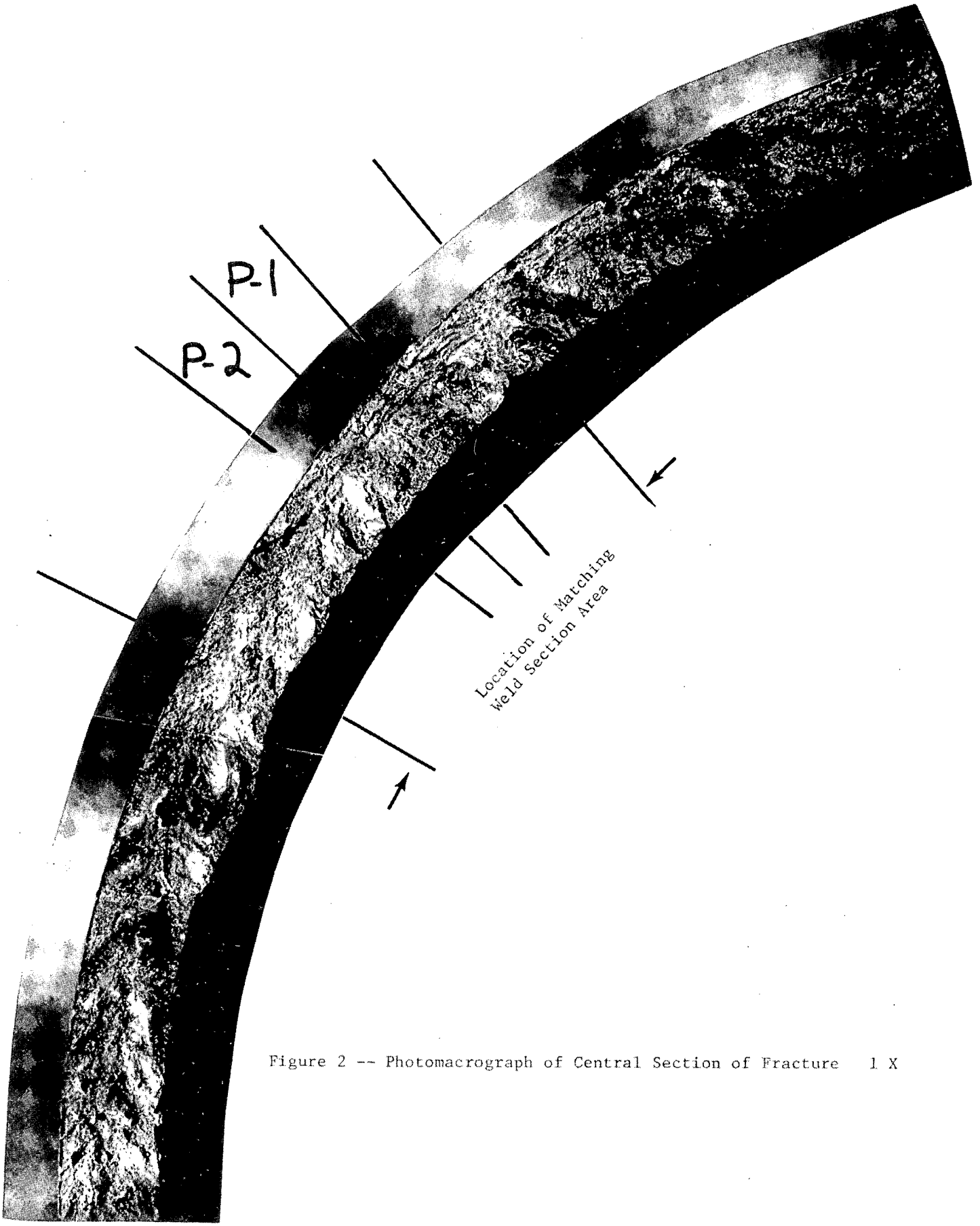

Figure 2 -- Photomacrograph of Central Section of Fracture 1 X

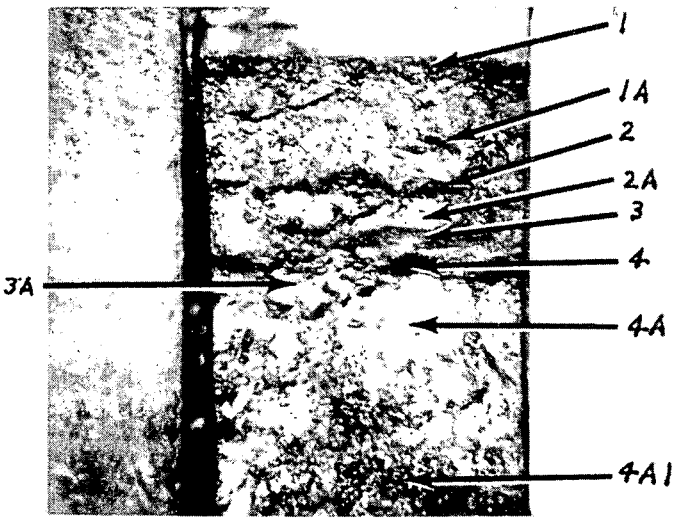

Figure 3 -- Photomacrograph of Section P-1 Showing Location of Fractographs in Following Five Figures. For Location of P-1 on Pipe Fracture, see Figure 2. 3.7 X

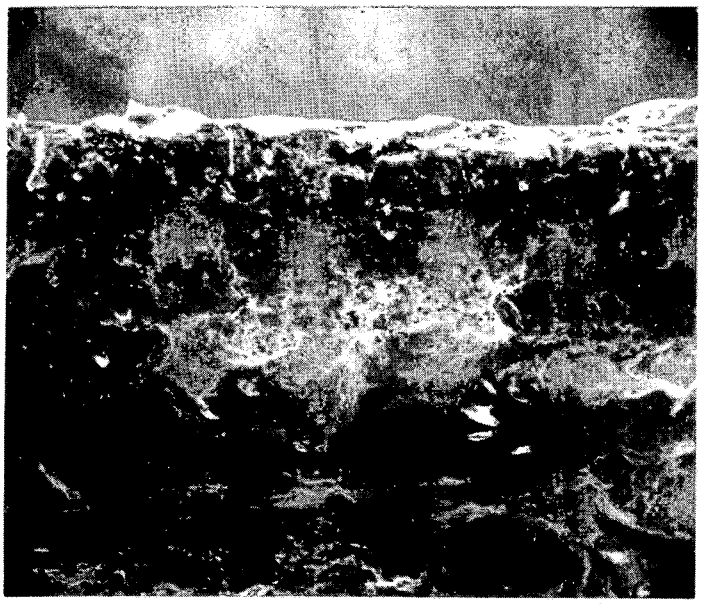

100 x

P-1

Area 1A

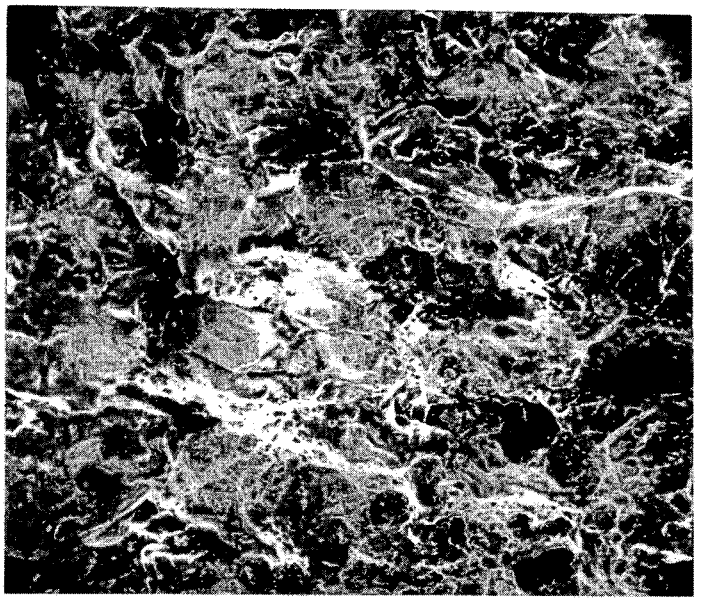

100 x

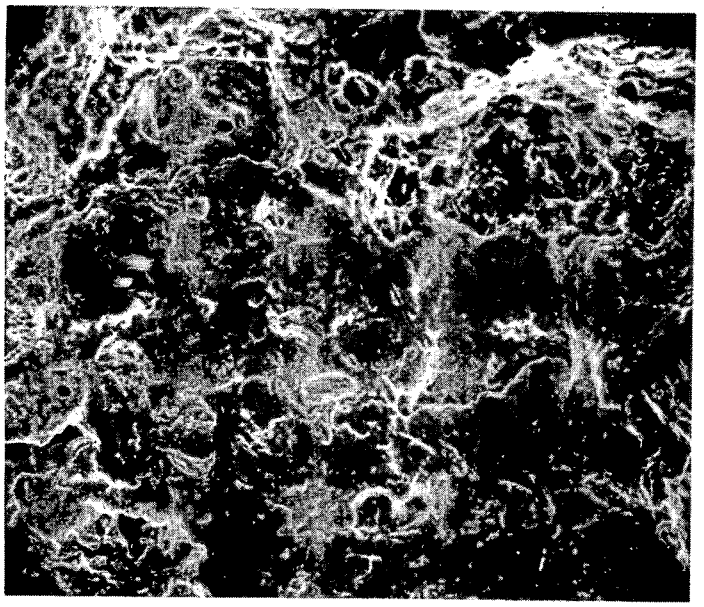

500 x

P-1

Area 1

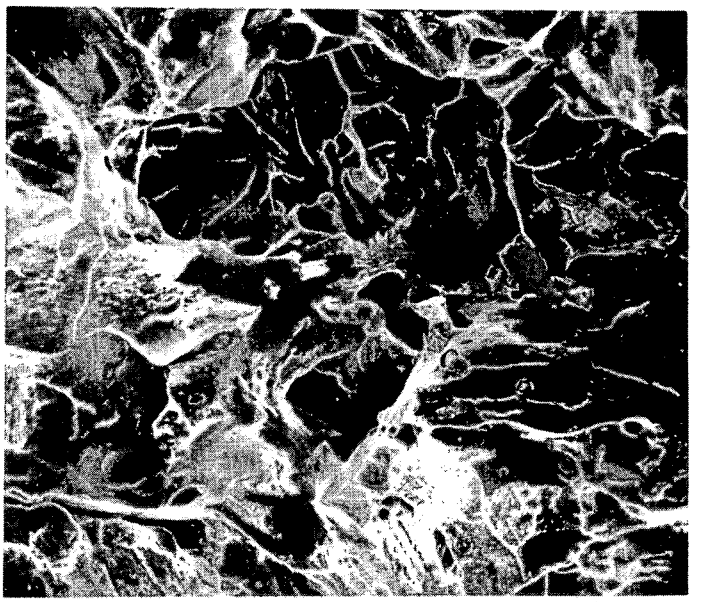

500 x

Figure 4 -- Fractographs of Areas 1 and 1A from Figure 3.

P-1

Area 2A

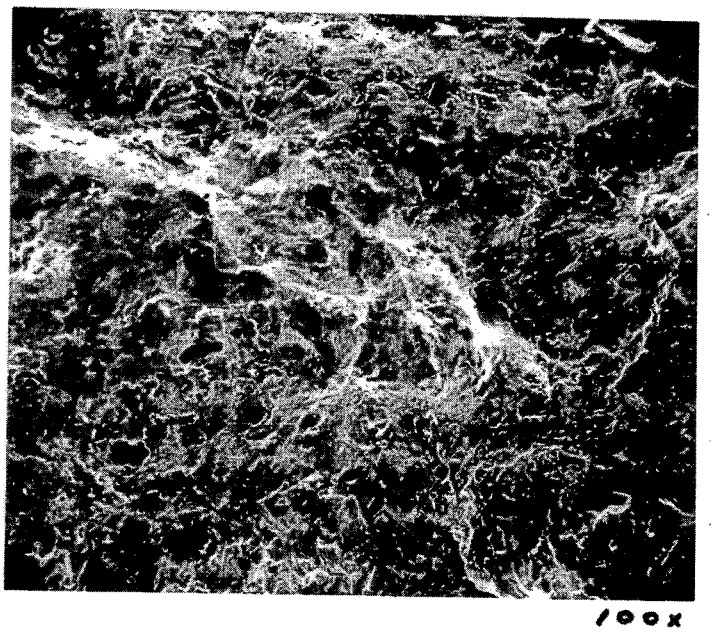

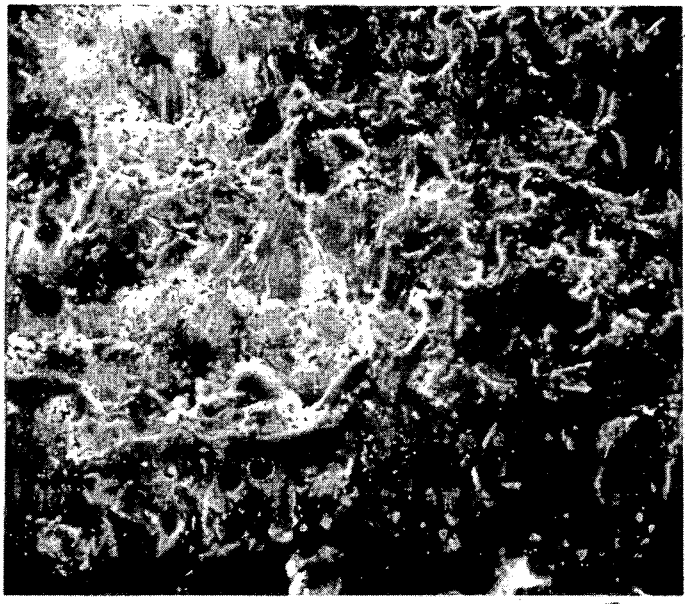

P-1

Area 2

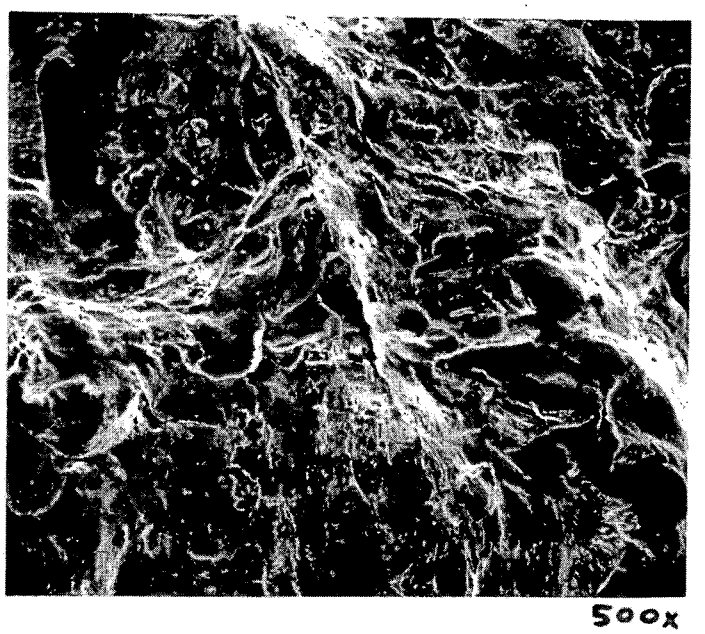

Figure 5 -- Fractographs of Areas 2 and 2A from Figure 3.

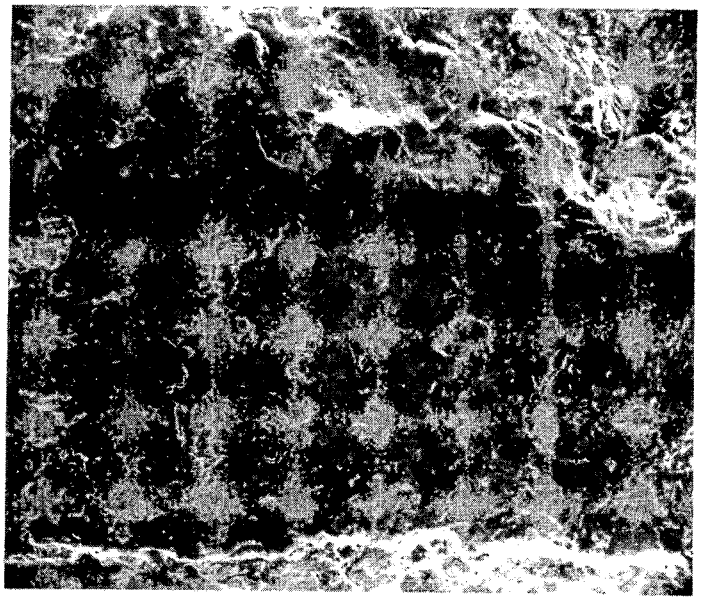

100x

P-1
Area 3A

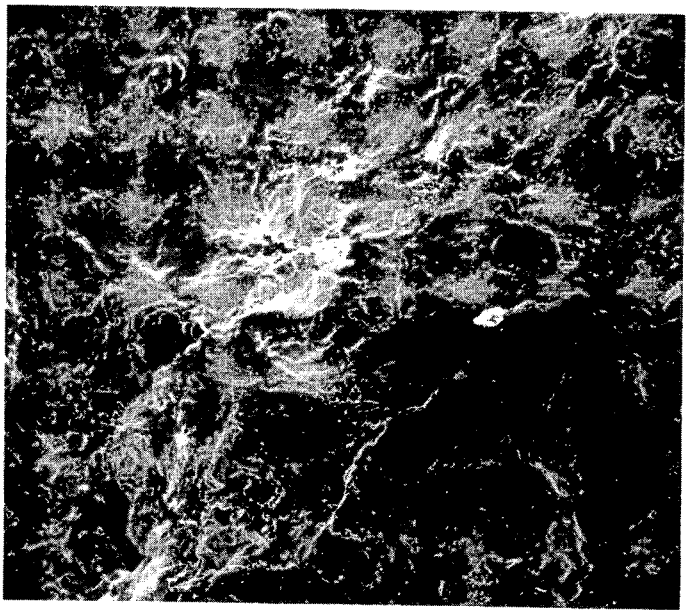

100x

500x

P-1
Area 3

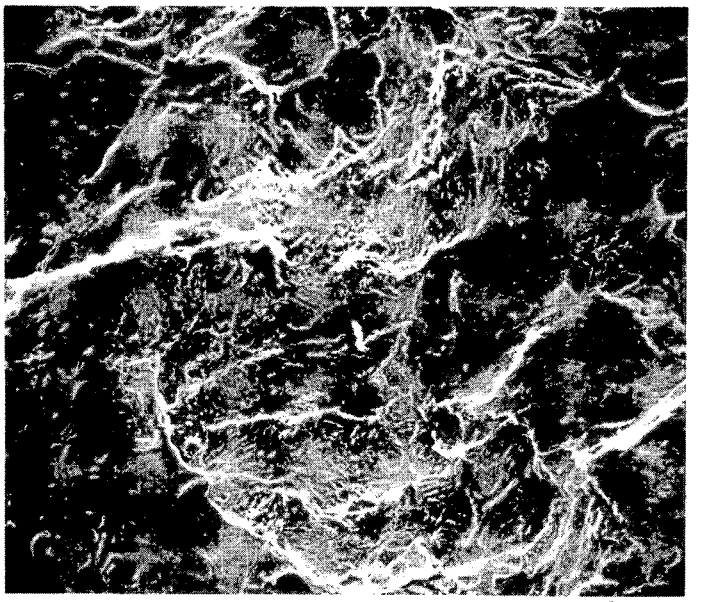

500x

Figure 6 -- Fractographs of Areas 3 and 3A from Figure 3.

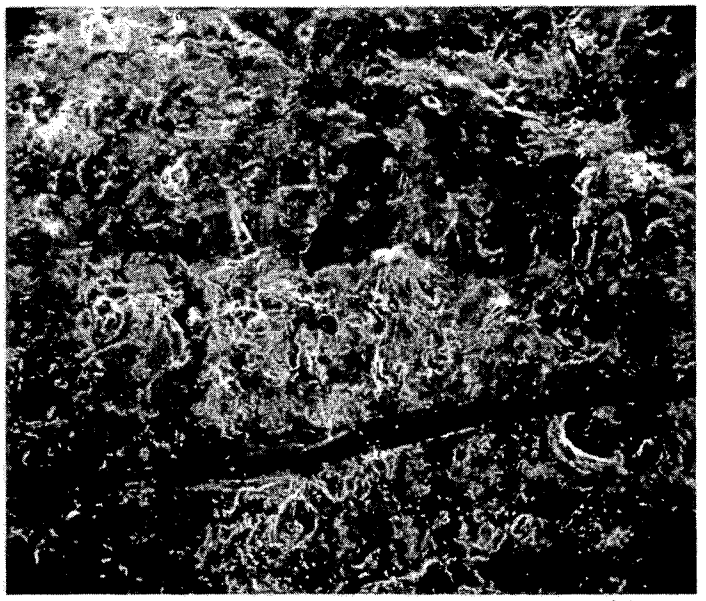

100x

P-1
Area 4A

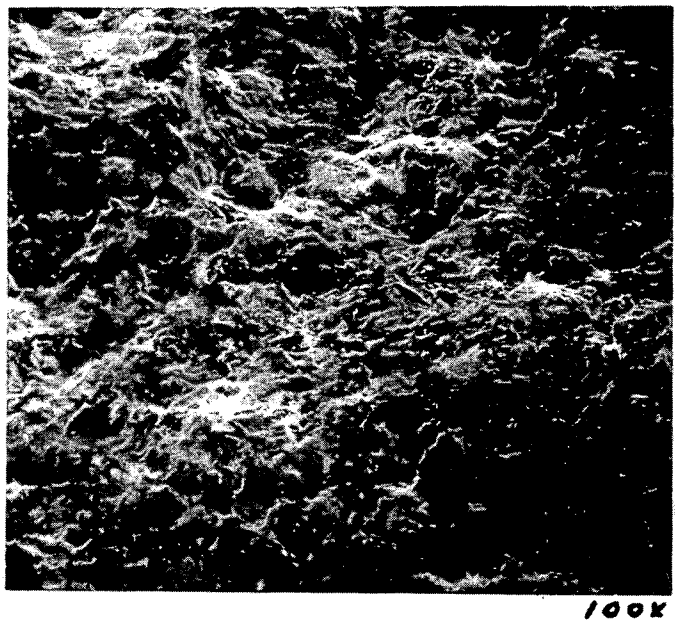

100x

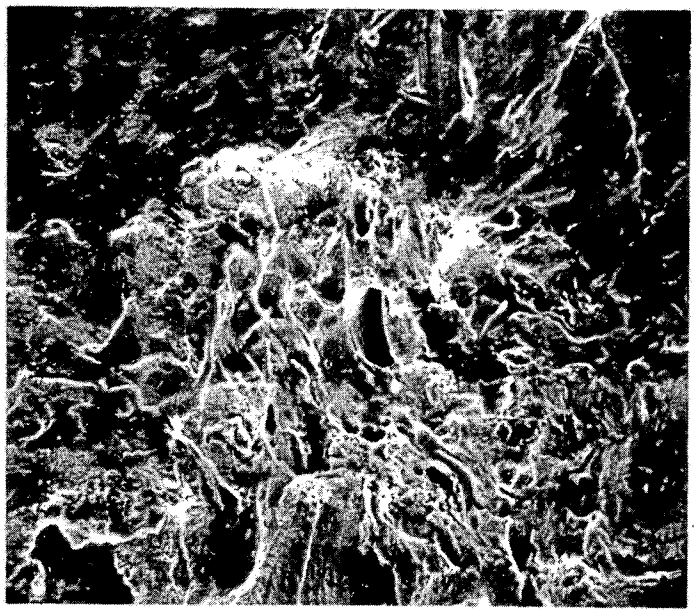

500x

P-1
Area 4

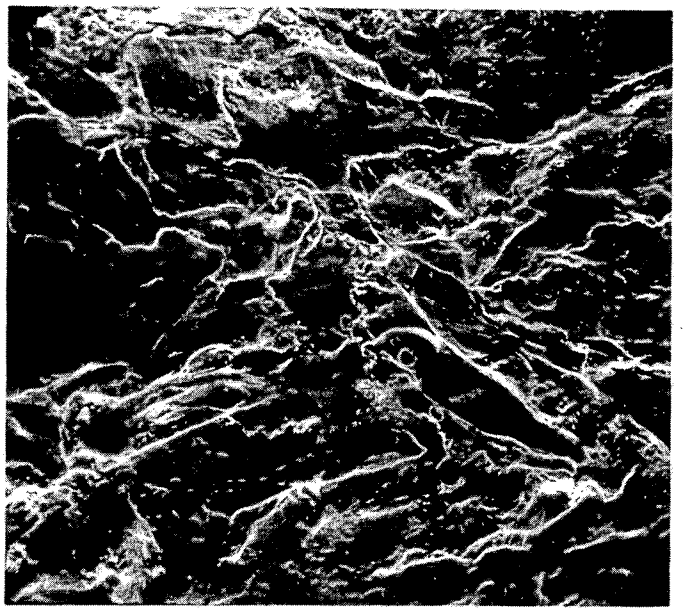

500x

Figure 7 -- Fractographs of Areas 4 and 4A from Figure 3.

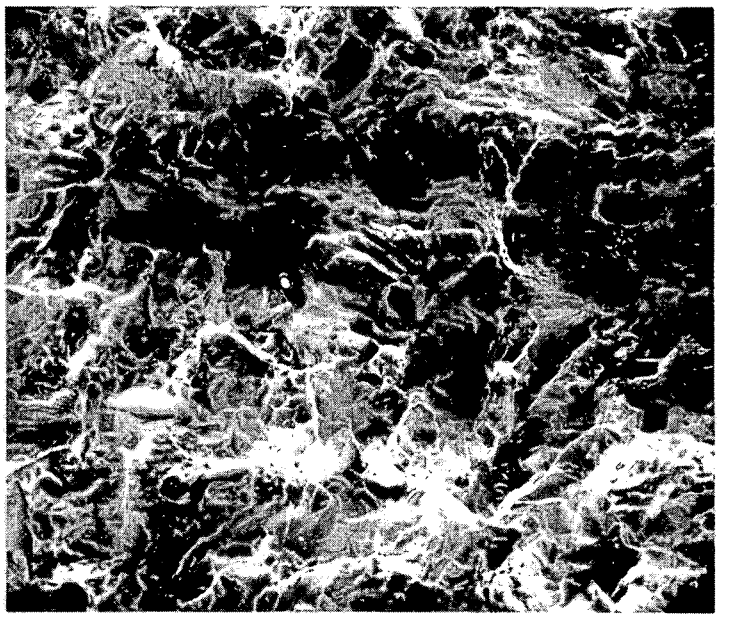

100 x

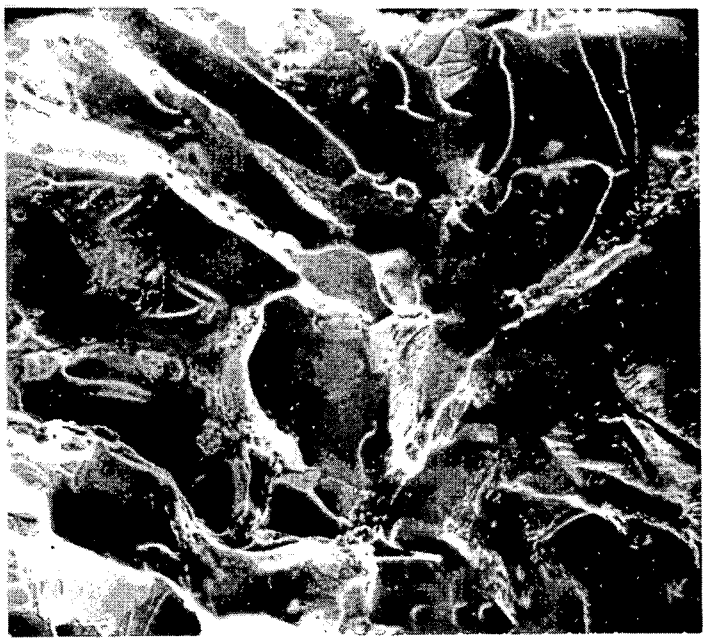

500x

Figure 8 -- Fractographs of Area 4A1 from Figure 3.

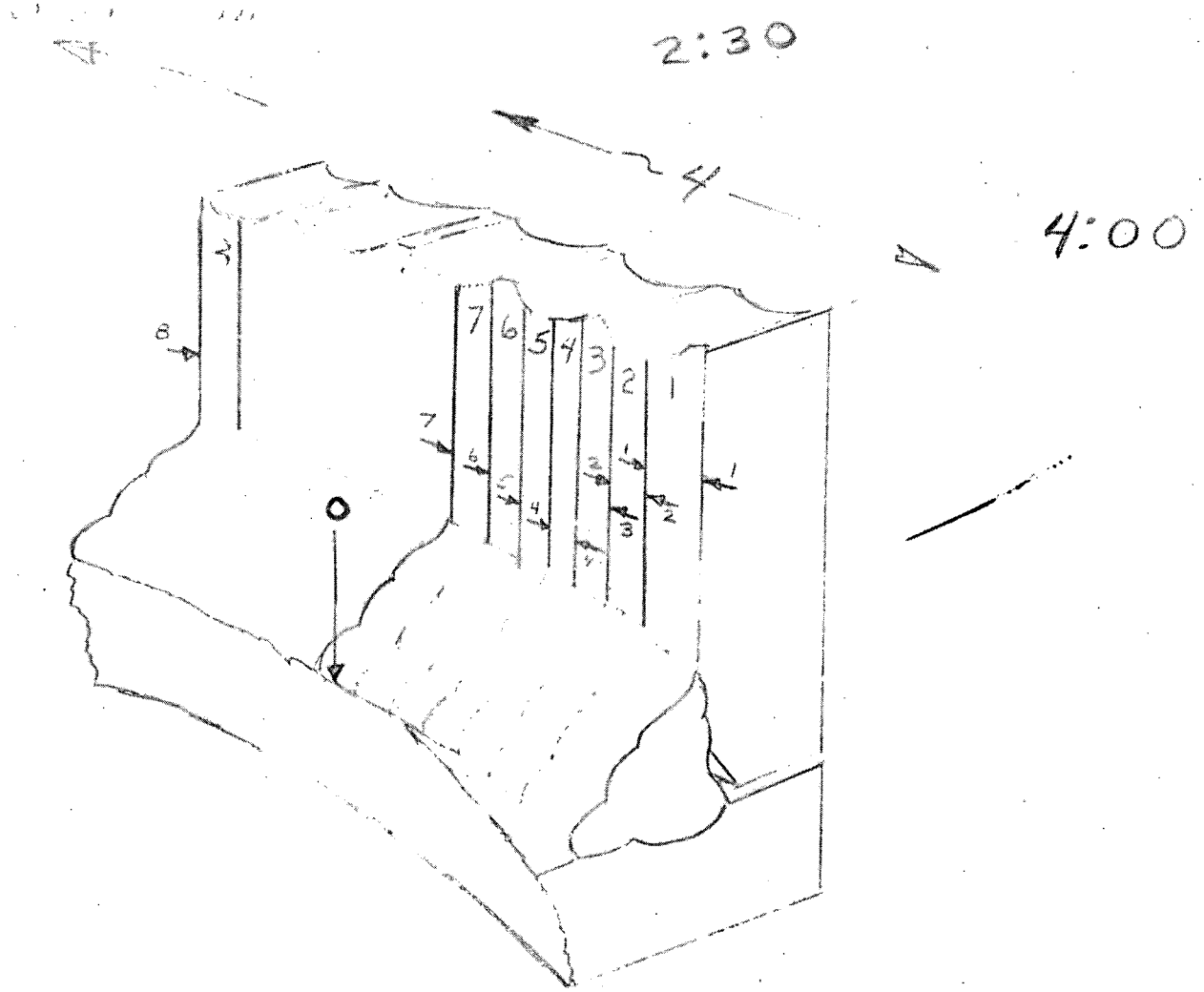

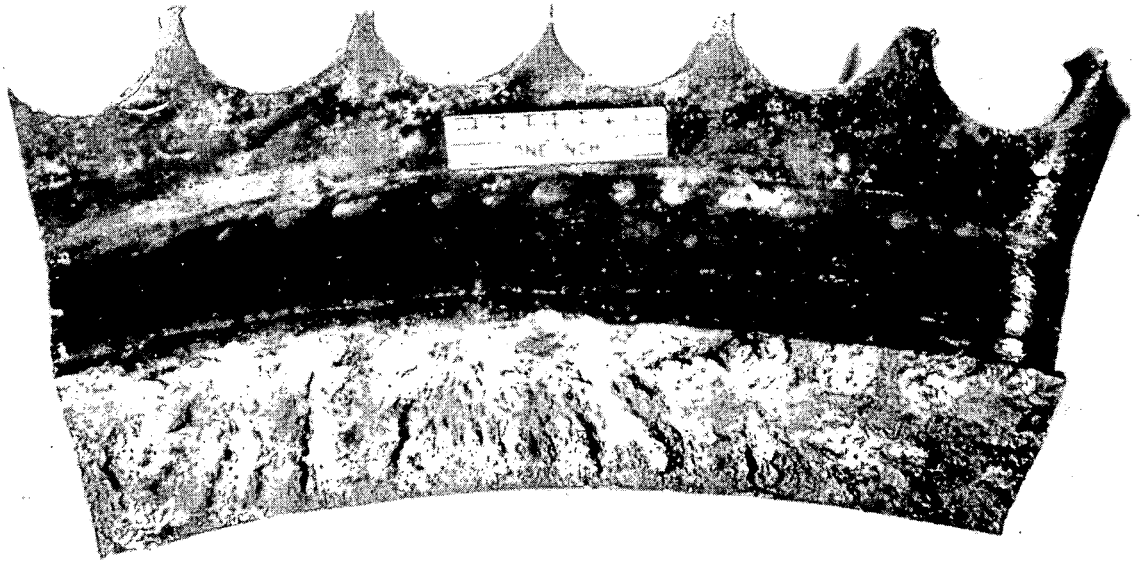

Figure 9 -- Sketch Showing Location of Fracture and Location of Sections Removed for Examination - Photomacrograph of Weld Section of Fracture 1 X

Pipe O.D.

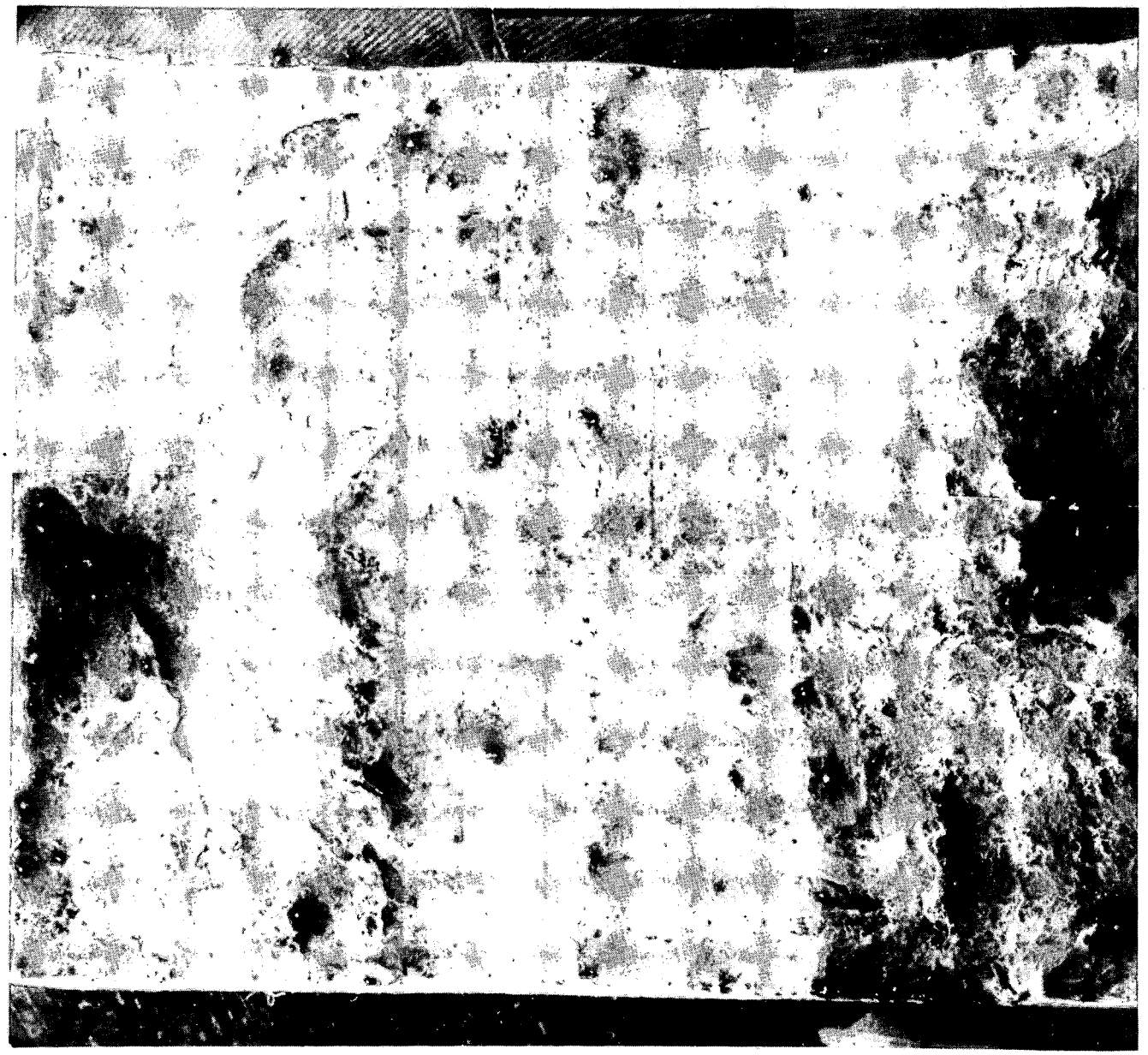

Figure 10 -- SEM Showing 1/2 of Fracture Surface of Weld Section. 20 X

Pipe I.D.

Figure 10A -- SEM Showing Second Half of Fracture Surface of Weld Section. 20 X

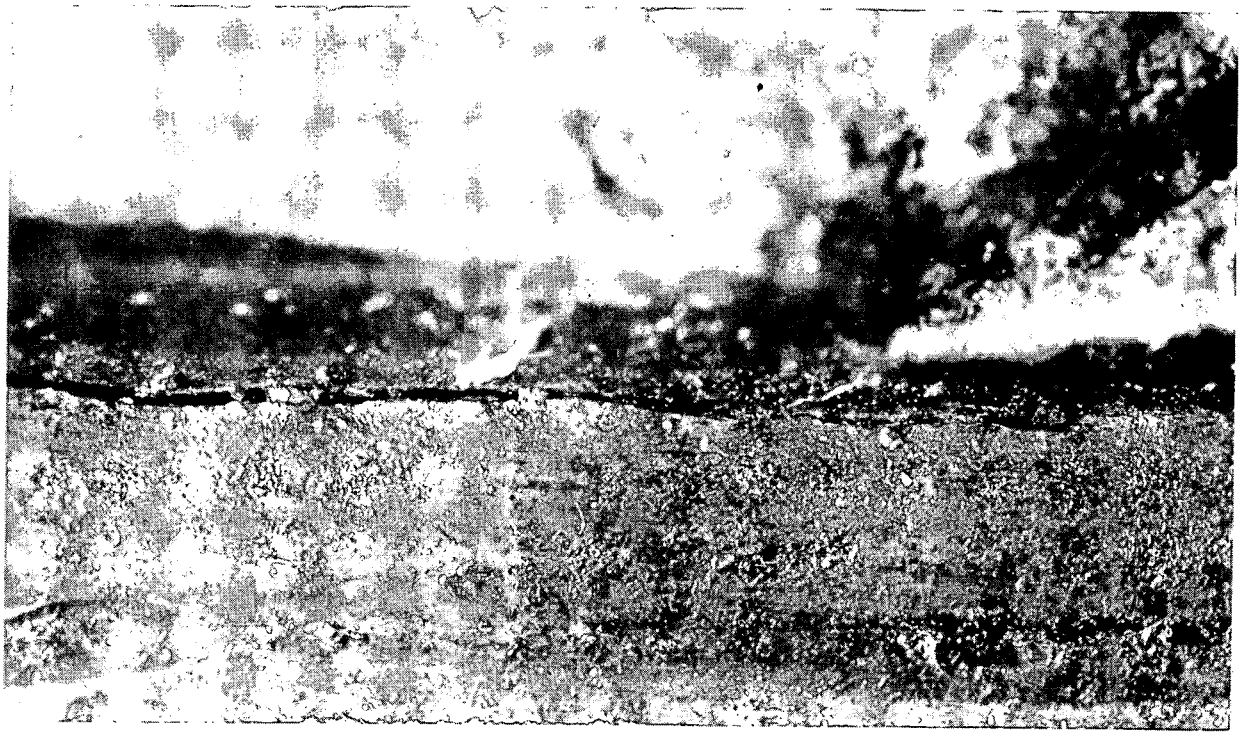

Figure 11 -- Photomacrographs of Weld Toe Crack. 10 X

Figure 12 -- Photomacrograph of a Weld Cross Section. Pipe Section is on the Left, Plate Section on the Right. 4 X

8X

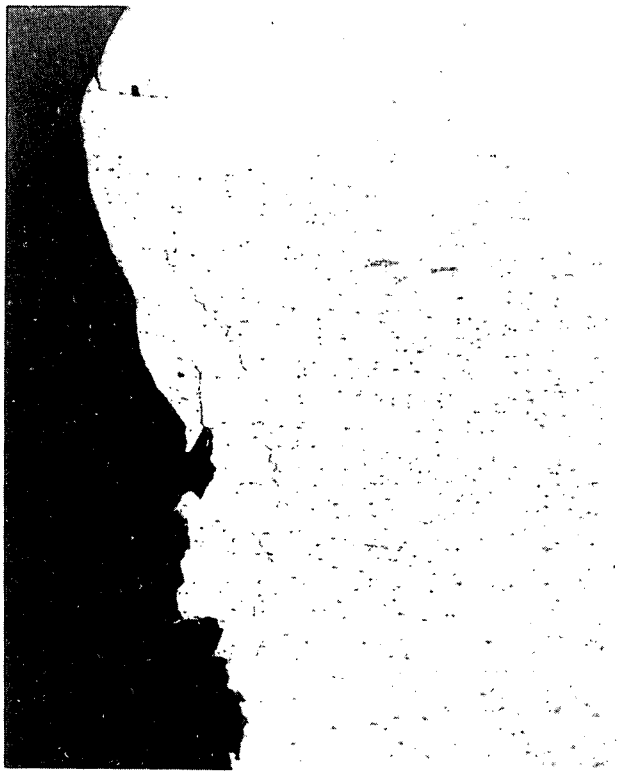

8X

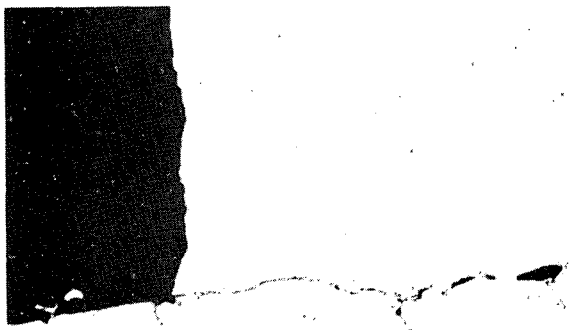

Section 5 100X

Section 6 100X

Figure 13 -- Photomicrographs, Etched and Unetched of Cross Section Through Weld Joint. See Figure 9 for Section Locations.

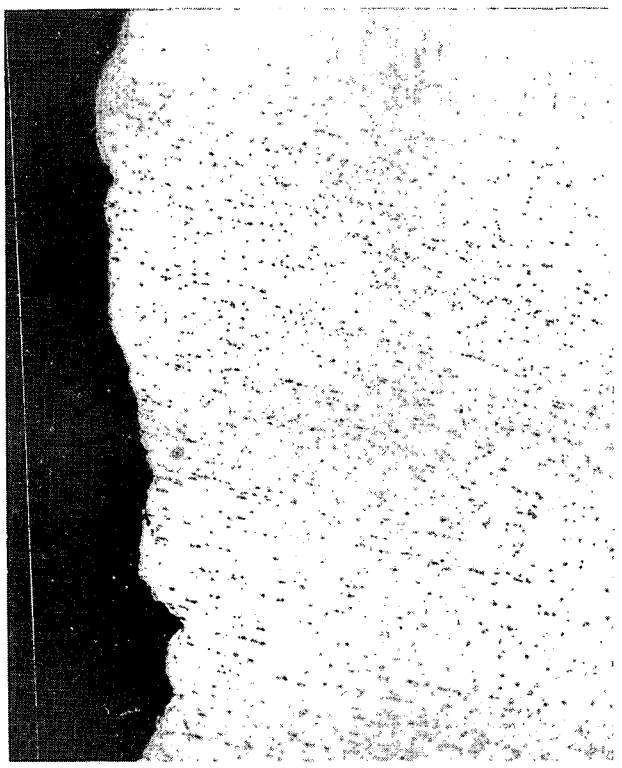

8X

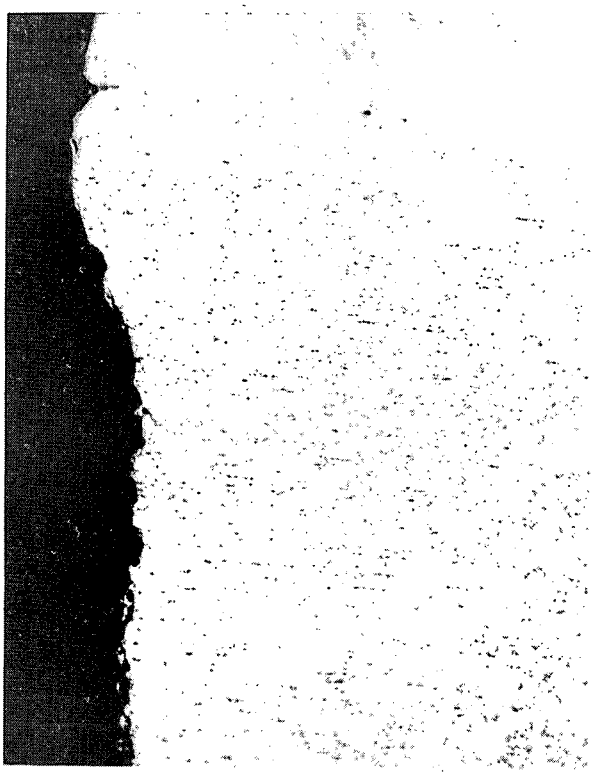

8X

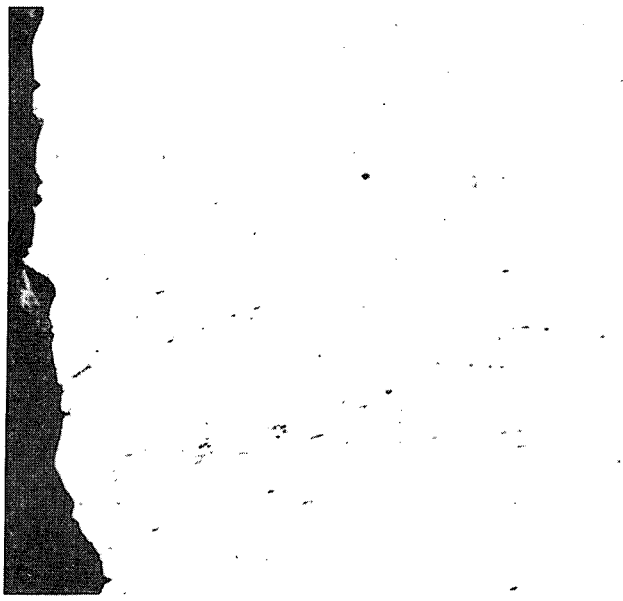

Section 7

100X

Section 8

100X

Figure 14 -- Photomicrographs, Etched and Unetched of Cross Sections Through Weld Joint. See Figure 9 for Section Locations.

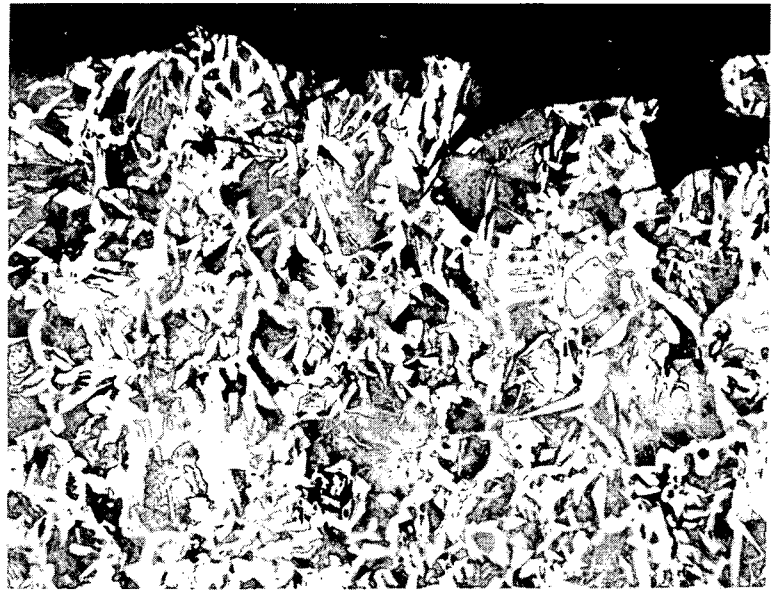

A

B

C

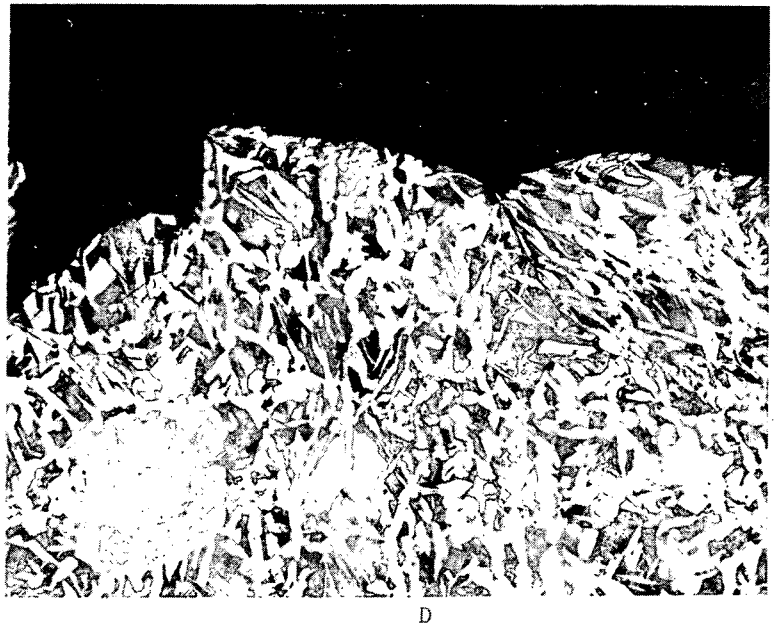

D

Figure 15 -- Photomicrographs Showing Sections of the Fracture Edge. 100 X

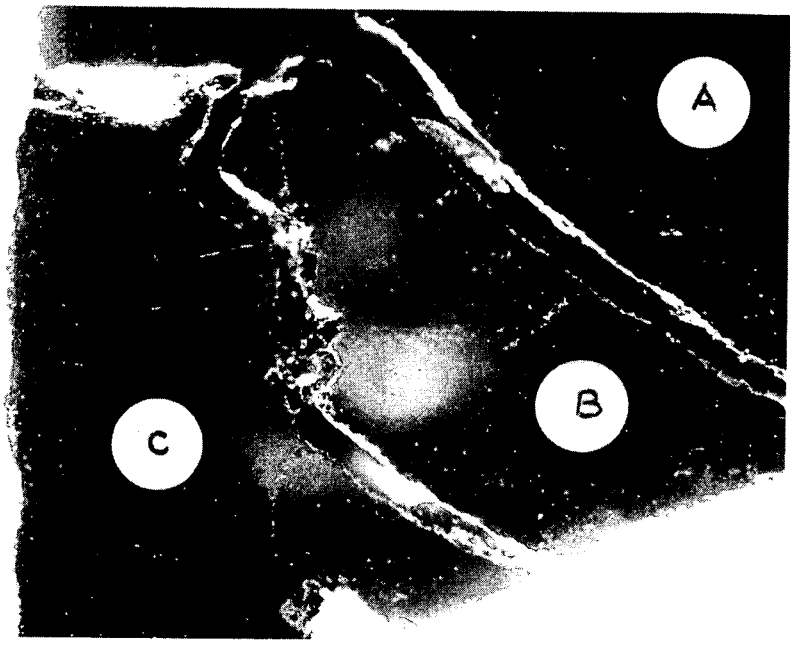

Figure 16 -- Photomacrographs Showing A Crack in Pipe Section (W-4) Under the Weld, Before and After Fracturing With Liquid Nitrogen. Subsequent Figures Show Fracture Faces of Sections A and B.

Figure 17 -- Photomacrograph of Fracture Face A. SEM Fractographs of Different Magnification of Area W-4-A3

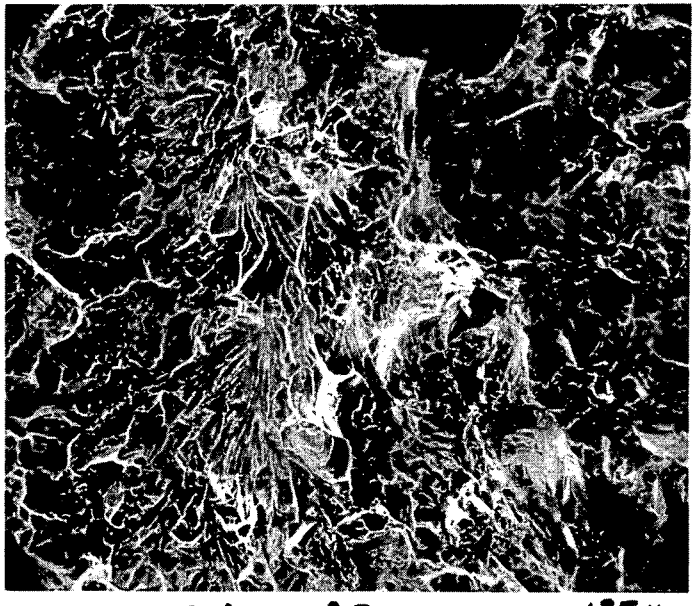

W-4-A3 135x

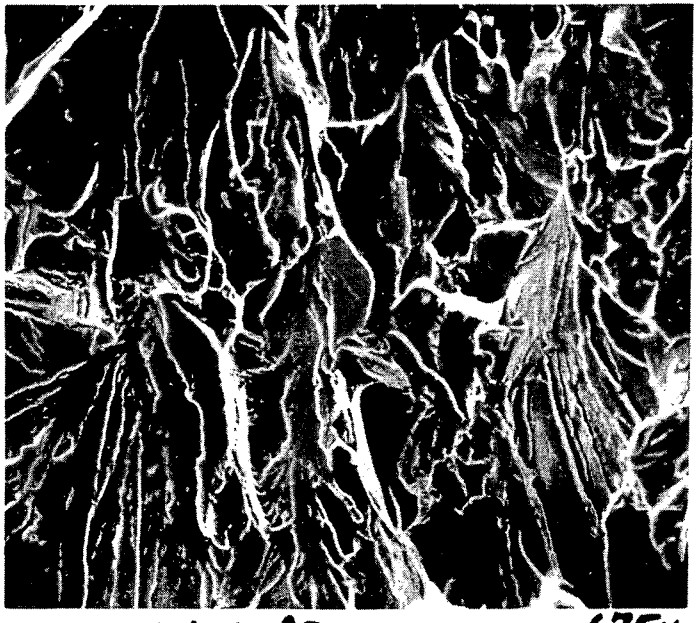

W-4-A3 675x

W-4-A1

Figure 18

W-4-A2

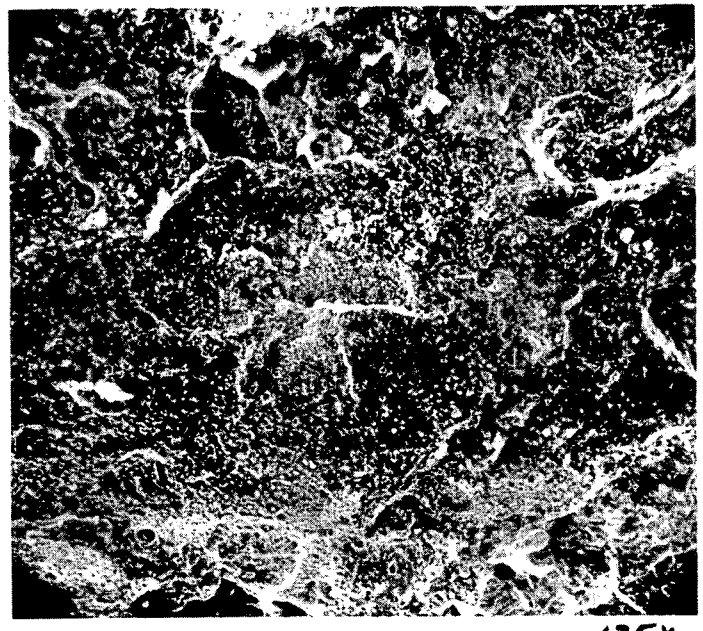

135x

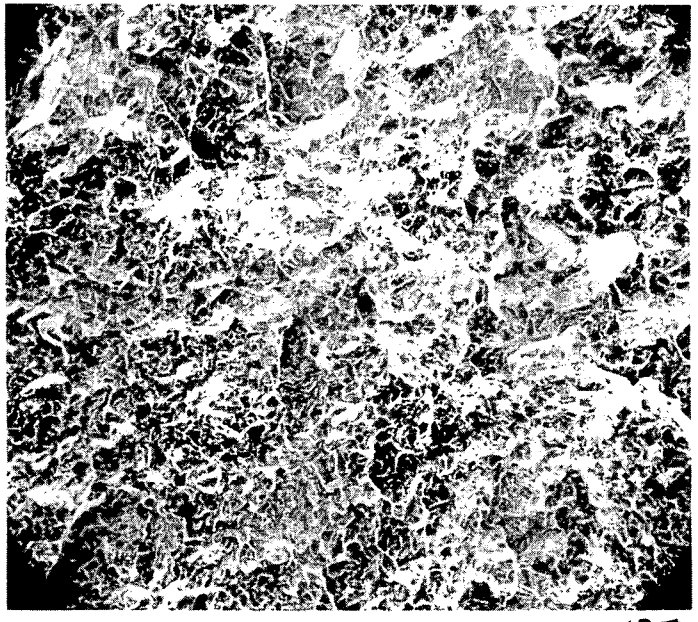

135x

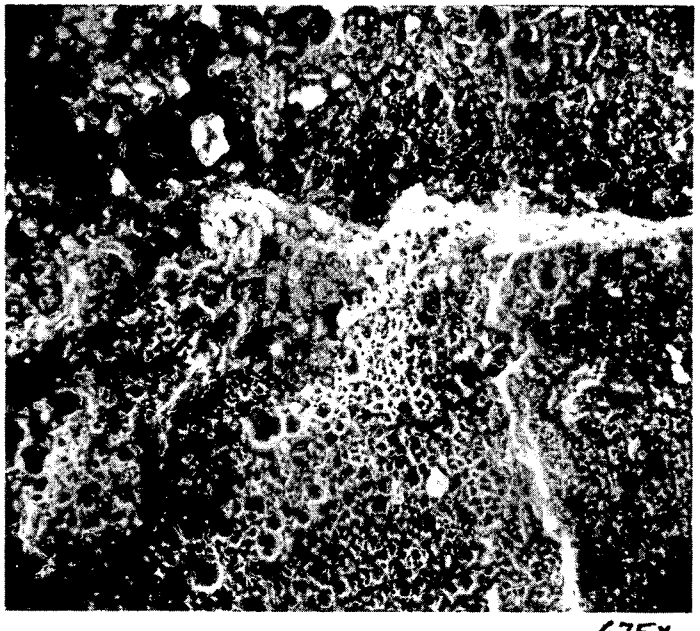

675x

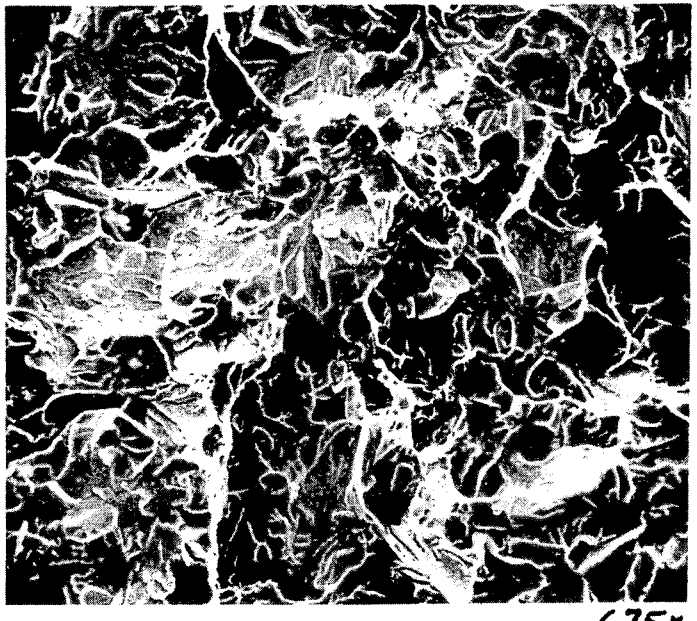

675x

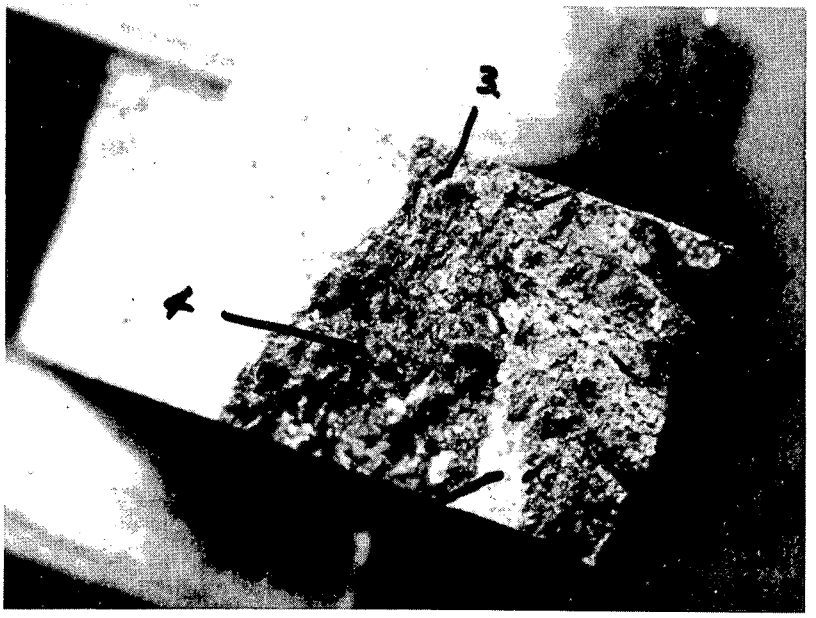

W-4-B

Figure 19 -- Photomacrograph of Fracture Face of Area W-4-B (From Figure 15) Showing Location of Fractographs in Following Three Figures.

W-4-B1

Figure 20

W-4-B2

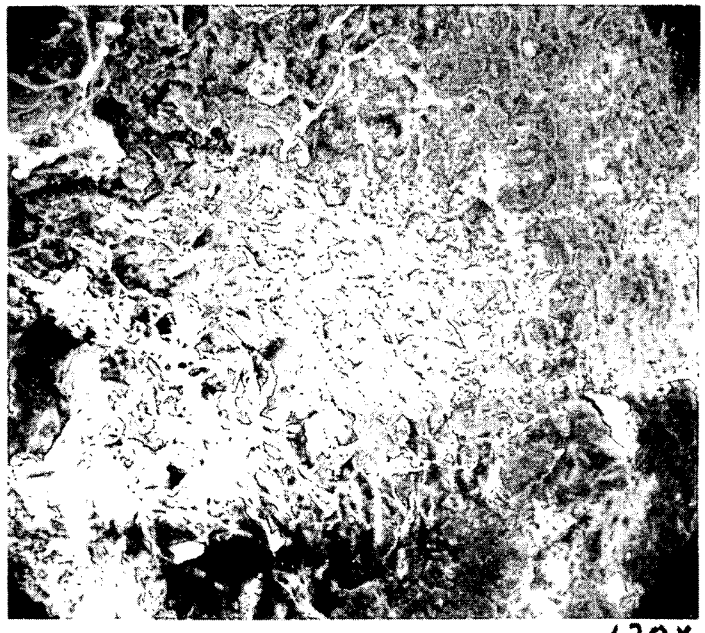

120x

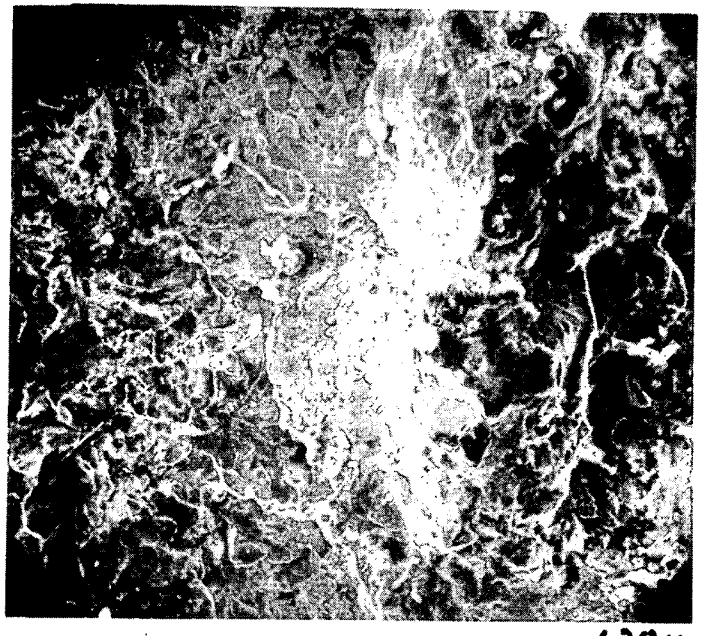

120x

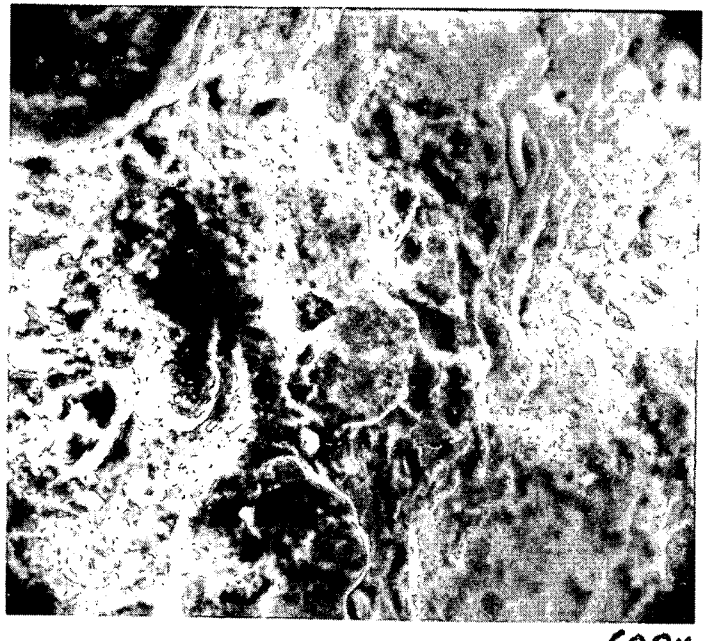

600x

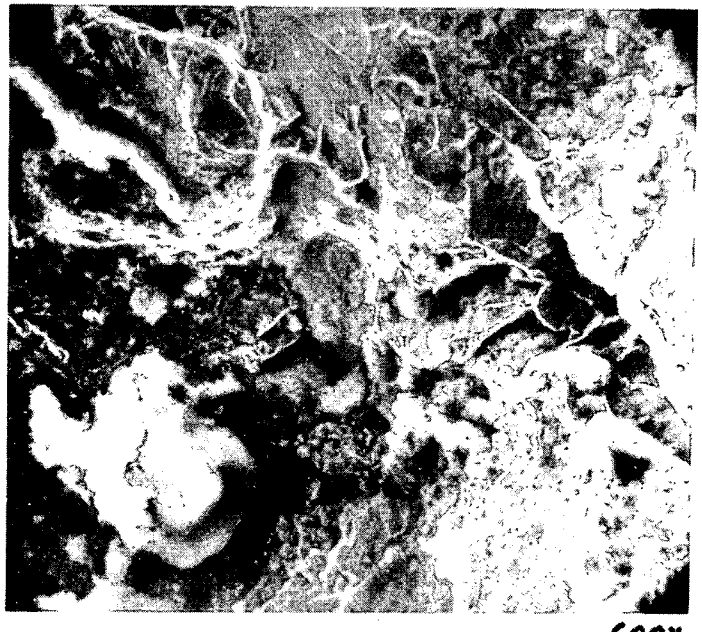

600x

Figure 21

W-4-B3

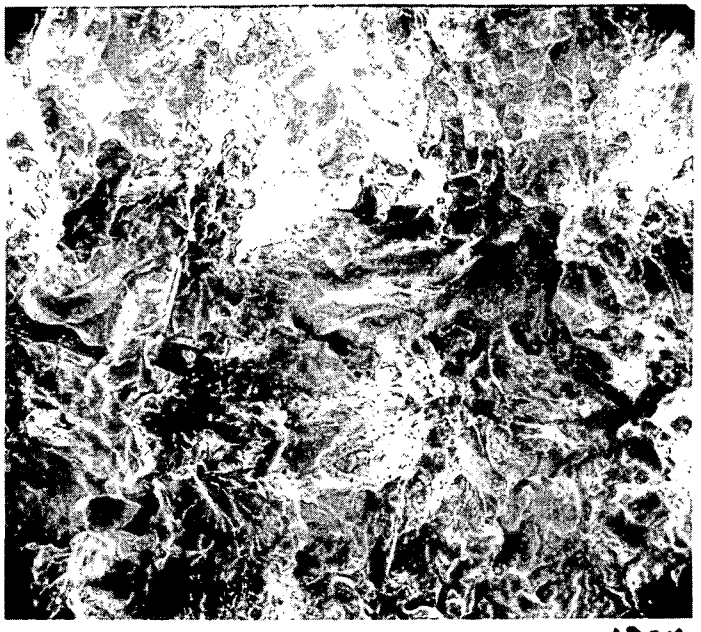

120x

600x

W-4-B4

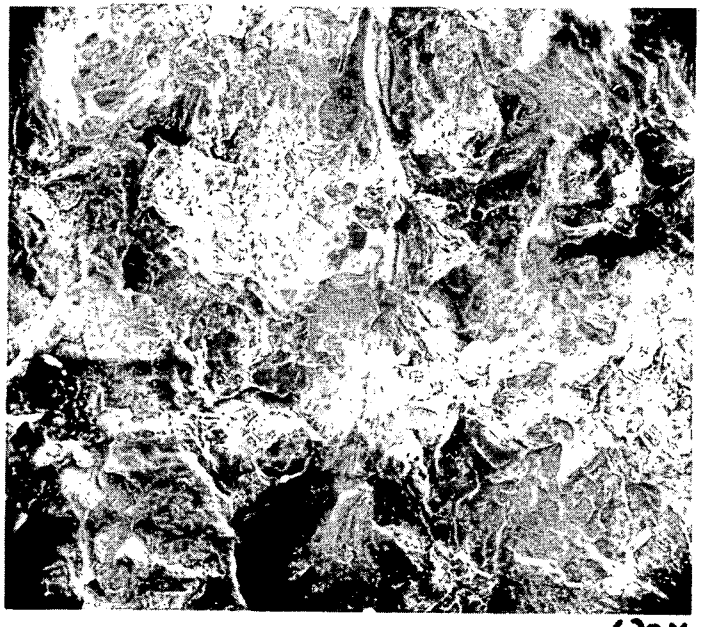

120x

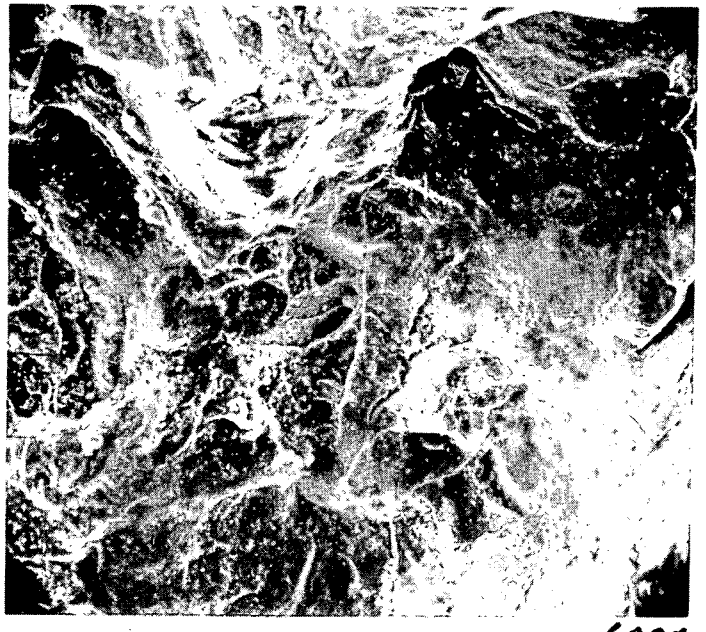

600x

W-4-B5

Figure 22

W-4-B6

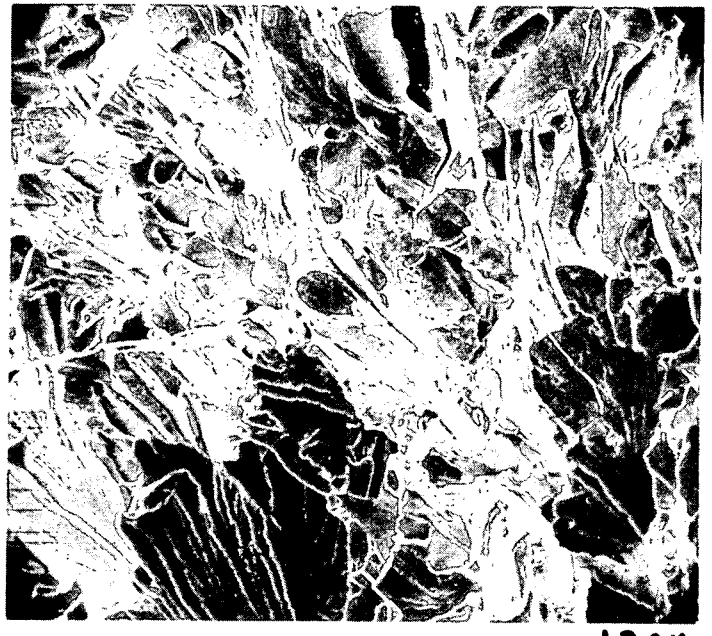

120x

120x

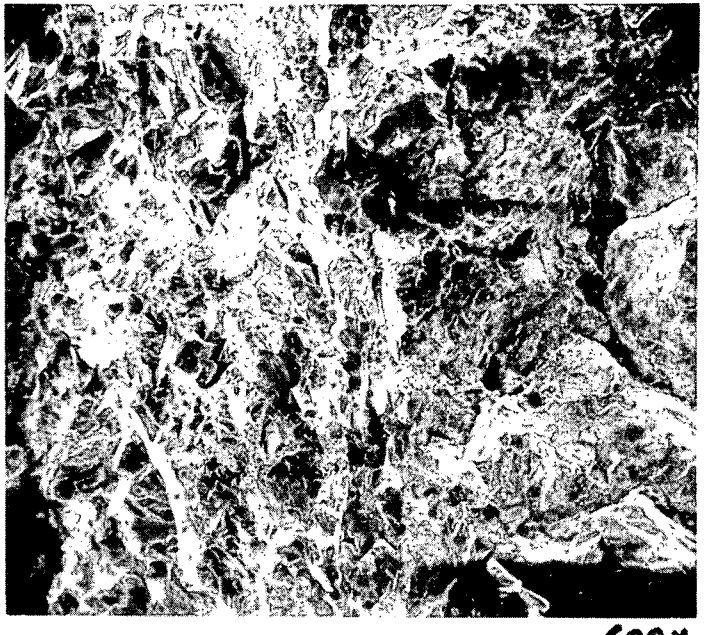

600x

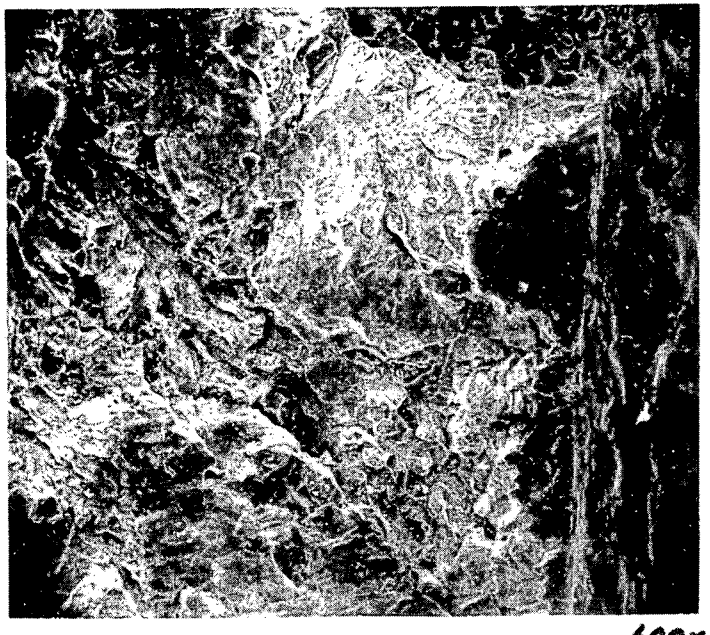

600x

11X

22X

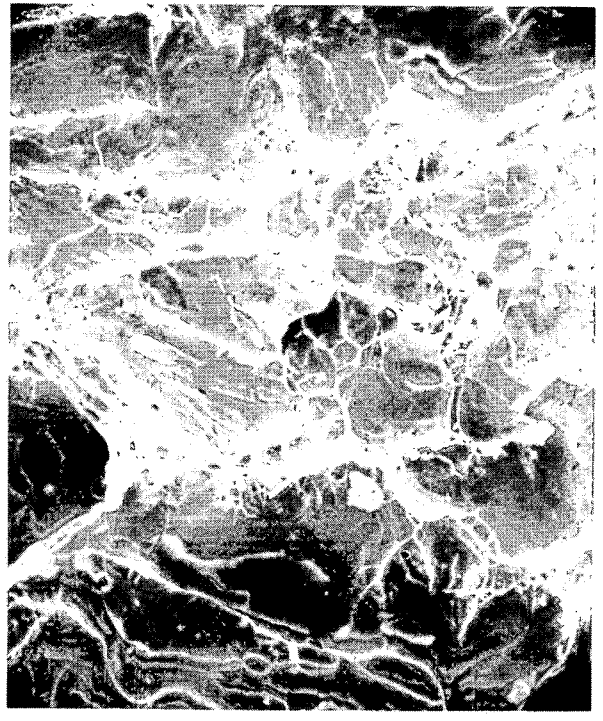

550X

Figure 23 -- Photomacrograph and SEM Fractographs of Fracture Surface of Simulated Triaxially Loaded Tensile Test of Material From Failed Pipe.

22X

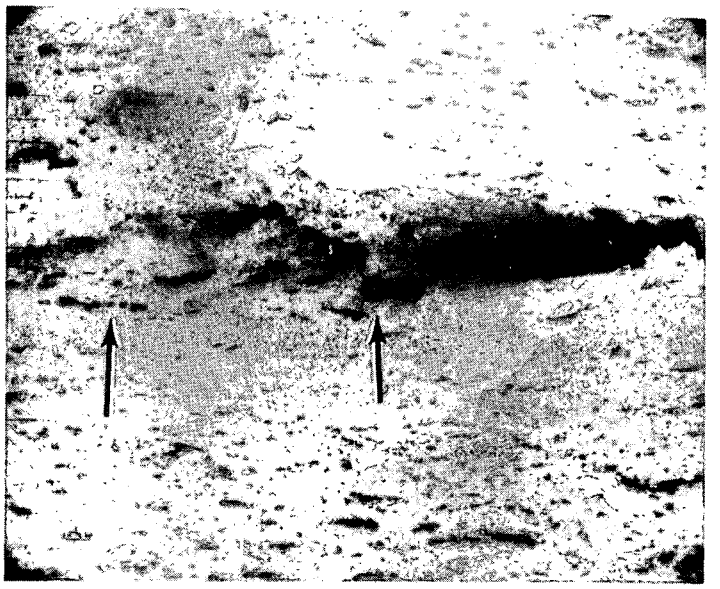

22X

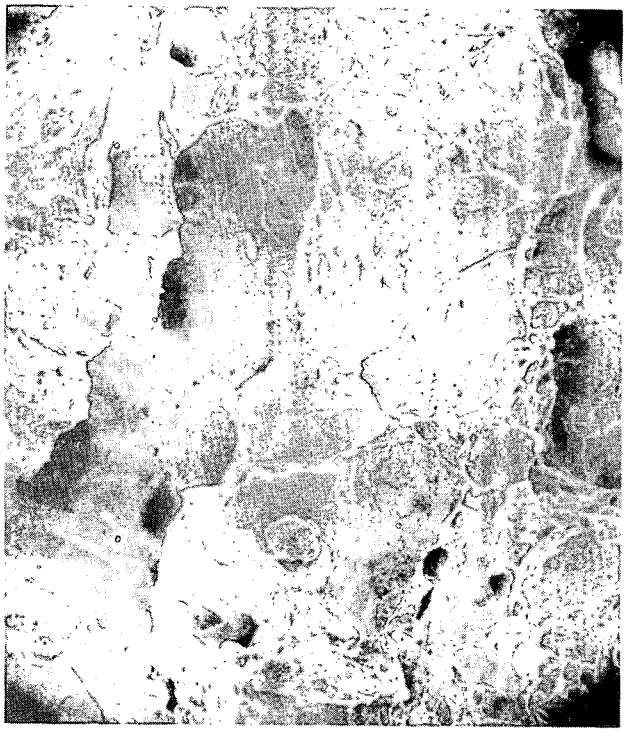

550X

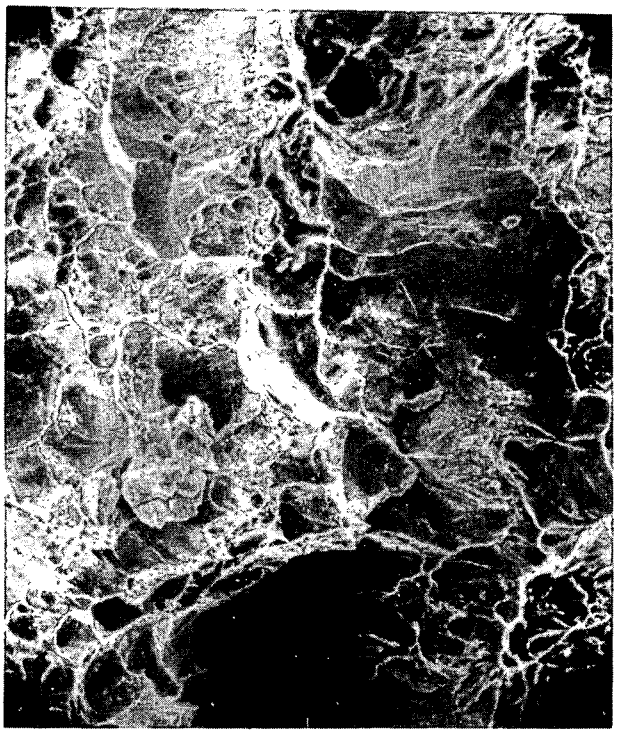

550X

Figure 24 -- SEM Fractographs of Fracture Surface Shown in Figure 23, at Different Magnifications. Arrows Identify Locations of the Higher Magnification Fractographs.

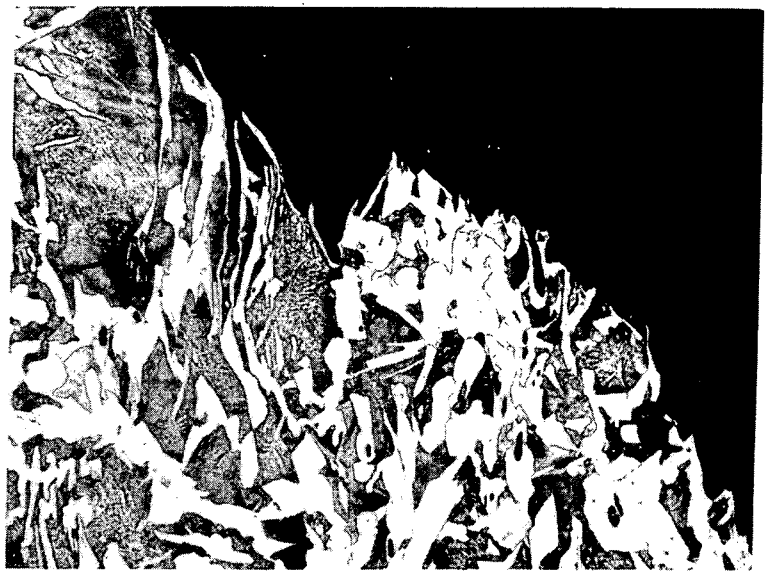

500X

500X

1000X

Figure 25 -- Photomicrographs of Fracture of Test Sample Shown in Figure 23.

Appendix IV

Analysis of Containment Liner

I. Description of Problem

A. Introduction

The report describes the damage observed in the Containment Liner following a pipe break in Boiler Feed Line No. 22, which penetrates the Containment 2'-0" south of west of the building east-west centerline at Elevation 57'-6". The circumferential break extended from the top of the penetration, clockwise, approximately 180°. The recommended liner fix and the analytical program undertaken to justify the recommendations are discussed along with response to various AEC questions resulting from a December 7, 1973 meeting with the Commission. A detailed description of the final recommended fixes is also presented.

B. Description of Structure

The liner function is to provide a leak-tight barrier to prevent releases of radioactivity, within the Commission's regulations, which could potentially endanger the health and safety of the public. The liner is not required to aid the reinforced concrete shell to carry structural load. Steel plates of ASTM A-442 material are welded together to form the liner. Continuously pressurized channels are placed over all weld seams and around all penetrations. The immediate area of the main steam and feedwater

penetrations consists of 3/4" thick plate to Elevation 72'-8-3/4". All other liner plate extending to this elevation is 1/2" thick. Above Elevation 72'-8-3/4", the plate thickness is reduced to 3/8". A polyvinylchloride thermal insulation extends to Elevation 63'-8-1/2" which also represents the top of the Main Steam penetrations.

The liner is attached to the 4-1/2" thick reinforced concrete containment shell by 1/2" diameter bent studs. The stud is 7" long with a 90°-2" leg. Below Elevation 77'-7-3/4", the studs are spaced at 28" vertically and 24" horizontally. Above this elevation, the cylinder studs are spaced 14" vertically and 24" horizontally. The construction drawings called for the vertical stud spacing to become 14" at Elevation 72'-7-3/4" at the start of the 3/8" plate, to preclude elastic buckling of the liner plate in accordance with the original design criteria. Due to the timing of mobilization of the liner contractor on and off the site, the first 5'-0" lift of concrete above the start of 3/8" thick liner plate was poured before the vertical stud spacing could be revised from 28" to 14". This resulted in two rows of missing studs around the containment structure. The original plant design criteria was

that the liner should not buckle or exceed yield strain under LOCA conditions. (Refer to Figure 1 for a complete description of the area).

There was no indication of deformation in the liner in the area of the feedwater penetration prior to the break in Feedwater Line No. 22.

C. Observations After Incident

After the incident, it was observed that an area of the liner plate above Feedwater Line No. 22 had liner deformations extending into the containment structure (away from the concrete). This area started at Elevation 72'-8-3/4" (15'-2-3/4" above the centerline of Feedwater Line No. 22) and extended about 2-1/2' to 3' in the vertical direction. In several areas, the deformation extended almost 5'-0" vertically. Circumferential extent was approximately from Building Column Lines 8 to 11 or 70'-0" with the most significant deformations contained in approximately a 50'-0" long band in the circumferential direction. The longest deformation occurred 1'-0" south of Column 9 and extended for approximately 56" in height with a bulge of approximately 1-1/16". The most highly strained area occurred in a deformation located 18' south of Column Line 9 where a 1-1/4" bulge occurred in 28"

of height. The maximum strain, determined by graphically developing the curvature from the deformed shape, was 1.33 percent. The above information was developed from Con Edison surveys of the deformed area which are shown in Figure 2. The information was obtained by measuring the distance of the liner from a plumb line from the floor above. This gave relative offsets of the liner in a vertical direction, but a base line had to be established to determine absolute deformations of the liner plate.

The base line was conservatively assumed to occur at Elevation 68'-0" and the concrete was conservatively assumed to be vertical although the original surveys taken of the liner plate prior to pouring of the concrete (shown in Figure 2), and subsequent surveys performed by Con Edison in the non-deformed area show a definite trend of the final concrete shape to the inside of the containment. It should be further noted that all deformations were measured in the 3/8" plate in the region of the two missing rows of studs.

In addition to the surveys, Con Edison performed an ultrasonic inspection to determine whether studs were broken behind the liner plate. (It was during the course of this examination that the two rows of missing studs were discovered). Based on the results of this

survey, it is believed that nine additional studs are broken in the row of studs at Elevation 74'-11-3/4" (the row of studs located between the two missing rows). The missing studs are indicated in Figure 1, and are generally located near deformations which show the longest vertical extension. In all further considerations and analytical work which followed, the effects of the missing and broken studs were included.

II. Investigations

Efforts undertaken to resolve the questions generated by the observations noted are as follows:

A. Analysis

Two major analyses were performed using the MARC-CDC Non-Linear Finite Element Analysis Program to determine the strain in the liner plate due to LOCA, earthquake, and test pressure loads, and to determine the extent to which the liner insulation should be extended. The first analysis considered

each discrete stud element (strip model) while the second analysis was an axisymmetric analysis which smeared the studs as additional liner plate thickness for 360° around the containment at the stud row location. The axisymmetric analyses was included as a check on the more sophisticated strip model analysis.

B. Inspection and Tests

In addition to the analysis, several tasks were performed to ascertain the acceptance of extending the liner insulation and also to provide additional confidence in the results of the computer analysis. These included:

1. A magnetic particle examination of the deformed area was performed. This examination was to determine the existence of cracks and assure that the liner in its present deformed state meets the leak tightness requirement which is the primary purpose of the liner plate. Although the present maximum strain of 1.5 percent in liner plate exceeds the allowable strain in Table CC-3700-1 of ASME, Section III, Division 2 Code, the MP inspection has shown that no cracks exist which eliminates this concern since the liner will maintain leak tightness in its present form.

2. Bend Tests of 3/8" Plate

These tests were performed to determine the ability of a 3/8" plate with inward curvature to straighten under yield tension load without cracking. In this test, a 6" by 28" plate was given an initial deformation of 1-1/2" (larger than measured deformation) and straightened with the yield tension load. In addition, the specimens were subjected to twenty cycles of 1/2 yield tension load to determine the effect of cyclic loads which would be expected due to the periodic integrated leak rate tests performed during the life of the plant. The samples tested included a vertical weld to simulate the worst condition at the site as requested by the AEC. The samples were MP tested at the conclusion of the tests to assure that no cracks exist. Although the above test does not simulate the pressure load normal to the deformation which will exist during test or LOCA conditions, it gives confidence that the vertical elongation of the structure during these conditions will not cause violation of liner integrity at the maximum deformation.

3. Full Pressure Test

A pressure test at 47 psig has been performed to assure that the effect of tension loads on the plate and pressure load normal to the plate will

not cause liner plate cracking. At the conclusion of the test, the area of the liner deformations was MP tested and resurveyed to detect any changes in shape. Cameras recorded movement of the liner plate during the test to measure the deflection of the deformed area.

With the UE&C analytical results backed in part by the pressure test, bend test, and magnetic particle tests, it will be shown in this report that by extending the liner insulation, the liner will not be stressed in excess of allowable strains discussed in Section IIIA of this report for test pressure, LOCA and/or seismic loadings.

III. Response to Questions

As a result of the December 7, 1973 AEC meeting (Reference No. 1), and as a consequence of the program undertaken in Section II of this report, the following questions must be addressed to justify our final recommendations which will be addressed in Section IV of this report.

Question A

Describe, in detail, the primary analytical effort undertaken to assure the adequacy of the deformed region of the containment liner. Discuss the results of this analysis and compare these with the acceptance criteria.

Answer

1) Statement of Problem

To verify that by extending the existing insulation

to cover the deformed region of the containment liner, the strains determined under test, normal and LOCA loads will be within acceptable limits.

2) Statement of Criteria

The acceptable limits of liner strain under the postulated loading conditions are taken as:

a) For membrane strain - 0.1 e_u

b) For membrane plus bending strains - 0.2 e_u

where e_u is defined as the uniform ultimate strain of the liner material. The uniform ultimate strain of ASTM A442 steel is 22 percent. Hence, the strain limits defined by criteria (a)(b) may be taken as:

a) For membrane strain $e = 0.1 \times 0.22 = 0.022$ in/in

b) For membrane plus bending strains

$$e = 0.2 \times 0.22 = 0.044 \text{ in/in}$$

3) Analysis Methods

Two series of finite element analyses have been performed to verify that the strains in the deformed region of the newly insulated liner under the loads produced by test, normal, and LOCA meet the criteria stated in Item (2) above.

The first series of analyses considered a vertical strip of a portion of the containment including the deformed area. The second series was an axisymmetric analysis considering the same portion of the containment. A

Detailed description of these analyses, including the effects considered, the assumptions inherent in them and the loading conditions, are described in the following paragraphs.

a) Liner-Stud-Reinforced Concrete Interaction Study Strip Model

The basic requirements of this analysis were established as:

1. The liner plate, studs, and reinforced concrete were to be modelled.
2. Both material and geometric nonlinearities were to be accounted for.
3. Provisions were to be made to prevent the liner from deflecting into the concrete.
4. The deformed shape of the liner plate was to be represented and the effect of any missing or broken studs was to be included.
5. The strains in the liner and the displacements in the studs were to be determined.

Based on these requirements, the analysis was performed using the MARC-CDC Non-Linear Finite Element Analysis Program. The details of the finite element model are shown in Figure 3.

Elements: The liner plate and reinforced concrete were represented by eight-node quadrilateral shell elements. These are reduced integration elements

derived from the twenty-node brick element. The deformed geometry of the liner may be accurately represented by this element and the large displacement terms were included so that the actual stiffness of the deformed liner is accounted for. The studs were represented by one-dimensional elements. At each stud location, three elements, two for shear and one for tension, were used to connect the concrete to the liner. Gap elements were used to insure that the liner would not deform into the concrete. These elements also permit free movement of the liner off the concrete.

Material Properties: The liner material was assumed to be elastic-perfectly plastic with a yield stress of 32 ksi. Non-linear load-deformation curves in the form of equivalent non-linear stress-strain curves for both tension and shear were used for studs. These curves are shown in Figure 4 and are based on the information contained in Reference (3). Anisotropic material properties were used for the concrete to properly represent the appropriate concrete cracking patterns.

Extent of Model: The width of the model was chosen to represent the liner and concrete containment wall between two columns of studs which

have a circumferential spacing of 24". The vertical spacing of the elements was chosen so that the corner nodes corresponded to stud locations. Hence, in the lower portion of the model, the elements are spaced at 28 inches, while in the upper portion of the model, the elements are spaced at 14 in. The elevation z = 112 in. on the model (Figure 3) corresponds to Elevation 72'-8-3/4" in the containment (i.e., the transition from 3/4" or 1/2" plate to the 3/8" plate). The largest significant deformation to be investigated was 56 in. high (z = 112 in. to z = 168 in.), the model was extended an additional 112 in. on each end (z = 0 in. to z = 280 in.) to assure that there would be no interaction between the ends of the model and the deformed region.

Boundary Conditions: Since the top edge of the model is well within the membrane behavior region of the containment, the concrete and liner elements were tied to preclude relative rotations and assure uniform vertical growth. The overall behavior of the containment should remain axi-symmetric, hence no rotation or tangential motion was allowed along the vertical edges. To preclude rigid body motion, the bottom edge of the model was fixed against vertical growth.

Geometry of Deformation: Two existing deformations were considered in the analysis. The first assumed deformation corresponds to the largest vertical deformation observed in the liner. It extends from z = 112 in. to z = 168 in. and corresponds to the case with studs missing at z = 126 in. and z = 154 in. For this case, the studs at z = 140 in. were assumed broken, and hence not acting. The liner deformation was defined by a cubic equation with zero slope at its extremities and at z = 140 in. The peaking deformation at z = 140 in. was taken as 1.08 in. The plate below this deformed region is 1/2 in. thick.

The second assumed deformation corresponds to the largest calculated existing bending strain in the deformed liner. This deformation was also defined by a cubic equation extending from z = 112 in. to z = 140 in. and having a peak displacement of 1.25 in. at the location of the missing studs at z = 126 in. The plate below this deformed region is 3/4 in. thick.

Loading Conditions: Four load cases were run for each of the deformations described above. These are summarized in Table I. In all load cases, the liner was assumed to be thermally insulated.

1. This load case considers a pressure test of 54 psig. To produce the maximum tension in the liner and concrete 95 percent of the calculated dead load and no thermal gradient through the containment wall was assumed.

2. This load case considers the loss-of-coolant accident pressure of 47 psi and assumes the deformed region is on the tension side of the resultant containment seismic loads. Again, to produce maximum tension, 95 percent of the calculated dead load and no thermal gradient was assumed.

3. This load case again considers the LOCA pressure of 47 psi, but assumes the compression side of the resultant containment seismic loads. To produce the maximum compression in the liner, 105 percent of the dead load was assumed, as was a winter thermal gradient of 120°F.

   This load case simulates normal operating conditions under the winter thermal gradient.

In the first two load cases, the concrete was assumed to be cracked in both the circumferential and vertical directions. In the third load case, only circumferential cracking was assumed, while no cracking was assumed in the fourth load case.

Load Incrementation: Since the model includes non-linear material behavior as well as large displacement terms for the liner, a load incrementation solution was used. All loads were considered proportional. Results were reviewed after each increment of loading in order to determine an appropriate size for the next load increment. If too large an increment of load was applied, the gap elements would not perform properly and, hence, would allow the liner to deform into the concrete. On the average, twelve load increments were required for each load case to bring the loads to their full value.

b) Liner Stud Reinforced Concrete Interaction Study--Axisymmetric Model

The basic requirements of this analysis were established as:

1. To represent, as completely as possible, those items included in the strip model.

2. To provide an independent confirmation of results.

3. To reduce the number of degrees-of-freedom considered in the analysis so that the solution could be more readily obtained.

Based on these requirements, the analysis was again performed using the MARC-CDC non-linear Finite Element Analysis Program. However, for this case, an axisymmetric model was used. A detailed view of the finite element model is shown in Figure 5.

Elements: The liner plate was represented by an axisymmetric thin-shell elements with two nodes per element having four degrees-of-freedom at each node. The deformed geometry of the liner may be accurately represented with this element and the large displacement terms were included in the formulation so that the appropriate stiffness of the deformed liner is accounted for. The concrete was represented by axisymmetric rings of quadrilateral cross-section. Four elements through the thickness were taken to represent the wall. The circumferential rows of studs were represented by axisymmetric membrane elements. Two elements, one to resist axial forces and one to resist vertical shear, were used for each row of studs. Gap elements were again used to insure that the liner will not deform into the concrete and yet still be allowed to grow away from the concrete.

Material Properties: The same material properties as assumed for the strip model were used in this analysis. The properties of the studs, however, had to be smeared because of the axisymmetric nature of the analysis.

Extent of Model: The model extended over the same length of the containment included in the strip analysis.

Boundary Conditions: The same boundary conditions were used on top and bottom edges of the model as assumed for the strip model.

Geometry of Deformation: The same deformations as considered in the strip analysis were included in this analysis.

Loading Conditions: The same four load cases (Table I) described for the strip analysis were used in this analysis.

Load Incrementation: Twenty load steps were used to take the loads to their full value.

4) Results and Conclusions

The results of the computer analysis included the element stresses and strains at each increment of loading as well as the accumulated stresses and strains at the end of each increment. Stress and strain is

obtained at each integration point in the element. In addition, both incremental and accumulated displacements were obtained at each element node. The strain results obtained from the analyses are the changes in strain from the initial deformed configuration. Hence, these results should be added to the existing strains in the deformed liner plate.

Existing Strains: The existing bending strains weee calculated from the actual deformed geometry ± 0.0009 in/in and ± 0.0133 in/in for the largest and highest strained deformations, respectively. The existing membrane strains were calculated by fitting a cubic curve to the deformations and evaluating the resulting changes in length. These strains are evaluated as +0.0009 in/in and +0.0050 in/in for largest and highest strained deformations, respectively.

The resulting extreme fiber strains for the existing deformations are therefore:

a) Large deformation

$$e_{inside} = 0.0009 + 0.0009 = 0.0018$$

$$e_{outside} = 0.0009 - 0.0009 = 0.0000$$

b) Highest strained deformation

$$e_{inside} = 0.0050 + 0.0133 = 0.0183$$

$$e_{outside} = 0.0050 - 0.0133 = -0.0083$$

Resulting Strains: The meridional strains at the extreme fibers of the liner at the crest of the assumed deformations are presented in Table II for both the strip and axisymmetric models.

The results indicate that:

a) the large deformation will move back to the concrete under the loads associated with the loss-of-coolant accident or the test condition;

b) the highest strained deformation will remain in essentially the same condition under these loads;

c) all resulting strains are substantially below the acceptable value of 0.044 for combined membrane and bending;

d) the results of the two independent analyses are in good agreement.

Stud Displacements: In addition to verifying that the resulting strains for the insulated liner meet the acceptance criteria, a check was made of the maximum stud shear deformations. These values were compared to the ultimate shear displacement capacity of 0.167 inches gives in Reference 3. These displacements are tabulated in Table III. The values presented are for the studs directly above and below the linear deformations.

The results indicate that:

a) the largest stud displacement occurs below the highest strained deformation under the loads associated with a LOCA:

b) this displacement is well below the ultimate stud capacity;

c) the strip and axisymmetric models substantially the same results.

Question B

Determine whether or not it will be necessary to insulate the liner in the non-deformed area where studs have been found to be missing.

Answer

The liner has been insulated around the full 360° to cover the non-deformed area where studs have been found to be missing.

Question C

Determine the effects of the transmition between the insulated and non-insulated area of the liner.

Answer

1. Statement of Problem

To verify that considering the effect of thermal load above the insulated portion of the liner does not cause the containment liner strains to exceed acceptable limits.

2) Statement of Criteria

See Section III-A of this report.

3) Analysis Methods

The same analysis procedure as described in Section IIIA was used for this problem. However, only a strip analysis was used for the liner model with the long deformation and only the axisymmetric analysis was used for the liner model with the highest strain deformation.

In this analysis, the top four elements of the model (see Figures 3 and 5) were considered not to be insulated. In this area, a thermal gradient consisting of 245°F on the liner and 120°F to 0°F in the concrete was assumed. This corresponds to the LOCA thermal gradient.

The other loads included:

Pressure = 47 psi

Dead Load = 1.05(105.6) = 110.9^k/ft (applied at top of model)

Seismic = 125^k/ft compression (applied at top of model)

4) Results and Conclusions

a) The results of the strip analysis for the model with long deformation show that the final liner plate strains at the crest of the deformation are:

$$e_{outside} = -0.0001 + 0.0000 = -0.00001$$

$$e_{inside} = -0.0023 + 0.0018 = -0.0005$$

These strains are within the acceptable limits.

The stud displacements above and below the deformation for this case are:

0.004 in.

0.023 in.

These displacements are also within acceptable limits.

Comparing these results to those reported for load Case 3 in Table II indicates that no significant change occurred in the liner strains, however, some change was observed in the stud displacements.

b) The results of the axisymmetric analysis for the model with the highest strain deformation show that the final liner plate strains at the crest of the deformation are:

$$e_{outside} = 0.0006 - 0.0083 = -0.0089$$
$$e_{inside} = +0.0009 + 0.0183 = +0.0192$$

These strains are within acceptable limits.

The stud displacements above and below the deformation for this case are:

0.028 in.

0.009 in.

These displacements are also within the acceptable limits.

Comparing these results to those resulted for load Case 3 in Table II indicates that no significant change occurred in the liner strains, however, some change was observed in the stud displacements.

Question D

What is the effect of the interruption of the meridional stress flow caused by the presence of the deformations?

Answer

Based on the results of the axisymmetric and strip models, which indicate that the predominant strains are flexural, there will be no significant effects caused by the interruption of the meridional stress flow by the presence of the deformations.

Question E

What is the effect of cyclic Earthquake Loads and Periodic Leak Rate Testing Loads on the allowable strains.

Answer

Based on test results in Reference (4), we have determined that a strain range of 6.5 percent has a fatigue endurance limit in excess of 400 cycles. The allowable strains are 4-5 percent which is less than the above-mentioned 6.5 percent. The number of cycles of pressure testing during the plant life is about seven cycles. These cycles of load will be approximately 1/2 of the pressure load during initial plant

testing, therefore, the maximum allowable strains will be 1/2 of the specified allowables. The answer to Question 2.8(f) of the Unit No. 3 PSAR indicates a range of 25-50 significant earthquake cycles. More recent work indicates that a typical earthquake used in designing Nuclear Power Plants produces twenty equivalent maximum earthquake cycles. The strains produced by the earthquake will be well below the specified allowable strains.

Based on the above information from Reference (4), fatigue will have negligible effects on the allowable strains specified at the December 7, 1973 AEC meeting for the following reasons:

1. Magnitude of allowable strains and number of cycles will be below the values developed from Reference (4).

2. The results of analyses which are discussed in Section IIIA of the report indicate that the maximum change in strain under LOCA, test pressure or seismic conditions is approximately .4 percent, which is well below the specified allowable of 4.4 percent.

The information in Reference (4) is based on AISI-1018 steel which is a low carbon steel. It is felt that the properties of this steel are sufficiently close to the ASTM A-442 liner material to make the above comparisons, especially when considering the wide margin of safety which apparently exists.

Question F

What is the effect of the two-dimension loading on the allowable strains presented during the AEC meeting of December 7, 1973 which are evolved from ASME Section III, Division I allowable which considers uniaxial loading conditions.

Answer

The effect of two-directional strain on the allowable strains for the analysis of the deformed liner plate was considered in the following manner:

The Von Mises-Henky yield criteria for yielding states that the distortion energy for all conditions of loading is constant. The formula for distortion energy is:

$$U_d = \frac{1+\mu}{3}\left[\sigma_1^2 + \sigma_2^2 + \sigma_3^2 - \sigma_1\sigma_2 - \sigma_2\sigma_3 - \sigma_3\sigma_1\right]$$

equating the simple tension case where:

$$\sigma_1 = \sigma_y$$
$$\sigma_2 = 0$$
$$\sigma_3 = 0$$

to the biaxial tension case

$$\sigma_3 = 0$$

one obtains:

$$\sigma_y^2 = \sigma_1^2 + \sigma_2^2 - \sigma_1\sigma_2 \qquad \text{(Equation (1))}$$

For our case, the allowable strain could be as high as 5% in the meridional direction with a maximum strain of .1% in the circumferential direction.

Solving Equation (1) for the case where the allowable strain is 50 times the strain in one direction, we find that the strain in the other orthogonal direction can be 49.50 or almost equal to the allowable.

Although it is recognized that the Von Mises criteria above is for stresses within yield and is not necessarily applicable to strains in excess of yield. The above exercise shows that a strain of low magnitude has negligible effect on much higher

strains due to the quadradic nature of the relationship in Equation (1). As shown in Section IIIA, Table II, the maximum calculated strain for LOCA, test pressure and seismic loadings is less than 2%, or 1/2 of allowables; therefore, a slight reduction in the allowable due to a small strain in the orthoganal direction will have little effect on our conclusions in Section IV.

Question G

What was the temperature of the concrete during the Feedwater Line Break Incident.

Answer

As indicated in the main body of the report, the maximum steam temperature at Loop No. 22 outside of the break was 325°F. Considering the extensive dilution of the steam with air and water which must have occurred, the resulting liner temperature at point of impingement was less than 300°F.

ASME Section III, Drawing 2, Section CC3430, states that, "local areas are allowed to reach 650°F from steam and/or water jets in the event of a pipe failure". Consequently, it is not believed that the concrete was damaged due to temperature effects.

Question H

Discuss the details of the plate taper at the transition of the 1/2" or 3/4" plate to 3/8" plate.

Answer

All transitions from thicker plate to thinner plate in the area of the deformed liner are taped to a slope of 4 to 1 to minimize stress concentrations.

Question I

Do the technical specifications indicate a maximum bulge in the liner plate above which the plant cannot operate until formal resolution of the problem is documented with the AEC.

Answer

Technical Specifications indicate that no such requirement exists for Indian Point Unit No. 2.

Question J

What is the effect of a postulated row of sheared studs at the top of the 3/4" plate.

Answer

A row of sheared stud, at the top of the 3/4" plate has no effect on our conclusions in Section V of this report since insulation has been extended approximately 18'-0" beyond this location. In addition, there is no measured information in the 3/4" plate. Therefore, shear loads will not be significant in this area.

IV. Addition of Insulation

As a result of the analysis of the deformed liner plate, and its ability to resist LOCA, test pressure and seismic loads within the allowable strains proposed during the AEC meeting of December 7, 1973, as discussed in Section IIIA of this report, the liner plate thermal insulation has been extended as follows:

a) The full 360° around containment from Elevation 63'-8-1/2" to Elevation 81'-9".

b) In addition, insulation is required where the Main Steam and Feedwater Lines extend up and over the crane wall to the operating floor level. This means insulation is required to Elevation 90'-9-1/4" in the following areas:

1. 6'-0" counterclockwise of Column 6 to 6'-0" clockwise of Column 5.

2. 7'-0" clockwise of Column 13 to 2'-0" counterclockwise of the south extension of the North South Building center line. See Figure 7 for a clearer representative of this required information.

The sandwich insulation which will be used in the areas specified above will consist of the following materials (see Figure 6).

1. 1/16" commercial grade pure asbestos paper backing adjacent to the liner plate on the unexposed face.

2. 1-1/2" thick FOAMGLAS^R insulation with density of 9 #/ft^3, as manufactured by Pittsburgh Corning Corporation.

3. 0.025" stainless steel jacket on the exposed face.

4. The adhesive bonding the FOAMGLAS^R to the asbestos paper is Cadoprene No. 434 and bonding the stainless steel jacket to the FOAMGLAS^R is Cadoseal No. 700 by Epolux Manufacturing Corporation.

The above insulation sandwich is nearly identical to that specified as the second alternate to UE&C Specification 9321-05-16-5. This insulation was

approved by Westinghouse for use in the containment and meets the requirements of NEPIA for use inside the containment structure. The only difference is that the approved insulation had a 0.019" stainless steel jacket, and the adhesives were EC-1357 by 3M Company. These minor changes will not affect the thermal insulating properties of the sandwich.

V. Summary and Conclusions

As the apparent result of the break in Boiler Feed Line No. 22, an area of the Containment Liner Plate was deformed and nine studs appeared to be damaged. During the course of Con Edison's investigation, it was discovered that two rows of studs were missing for 360° around the containment. The deformed liner area was MP tested to show that liner integrity had not been violated by the incident. A program of analysis by UE&C and testing by Con Edison was developed to show that the proper fix for the situation was to extend liner insulation into the the deformed region. The analysis showed that liner strains under LOCA, test pressure, and seismic conditions would remain within allowable strains specified during an AEC meeting of December 7, 1973. At this meeting, the AEC indicated general agreement with our recommended program. The bend tests on liner plate bent according to the observed deformations, and the results of a 47 psi pressure test by Con Edison increased the confidence in the analytical results and supported the recommendation to extend liner insulation. On the basis of the above analysis and tests, the liner insulation was extended as discussed in

Section V of the Report with FOAMGLAS^{R} sandwich insulation which had previously been approved for use on Indian Point Unit No. 3.

References

(1) "Summary of Meeting Held December 7, 1973, Rethe Containment Liner", as Issued December 14, 1973 by R. W. Woodruff, Operating Reactors Branch #1, USAEC Washington, D. C.

(2) MARC-CDC User Information Manual, Volumes I, II and III, Control Data Corporation, Cybernet Publications Department, Minneapolis, Minnesota.

(3) "Design Data-Nelson Concrete Anchor", Gregory Industries, Inc., Lorain, Ohio 1961.

(4) Benham, P. P. and Ford, H., "Low Endurance Fatigue of a Mild Steel and Arc Aluminum Alloy", Journal of Mechanical Engineering Science, Volume 3, No. 2, 1961, pp. 119-132.

TABLE I

Load Cases

LOAD	LOAD CASE	PRESSURE(1)	DEAD LOAD(2)	SEISMIC(3	THERMAL(4)	REMARKS
I) 1.08 in. peak deformation in 56 in. above ½ in. plate						
1.	Test	1.15 Pa	0.95D	0	0	Concrete cracked in two directions
2.	LOCA	1.0 Pa	0.95D	1.0E(tension)	0	Concrete cracked in two directions
3.	LOCA	1.0 Pa	1.05D	1.0E(comp)	$1.0T_0$	Concrete cracked circumferentially
4.	Normal	0	1.05D	0	$1.0T_0$	
II) 1.25 in. peak deformation in 28 in. above 3/4 in. plate						
1.	Test	1.15 Pa	0.95D	0	0	Concrete cracked in two directions
2.	LOCA	1.0 Pa	0.95D	1.0E(tension)	0	Concrete cracked in two directions
3.	LOCA	1.0Pa	1.05D	1.0E(comp)	$1.0T_0$	Concrete cracked circumferentially
4.	Normal	0	1.05D	0	$1.0T_0$	

(1) Pa = 47 psi

(2) D = 105.6 k/ft. applied at top of model (z = 280 in.)

(3) E = 125 k/ft. applied at top of model (z = 280 in.)

(4) T_0 taken as 0° F outside 120° inside

TABLE II

Extreme Liner Meridional Fiber Strain
at Mid-Height of Deformation
(Strain in inches/inch)

	LOAD CASE	STRIP MODEL						AXISYMMETRIC MODEL					
		INSIDE FIBER(1)			OUTSIDE FIBER(2)			INSIDE FIBER			OUTSIDE FIBER		
		e_o(3)	Δe(4)	e_T(5)	e_o	Δe	e_T	e_o	Δe	e_T	e_o	Δe	e_T
I) 1.08 inch deformation in 56 inches	1. Test	+0.0018	-0.0015	+0.0003	0.0000	+0.0008	+0.0008	+0.0018	-0.0018	0.0000	0.0000	+0.0010	+0.0010
	2. LOCA	+0.0018	-0.0012	+0.0006	0.0000	+0.0013	+0.0013	+0.0018	-0.0014	+0.0004	0.0000	+0.0014	+0.0014
	3. LOCA	+0.0018	-0.0019	-0.0001	0.0000	-0.0001	-0.0001	+0.0018	-0.0010	+0.0008	0.0000	-0.0003	-0.0003
II) 1.25 inch deformation in 28 inches	1. Test	+0.0183	-0.0039	+0.0144	-0.0083	+0.0040	-0.0043	+0.0183	-0.0033	+0.0150	-0.0083	+0.0021	-0.0062
	2. LOCA	+0.0183	-0.0032	+0.0151	-0.0083	+0.0043	-0.0040	+0.0183	-0.0024	+0.0159	-0.0083	+0.0028	-0.0055
	3. LOCA	+0.0183	+0.0001	+0.0184	-0.0083	-0.0002	-0.0085	+0.0183	+0.0003	0.0186	-0.0083	-0.0002	-0.0085

(1) Inside fiber refers to fiber on the interior of Containment
(2) Outside fiber refers to fiber on concrete side of liner
(3) e_c is the initial (i.e. existing) fiber strain
(4) Δe is the calculated fiber strain due to the various loadings
(5) e_T is the total resulting fiber strain

TABLE III

Stud Displacements in Meridional Shear Direction at Extremeties of Deformed Area (Displacements in Inches)

	Load Case	STRIP MODEL (Above) (Below)	AXISYMMETRICAL MODEL (Above) (Below)
I. 1.08 inch deformation in 56 inches	1. Test	-0.0162 0.0261	-0.0094 0.0214
	2. LOCA	-0.0148 0.0288	-0.0109 0.0238
	3. LOCA	-0.0163 0.0084	-0.0110 0.0022
II. 1.25 inch deformation in 28 inches	1. Test	-0.0500 0.0584	-0.0287 0.0538
	2. LOCA	-0.0496 0.0674	-0.0334 0.0647
	3. LOCA	-0.0027 -0.0108	0.0010 -0.0109

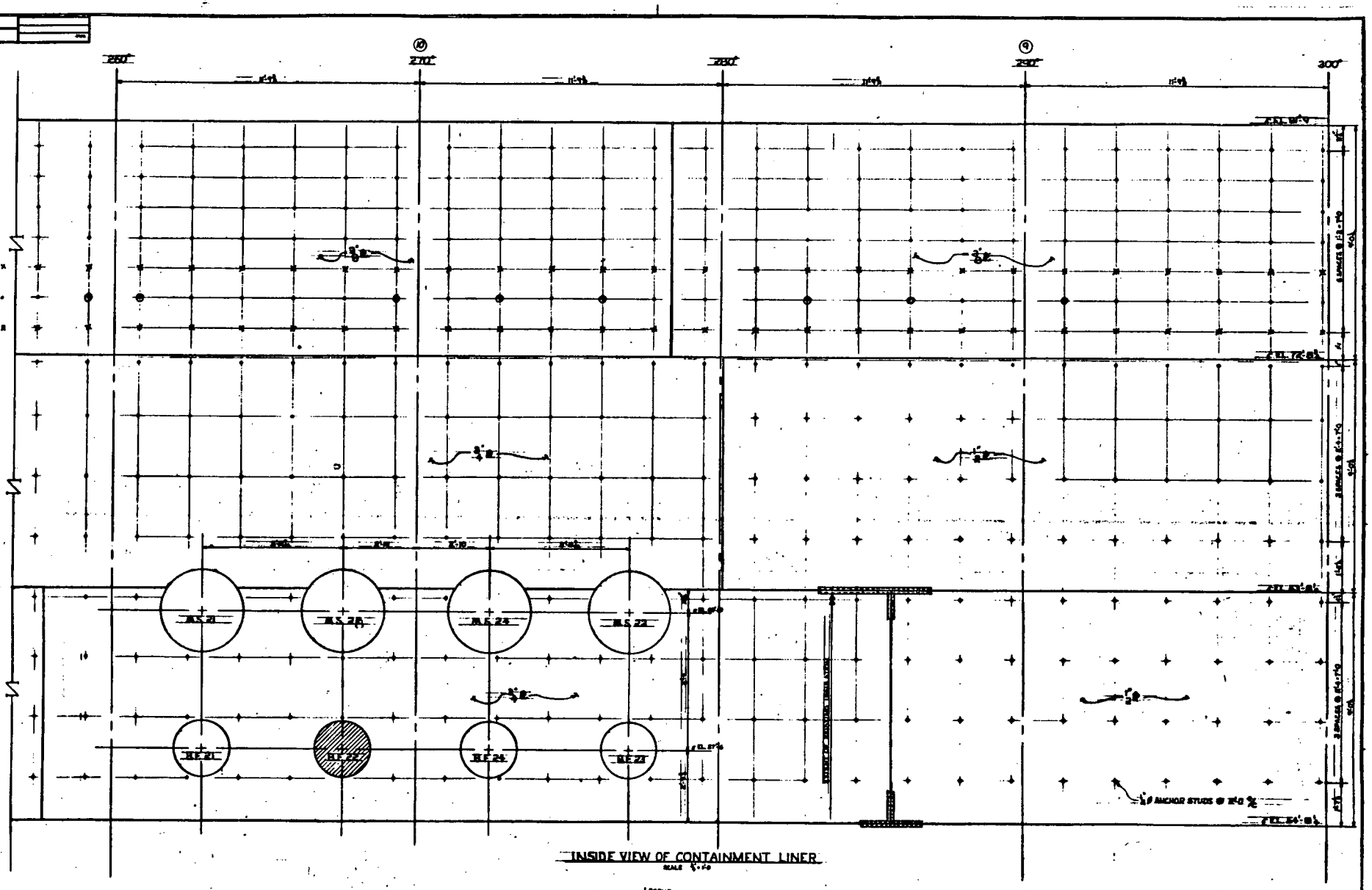

CONSOLIDATED EDISON CO.

STUD SURVEY

FIGURE 1

IV-35

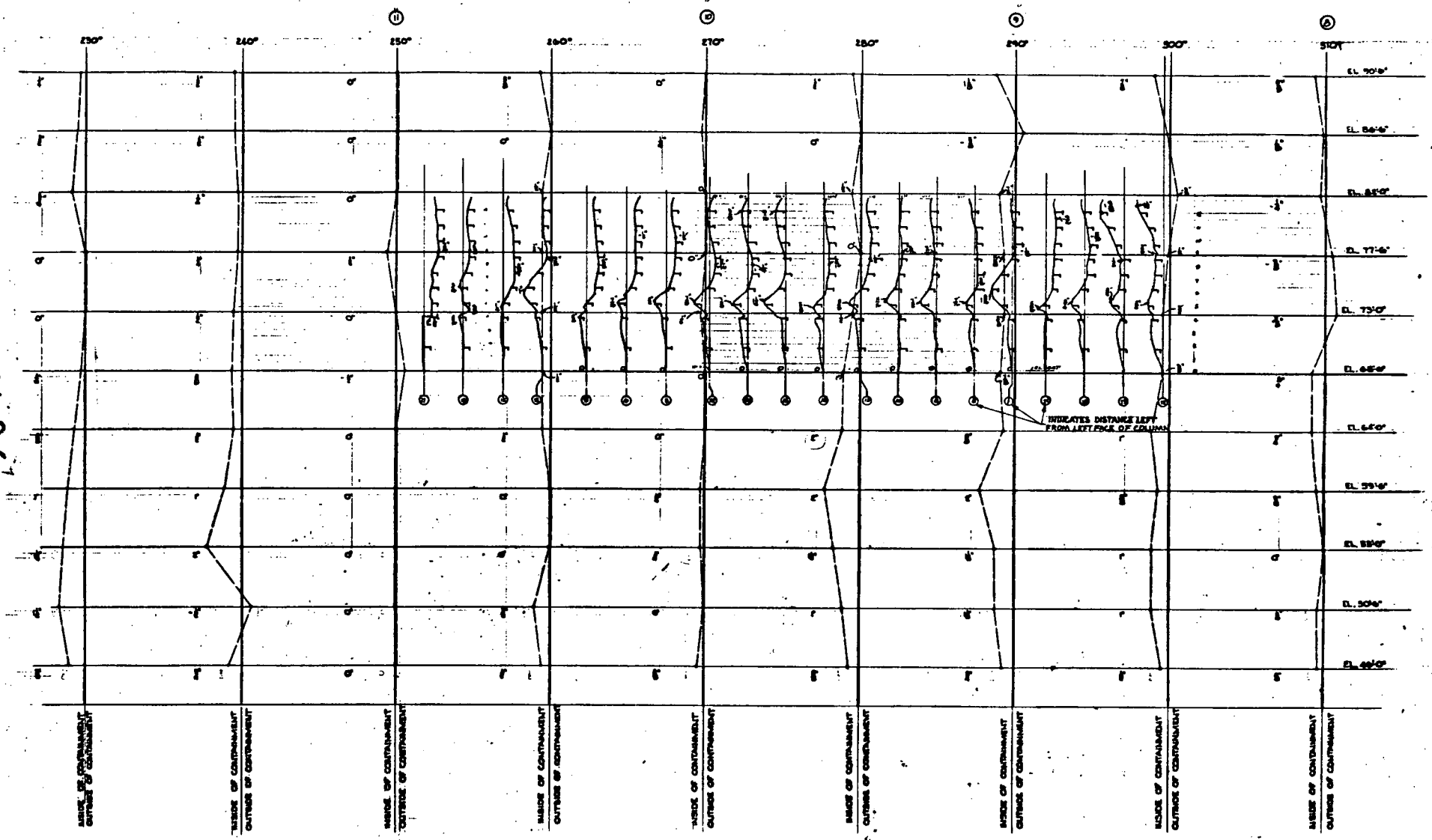

LINER SURVEY PROFILES

SCALE: 1/8"=1'-0" VERT.
SCALE: 1/8"=1' HORIZ.
— — — INDICATES SURVEY TAKEN 2-19-68 TO 2-28-68
——— INDICATES SURVEY TAKEN 11-17-72

CONSOLIDATED EDISON CO.
INDIAN POINT STA.
LINER SURVEY PROFILES

FIGURE 2

IV-36

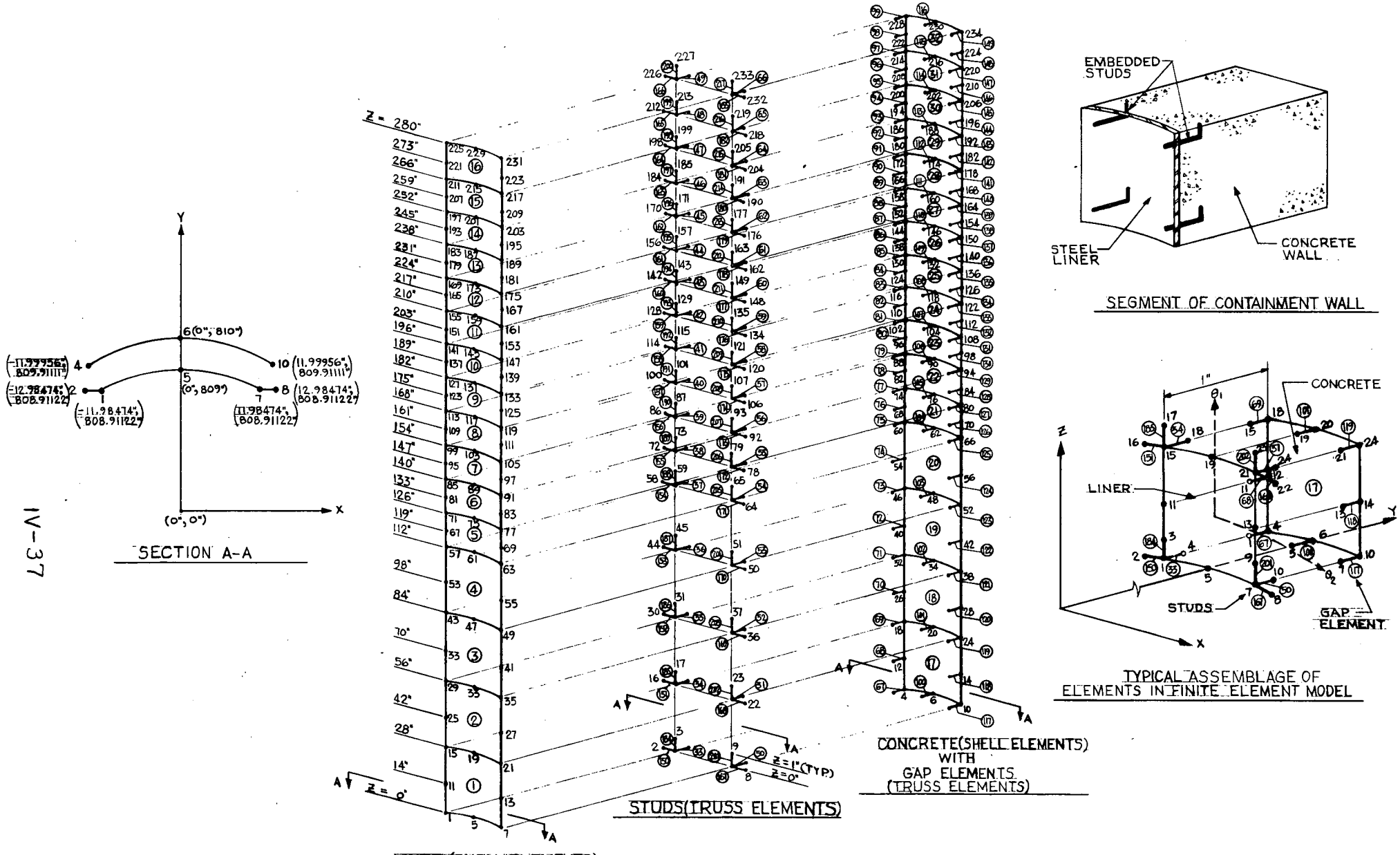

EXPLODED VIEW OF COMPLETE SHELL-SHELL FINITE ELEMENT MODEL

NOT TO SCALE

FIGURE 3

STRESS - STRAIN CURVE

FOR TENSION

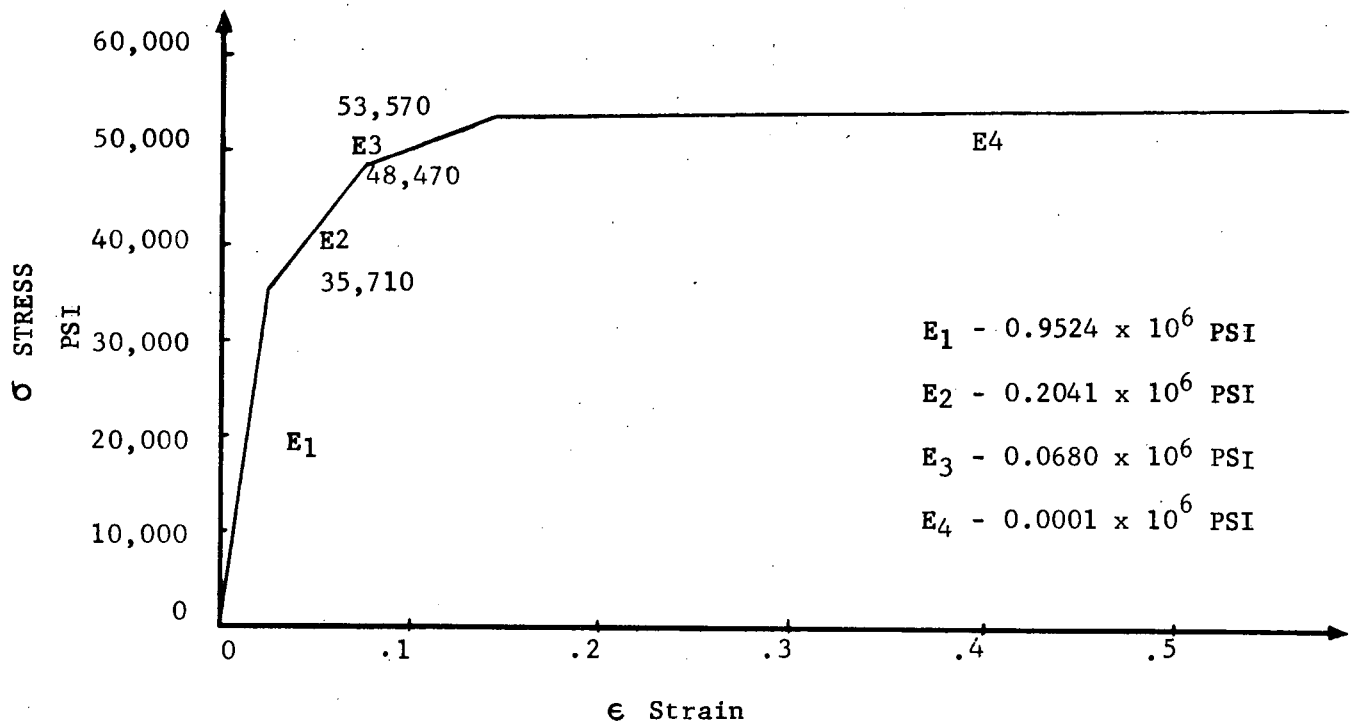

STRESS - STRAIN CURVE
FOR SHEAR

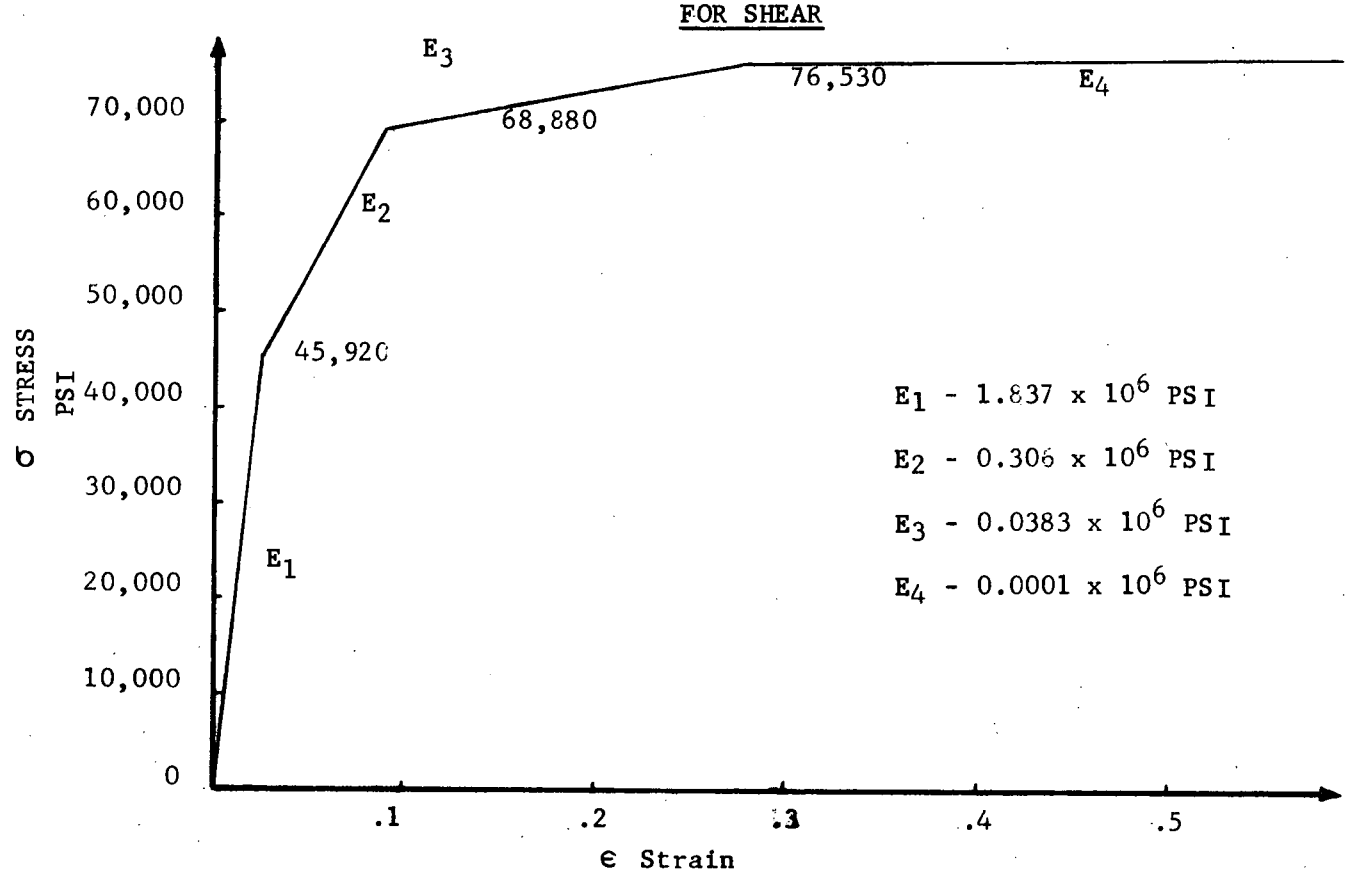

IDEALIZED STRESS STRAIN CURVES FOR STUDS FIGURE 4

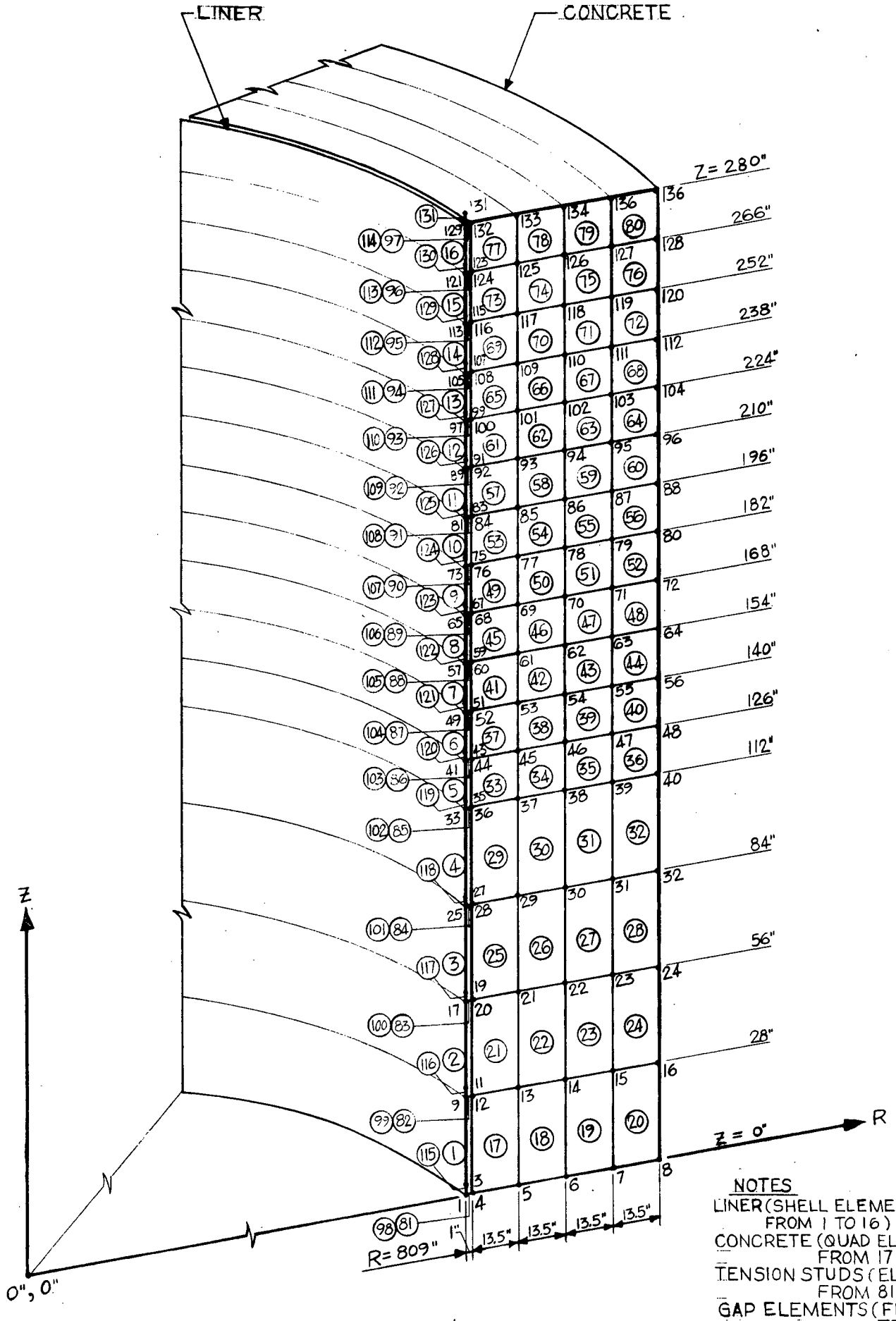

NOTES
LINER (SHELL ELEMENTS FROM 1 TO 16)
CONCRETE (QUAD ELEMENTS FROM 17 TO 80)
TENSION STUDS (ELEMENTS FROM 81 TO 97)
GAP ELEMENTS (FROM 98 TO 114)
SHEAR ELEMENTS (FROM 115 TO 131)

FIGURE 5 AXISYMMETRIC FINITE ELEMENT MODEL

NOT TO SCALE

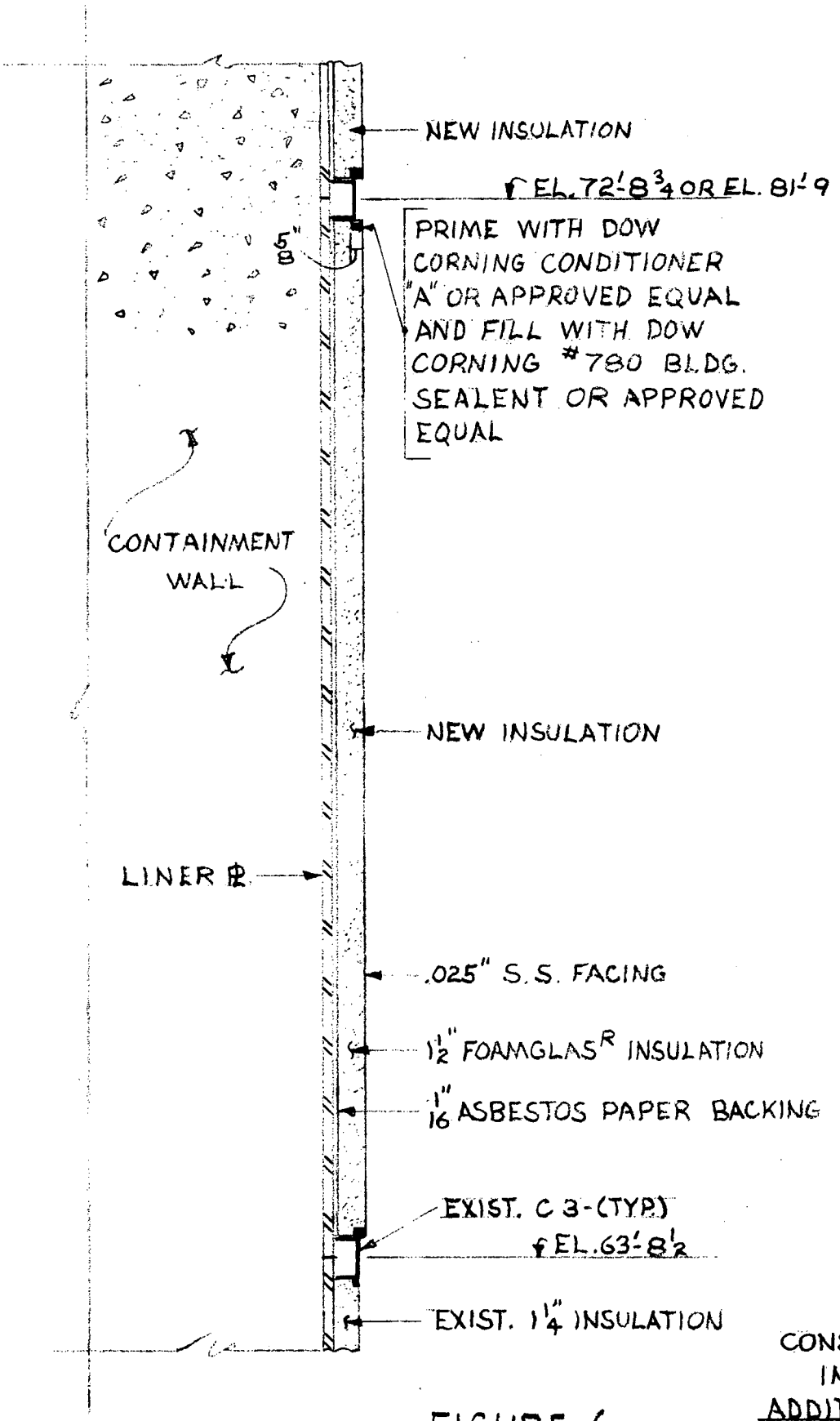

FIGURE 6

IV-40

CONSOLIDATED EDISON CO.
INDIAN POINT STATION
ADDITIONAL LINER INSULATION
FOR CONTAINMENT-UNIT # 2
DETAILS

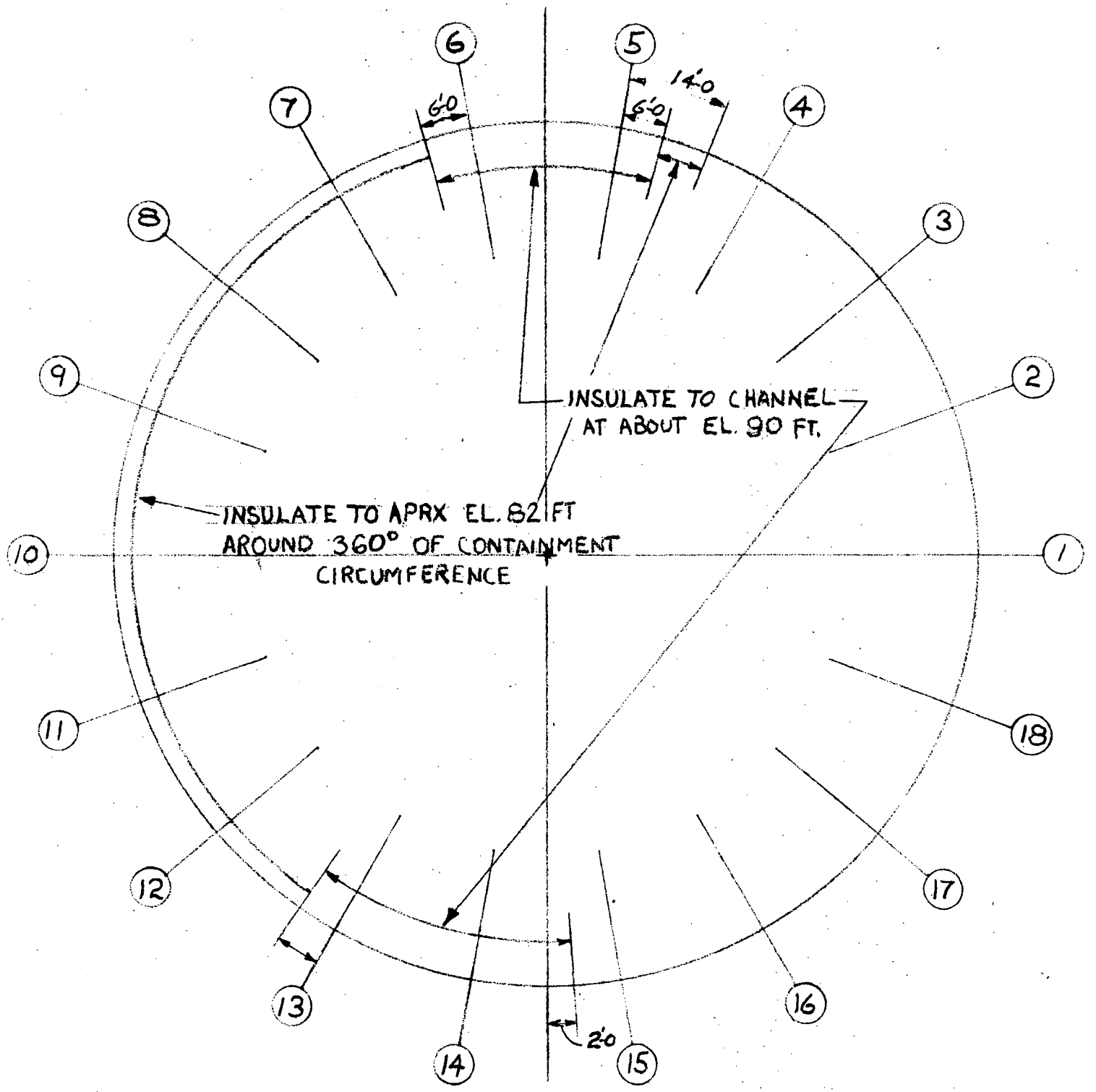

NO SCALE

CONSOLIDATED EDISON CO.
INDIAN POINT STATION
ADDITIONAL LINER INSULATION
FOR CONTAINMENT- UNIT 2
PLAN

FIGURE 7

Appendix V

Evaluation of Feedwater Line Check Valve

EVALUATION OF FEEDWATER LINE CHECK VALVE

INDIAN POINT UNIT NO. 2

January 11, 1974

Approved: J. Dainora

J. Dainora
Manager, Mechanical Systems Analysis

United Engineers & Constructors, Inc.
Philadelphia, Pennsylvania

INDIAN POINT UNIT NO. 2 - FEEDWATER LINE FAILURE

FEEDWATER LINE CHECK VALVE EVALUATION

TABLE OF CONTENTS

A. SUMMARY

I. OBJECT

II. INVESTIGATION PROGRAM

III. CONCLUSIONS

IV. RECOMMENDATIONS

B. CHECK VALVE EVALUATION PROGRAM

I. GENERAL

II. FIELD INSPECTION OF THE CHECK VALVES

III. CASE HISTORY

IV. PRELIMINARY TESTS

V. PERFORMANCE EVALUATION

C. ANALYSIS OF CHECK VALVE DESIGN

I. GENERAL DISCUSSION

II. TYPES OF CHECK VALVES

III. DESIGN FEATURES OF CRANE CHAPMAN TILTING DISC CHECK VALVES

A. Dynamic Characteristics
B. Materials of Construction

D. RESULTS AND CONCLUSIONS

E. EXHIBITS

DWG. PB - Crane List 973 Press. Seal Tilting Disc Check Valve

A. SUMMARY

I. OBJECT

The objectives of this evaluation are:

A. To determine if any malfunction or design deficiency of the four (4) Crane Chapman List 973 check valves was instrumental in causing a dynamic transient to occur in the feedwater system.

B. To recommend necessary modifications and or redesign of the valves.

II. INVESTIGATION PROGRAM

Investigation of the problem included:

A. Field observation of damage

B. Field testing of valve operation

C. Analysis of design features

D. Vendor consultation & discussions

E. Analysis of valve disc position at system failure conditions

F. Evaluation, conclusions and recommendations

The investigation indicated that the check valve in feedwater Line #22 was not the initiating mechanism causing the piping failure. Calculations at seven (7) percent power (200,000 lb/hr of water at 195°F), the condition at which the pipe failure took place, indicated that the check valve disc was just cracked off its seat (less than 25 percent open). At this partially open position, the sudden closing of the disc would not cause any appreciable water hammer effect on the piping system. The apparent loosening of the lock plate bolts in several of the valves was probably caused by slamming of the valve disc,

due to combination of reverse flow and fluttering during the low flow conditions. Reverse flow could have been caused by different pressure levels in the steam generator and fluttering by the hunting of the regulator control valves, at low flow conditions.

III. CONCLUSION

It is our opinion that once the proposed modifications to the regulator valve by-pass system, to the feedwater piping and steam generator level control are completed, the fluttering and slamming of the check valve disc should be eliminated or minimized sufficiently to enable the check valves to continue to perform satisfactorily without additional check valve modification.

IV. RECOMMENDATIONS

Because it appears that the Crane-Chapman check valve did not contribute to the feedwater piping failure, it is our recommendation that the check valves in the feedwater system should not be modified or redesigned, before returning them to service. However, it is recommended that the lock plate bolts be tightened to their original condition, before reassembling the valves.

B. CHECK VALVE EVALUATION PROGRAM

I. GENERAL

The program included the field inspection of the check valves and assessment of any past operational damage, a gathering of case history and background information, and a series of preliminary field tests. This information was then carefully analyzed and the performance evaluated to determine the adequacy of the check valves design.

In subsequent sections of this report, check valve designations such as number 22 for example; refers to the respective valve installed in the feedwater line to steam generator number 22.

II. FIELD INSPECTION OF THE CHECK VALVES

The Mechanical Systems Analysis Group of United Engineers and Constructors Inc., inspected the check valves and gathered other pertinent information relative to the evaluation program of the feedwater line check valves.

The following check valve components were inspected and observed:

A. Condition of Disc

Good condition - Stellite facing good condition

B. Condition of Seat Ring

Stellite facing good condition.

C. Condition of Hold-Down Lock Plate Bolts

Inspections, indicated clearance under the lock plate retainer clips on three (3) out of the four (4) check valves. The bolts apparently loosened within the helicoil inserts.

II. FIELD INSPECTION OF THE CHECK VALVES

D. Condition of the Spring Bumper

On disc-type check valves, the shape and weight distribution of the discs are such that, with the loss of flow in the normal flow direction, the disc will close to prevent reverse flow. In a horizontally-mounted check valve, gravity aids the closing of the disc, when the normal flow stops. However, when mounted in the vertical direction, the gravity component action on the disc in the closing direction is somewhat reduced, so that an auxiliary bumper device is sometimes used to aid closing from the full open position.

The spring bumper device on valve No. 23 was inspected and tested by compressing and then releasing. The stiffness of the spring was found to be so weak that it is doubtful whether any aid is given to help return the disc to the closed position. However, it was found that the weight distribution and center of gravity of the disc was such that the disc would normally return to the closed position, when the normal flow ceased, without a need for auxiliary devices.

Measurements were taken which indicate that when the disc is full open, the spring bumper is compressed approximately one inch of its three (3) inch compression stroke.

E. Condition of Stops

The design of the check valve is such that travel in the opening direction is limited by an internal stop. In the closing direction, the valve disc travel is limited by contact with

II. FIELD INSPECTION OF THE CHECK VALVES (continued)

E. Condition of Stops (continued)

the stellite seat on the seat ring. If damage or wear occurs on the seat, a secondary stop will limit travel after approximately 1/16" to 1/8" additional travel. On valve No. 23 the condition of the stops did not show any apparent wear or damage during its limited operating usage.

F. Condition of Hinge Pin

The disc was rotated through its normal range from full open to full closed, with an additional rocking motion on the hinge pin to check for freedom of motion. Information from the Engineering Department of the Crane Chapman Company gave the normal pin clearance as .001 to .0045." The freedom of motion and lack of looseness in the hinge, indicated that the valve components were properly manufactured within tolerances.

G. Other Structural Damage

The complete examination indicated that the valve design is basically sound with no apparent structural damage except for the slight loosening of the lock plate bolts, in three of the four valves. This unusual condition, may be attributed to flow at low power levels, or to unusual reverse flows in the system.

III. CASE HISTORY

On October 12, 1973, after a "loss of field trip" the check valve in feedwater Line No. 22 was inspected.

Examination of this check valve indicated that the two lock plate bolts holding the disc seat subassembly to the body were bent, the helicoil inserts damaged and the seat ring gasket below the seat was twisted. The damaged parts were replaced and the plant returned to service.

Examination of the four check valves in the feedwater system after the November 13, 1973 incident, indicated that the check valves in Lines No. 21, 22 and 24 were disturbed only to the extent that the lock plate bolts were loosened. Other parts of the valve were undamaged. The check valve in Line No. 22 which had been damaged previously on October 12, 1973, received the greatest shock, as indicated by the amount of clearance the lock plates developed. The lock plate held by these bolts showed a clearance of 0.056" and 0.157" respectively for the left and right sides. The check valve in Lines No. 21 & 24 showed the lock plate bolts slightly loosened, while the check valve in Line 23 indicated no clearance at the lock plates.

IV. PRELIMINARY TESTS

A. Disc Closing Action Due to Gravity in the Dry Condition

On valve No. 23, which had been dismantled for inspection, the disc was checked for operation in the dry condition. It was found that the weight and center of gravity was so distributed, that from the full open position the disc would tend to close normally, even without any assistance from the spring-loaded bumper device.

IV. PRELIMINARY TESTS (continued)

B. Effectiveness of Stops in the Closing and Opening Modes

The stop in the open direction does limit disc travel in the open position. The full open limit is designed by the manufacturer to permit the maximum flow with a minimum of pressure drop.

In the closed position, contact is made by the disc on the seat. The stop on the closed direction is secondary, not coming into action, unless wear or damage to the seat permits an additional 1/16" to 1/8" travel.

C. Effectiveness of the Spring Bumper

As discussed earlier under the valve inspection section, the spring bumper installed in valve No. 23 appears to be too weak to be effective. However, our study indicated that the valve disc tends to close normally even without this device.

D. Pin Clearance and Friction Effects

The movement of the disc (valve No. 23) about the hinge pins appears to be free and smooth, indicating that the valve components were properly manufactured.

E. Position of the Disc in the Full Open Mode

Observations made with the disc full open against the stop indicated that the downstream end of disc was in line with the outer wall of the the valve body.

V. PERFORMANCE EVALUATION

The field observations, inspections, field tests, together with the case history and background information were then carefully analyzed. Results and conclusions are discussed subsequently.

C. ANALYSIS OF CHECK VALVE DESIGN

I. GENERAL DISCUSSION

Slamming of check valves is the result of the failure of the valve disc to reach its closed position before fluid flow reversal. The reversal flow velocity at instant of closure, the physical characteristics, particularly density and compressibility of the fluid and the length of pipe downstream from the valve all affect the severity of the pressure surge resulting from check valve slams.

In the Indian Point No. 2 pipe system, the slamming of check valves could conceivable have been initiated by reverse flow originated by different pressure levels in the steam generators. If the reverse flow from the operating loop rapidly closed the check valve in the non-operating loop, the slam could possibly have caused a destructive pressure pulse.

To determine if this was the case, the position of the check valve disc at low power condition (7 percent flow) at which the pipe system damage took place, was throughly investigated. Calculations indicated that the check valve tilting disc was just cracked off the seat (less than 25 percent open) at this condition. At this almost closed position, it can be concluded that there is no possibility of the check valve remaining open, during periods of backward flow. Should the disc be slammed closed from this almost closed position by reverse flow, the impact effect would be minimum, and would not contribute any excessive pressure surges to the piping system, even if it should create a loud noise.

II. TYPES OF CHECK VALVES

There are three basic type check valves, including the swing check, the lift check and the stop check valve. A variation of the swing check is the tilting disc type.

II. TYPES OF CHECK VALVES

By far, the tilting disc is the simplest and most reliable type having a relative low pressure drop through a high cross sectional area with little change of direction of flow. The other types (lift and stop check) not only have a greater pressure loss through the valve body, but there is also a greater tendency for the disc to stick after periods of operation. The choice of the tilting disc check valve for this application was the best type from an engineering standpoint.

III. DESIGN FEATURES OF CRANE CHAPMAN TILTING DISC CHECK VALVE

A. Dynamic Characteristics

1) Closing with minimum slamming effect

The disc on the tilting disc type check valve has a shorter distance to travel, hence arrives at the seat earlier, with a lower velocity, which in turn minimizes or eliminates the slamming effect on the seat.

2) Reduced Loss of Head

The Crane Chapman tilting disc valve design is pivoted just above its center, and being partially balanced, the greater part of its weight is carried by the hinge pins. Therefore, the effort to maintain it in the open position is very slight. The disc also has an "Aero Foil Section" shape giving desirable lifting properties and very low resistance to the flow when in the the full open position. Disturbances to the flow appear to be kept to a minimum, since the internal streamlined body is designed to have no pockets or sudden enlargements.

III. DESIGN FEATURES OF CRANE CHAPMAN TILTING DISC CHECK VALVE (continued)

A. Dynamic Characteristics (continued)

3) Minimum Flutter of Disc at Full Open Position

The disc of the Crane Chapman tilting disc is partially balanced. Therefore, under normal flow in the full open position it is held firmly against the stops in the body. In this position the disc is at rest and does not swing or flutter, minimizing wear on the pivot pins.

4) Stability of Disc at Partial Position

The "Aerofoil Section" and partially balanced disc, while quite helpful in performance in the full open position could possibly cause some disc flutter at very low flow conditions. Operation at this condition is usually rare or for short periods of time. If operations are frequent at small openings, a dashpot should be considered to absorb some of the energy in the disc.

B. Materials of Construction Used in Crane Chapman Tilting Disc Check Valve List 973

Body	A216	WCB
Seat Ring	A216	WCB
Disc	A216	WCB
Bonnet	A201	B
Retaining Cap	A216	WCB
Lock Ring	A216	WCB
Pivot Pin	A276	Type 410 Malcomized
Bushings	A276	Type 304
Facing Surfaces	Stellite overlay	

The body, seating disc, retaining cap and lock ring are all made of A216 WCB, a cast carbon steel material. This material is excellent for high pressure system components, has high strength at elevated temperature and can be easily field-welded into the piping system. While carbon steel is not corrosion resistant, an allowance can be designed into the valve for long service life. Corrosion can also

B. Materials of Construction Used in Crane Chapman Tilting Disc Check Valve List 973 (continued)

be reduced to a very low value by controlling the oxygen in the process fluid.

The pivot pin and bushings are made from A276 Type 410 and Type 304 stainless steel respectively, both possessing high strength, good corrosion resistance and good resistance to high temperatures. In addition the pin is Malcomized, a process for surface hardening stainless steel to 1000 Brinell. The materials are dissimilar enough that they will not seize or gall. The coefficient of expansion of these materials are similar enough, so that no interference problems can be expected at elevated temperature operation.

Excellent wear properties are achieved by applying a stellite facing material to the seat ring and to its mating surface on the disc.

The above study indicated that all materials used in the valve construction are structurally adequate for the expected service conditions of the valve application.

D. RESULTS AND CONCLUSIONS

A complete analysis of the check valve installation has been made as to field observations and findings, types of check valves available and reasons for the choice of the tilting disc type, a study of the design features and dynamic characteristics of the valves, an evaluation of the materials used in the valve construction and its structural adequacy for the service application.

It is our opinion that the valve as presently designed and installed in the feedwater line is satisfactory as is, for the intended service. The apparent looseness of the lock plate bolts that retains the disc and seat subassembly to the valve body, was the result of an unusual disturbance to the pipe system. The proposed modification to the regulating control valve system, piping system, and steam generator level control, should enable the check valves to function in a satisfactory manner.

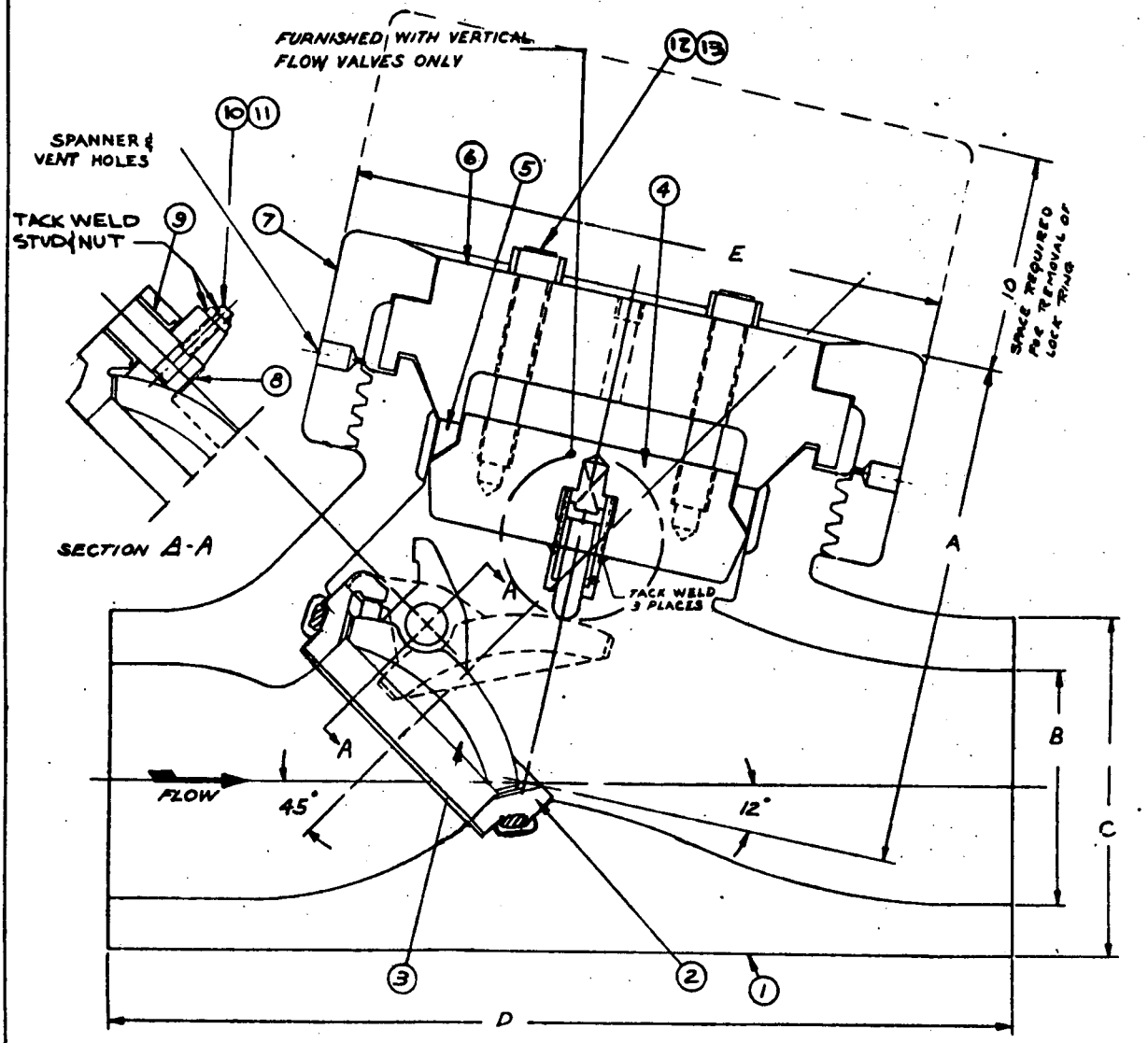

WEIGHT	SIZE	DIM. A	DIM. B	DIM. C	DIM. D	DIM. E
4310	18	25 7/8	14 5/16	18 1/2	48	32 5/16

CRANE CO.

List 973 Press. Seal
Tilting Disc Check Valves

PB

Appendix VI

Analytical Investigation of Feedwater Line Response

To Postulated Water Hammer Effects

ANALYTICAL INVESTIGATION OF FEEDWATER LINE RESPONSE TO POSTULATED WATER HAMMER EFFECTS FOR INDIAN POINT UNIT NO. 2

JANUARY 11, 1974

Approved: J. Dainora

J. Dainora
Manager, Mechanical Systems Analysis

United Engineers & Constructors, Inc

Philadelphia, Pa.

TABLE OF CONTENTS

1.0 ABSTRACT

2.0 LIST OF TABLES

3.0 LIST OF FIGURES

4.0 INTRODUCTION

5.0 HYPOTHESIS NO. 1 WATER HAMMER

5.1 Method of Analysis

5.2 Analysis of Water Hammer Hydraulic Effect

5.2.1 Description of WHAM Program

5.2.2 Description of Mathematical Model

5.2.3 Results

5.3 Dynamic Time-History Analysis of Feedwater Line

5.3.1 Description of STARDYNE Program

5.3.2 Description of Mathematical Model

5.3.3 Operating Conditions and Configurations Analyzed

5.3.4 Results

5.4 Stress Evaluation Due to Equivalent Static Loads

5.4.1 Description of MEL-40 Program

5.4.2 Results

5.5 Conclusions

1.0 ABSTRACT

A dynamic transient analysis was performed to investigate the response of feedwater line #22 to postulated water hammer effects from rapid control valve closure. The flow conditions associated with a power level of 360 Mw(e) for plant operation on September 27, 1973 were used in the analysis. Results of the analytical investigation indicate a stress level in the feedwater piping at the containment penetration higher than the minimum specified yield strength for the pipe material.

2.0 LIST OF TABLES

Table No.		
5.1	Hydraulic Force-Time History for Instantaneous Control Valve Closure with Check Valve Active	
5.2	Hydraulic Force-Time History for Instantaneous Control Valve Closure with Check Valve not Active	
5.3	Case 1H1S1	Maximum Deflections from STARDYNE Dynamic Analysis
5.4	Case 1H1S2	Maximum Deflections from STARDYNE Dynamic Analysis
5.5	Case 1H1S3	Maximum Deflections from STARDYNE Dynamic Analysis
5.6	Case 1H1S4	Maximum Deflections from STARDYNE Dynamic Analysis
5.7	Case 2H1S1	Maximum Deflections from STARDYNE Dynamic Analysis
5.8	Case 5H1S1	Maximum Deflections from STARDYNE Dynamic Analysis
5.9	MEL-40	Dynamic Transient Stresses
5.10	MEL-40	Dynamic Transient Forces & Moments
5.11	Case 1H1S5	Maximum Deflections from STARDYNE Dynamic Analysis
5.12	Case 1H1S6	Maximum Deflections from STARDYNE Dynamic Analysis
5.13	Case 2H1S6	Maximum Deflections from STARDYNE Dynamic Analysis
5.14	Case 5H1S6	Maximum Deflections from STARDYNE Dynamic Analysis
5.15	Maximum Forces - Seismic Restraints and Pipe Supports	
5.16	MEL-40	Dynamic Transient Stresses

3.0 LIST OF FIGURES

Figure No.	
5.1	Flow Chart of Analytical Investigation
5.2	WHAM Hydraulic Transient Mathematical Model — Outside Containment
5.3	WHAM Hydraulic Transient Mathematical Model — Inside Containment
5.4	Hydraulic Force-Time History for Control Valve Closure in 50 Milliseconds with Check Valve Active - Leg 8
5.5	Hydraulic Force-Time History for Control Valve Closure in 50 Milliseconds with Check Valve Active - Leg 16
5.6	STARDYNE Mathematical Model for Feedwater Line Outside Containment
5.7	STARDYNE Mathematical Model for Feedwater Line Inside Containment
5.8	Case 1H1S1 Force-Time History at Containment Penetration
5.9	Case 1H1S1 Moment-Time History at Containment Penetration
5.10	Case 1H1S1 Force-Time History at Steam Generator Nozzle
5.11	Case 1H1S1 Moment-Time History at Steam Generator Nozzle
5.12	Case 1H1S2 Force-Time History at Containment Penetration
5.13	Case 1H1S2 Moment-Time History at Containment Penetration
5.14	Case 1H1S2 Force-Time History at Steam Generator Nozzle
5.15	Case 1H1S2 Moment-Time History at Steam Generator Nozzle
5.16	Case 1H1S3 Force-Time History at Containment Penetration
5.17	Case 1H1S3 Moment-Time History at Containment Penetration
5.18	Case 1H1S3 Force-Time History at Steam Generator Nozzle
5.19	Case 1H1S3 Moment-Time History at Steam Generator Nozzle

3.0 LIST OF FIGURES (con't)

Figure No.	
5.20	Case 1H1S4 Force-Time History at Containment Penetration
5.21	Case 1H1S4 Moment-Time History at Containment Penetration
5.22	Case 1H1S4 Force-Time History at Steam Generator Nozzle
5.23	Case 1H1S4 Moment-Time History at Steam Generator Nozzle
5.24	Case 2H1S1 Force-Time History at Containment Penetration
5.25	Case 2H1S1 Moment-Time History at Containment Penetration
5.26	Case 2H1S1 Force-Time History at Steam Generator Nozzle
5.27	Case 2H1S1 Moment-Time History at Steam Generator Nozzle
5.28	Case 5H1S1 Force-Time History at Containment Penetration
5.29	Case 5H1S1 Moment-Time History at Containment Penetration
5.30	Case 5H1S1 Force-Time History at Steam Generator Nozzle
5.31	Case 5H1S1 Moment-Time History at Steam Generator Nozzle
5.32	MEL-40 Mathematical Model for Feedwater Line Outside Containment
5.33	MEL-40 Mathematical Model for Feedwater Line Inside Containment

4.0 INTRODUCTION

This report covers UE&C's contribution to the analysis of the Con Edison feedwater line break of November 13, 1973. The report is part of the full investigation of the incident and is intended to provide postulated water hammer effects.

5.1 METHOD OF ANALYSIS

A parametric evaluation of the dynamic response of feedwater line #22 to postulated water hammer effects was performed for flow conditions associated with the 360 Mw(e) power level. The flow chart summarizing the method of analysis is given in Figure 5.1.

The first step in the analytical investigation was the determination of hydraulic forces acting on the piping system. The event initiating water hammer effects was postulated to be the rapid control valve closure in feedwater line #22. A force time-history was calculated for each water hammer event using the WHAM computer program. Forcing functions were generated for the feedwater piping extending from the control valve to the steam generator nozzle. The following three water hammer events were considered in the analysis:

a. Instantaneous control valve closure with check valve acting.

b. Control valve closure in 50 milliseconds with check valve acting.

c. Instantaneous control valve closure without check valve.

The transient response of the feedwater piping to the hydraulic forcing functions was calculated using the STARDYNE computer program. The piping system was uncoupled mathematically at the containment penetration. Separate mathematical models were developed for the piping inside and outside the containment for several possible pipe support configurations. STARDYNE results consisting of displacement, force, and moment time-histories were reviewed to determine the critical time periods of maximum response.

At the critical time periods, results from the STARDYNE program were used as input to the MEL-40 computer program to determine stresses from the equivalent static loads in accordance with B31.1 code requirements. The output from the MEL-40 program consisted of stresses in the piping system and reactions at anchor and support locations.

5.2 ANALYSIS OF WATER HAMMER HYDRAULIC EFFECT

5.2.1 Description of WHAM Program

Water hammer hydraulic effects are computed by the WHAM digital computer program. The WHAM program is applicable to piping networks consisting of dead ends, elbows, orifices, multiple branch tees, non-uniform flow cross-sections, check valves, pumps, pressurizers or tanks, and exit valves. The program considers hydraulic losses and transients which can be initiated by a closing/opening of an exit valve, by a prescribed change in the pressurizer/tank pressure, and/or by a pump power failure.

Input data required to initiate program WHAM consists of a definition of system initial conditions prior to transient initiation, system geometry definition, and a definition of certain physical parameters in the system. Transients in feedwater line #22 result from valve closure and for this type of transient initiation, the following specific input parameters are required:

a. Fluid initial velocity and pressure for each leg in the system.

b. Fluid density and viscosity.

c. Shock wave velocity for each leg in the system.

d. Geometry, area and length, for each leg in the system.

e. Valve operating time and discharge coefficient.

f. Velocity below which check valve closes.

Output data from WHAM consists of inertia loads on each leg of the system, pressure at the beginning and end of each leg in the system, and fluid velocity at the beginning and end of each leg in the system. This set of output data is presented for each leg in the system at preselected times from start of transient.

5.2.2 Description of Mathematical Model

Water hammer hydraulic effects were investigated for the following three conditions:

(1) instantaneous control valve closure with check valve active,

(2) control valve closure in 50 milliseconds with check valve active,

(3) instantaneous control valve closure with the check valve not active.

The flow in feedwater line #22 for the above cases was taken as 1.0×10^6 lb/hr corresponding to a power level of 360 Mw(e). System losses were considered in establishing the initial flow conditions and were accounted for during the hydraulic transient evaluation by the WHAM computer program.

The mathematical model used for the hydraulic transient analysis is presented in Figures 5.2 and 5.3. The model boundaries were taken as the control valve and steam generator nozzle. A calculation time increment of 0.1 milliseconds was used in conjunction with a sonic velocity of 5000 ft/sec to establish a node spacing of 0.5 feet in the WHAM model.

5.2.3 Results

Instantaneous Control Valve Closure with Check Valve Active

During an instantaneous control valve closure, the following sequence of events occur on the downstream side of the valve:

(1) The valve closure produces a shock wave which travels downstream from the valve toward the steam generator at a speed equal to the sonic velocity.

(2) As the shockwave passes any given point in the system it reduces the initial fluid velocity to zero and additionally reduces the pressure in the pipeline to a value lower than its initial value.

(3) As the shock wave passes the check valve and reduces the fluid velocity to zero, the check valve closes.

(4) The shock wave continues down the pipeline to the steam generator.

(5) Conditions at the steam generator are such that the reduced pressure level in the pipeline cannot be sustained and the shockwave is reflected back toward the check valve.

(6) As the reflected wave passes any given point in the pipeline the reduced pressure is returned to the pressure level of the steam generator and the fluid in the pipeline begins to flow toward the check valve.

(7) When the shock wave reaches the closed check valve the boundary is such that the flow velocity cannot be sustained.

(8) The velocity of the fluid reduces again to zero accompanied by a pressure increase in the pipeline and a wave reflection.

(9) The reflected wave travels toward the steam generator reducing the fluid velocity to zero and increasing the system pressure to a value above that in the steam generator.

(10) Upon reaching the steam generator, the increased pipeline pressure cannot be sustained. The shockwave is reflected and travels back toward the check valve reducing the pipeline pressure to that in the steam generator and fluid begins to flow into the steam generator.

(11) At the time when the shockwave reaches the check valve, one cycle of the water hammer is completed.

(12) The cycle will then repeat itself until system losses cause it to become negligible.

For rapid control valve closures shock waves are developed and load the system continuously as they move through the system. For purpose of analysis, continuous systems are modeled by a finite number of discrete legs. Each leg

is subjected to load during that period of time while the shock wave is traveling through the leg. This results in a series of pulse loads applied to any given leg during the appropriate time interval. The hydraulic force-time history for the instantaneous control valve closure with the check valve in the system is presented in Table 5.1. The shock wave passes the check valve (end of leg 7 see Fig. 5.2) 16 milliseconds after start of transient (i.e. valve closure). At this time the check valve closes and no additional forces are developed on legs 1 through 7. For time in excess of 16 milliseconds the closed check valve and the steam generator are the system boundaries and the force-time history in legs 8 to 20 is as delineated in Table 5.1.

Control Valve Closure in 50 Milliseconds with Check Valve Active

During slower valve closures, the pressure in the system builds up slower being inversely proportional to the valve closure time. A series of continuous shock waves are generated by the valve as it closes. As long as the valve closes before the initial shock pulse (generated at time zero) can travel to the steam generator and back again to the valve the maximum differential pressure developed at the valve location will be identical to that developed in the case when the valve closes instantly. The slower pressure built up results in smaller hydraulic forces being applied to any given leg than those obtained during the instantaneous valve closure. However, the smaller force acts for a longer period of time on any given leg.

Results of the analysis indicate that for a 50 millisecond control valve closure the fluid velocity in legs 1 through 7 (see Figure 5.2) will be reduced to zero and the check valve will close 66 milliseconds after the start of the transient. Representative force-time histories for legs 8 and 16 (Figures 5.2 - 5.3) for the first 200 milliseconds of the transient are presented in Figures 5.4 and 5.5.

Instantaneous Control Valve Closure with Check Valve not Active

Table 5.2 summarizes the hydraulic force-time history for the case of an instantaneous control valve closure with the check valve not active. This case was analyzed to establish hydraulic transients for the assumed condition that the check valve malfunctioned. The WHAM computer program calculations were based on a mathematical model with the check valve deleted from the system. An evaluation of the check valve design was performed and the results are summarized in Section 8.0. The check valve was found to be satisfactory for the intended service and the results of this analysis represent "worst case" assumptions.

5.3 DYNAMIC TIME HISTORY ANALYSIS OF FEEDWATER LINE

5.3.1 Description of STARDYNE Program

The STARDYNE program provides elastic analysis of structural models in the static and dynamic regimes. The static capability includes the computation of structural deformations and member loads and stresses caused by an arbitrary set of thermal, nodal applied loads and/or prescribed displacements. In the dynamic regime, the program can be used for the computation of natural frequencies, mode shapes, and participation factors. The program input consists of structural geometry, element mass and stiffness properties, and boundary conditions.

Dynamic response analysis utilizing the normal mode techniques can be performed for a wide range of loading conditions, including transient, steady state harmonic, random and shock spectra. Dynamic response results are presented as time-history structural deformations (displacements, velocities, or accelerations) and/or internal member loads/stresses.

The library of finite elements consists of elastic and rigid beams, triangular and quadrilateral plates, solid tetrahedrons and hexahedrons.

5.3.2 Description of Mathematical Model

The dynamic response of feedwater line #22 was calculated using the STARDYNE program. The mathematical models for structural dynamic analysis are given as Figures 5.6 and 5.7. The piping system was represented by an assemblage of finite beam elements interconnected at nodal points. The mass of the piping system was simulated using a lumped mass representation at the various nodal points in the model. A damping value of 1 percent of critical damping was used in the dynamic analysis.

Figure 5.6 is the STARDYNE mathematical model for feedwater line #22 outside the containment. The section of piping represented by this mathematical model is bounded on one end by the junction of the 18-inch line to the 30-inch header and at the other end by the containment penetration. The boundary points are considered to be anchor points with all degrees of freedom fixed.

Figure 5.7 is the STARDYNE mathematical model for the feedwater piping inside the containment. The section of the piping system inside the containment is bounded by the containment penetration at one end and the steam generator nozzle at the other end. These terminal locations are defined as anchor points.

5.3.3 Operating Conditions and Configurations Analyzed

The operating conditions assumed for the water hammer analysis consisted of the following cases:

Case 1

a. Power 360 MWe

b. Valve No. 22 closes instantly

c. Check valve active

Case 2

a. Power 360 MWe

b. Valve No. 22 closes in 50 milliseconds

c. Check valve active

Case 3

a. Power 360 MWe

b. Valve No. 22 closes instantly

c. Check valve not active

The mathematical models (Figures 5.6 - 5.7) were modified to reflect various piping/support configurations. The parametric investigation was performed to investigate the effect of clearances between piping and supports and possible support failure on the response of the system. If a support or restraint was postulated to fail, two separate mathematical models were generated. The stiffness of the support was included in one mathematical model and deleted from the other. Each configuration analyzed was designated by a number which identifies the operating case and the piping configuration as follows:

Case 1

1 H1S1 (Inside Containment - Ref. Figure 5.7)

a. No Pipe Whip Restraint Pins

b. No Support No. 31 (Restraint at 2 feet from containment penetration)

1 H1S2 (Inside Containment)

a. With Pipe Whip Restraint Pins

b. No Support No. 31

1 H1S3 (Inside Containment)

a. No Pipe Whip Restraint Pins

b. With Support No. 31

1 H1S4 (Inside Containment)

a. With Pipe Whip Restraint Pins

b. With Support No. 31

1H1S5 (Outside Containment - Ref. Figure 5.6)

a. Seismic Restraint SR-B3 acting

1H1S6 (Outside Containment)

a. Seismic Restraint SR-B3 not acting

Case 2

2H1S1 (Inside Containment)

a. No Pipe Whip Restraint Pins

b. No Support No. 31

2H1S6 (Outside Containment)

a. Seismic Restraint SR-B3 not acting

Case 3

5H1S1 (Inside Containment)

a. No Pipe Whip Restraint Pins

b. No Support No. 31

5H1S6 (Outside Containment)

a. Seismic Restraint SR-B3 not acting

All of the above conditions were analyzed for time-history of displacements using the STARDYNE program.

5.3.4 Results

Figures 5.8 through 5.31 summarize the force or moment time histories at the containment penetration and steam generator nozzle for Cases 1H1S1, 1H1S2, 1H1S3, 1H1S4, 2H1S1 and 5H1S1. The time-history record out to 0.200 seconds includes the maximum response of the system.

The present analysis indicates a loading in excess of the design allowable force of 20.0 kips for the seismic restraint SR-B4. Field observations did not indicate structural damage to this restraint.

The 2½ inch schedule 80 pipe spacer on the end of the hydraulic seismic restraint SR-B9 was observed to be visibly bent. The present analysis shows 0.755-inch movement of the pipe in the south direction corresponding to the above qualitative observation. The analysis also indicates possible structural damage.

The insulation was observed to have been compressed on the north side of the sliding support BFD-41, leaving a 1 inch open gap between the sliding support BFD-41, and a 1 inch open gap between the insulation face and the vertical face of the top plate of the sliding support. The analysis indicated a movement of 0.774-inch of the pipe (node 36) in the south direction correlating with the physical observations.

It is important to note that the majority of the field observations are qualitative in nature especially those displacements based on displacement of insulation.

5.4 Stress Evaluation Due to Equivalent Static Loads

5.4.1 Description of MEL-40 Program

The MEL-40 computer program analyzes the flexibility of multiple branch and closed-loop piping systems subject to pressure variations, temperature variations, anchor movements, weight, and/or other prescribed loading conditions. The program determines the forces, moments, stresses, deflections and rotations at the anchor and balance points; at the middle and ends of each bend and the ends of each tangent or joint; and at the point of attachment of all restraints. Elements may be subject to any degree of skewness; any number of anchors and restraints may be included; anchors may have

flexibility (elasticity) as well as extraneous movements.

The MEL-40 program computes pipe stresses in accordance with B31.1 code requirements. Piping flexibility properties and stress intensification factors for elbows and bends are incorporated in the program.

Input to the MEL-40 program consisted of equivalent static loads obtained from the STARDYNE dynamic analysis for selected critical time periods. The MEL-40 mathematical model is given in Figures 5.32 and 5.33. The stiffness characteristics of the STARDYNE and MEL-40 mathematical models are compatible but the two programs have different node numbering schemes.

5.4.2 Results

Maximum stresses fot the section of feedwater piping inside the containment are presented in Table 5.9. The stresses in Table 5.9 are only for the dynamic transient loading condition resulting from the postulated water hammer effects and must be added to the dead weight and pressure stresses to compute total stresses in the system. The maximum stress for the section of piping at the penetration anchor is estimated to be (35.53 + 0.46 + 5.31) = 41.10 ksi due to water hammer loading, dead weight, and line pressure. The total stress value exceeds the code allowable stress of 21.0 ksi as well as the specified minimum yield strength of 40.0 ksi.

Maximum forces and moments at the containment penetration and the steam generator nozzle are given in Table 5.10. The maximum moment at the steam generator nozzle is less than the design allowable.

The dynamic transient stresses in the feedwater piping outside of the containment are summarized in Table 5.16. The maximum dynamic transient stress is 8.43 psi at the junction of feedwater line #22 to the 30-inch header. The total stresses including dynamic transient, dead weight and pressure loadings are less than the B31.1 code allowable.

Tables 5.3 through 5.8 summarize the maximum displacements at various nodes in the piping system inside the containment for the six cases investigated. The maximum displacement at the bend (nodes 18 - 21) as computed by the STARDYNE analysis is 1.210 inches (Table 5.5) and the vertical component of displacement (node 22) for BFD-2 is 0.752 inch acting downward (Table 5.4). These calculated displacements are slightly lower than the displacements obtained from field observations of feedwater line motion inside the containment.

The maximum displacements of the feedwater line outside the containment for Cases 1H1S5, 1H1S6, 2H1S6, and 5H1S6 are summarized in Tables 5.11 through 5.14. The computed displacements are smaller than field observations of apparent line movement.

Table 5.15 presents the maximum forces calculated in the seismic restraints and supports for the section of feedwater piping outside the containment. Seismic SR-B3 was deleted from the mathematical model for Cases 1H1S6, 2H1S6, and 5H1S6 and, therefore, no forces are given for this member. The loading of 25.92 ksi on the seismic restraint SR-B3 exceeds the maximum allowable force of 20.0 kips. Similarly, the calculated force acting on SR-B9 was at or above the design allowable force of 20 kips.

The direction of displacement of node-48 is in the direction that would cause the anchor plate carrying the horizontal load from the hydraulic seismic restraint SR-B3, to be rotated in the observed direction (rotation of 3/16 inch was measured at the corners) and pulled away from the concrete (a 1/2 inch gap on thw north side and 3/32 inch gap at the fastener nuts on the south side was measured).

5.5 CONCLUSIONS

The applicability of the water hammer hypothesis as a credible dynamic transient is mainly dependent on two conditions. The first condition is the requirement for rapid closure of the control valve. The normal closing time of the control valve is several orders of magnitude higher than the closure time required to initiate water hammer shock waves. Because the control valve is spring loaded, the failure of a component of the control valve assembly is required to initiate the water hammer dynamic transient. The second condition is the requirement for large flow in the feedwater system and consequently higher plant power levels. The analytical investigation is based on the plant operating conditions of September 27, 1973 when the plant was operating at 360 Mw(e) or approximately 30 percent power. Some operating problems were experienced with the control valve in feedwater line #22 on the above date which may have initiated rapid valve closure.

On the basis of an analytical investigation of the hydraulic forces generated at flows associated with approximately 7 percent power operation, it is our conclusion that the magnitude of the hydraulic forces is sufficiently low to preclude pipe failure at this power level. The pipe stress levels generated by the water hammer effects at the 30 percent power level were slightly above specified minimum yield strength at the containment penetration but below code allowables for most of the system.

The calculated displacements at various support points were generally lower than the results of field observations. The analytical results did predict accurately conditions of overload at seismic restraints SR-B3 and SR-B9 which were confirmed by field observations.

Table 5.1 Hydraulic Force-Time History for Instantaneous Control Valve Closure with Check Valve Active

Leg	Force (Pounds)	Force Application Time From (Millisec)	To (Millisec)
1	43170	0	0.9
1	43170	98.9	99.8
1	- 43170	99.8	100.7
1	- 43170	198.7	199.6
2	43170	0.9	3.0
2	43170	96.8	98.9
2	- 43170	100.7	102.8
2	- 43170	196.6	198.7
3,4,5	43170	3.0	12.3
3,4,5	43170	87.5	96.8
3,4,5	- 43170	102.8	112.1
3,4,5	- 43170	187.3	196.6
6	43170	12.3	13.7
6	43170	86.1	87.5
6	- 43170	112.1	113.5
6	- 43170	185.9	187.3
7	43170	13.7	16.0
7	43170	83.8	86.1
7	- 43170	113.5	115.8
7	- 43170	183.6	185.9
8	43170	16.0	19.0
8	43170	80.8	83.8
8	- 43170	115.8	118.8

Table 5.1 (continued)

Hydraulic Force-Time History for Instantaneous

Control Valve Closure with Check Valve Active

Leg	Force (Pounds)	Force Application Time From (Millisec)	To (Millisec)
8	- 43170	180.6	183.6
9	43170	19.0	20.9
9	43170	78.9	80.8
9	- 43170	118.8	120.7
9	- 43170	178.7	180.6
10	43170	20.9	22.1
10	43170	77.7	78.9
10	- 43170	120.7	121.9
10	- 43170	177.5	178.7
11	43170	22.1	24.1
11	43170	75.7	77.7
11	- 43170	121.9	123.9
11	- 43170	175.5	177.5
12	43170	24.1	28.1
12	43170	71.7	75.7
12	- 43170	123.9	127.9
12	- 43170	171.5	175.5
13	43.70	28.1	32.1
13	43170	67.7	71.7
13	- 43170	127.9	131.9
13	- 43170	167.5	171.5
14	43170	32.1	34.3
14	43170	65.5	67.7

Table 5.1 (continued)

Hydraulic Force-Time History for Instantaneous

Control Valve Closure with Check Valve Active

Leg	Force (Pounds)	Force Application Time From (Millisec)	To (Millisec)
14	- 43170	131.9	134.1
14	- 43170	165.3	167.5
15	43170	34.3	37.6
15	43170	62.2	65.5
15	- 43170	134.1	137.4
15	- 43170	162.0	165.3
16	43170	37.6	39.9
16	43170	59.9	62.2
16	- 43170	137.4	139.7
16	- 43170	159.7	162.0
17	43170	39.9	43.9
17	43170	55.9	59.9
17	- 43170	139.7	143.7
17	- 43170	155.7	159.7
18	43170	43.9	45.3
18	43170	54.5	55.9
18	- 43170	143.7	145.1
18	- 43170	154.3	155.7
19	43170	45.3	46.8
19	43170	53.0	54.5
19	- 43170	145.1	146.6
19	- 43170	152.8	154.3
20	43170	46.8	49.9
20	43170	49.9	53.0

Table 5.1 (continued)

Hydraulic Force-Time History for Instantaneous

Control Valve Closure with Check Valve Active

Leg	Force (Pounds)	Force Application Time From (Millisec)	To (Millisec)
20	- 43170	146.6	149.7
20	- 43170	149.7	152.8

Table 5.2 Hydraulic Force-Time History for Instantaneous Control Valve Closure with Check Valve Not Active

Leg	Force (Pounds)	Force Application Time From (Millisec)	To (Millisec)
1	43170	0	0.9
2	43170	0.9	3.0
3,4,5	43170	3.0	12.3
6	43170	12.3	13.7
7	43170	13.7	16.0
8	43170	16.0	19.0
8	42898	80.9	83.9
8	- 42852	83.9	86.9
8	- 41781	148.7	151.7
8	42283	151.7	154.7
9	43170	19.1	21.0
9	42931	79.0	80.9
9	- 42713	86.9	88.8
9	- 42191	146.8	148.7
9	43270	154.7	156.6
10	43170	21.0	22.2
10	42950	77.8	79.0
10	- 42655	88.8	90.0
10	- 42695	145.6	146.8
10	41904	156.6	157.8
11	43170	22.2	24.2
11	42978	75.8	77.8
11	- 42446	90.0	92.0
11	- 43807	143.6	145.6

Table 5.2 (continued)

Hydraulic Force-Time History for Instantaneous

Control Valve Closure with Check Valve Not Active

Leg	Force (Pounds)	Force Application Time From (Millisec)	To (Millisec)
11	41752	157.8	159.8
12	43170	24.2	28.2
12	43018	71.8	75.8
12	- 42437	92.0	96.0
12	- 43403	139.6	143.6
12	42761	159.8	163.8
13	43170	28.2	32.2
13	43052	67.8	71.8
13	- 42349	96.0	100.0
13	- 43800	135.6	137.6
13	42780	163.8	167.8
14	43170	32.2	34.4
14	43068	65.6	67.8
14	- 42493	100.0	102.2
14	- 44978	133.4	135.6
14	43782	167.8	170.0
15	43170	34.4	37.7
15	43093	62.3	65.6
15	- 42856	102.2	105.5
15	- 43176	130.1	133.4
15	42120	170.0	173.3
16	43170	37.7	40.0

Table 5.2 (continued)

Hydraulic Force-Time History for Instantaneous

Control Valve Closure with Check Valve Not Active

Leg	Force (Pounds)	Force Application Time From (Millisec)	To (Millisec)
16	43108	60.0	62.3
16	- 42570	105.5	107.8
16	- 43907	127.8	130.1
16	43463	173.3	175.6
17	43170	40.0	44.0
17	43133	56.0	60.0
17	- 42956	107.8	111.8
17	- 42715	123.8	127.8
17	43527	175.6	179.6
17	42623	191.6	195.6
18	43170	44.0	45.4
18	43138	54.6	56.0
18	- 42080	111.8	113.2
18	- 44294	122.4	123.8
18	42637	179.6	181.0
18	44152	190.2	191.6
19	43170	45.4	46.9
19	43150	53.1	54.6
19	- 41740	113.2	114.7
19	- 44070	120.9	122.4
19	42507	181.0	182.5
19	42059	188.7	190.2
20	43170	46.9	50.0

Table 5.2 (continued)

Hydraulic Force-Time History for Instantaneous

Control Valve Closure with Check Valve Not Active

Leg	Force (Pounds)	Force Application Time From (Millisec)	To (Millisec)
20	43150	50.0	53.1
20	- 42400	114.7	117.8
20	- 43027	117.8	120.9
20	43800	182.5	185.6
20	42726	185.6	188.7

Table 5.3 Case 1H1S1 Maximum Deflections

From STARDYNE Dynamic Analysis

Node	Type	Maximum Deflections						Actual Component No.
		Time	ΔX (In.)	Time (Sec.)	ΔY (In.)	Time (Sec.)	ΔZ (In.)	
31	RST	0.115	-.037	0.157	.002	0.185	-.003	
8	RST	0.115	-.183	0.115	-.068	-----	0.	HBF-17
10	RST	0.118	-.148	0.108	-.202	0.688	.028	PR-4
12	RST	0.112	-.174	0.112	-.149	-----	0.	HBF-18
14	RST	0.169	-.171	0.108	-.227	0.160	.062	PR-5
16	RST	0.112	-.122	0.112	-.213	-----	0.	HBF-19
17	TGNT	0.169	.264	0.115	-.213	0.173	-.087	
22	RST	0.148	.364	0.124	-.599	0.176	-.583	SPRING
2 to 5	ELB	0.115	-.210	0.112	.067	0.185	-.023	
18 to 21	ELB	0.160	.751	0.191	.535	0.179	-.605	
23 to 26	ELB	0.185	-.507	0.166	-.796	0.176	-.773	

Directions: +X = south
+Y = east
+Z = vertical up

Table 5.4 Case 1H1S2 Maximum Deflections

From STARDYNE Dynamic Analysis

Node	Type	Maximum Deflections						Actual Component No.
		Time	ΔX (In.)	Time (Sec.)	ΔY (In.)	Time (Sec.)	ΔZ (In.)	
31	RST	0.118	-.036	0.163	-.001	0.173	-.002	
8	RST	0.115	-.184	0.115	-.068	-----	0.	HBF-17
10	RST	0.118	-.150	0.108	-.202	-----	0.	PR-4
12	RST	0.112	-.175	0.112	-.149	-----	0.	HBF-18
14	RST	0.169	-.171	0.108	-.230	-----	0.	PR-5
16	RST	0.191	.086	0.191	.151	-----	0.	HBF-19
17	TGNT	0.169	.261	0.115	-.211	0.084	.094	
22	RST	0.148	.306	0.121	-.588	0.176	-.752	SPRING
2 to 5	ELB	0.115	-.210	0.112	.067	0.173	-.013	
18 to 21	ELB	0.160	.743	0.188	.545	0.176	-.062	
23 to 26	ELB	0.185	-.488	0.166	-.913	-.176	-.788	

Directions: +X = south
+Y = east
+Z = vertical up

Table 5.5 Case 1H1S3 Maximum Deflections

From STARDYNE Dynamic Analysis

Node	Type	Maximum Deflections						Actual Component No.
		Time Sec.	ΔX (In.)	Time (Sec.)	ΔY (In.)	Time (Sec.)	ΔZ (In.)	
31	RST	-----	0.	-----	0.	-----	0.	
8	RST	0.179	.189	0.179	.071	-----	0.	HBF-17
10	RST	0.182	.140	0.108	-.271	0.163	-.050	PR-4
12	RST	0.179	.192	0.179	.164	-----	0.	HBF-18
14	RST	0.169	.329	0.105	-.242	0.160	.096	PR-5
16	RST	0.145	.398	0.179	.246	-----	0.	HBF-19
17	TGNT	0.169	.329	0.182	.212	0.099	.125	
22	RST	0.145	.398	0.188	.554	0.176	-.694	SPRING
2 to 5	ELB	0.182	.198	0.182	-.076	0.182	-.020	
18 to 21	ELB	0.173	.781	0.182	.695	0.176	-.608	
23 to 26	ELB	0.182	-.543	0.163	-.933	0.176	-.753	

Directions: +X = south
+Y = east
+Z = vertical up

Table 5.6 Case 1H1S4 Maximum Deflections

From STARDYNE Dynamic Analysis

Node	Type	Maximum Deflections						Actual Component No.
		Time Sec.	ΔX (In.)	Time (Sec.)	ΔY (In.)	Time (Sec.)	ΔZ (In.)	
31	RST	-----	0.	-----	0.	-----	0.	
8	RST	0.179	0.190	0.179	0.079	-----	0.	HBF-17
10	RST	0.179	0.144	0.105	-0.260	-----	0.	PR-4
12	RST	0.179	0.192	0.179	0.164	-----	0.	HBF-18
14	RST	0.154	0.182	0.173	0.262	-----	0.	PR-5
16	RST	0.179	0.141	0.179	0.247	-----	0.	HBF-19
17	TGNT	0.169	0.327	0.157	-0.280	0.157	-0.096	
22	RST	0.145	0.340	0.121	-0.602	0.173	-0.727	SPRING
2 to 5	ELB	0.182	0.201	0.182	-0.077	0.169	-0.010	
18 to 21	ELB	0.169	0.778	0.182	0.709	0.179	-0.633	
23 to 26	ELB	0.185	-0.538	0.163	0.929	0.176	-0.764	

Directions: +X = south
+Y = east
+Z = vertical up

Table 5.7 Case 2H1S1 Maximum Deflections

From STARDYNE Dynamic Analysis

Node	Type	Maximum Deflections						Actual Component No.
		Time Sec.	ΔX (In.)	Time (Sec.)	ΔY (In.)	Time (Sec.)	ΔZ (In.)	
31	RST	.1974	-.0012	0.135	.00002	.174	.0001	
8	RST	.089	-.010	.158	-.010	----	-----	HBF-17
10	RST	.099	-.010	.099	-.010	.197	.002	PR-4
12	RST	.166	-.011	.174	.011	----	-----	HBF-18
14	RST	1081	.011	.109	.011	.068	.011	PR-5
16	RST	.120	.010	.114	.010	----	-----	HBF-19
17	TGNT	.073	.0105	.107	.011	.102	.011	
22	RST	.156	.130	.127	.200	.125	.271	SPRING
2 to 5	ELB	.060	.039	.060	-.011	.143	.0029	
18 to 21	ELB	.184	.238	.148	-.097	.127	.233	
23 to 26	ELB	.200	-.120	.181	.221	.122	.263	

Directions: +X = south
+Y = east
+Z = vertical up

Table 5.8 Case 5H1S1 Maximum Deflections

From STARDYNE Dynamic Analysis

Node	Type	Maximum Deflections						Actual Component No.
		Time Sec.	ΔX (In.)	Time (Sec.)	ΔY (In.)	Time (Sec.)	ΔZ (In.)	
31	RST	0.185	-0.036	0.179	-0.001	0.185	-0.002	
8	RST	0.185	-0.170	0.185	-0.062	-----	------	HBF-17
10	RST	0.185	-0.130	0.188	-0.180	0.200	-0.051	PR-4
12	RST	0.188	-0.163	0.188	-0.138	-----	------	HBF-18
14	RST	0.185	-0.193	0.163	0.169	0.200	0.121	PR-5
16	RST	0.188	-0.102	0.188	-0.179	-----	------	HBF-19
17	TGNT	0.163	0.281	0.188	-0.274	0.200	-0.218	
22	RST	0.179	0.391	0.124	-0.584	0.200	-0.962	SPRING
2 to 5	ELB	0.185	-0.189	0.185	0.055	0.185	-0.018	
18 to 21	ELB	0.173	0.811	0.121	-0.440	0.200	-0.866	
23 to 26	ELB	0.185	-0.532	0.179	-0.695	0.200	-1.003	

Directions: +X = south
+Y = east
+Z = vertical up

Table 5.9 MEL-40 Dynamic Transient Stresses

Data Point (Fig. 5.33)	Stress, ksi					
	1H1S1 0.111 Sec.	1H1S1 0.169 Sec.	2H1S1 0.058 Sec.	2H1S1 0.107 Sec.	5H1S1 0.185 Sec.	5H1S1 0.200 Sec.
5	34.46	7.40	7.15	0.61	35.33	3.65
20	12.56	13.99	1.03	3.49	16.23	16.89
30	2.14	4.06	0.09	0.57	5.77	2.50
52	5.94	6.56	0.26	1.26	11.14	6.06
70	1.11	0.44	0.13	0.33	3.29	3.81
80	2.81	8.67	0.65	1.24	9.12	9.20
90	3.68	8.58	0.10	0.73	2.70	3.71
100	6.61	6.02	0.55	0.61	0.43	2.43
110	4.24	1.66	0.53	0.16	2.68	2.01
120	2.23	2.08	0.50	0.18	2.32	0.54
145	13.82	3.13	2.33	0.25	11.76	0.97

Table 5.10 MEL-40 Dynamic Transient Forces & Moments

Case	Time (secs)	Location	Force, Kips			Moment, ft-lbs x 10^3		
			F_x	F_y	F_z	M_x	M_y	M_z
1H1S1	0.111	P	90.7	-1.5	-19.9	3.5	483.2	4.5
1H1S1	0.111	SGN	-47.6	10.1	-15.6	69.1	156.5	-42.1
1H1S1	0.169	P	19.3	2.5	24.1	-6.4	103.4	-7.1
1H1S1	0.169	SGN	4.9	-11.9	-34.0	-158.3	-69.8	92.5
2H1S1	0.058	P	-19.9	0.3	5.6	-1.6	-100.3	-0.4
2H1S1	0.058	SGN	4.5	0.6	2.3	9.5	-7.1	-8.1
2H1S1	0.107	P	2.1	0.1	0.7	-1.8	8.4	0.4
2H1S1	0.107	SGN	-1.8	5.0	1.4	35.8	17.4	-28.4
5H1S1	0.185	P	99.7	-4.2	7.7	21.5	494.9	6.7
5H1S1	0.185	SGN	1.4	-21.6	0.6	-149.1	-134.3	107.4
5H1S1	0.200	P	11.1	3.3	-1.1	-11.4	49.3	-7.3
5H1S1	0.200	SGN	4.0	-17.5	-23.1	-176.3	-77.8	137.6

Note: +X = north
+Y = vertical up
+Z = east

P = Pipe at Containment Penetration
SGN = Pipe at Steam Generator Nozzle

Table 5.11 Case 1H1S5 Maximum Deflections

From STARDYNE Dynamic Analysis

Node	Component	Maximum Deflections					
		Time (Sec.)	X (In.)	Time (Sec.)	Y (In.)	Time (Sec.)	Z (In.)
28	BFD-38	0.032	0.197	0.104	-0.192	0.108	0.117
36	BFD-41	0.034	0.199	0.060	-0.152	0.042	-0.042
42	SR-B9	0.034	0.154	0.060	-0.108	0.078	-0.039
48	SR-B3	0.032	0.057	0.018	0.029	0.074	-0.094
54	BFD-45	0.024	0.012	0.068	0.026	0.074	-0.092

Directions: +X = south
+Y = east
+Z = vertical up

Table 5.12 Case 1H1S6 Maximum Deflections

From STARDYNE Dynamic Analysis

Node	Component	Maximum Deflections					
		Time (Sec.)	X (In.)	Time (Sec.)	Y (In.)	Time (Sec.)	Z (In.)
28	BFD-38	0.074	0.392	0.128	-0.129	0.076	-0.176
36	BFD-41	0.072	0.393	0.086	-0.089	0.090	0.045
42	SR-B9	0.064	0.389	0.062	-0.077	0.090	0.401
48	SR-B4	0.062	0.332	0.096	-0.023	0.030	0.071
54	BFD-45	0.054	0.051	0.034	-0.024	0.030	0.072

Directions: +X = south
+Y = east
+Z = vertical up

Table 5.13 Case 2H1S6 Maximum Deflections

From STARDYNE Dynamic Analysis

Node	Component	Maximum Deflections					
		Time (Sec.)	Δ X (In.)	Time (Sec.)	Δ Y (In.)	Time (Sec.)	Δ Z (In.)
28	BFD-38	0.136	0.170	0.172	- 0.326	0.110	- 0.335
36	BFD-41	0.136	0.170	0.188	- 0.265	0.130	- 0.185
42	SR-B9	0.136	0.162	0.178	- 0.156	0.092	- 0.048
48	SR-B4	0.142	1.271	0.200	- 0.021	0.138	0.111
54	BFD-45	0.172	0.267	0.132	- 0.023	0.138	0.109

Directions: +X = South
+Y = East
+Z = Vertical Up

Table 5.14 Case 5H1S6 Maximum Deflections

From STARDYNE Dynamic Analysis

Node	Component	Maximum Deflections					
		Time (Sec.)	Δ X (In.)	Time (Sec.)	Δ Y (In.)	Time (Sec.)	Δ Z (In.)
28	BFD-38	0.110	0.780	0.198	- 0.262	0.198	0.200
36	BFD-41	0.108	0.774	0.158	- 0.181	0.108	- 0.136
42	SR-B9	0.108	0.755	0.154	- 0.128	0.198	- 0.099
48	SR-B4	0.120	0.611	0.158	- 0.064	0.102	0.144
54	BFD-45	0.146	0.207	0.136	0.042	0.102	0.143

Directions: +X = South
+Y = East
+Z = Vertical Up

Table 5.15 Maximum Forces - Seismic Restraints

And Pipe Supports

Beam Nodes (Fig. 5.6)	Component	Member Force, Kips			
		1H1S5	1H1S6	2H1S6	5H1S6
28-62	BFD-38	- 0.20	0.30	0.57	- 0.34
36-64	BFD-41	- 0.03	- 0.07	- 0.12	- 0.09
42-65	SR-B9	19.51	11.50	20.20	40.92
48-66	SR-B3	- 25.92	NA	NA	NA
48-67	SR-B4	14.56	- 9.68	- 0.86	- 26.83
54-68	BFD-45	0.42	- 0.33	- 0.49	0.65

Table 5.16 MEL-40 Dynamic Transient Stresses

Nodes (Fig. 5.32)	Location	Stress, KSI 1H1S6 0.024 sec.	2H1S6 0.140 sec.	5H1S6 0.146 sec.
400	30" Header	2.12	8.43	5.86
355-357	90° Elbow	0.81	5.06	1.67
340-342	Control Valve Guide	0.23	0.43	0.21
310-312	Control Valve Guide	0.96	3.93	1.40
285-287	90° Elbow	0.47	4.21	1.44
265-267	90° Elbow	1.86	3.68	1.52
220-222	Horizontal Pipe Run	2.11	5.37	2.55
186-188	45° Elbow	4.70	7.91	3.80
171-173	90° Elbow	3.78	6.12	4.38
150-152	Check Valve	0.16	0.53	0.44
115-117	90° Elbow	1.63	7.67	2.59

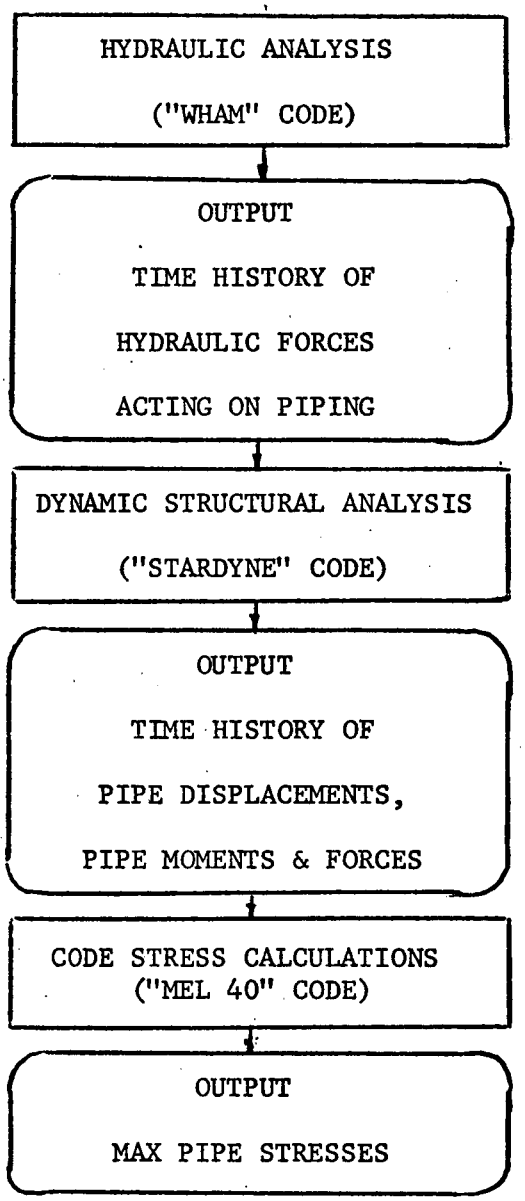

FIGURE 5.1 FLOW CHART OF ANALYTICAL INVESTIGATION

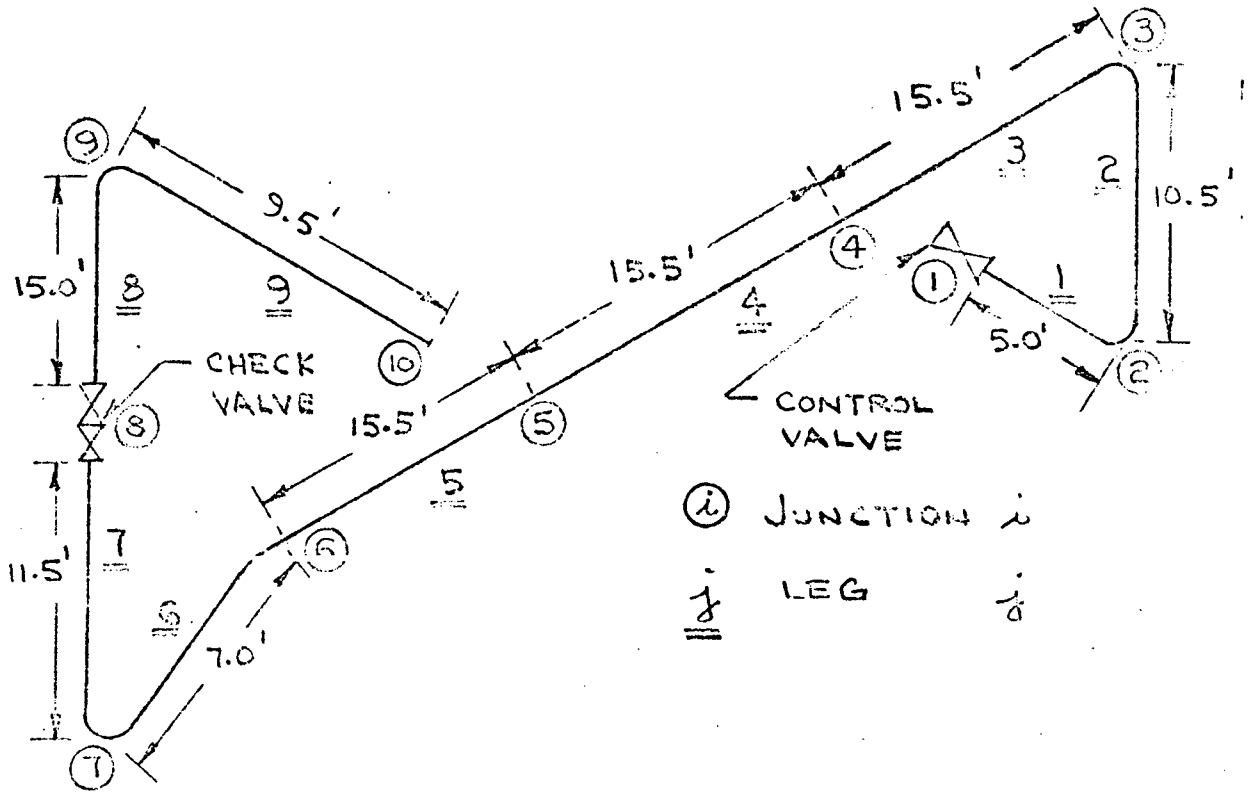

FIGURE 5.2 WHAM HYDRAULIC TRANSIENT MATHEMATICAL MODEL - OUTSIDE CONTAINMENT

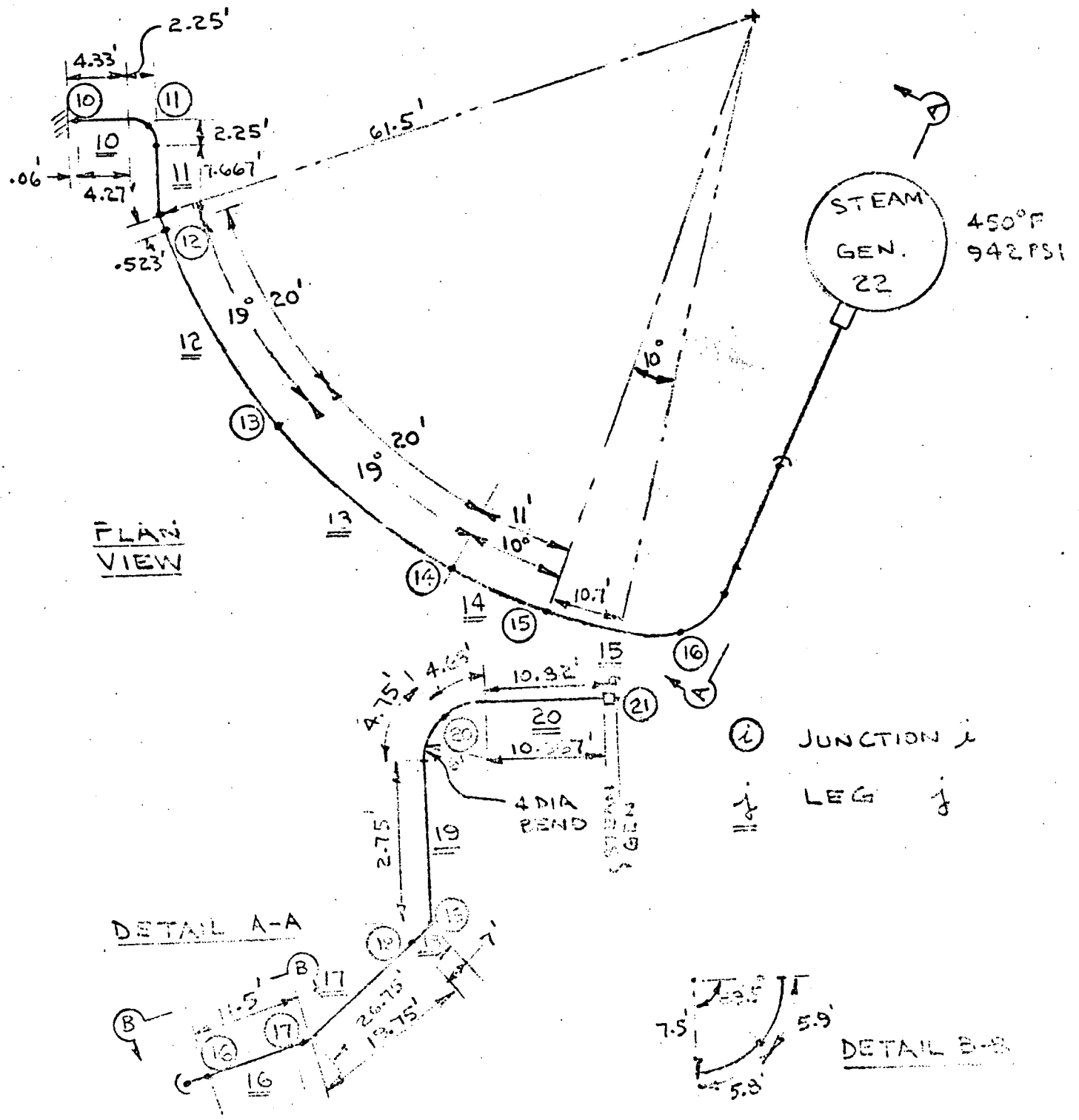

FIGURE 5.3 WHAM HYDRAULIC TRANSIENT MATHEMATICAL MODEL - INSIDE CONTAINMENT

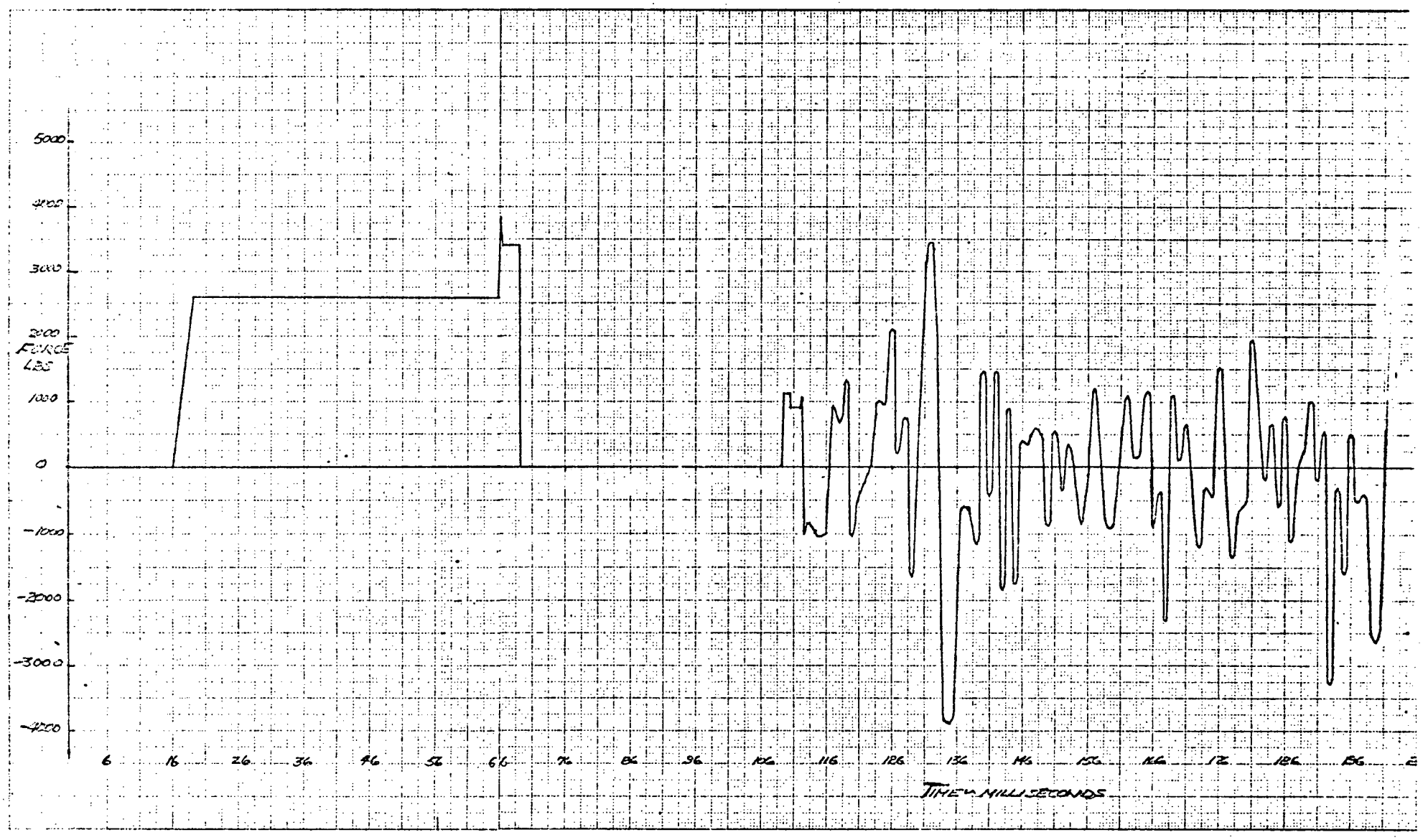

FIGURE 5.4 HYDRAULIC FORCE-TIME HISTORY FOR CONTROL VALVE CLOSURE IN 50 MILLISECONDS WITH CHECK VALVE ACTIVE - LEG 8

FIGURE 5.5 HYDRAULIC FORCE-TIME HISTORY FOR CONTROL VALVE CLOSURE IN 50 MILLISECONDS WITH CHECK VALVE ACTIVE - LEG 16

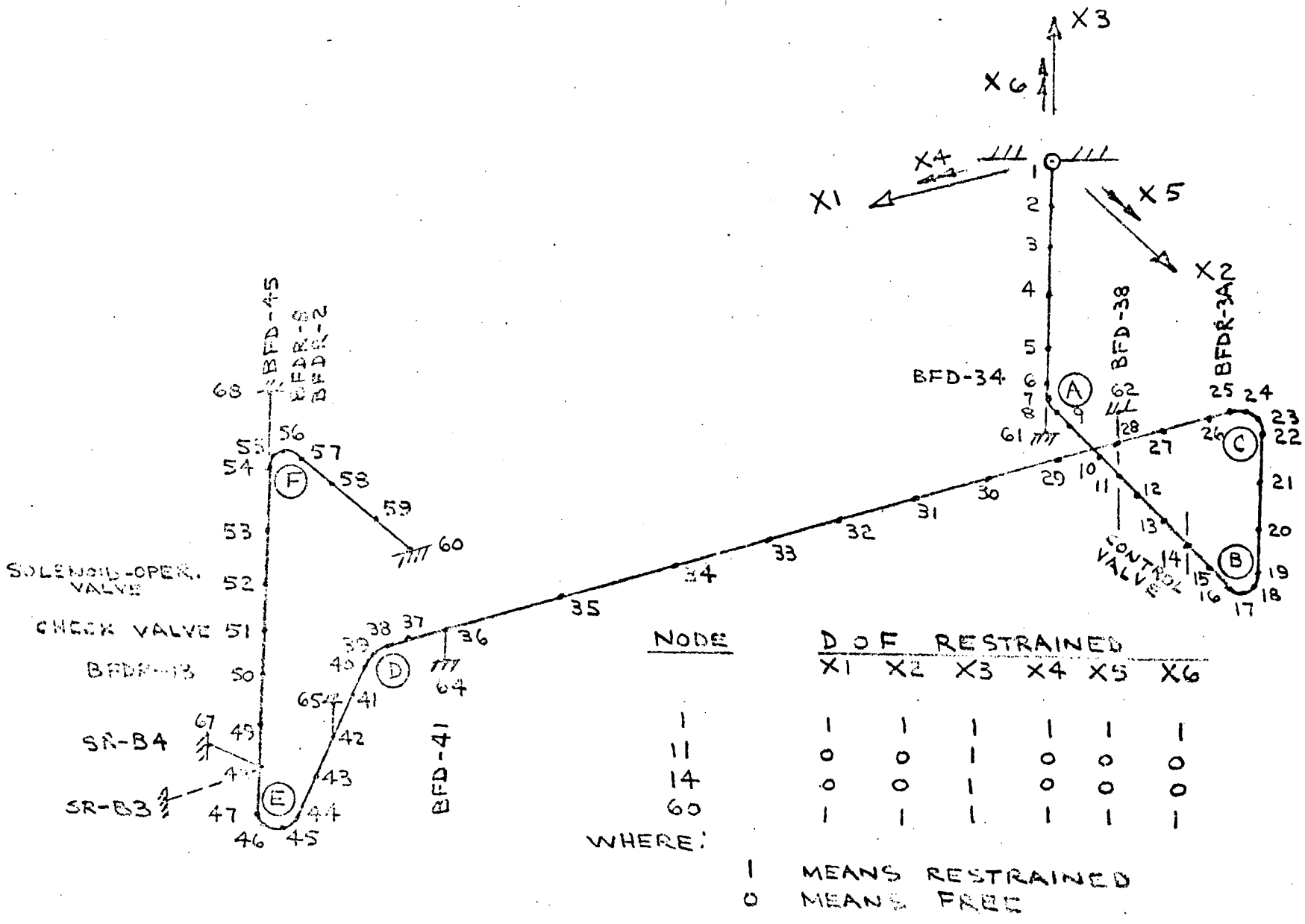

FIGURE 5.6 STARDYNE MATHEMATICAL MODEL FOR FEEDWATER LINE OUTSIDE CONTAINMENT

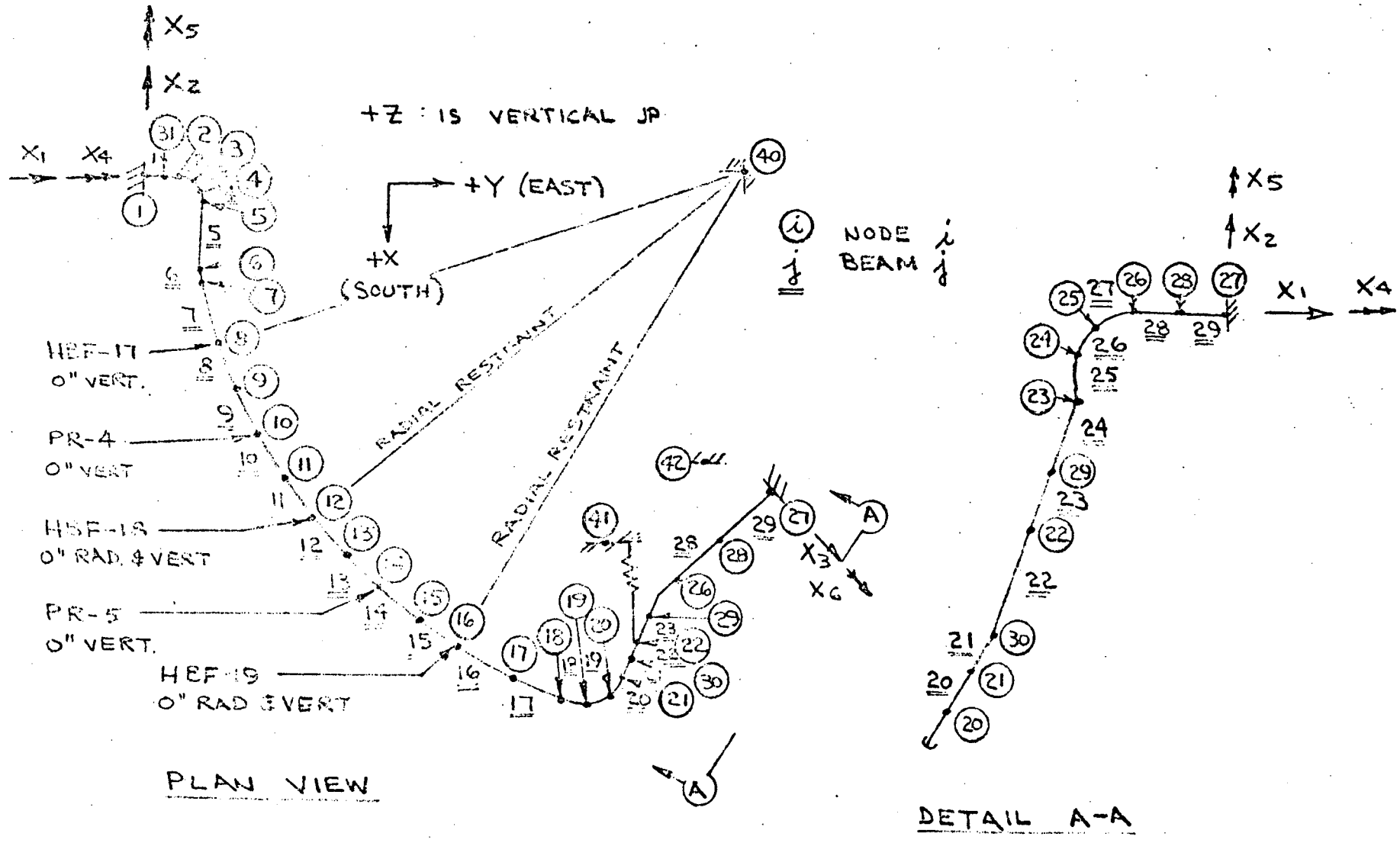

FIGURE 5.7 STARDYNE MATHEMATICAL MODEL FOR FEEDWATER LINE INSIDE CONTAINMENT

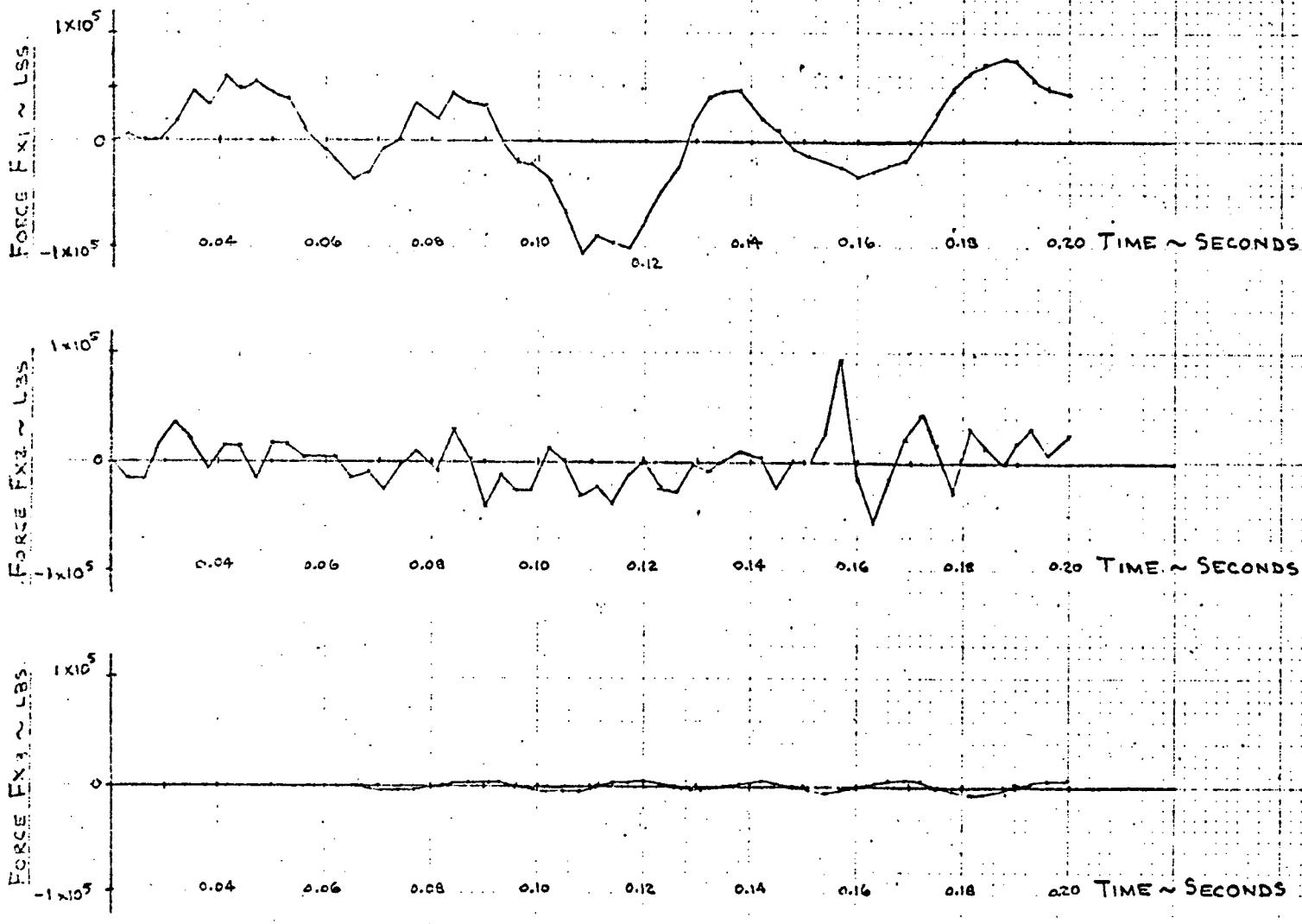

FIGURE 5.8 CASE 1H1S1 FORCE-TIME HISTORY AT CONTAINMENT PENETRATION

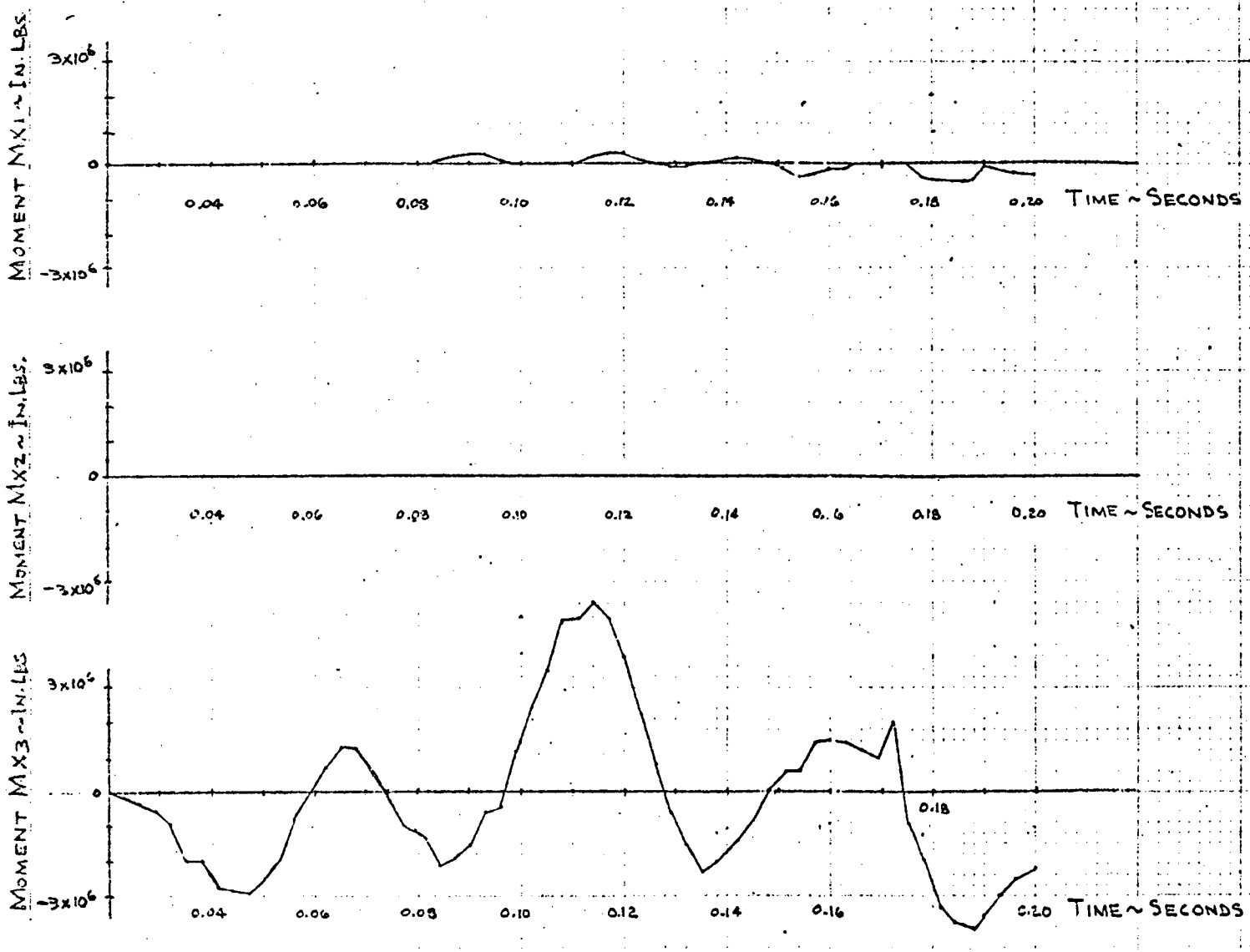

FIGURE 5.9 CASE 1H1S1 MOMENT-TIME HISTORY AT CONTAINMENT PENETRATION

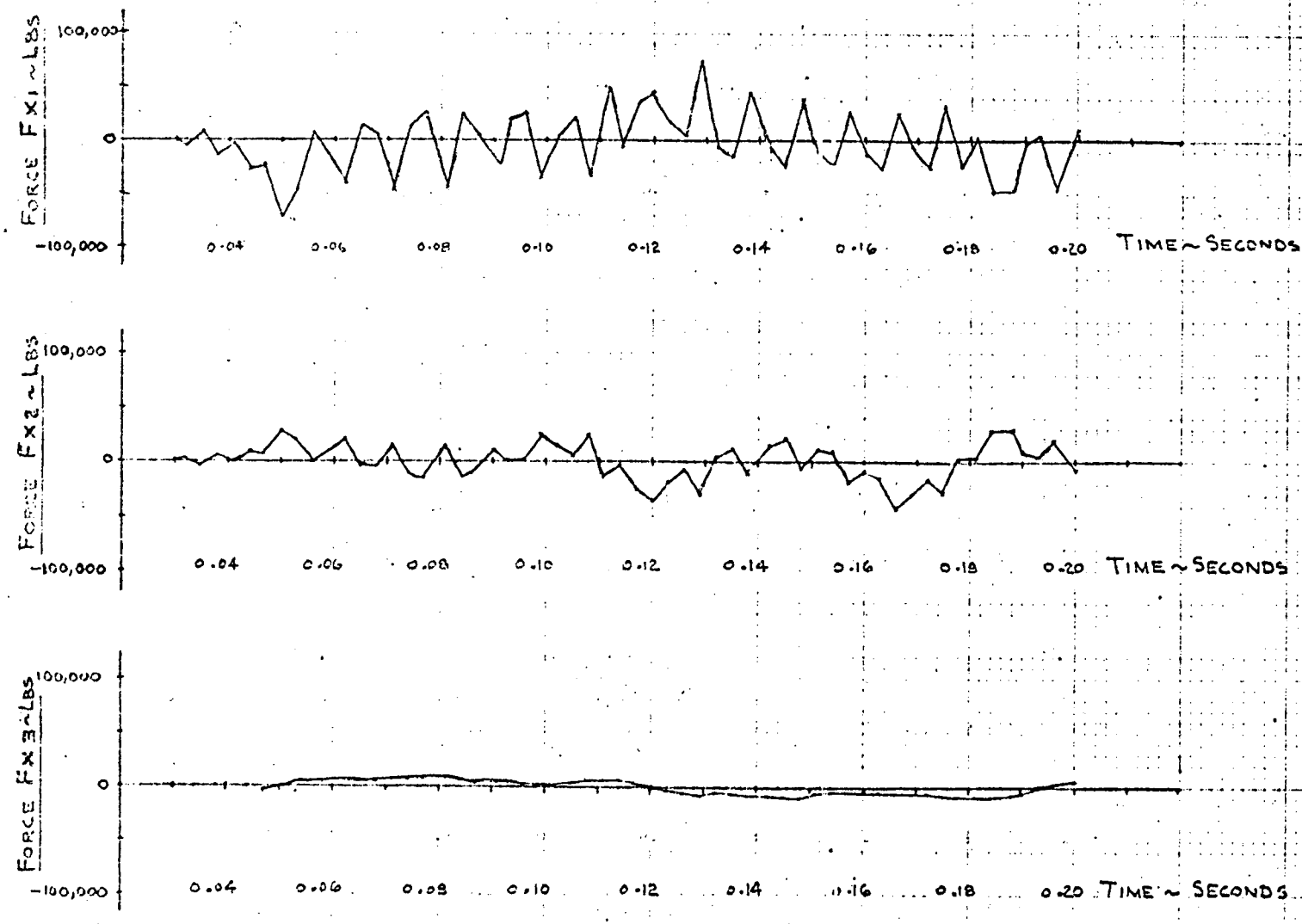

FIGURE 5.10 CASE 1H1S1 FORCE-TIME HISTORY AT STEAM GENERATOR NOZZLE

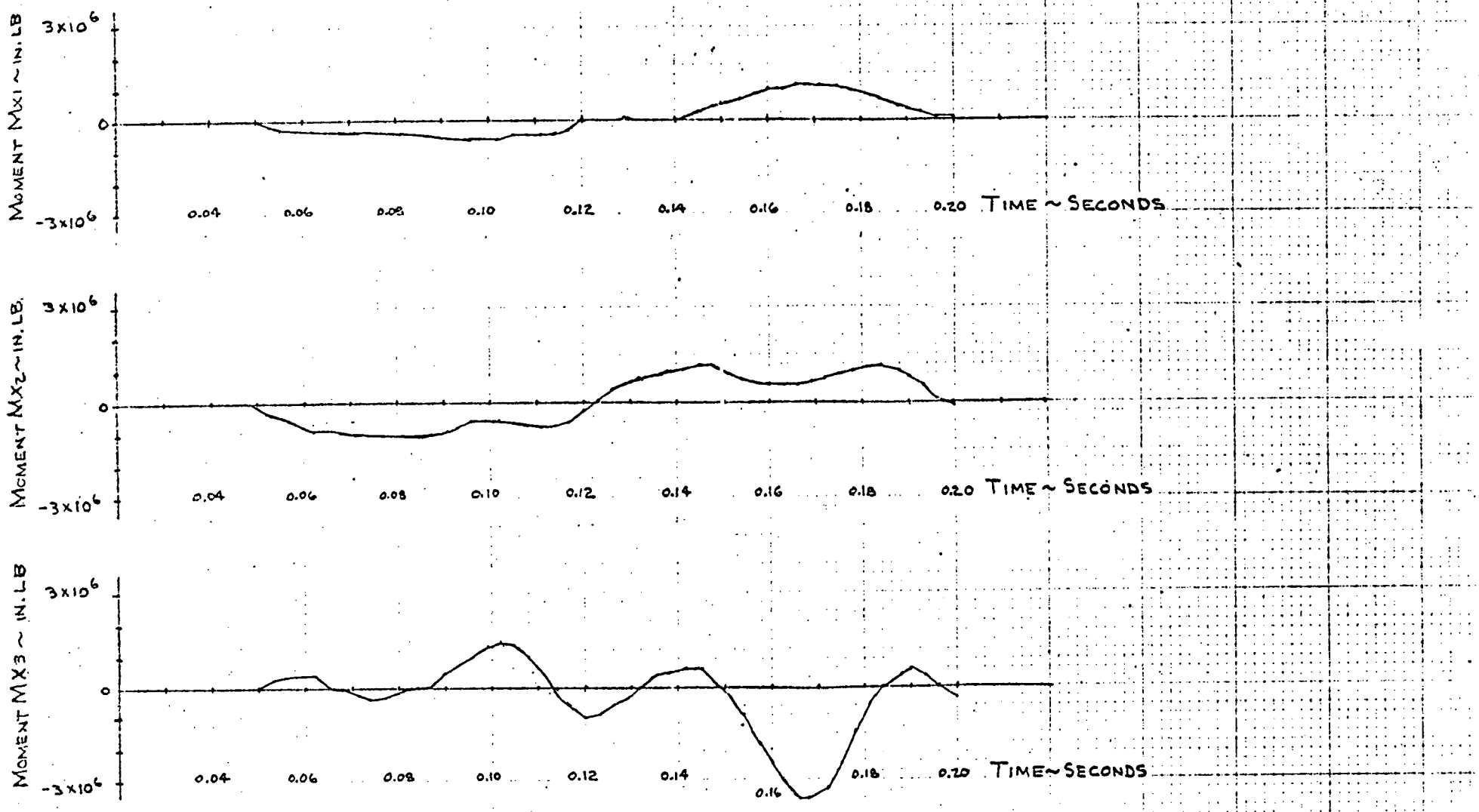

FIGURE 5.11 CASE 1H1S1 MOMENT-TIME HISTORY AT STEAM GENERATOR NOZZLE

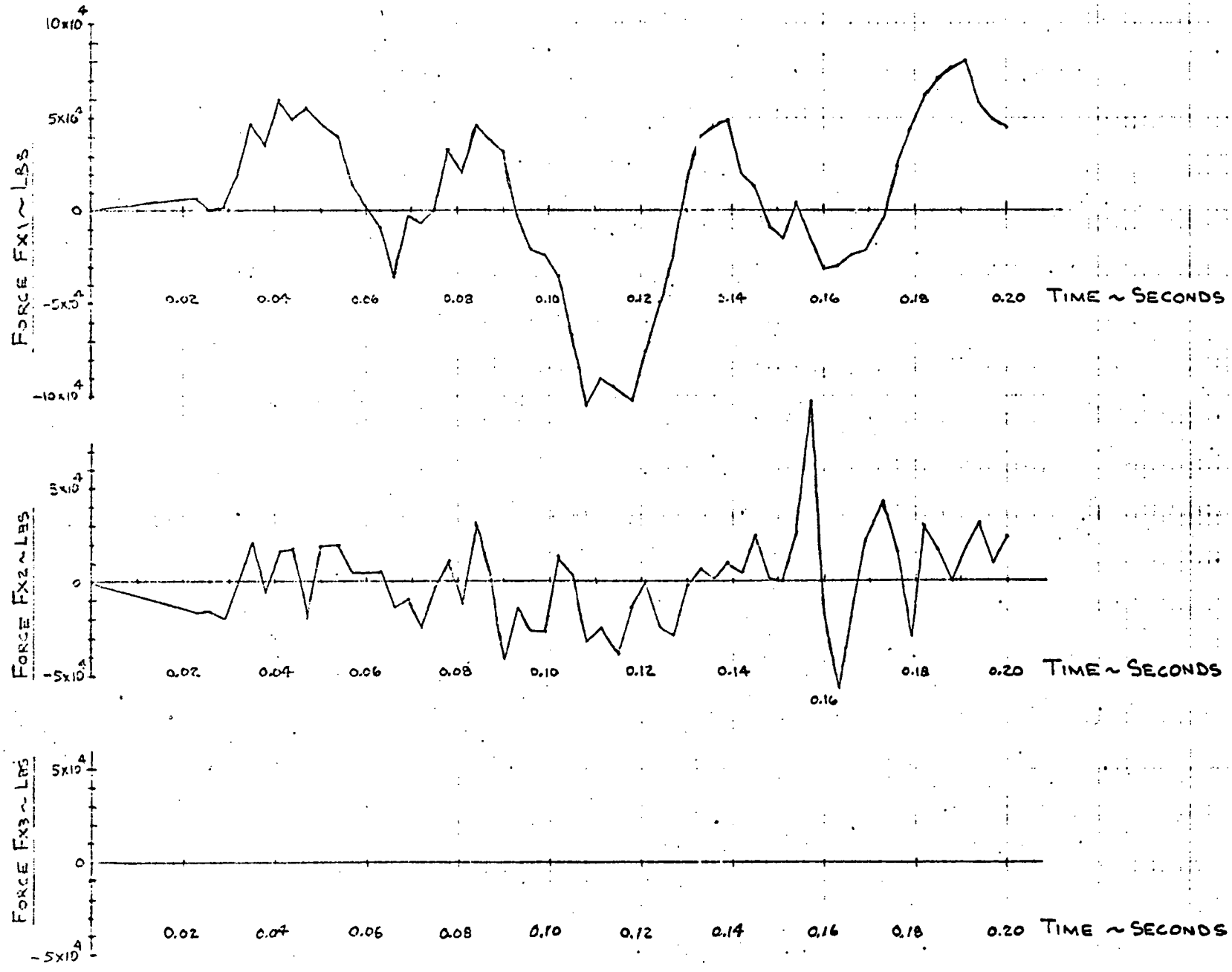

FIGURE 5.12 CASE 1H1S2 FORCE-TIME HISTORY AT CONTAINMENT PENETRATION

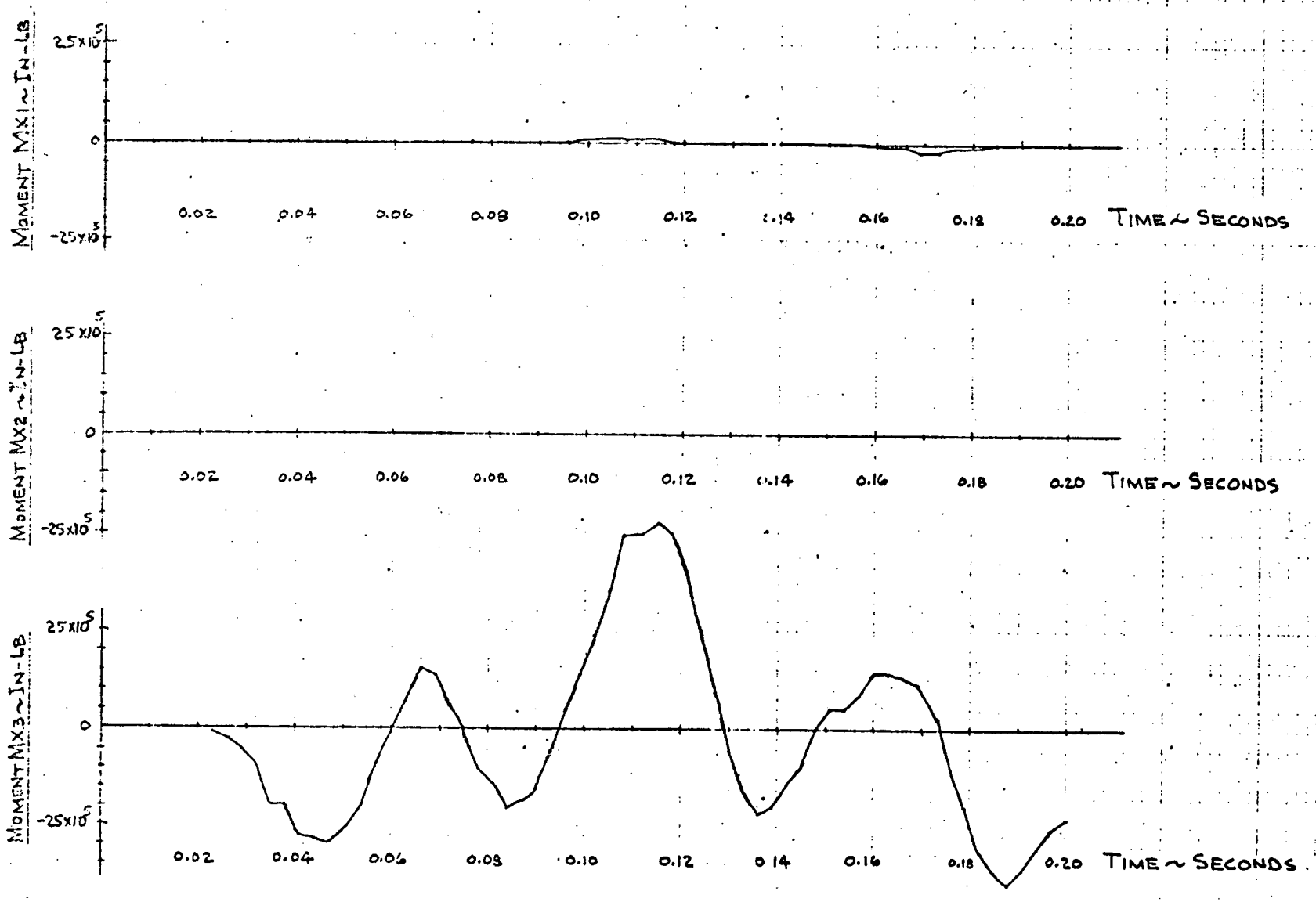

FIGURE 5.13 CASE 1H1S2 MOMENT-TIME HISTORY AT CONTAINMENT PENETRATION

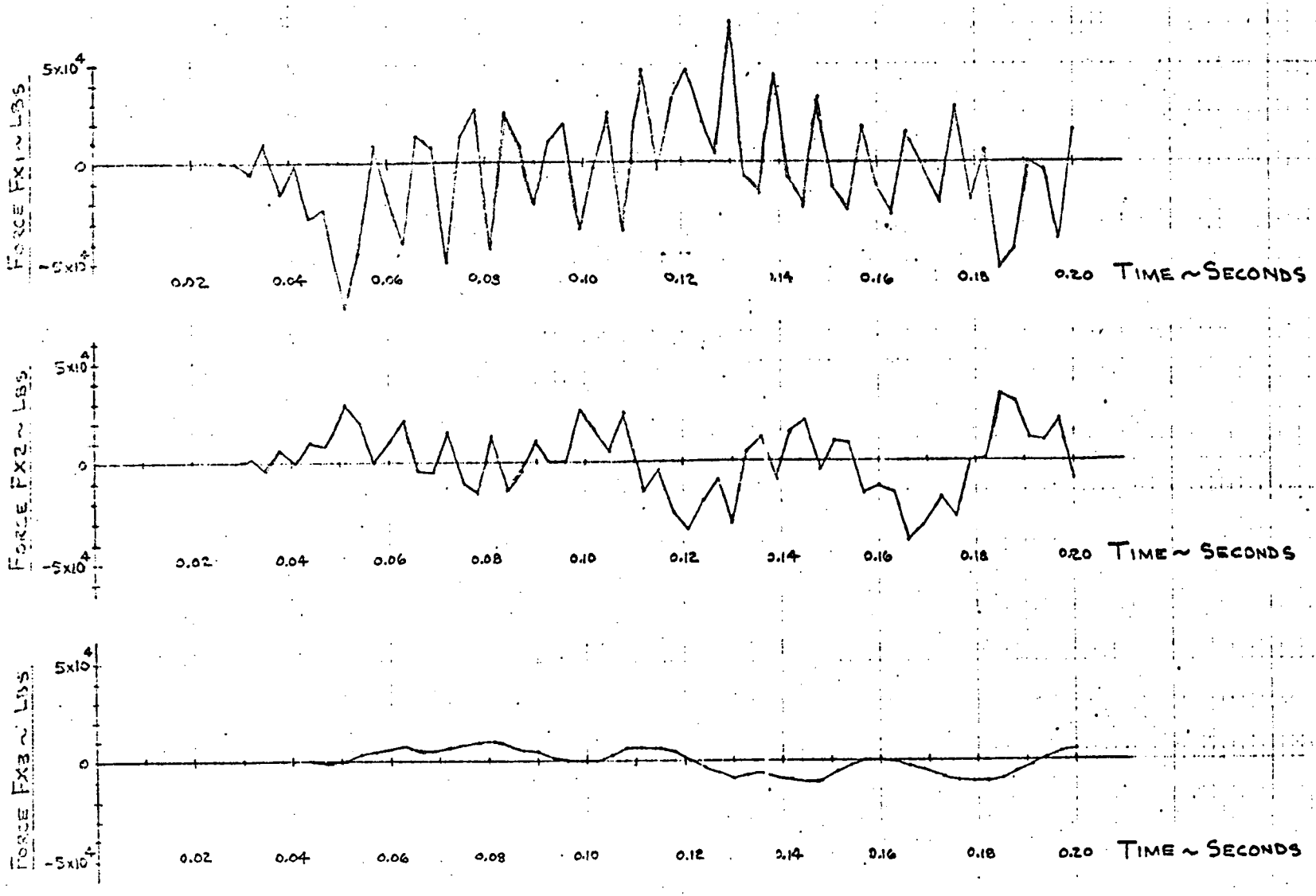

FIGURE 5.14 CASE 1H1S2 FORCE-TIME HISTORY AT STEAM GENERATOR NOZZLE

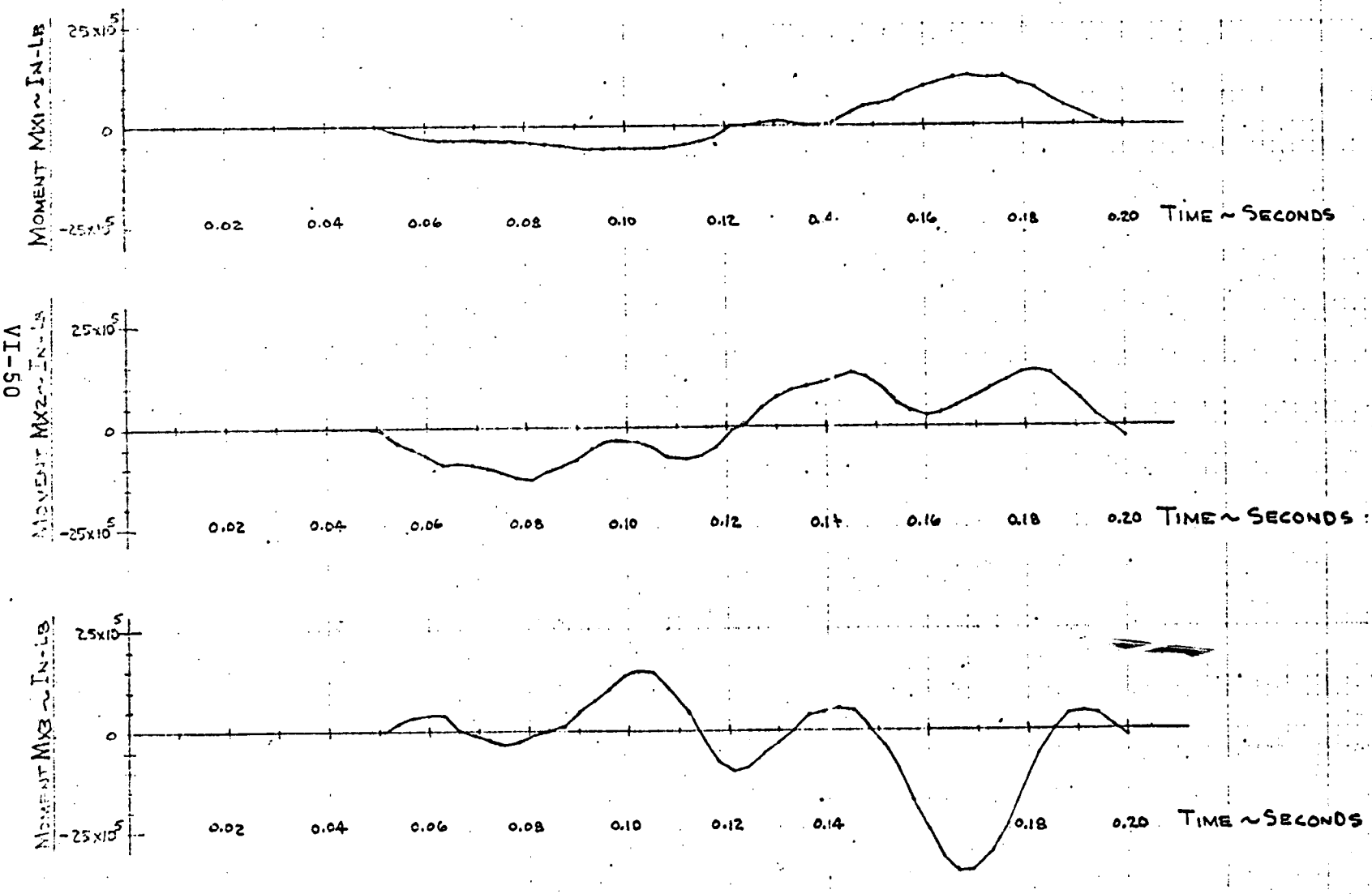

FIGURE 5.15 CASE 1H1S2 MOMENT-TIME HISTORY AT STEAM GENERATOR NOZZLE

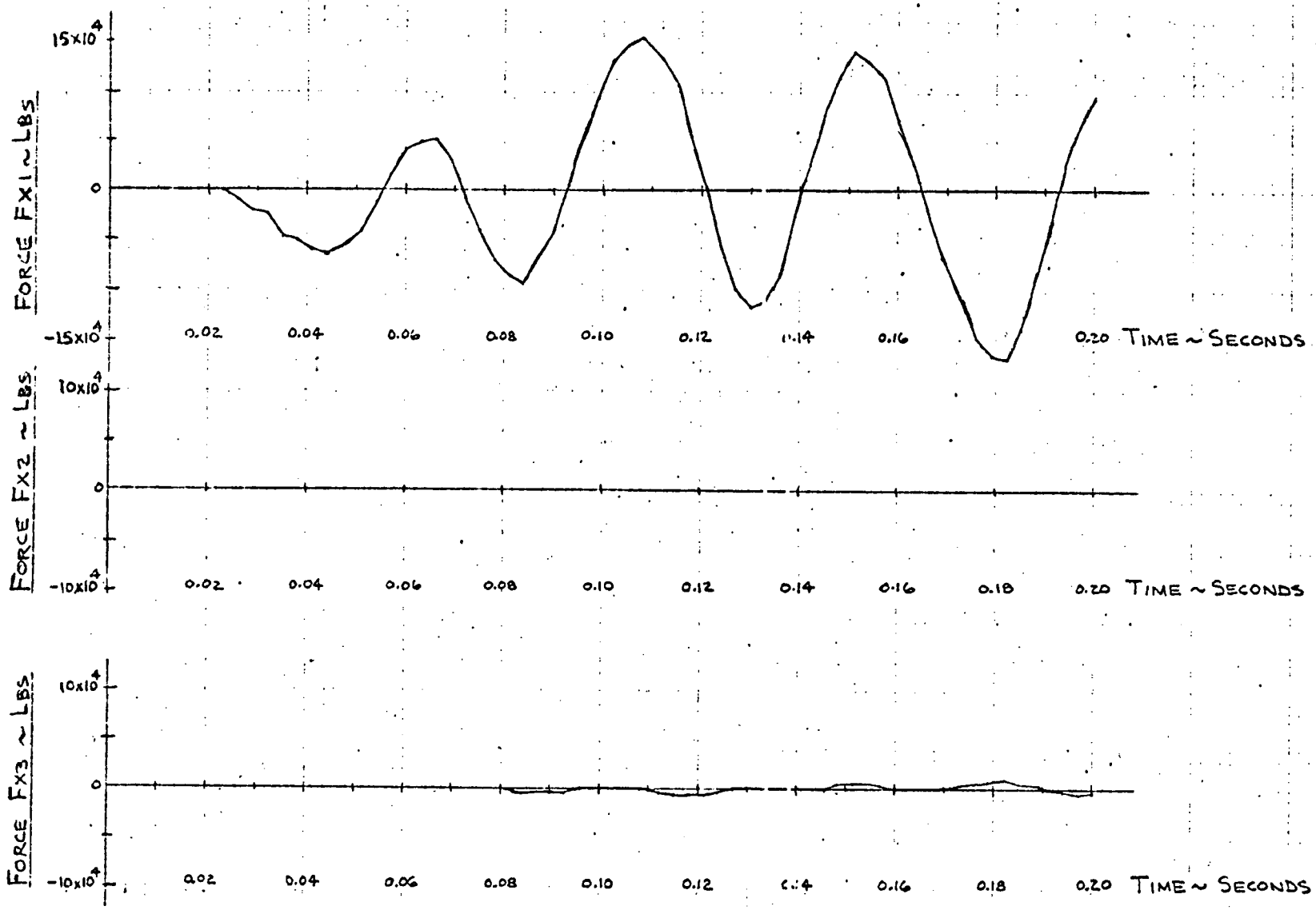

FIGURE 5.16 CASE 1H1S3 FORCE-TIME HISTORY AT CONTAINMENT PENETRATION

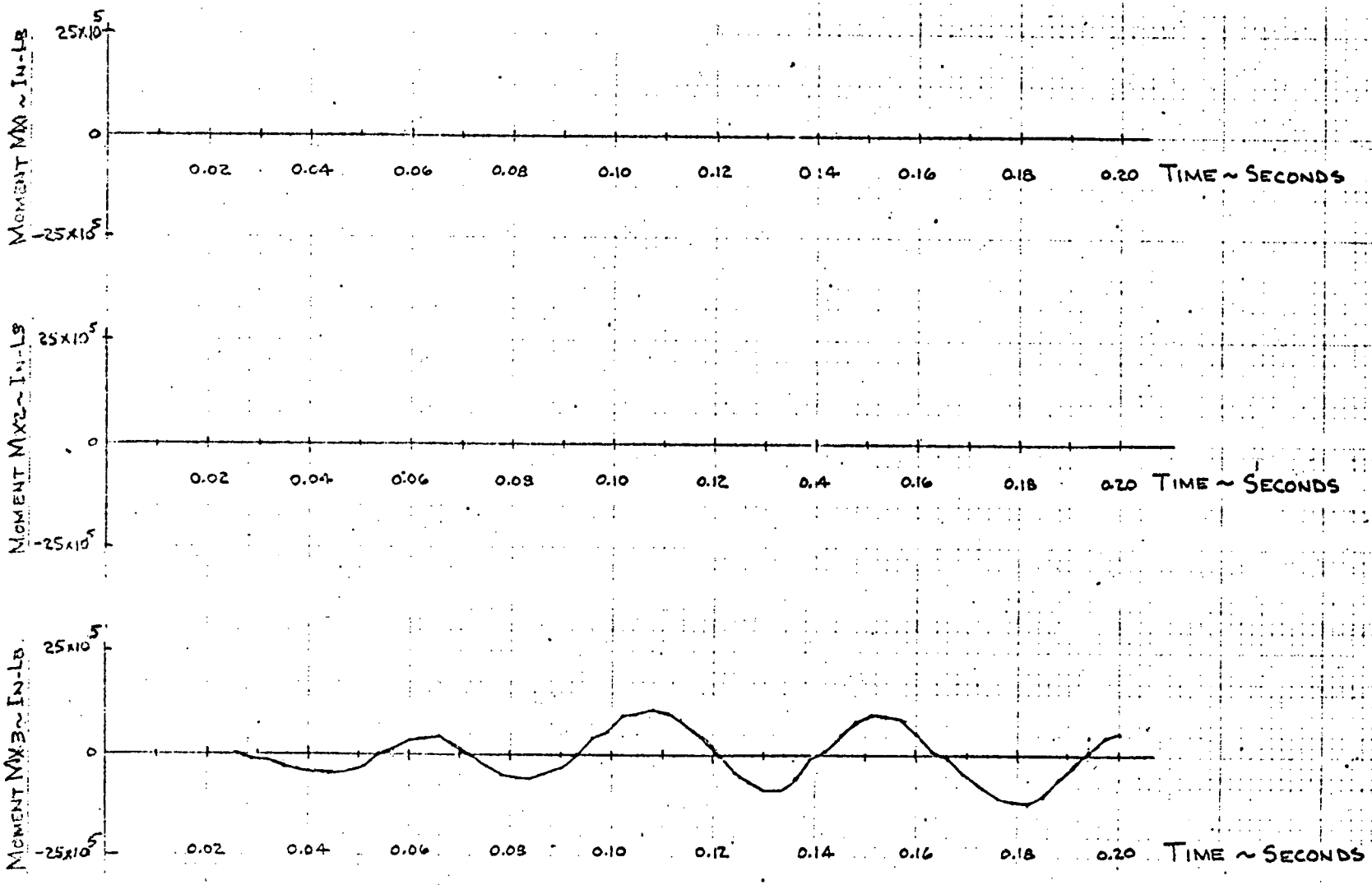

FIGURE 5.17 CASE 1H1S3 MOMENT-TIME HISTORY AT CONTAINMENT PENETRATION

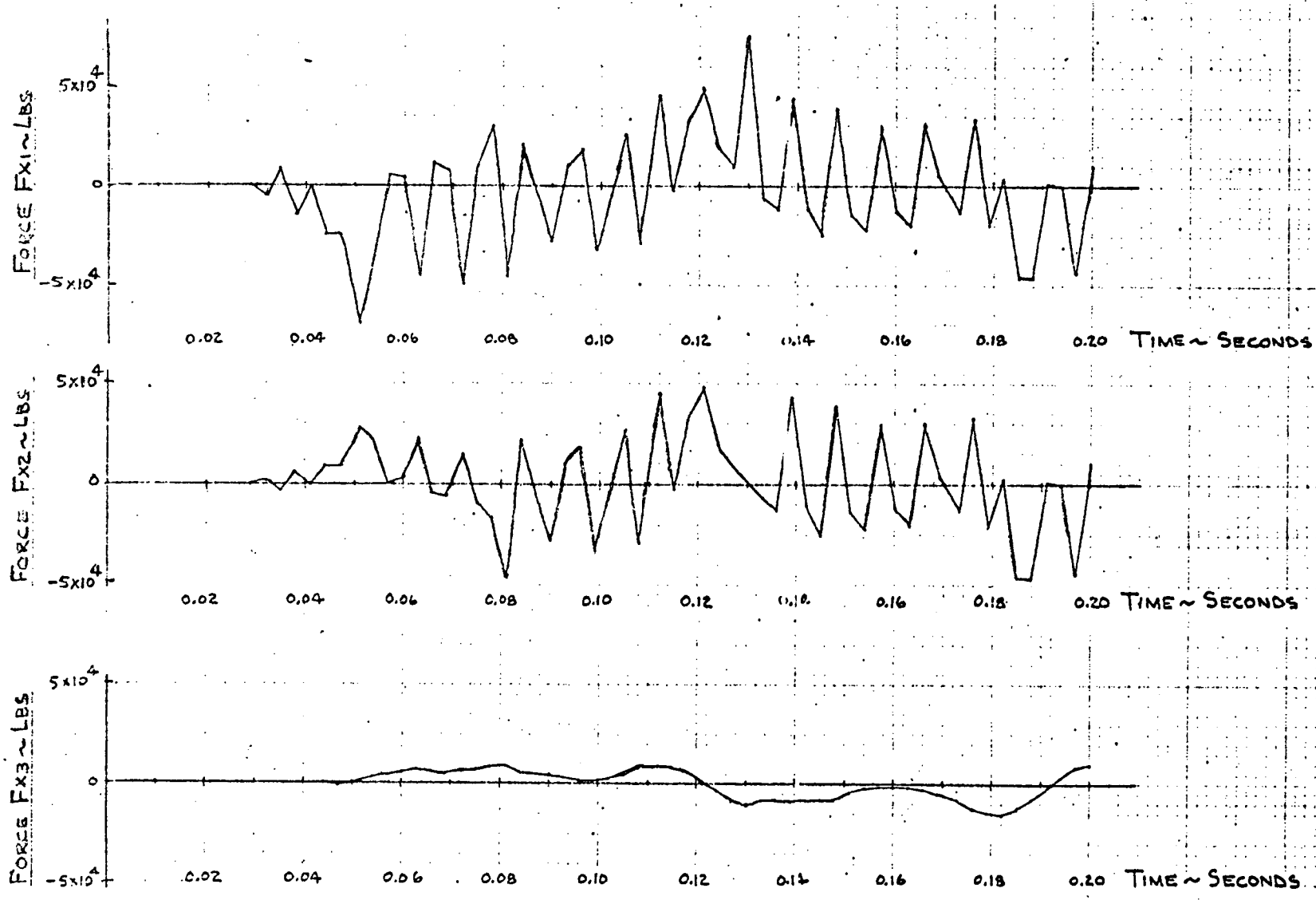

FIGURE 5.18 CASE 1H1S3 FORCE-TIME HISTORY AT STEAM GENERATOR NOZZLE

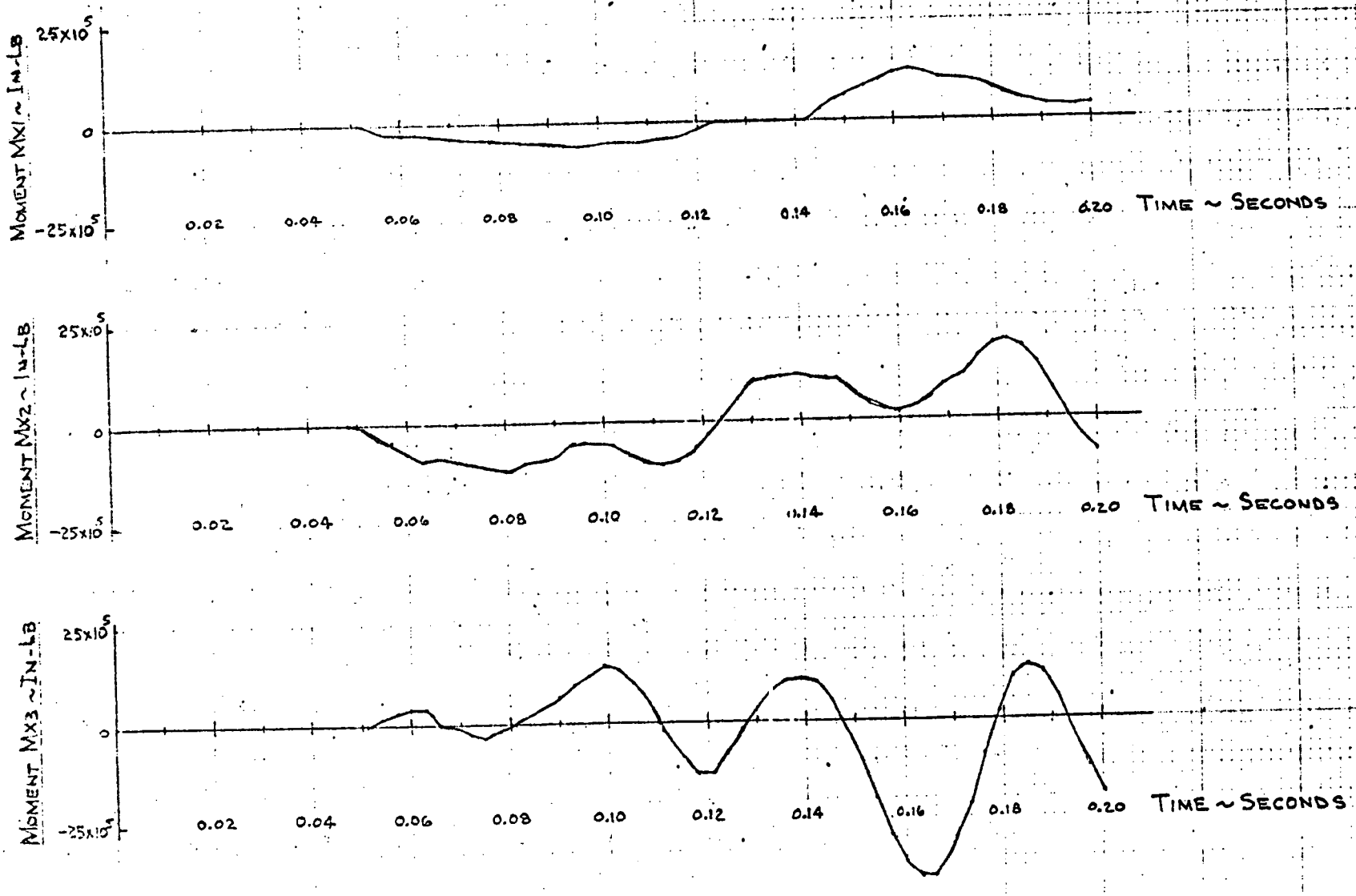

FIGURE 5.19 CASE 1H1S3 MOMENT-TIME HISTORY AT STEAM GENERATOR NOZZLE

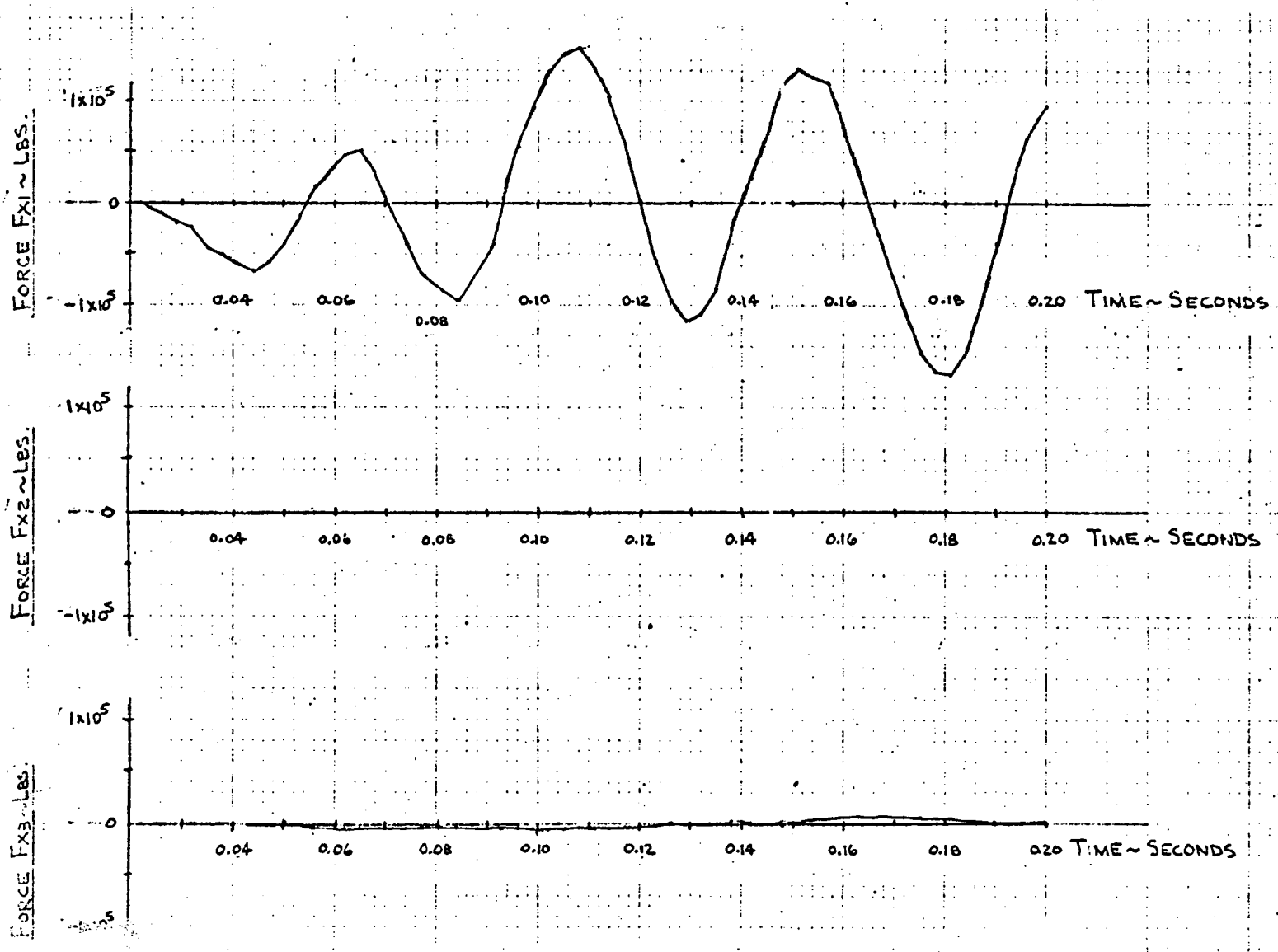

FIGURE 5.20 CASE 1H1S4 FORCE-TIME HISTORY AT CONTAINMENT PENETRATION

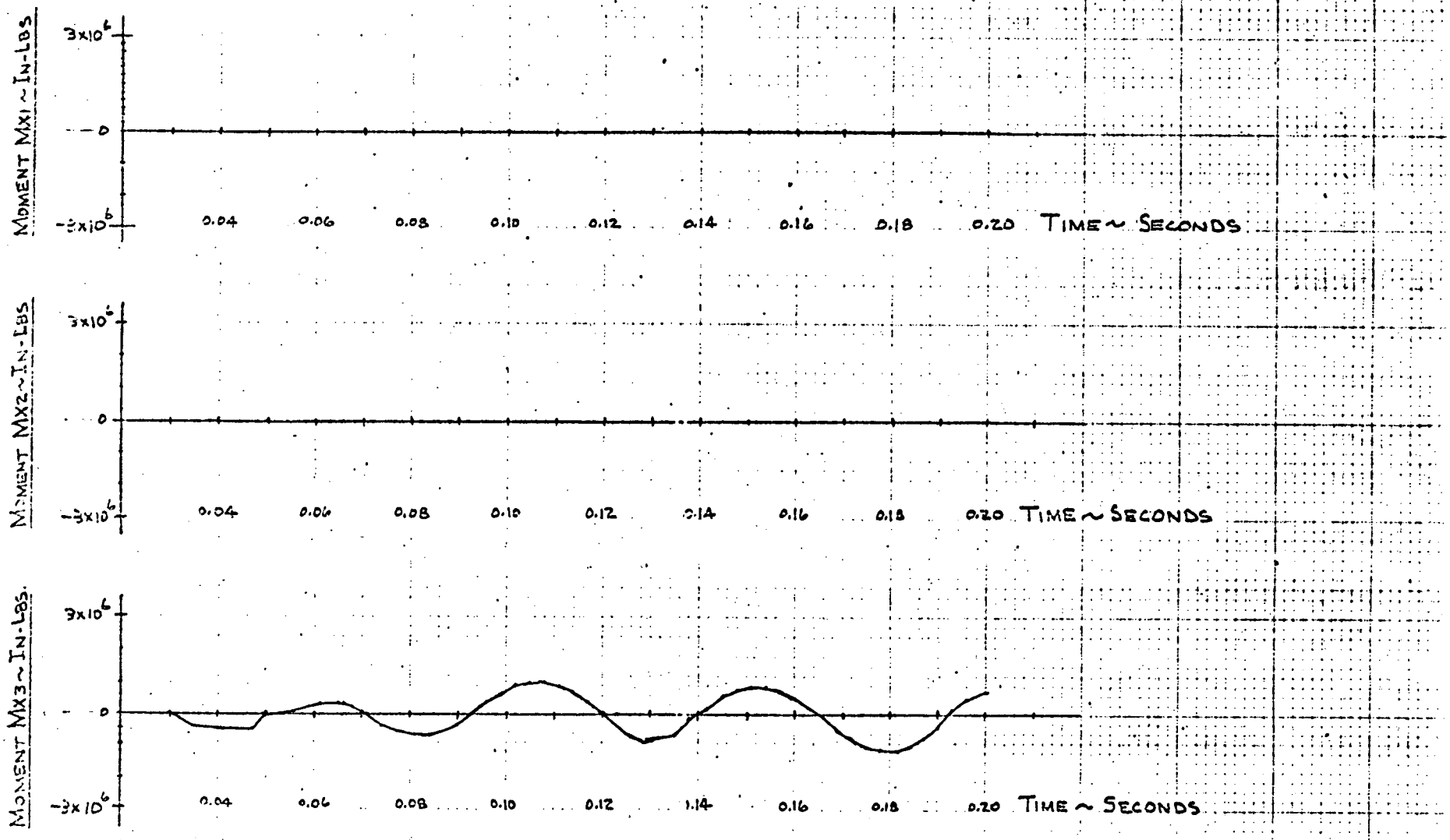

FIGURE 5.21 CASE 1H1S4 MOMENT-TIME HISTORY AT CONTAINMENT PENETRATION

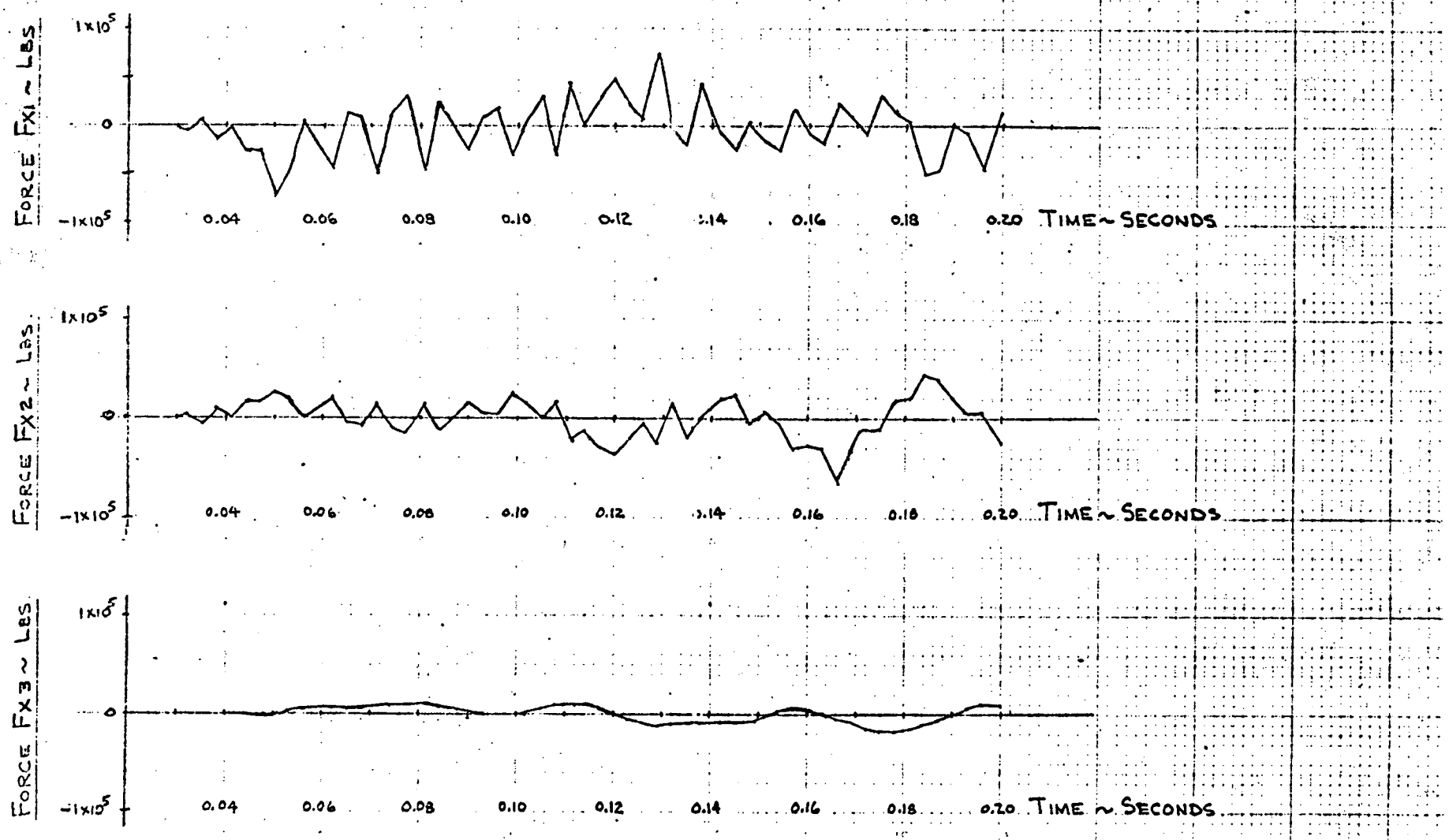

FIGURE 5.22 CASE 1H1S4 FORCE-TIME HISTORY AT STEAM GENERATOR NOZZLE

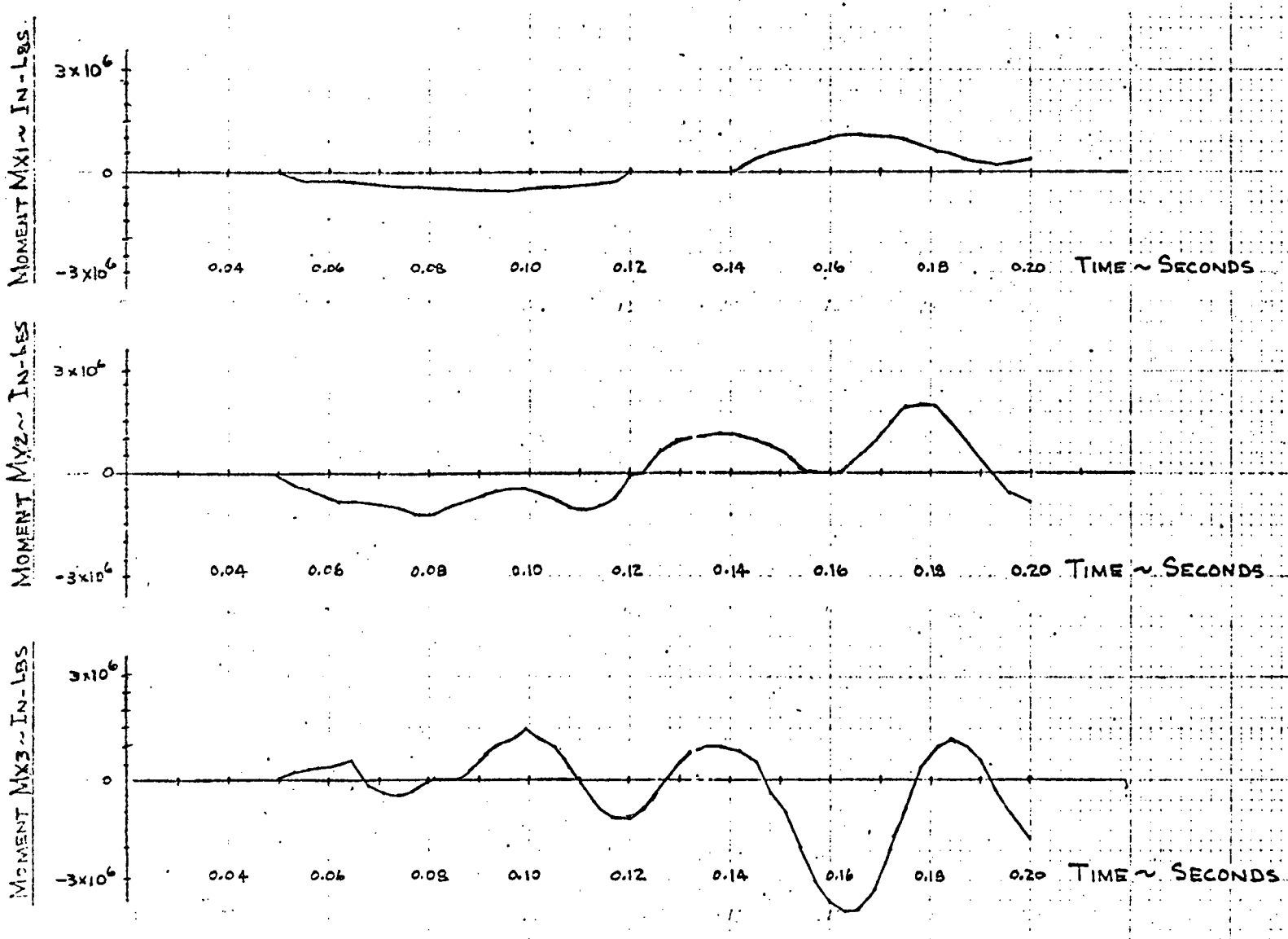

FIGURE 5.23 CASE 1H1S4 MOMENT-TIME HISTORY AT STEAM GENERATOR NOZZLE

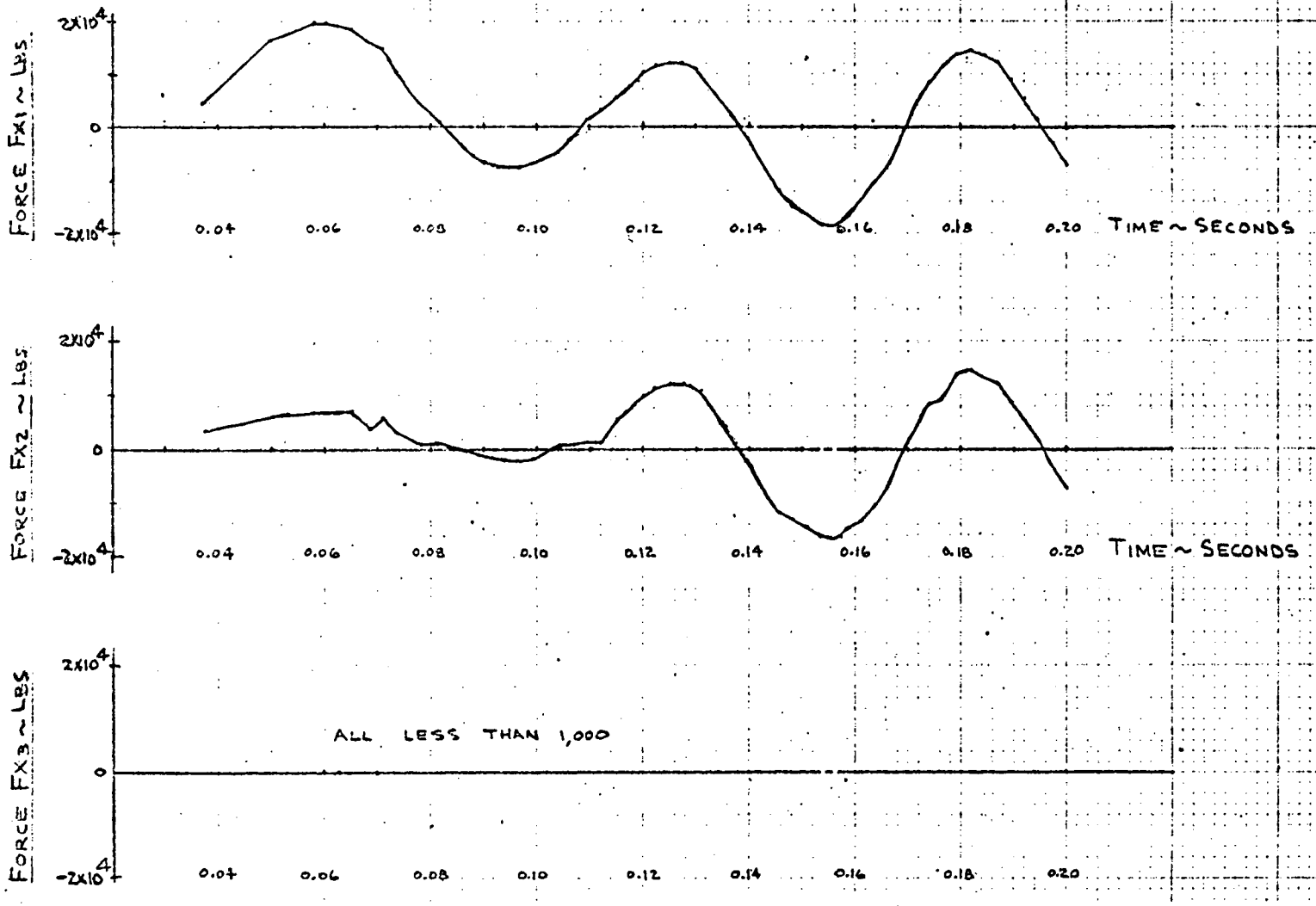

FIGURE 5.24 CASE 2H1S1 FORCE-TIME HISTORY AT CONTAINMENT PENETRATION

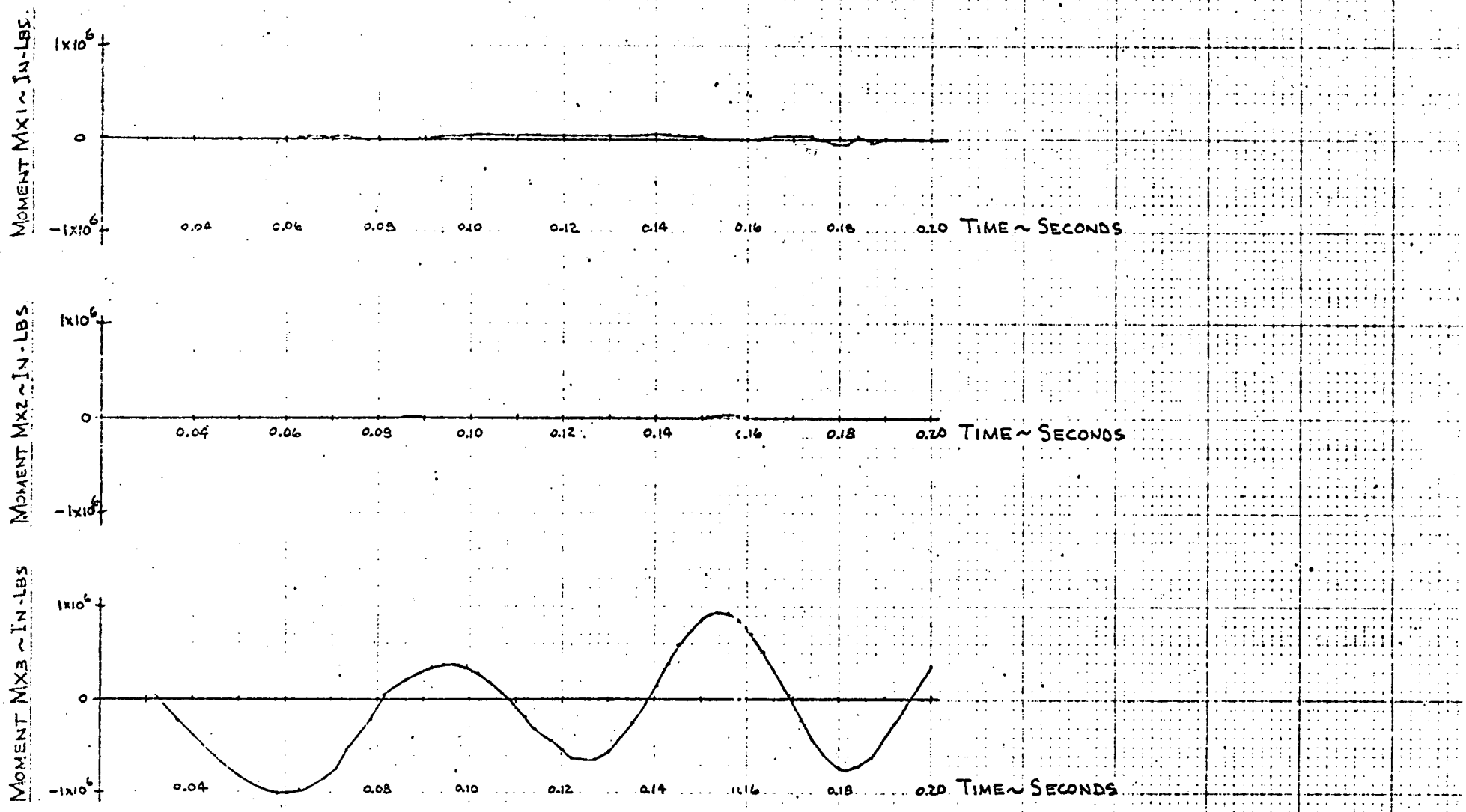

FIGURE 5.25 CASE 2H1S1 MOMENT-TIME HISTORY AT CONTAINMENT PENETRATION

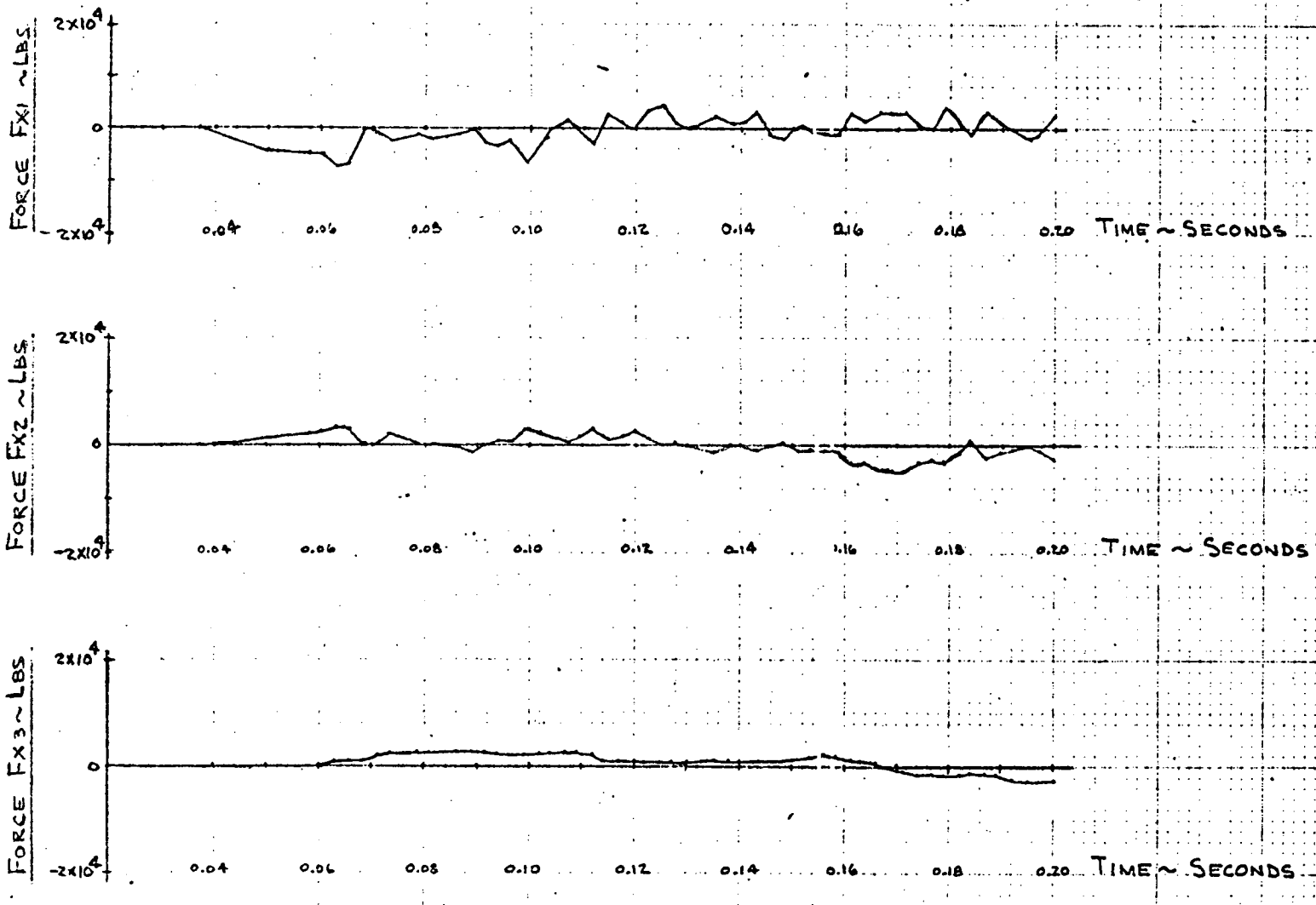

FIGURE 5.26 CASE 2H1S1 FORCE-TIME HISTORY AT STEAM GENERATOR NOZZLE

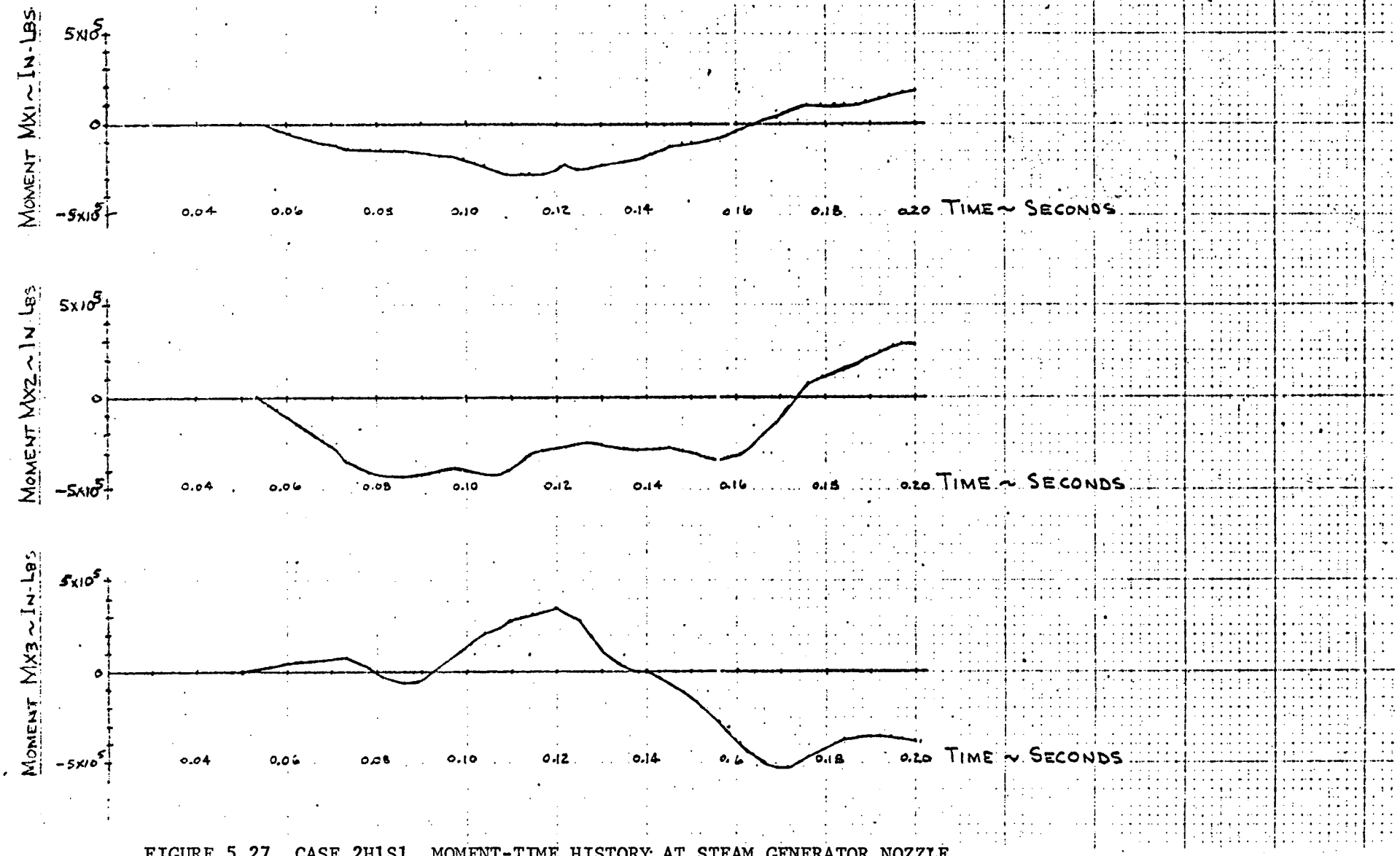

FIGURE 5.27 CASE 2H1S1 MOMENT-TIME HISTORY AT STEAM GENERATOR NOZZLE

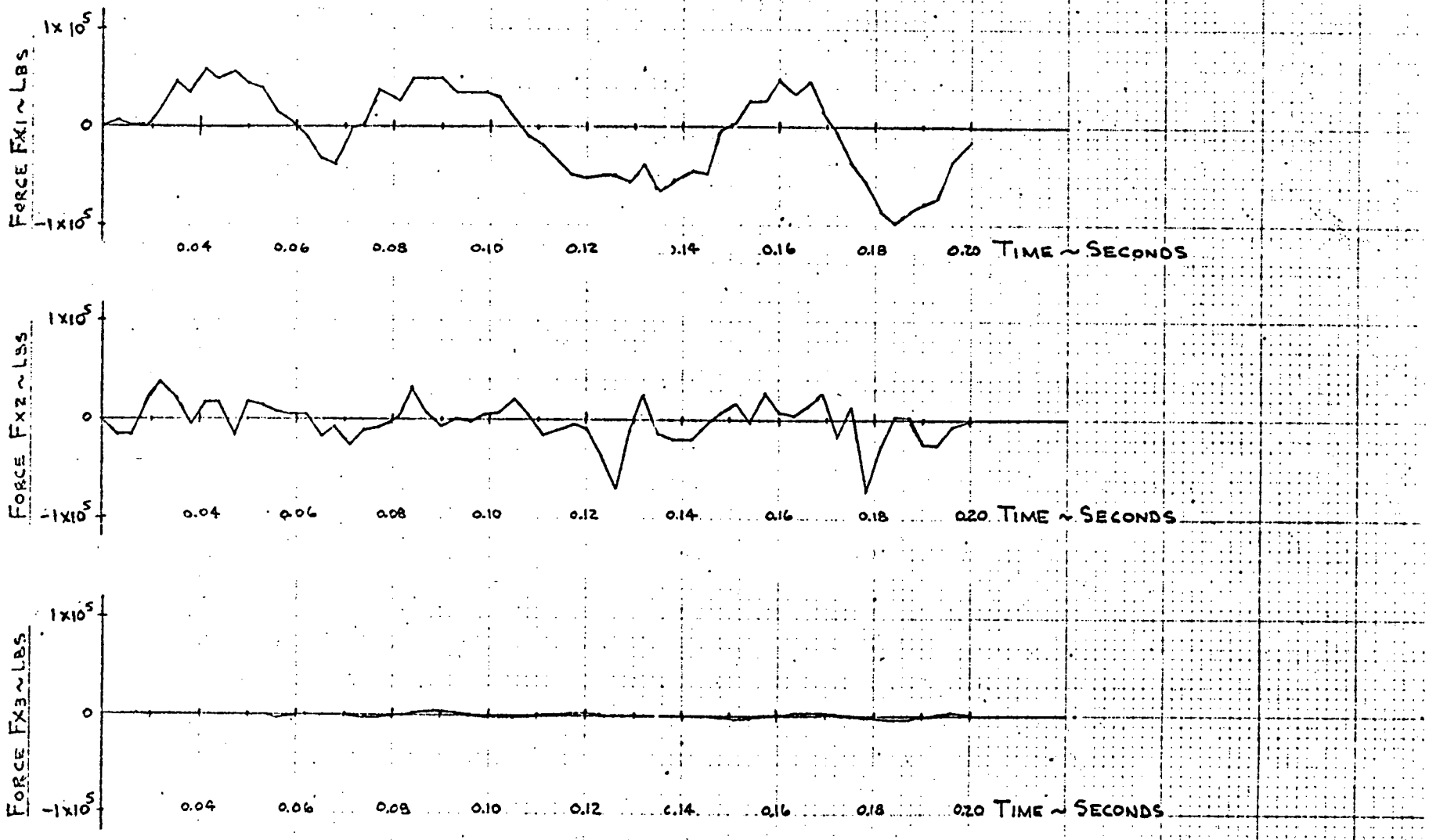

FIGURE 5.28 CASE 5H1S1 FORCE-TIME HISTORY AT CONTAINMENT PENETRATION

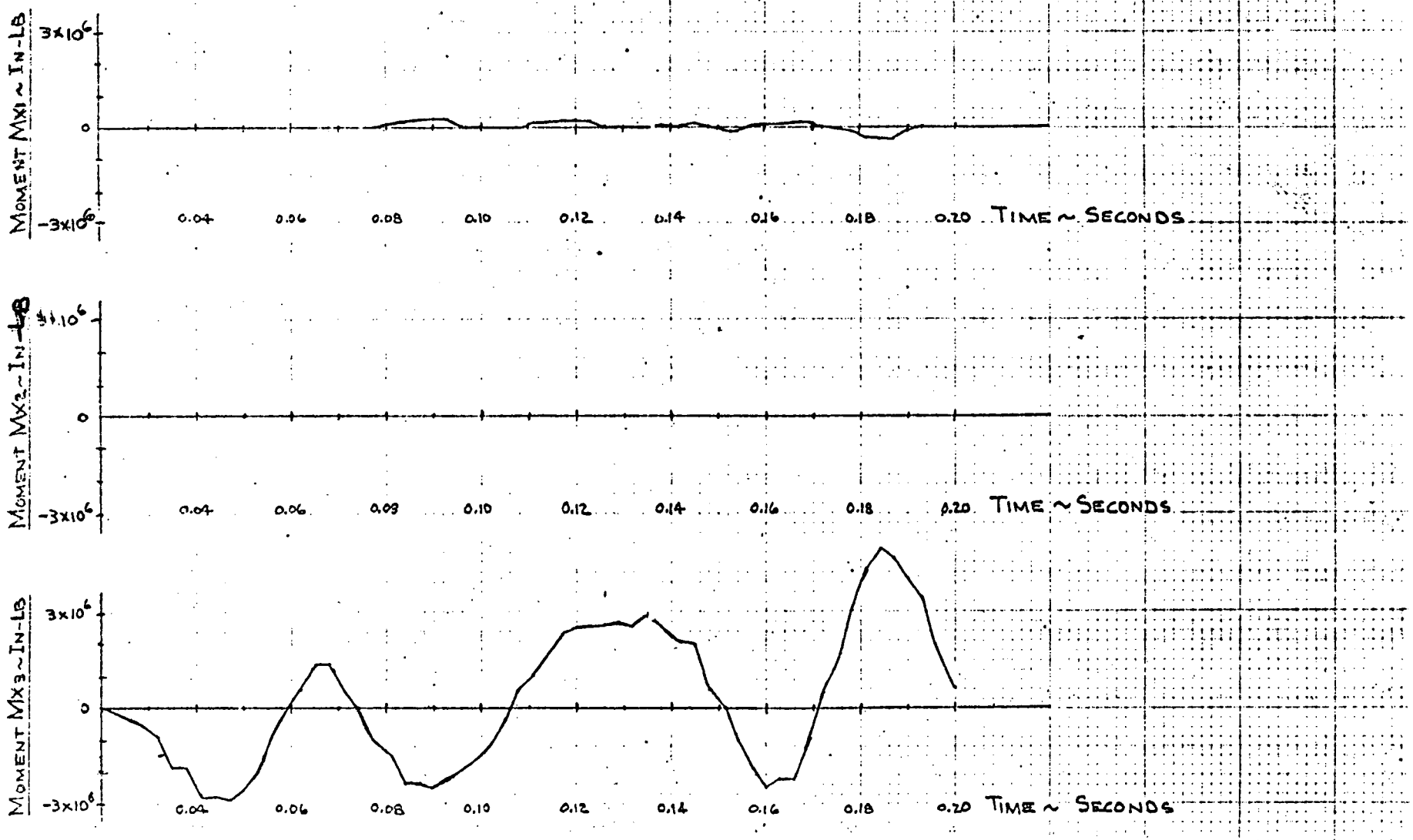

FIGURE 5.29 CASE 5H1S1 MOMENT-TIME HISTORY AT CONTAINMENT PENETRATION

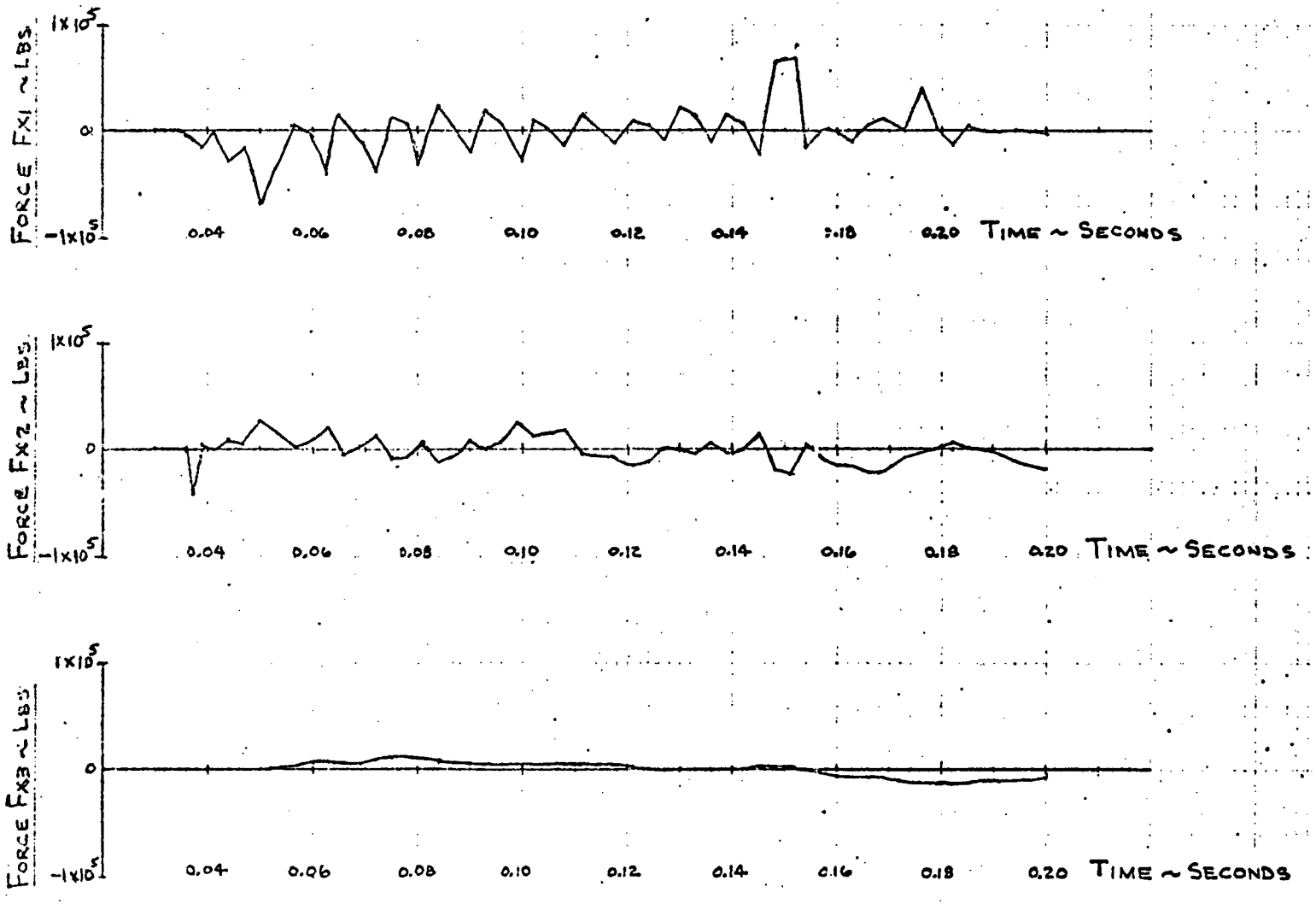

FIGURE 5.30 CASE 5H1S1 FORCE-TIME HISTORY AT STEAM GENERATOR NOZZLE

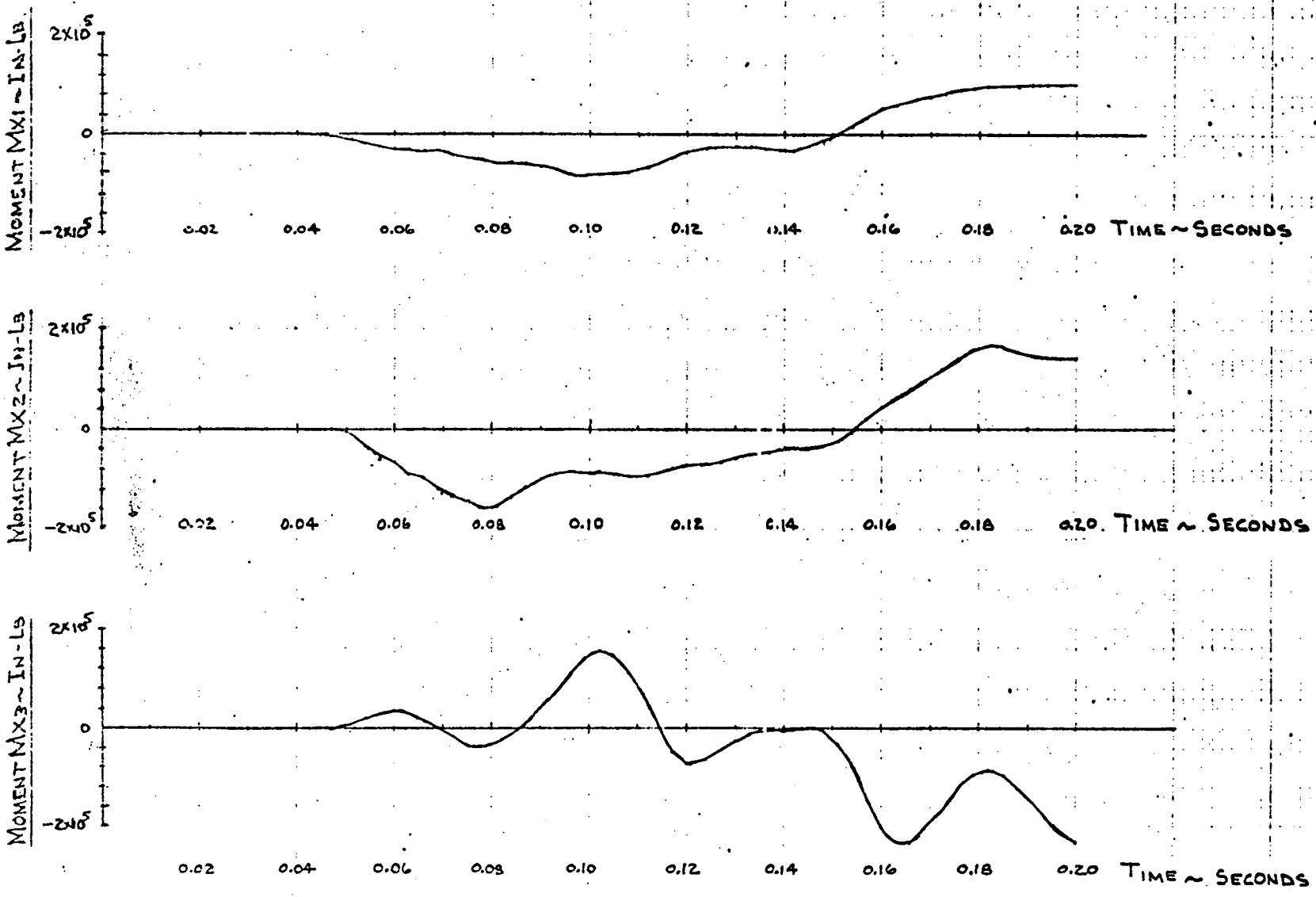

FIGURE 5.31 CASE 5H1S1 MOMENT-TIME HISTORY AT STEAM GENERATOR NOZZLE

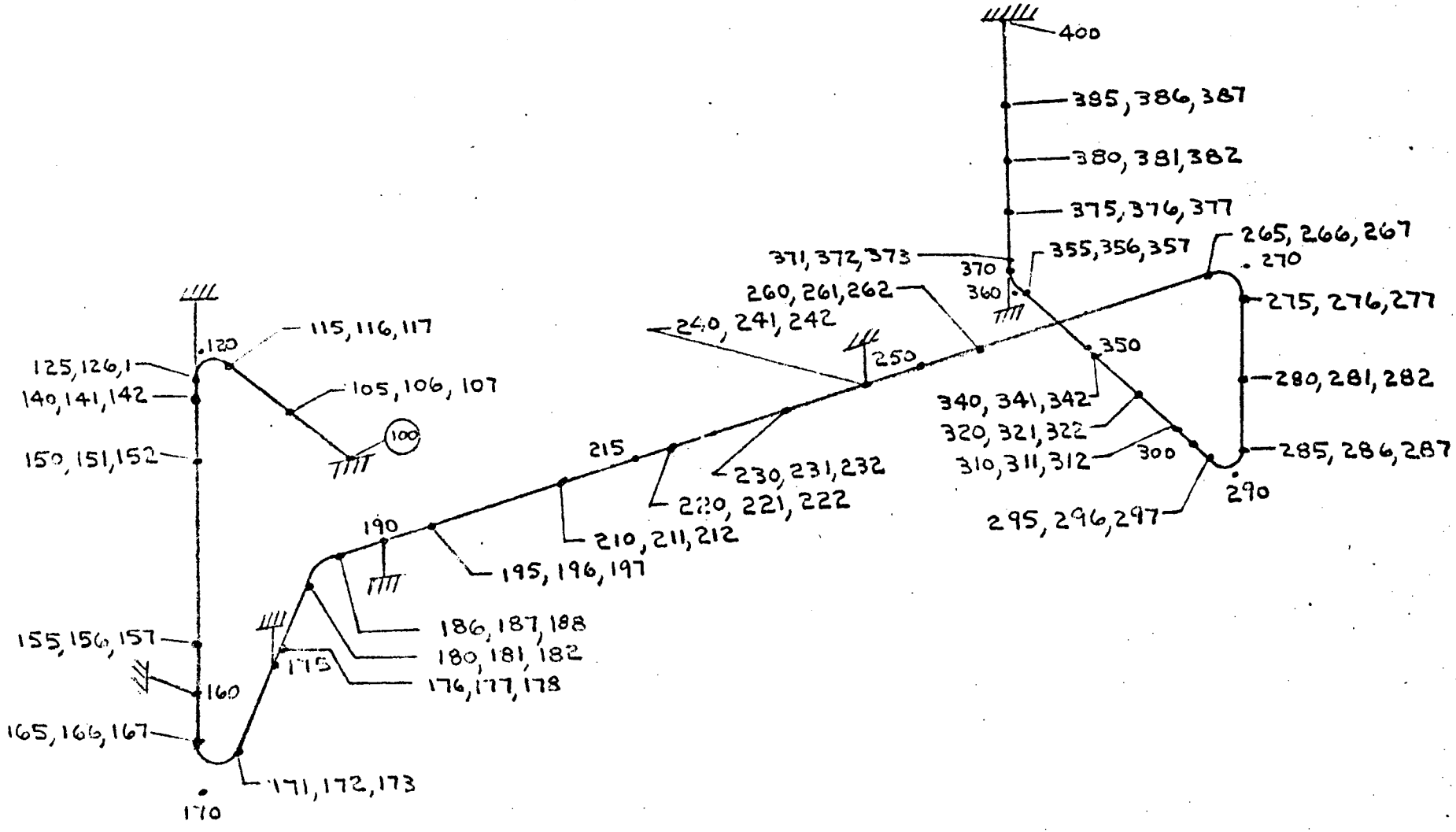

FIGURE 5.32 MEL-40 MATHEMATICAL MODEL FOR FEEDWATER LINE - OUTSIDE CONTAINMENT

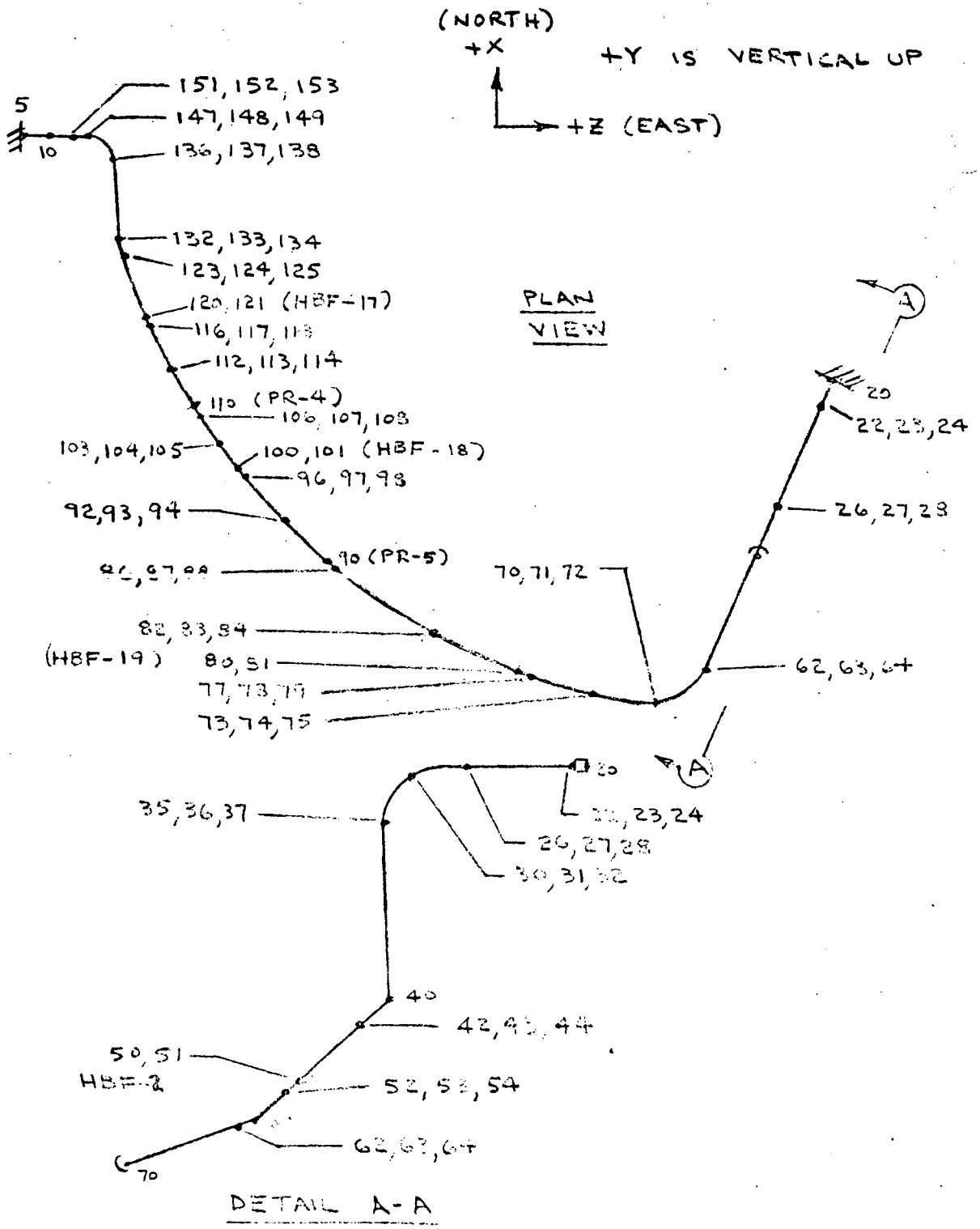

FIGURE 5.33 MEL-40 MATHEMATICAL MODEL FOR FEEDWATER LINE - INSIDE CONTAINMENT